Final Engineering Report

SPACE STATION STABILIZATION AND CONTROL STUDY

Prepared for
LANGLEY RESEARCH CENTER
NATIONAL AERONAUTICS AND SPACE ADMINISTRATION
LANGLEY FIELD, VIRGINIA

Contract No. NAS 1-2946

Prepared by
SPERRY RAND SYSTEM GROUP
SPERRY GYROSCOPE COMPANY
DIVISION OF SPERRY RAND CORPORATION
GREAT NECK NEW YORK

Sperry Report No. AB-1210-0020

December 1963

Final Engineering Report

SPACE STATION STABILIZATION AND CONTROL STUDY

Prepared for

LANGLEY RESEARCH CENTER
NATIONAL AERONAUTICS AND SPACE ADMINISTRATION
LANGLEY FIELD, VIRGINIA

Contract No. NAS 1-2946

Prepared by

SPERRY RAND SYSTEMS GROUP
SPERRY GYROSCOPE COMPANY
DIVISION OF SPERRY RAND CORPORATION
GREAT NECK NEW YORK

I.N. Hutchinson
R. Steuer
R. Morrison
K.Thomson

Approved by

J. Keller, Research Section Head
W. Zdan, Senior Research Section Head
D. Barnette, Engineering Section Head

Copy No. 21

Sperry Report No. AB-1210-0020

December 1963

TABLE OF CONTENTS

TABLE OF CONTENTS (Cont)

LIST OF ILLUSTRATIONS

LIST OF ILLUSTRATIONS (Cont)

LIST OF TABLES

LIST OF TABLES (Cont)

Section I

INTRODUCTION

A. BACKGROUND

This report documents a Stabilization and Control study of flexible, spinning, manned space stations. The study was performed by the Sperry Rand Systems Group of Sperry Gyroscope Company, Division of Sperry Rand Corporation, for the Langley Research Center, National Aeronautics and Space Administration under Contract No. NAS 1-2946.

The investigation of the stabilization and control problem for a flexible spinning vehicle was initiated to explore the feasibility of controlling this type of vehicle because such configurations provide a means of obtaining an artificial gravity station environment within near-term booster payload limitations.

The uncertainty of man's reaction to prolonged zero-gravity exposure has necessitated investigations of techniques which can be used in space station configuration design to provide an artificial gravity environment, either as an experimental tool or as a backup configuration in the event that extended zero-gravity operation proves unfeasible. One technique for providing artificial gravity, within constraints imposed by payload limitations and the desire for a large rotational radius, consists of spinning a manned space capsule and an empty booster case about their common mass center. A large spin radius can be achieved by separating the two bodies by means of a structural member. The desire to minimize the weight associated with the member connecting the separated bodies leads to vehicle configurations which use either cables or relatively thin struts or tubes as the coupling device. Such extension mechanisms are elastic structures and will behave as flexible or nonrigid members. Vehicles of this

type, therefore, can be generically referred to as flexibly coupled, spinning, space stations.

The dynamics of this type of flexible vehicle are more complex than those of a rigid body. Structural oscillations will be superimposed on, and will interact with, the rigid body motions. Thus, it can be expected that control concepts will be required which differ from those which have been reasonably well developed for vehicles more nearly exhibiting rigid body behavior. This study was undertaken with the purpose of defining the control and stabilization problems and generating promising control-system concepts for coping with it.

B. OBJECTIVES

The broad objectives of the study were:

1. To evaluate the feasibility of providing effective, reliable, control subsystems for flexibly coupled, spinning, manned vehicles during the extension or retraction maneuver, and during steady spinning operation.
2. To generate promising control-system concepts and investigate their performance characteristics.
3. To define the relationships among the control system, configuration, and control-requirement parameters. Knowledge of such relationships, i.e., sizing laws, provides the basis for the subsequent generation of control-system specifications and preliminary design.
4. To analyze and evaluate several cable-coupling configurations with the objective of minimizing the control problem imposed by the flexible structure.

C. SCOPE

This study has emphasized (1) dynamics and control of the vehicle in the spinning operational mode and (2) the transition from the spinning to the nonspinning mode. Most station concepts also envision operating the station in a nonspinning or zero-gravity mode, perhaps for considerable periods of time. However, consistent with the objectives of this study, consideration of the nonspinning control problem was restricted to insuring compatibility.

For study purposes, a nominal vehicle and a set of nominal control requirements were established. The effects of variations about these nominals were considered in generating sizing or scaling laws. Variations in such parameters as orbital altitude, inclination, eccentricity, and aerodynamic coefficients are not of significance with respect to vehicle short-term dynamics, and are therefore outside of the study scope. Detailed study in these and other areas will be required prior to preliminary design, establishment of fuel budgets, and similar subsequent development activities.

D. APPROACH

The study effort proceeded along the following lines:

1. The important vehicle dynamic characteristics were established and analytical models were generated.
2. Nominal control requirements and disturbance models were formulated for the various modes of space-station operation.
3. Based on the appropriate models, control concepts were synthesized.
4. Control-system simulations were performed for the nominal vehicle, establishing "nominal" performance characteristics.
5. Data was generated describing the relationship of such control-system parameters as weight and peak power to vehicle configuration, disturbance, and damping-requirement parameters.
6. The relative merits of variations in control approach for this application were examined and summarized.
7. Problem areas requiring further study were identified.

Section II of the report describes the technical approach and summarizes the study results. Subsequent sections treat the various aspects of the study at length.

Section II

SUMMARY OF RESULTS AND RECOMMENDATIONS

A. MAJOR RESULTS

1. The study established the feasibility of stabilizing and controlling a flexible, spinning space station.
2. The control system required for the station is of reasonable size, weight, and power, and is well within the state of the art.
3. The only unique component required in the control system is a large, two-degree-of-freedom control moment gyroscope. The development of such a gyro represents a standard gyro design problem. No technological break-throughs are required.
4. The cable configuration used to couple the manned body to the empty booster case is not critical from a controls standpoint. Several simple cable configurations are feasible, and the selection of a particular configuration can be largely based on deployment mechanism trade-offs, operational considerations, and other factors beyond the scope of a controls-oriented study. From a controls viewpoint, however, an eight crossed cable configuration appears to offer some slight advantages relative to others considered in the study.
5. The elastic structural modes, although of importance, pose as insurmountable control problems during either steady spinning operation or the transition from the spinning to the nonspinning state.
6. The extension and retraction of the station can be performed with good propellant economy. In the nominal case considered

here, the transition maneuver required only 6 percent more fuel than would be required to accelerate an equivalent rigid station to the same operating speed.

B. RECOMMENDED FOLLOW-ON EFFORTS

As a further result of this investigation, several areas requirin more detailed study have been identified. The specific tasks which are recommended as follow-on items are discussed in section IX, and summarized below:

- It is recommended that the scope of this study be enlarged to include other vehicle configurations. For example, vehicles having no inherent roll stability, or having asymmetric booster and/or cable configurations are practical candidates for near-future use, but were not considered in this study.
- It is recommended that further analysis of the extension/retraction problem be performed in order to insure that there are no hidden problem areas. In this study, attention was focused on the yaw axis since the pitch and roll axes did not appear as critical. This preliminary finding must, of course, be substantiated by detailed simulation of the pitch and roll axes. Further, a four cable configuration was considered in this study to simplify the cable slacking calculations. Other cable configurations should be analyzed. Finally, no attempt has been made to define detailed performance requirements for the mating device used to couple the manned body to the capsule. Allowable disturbance inputs at de-coupling and expected terminal conditions at coupling shoud be established.
- It is further recommended that system integration studies be performed. Control concepts suitable for use in the spinning modes have been established, and nonspinning mode control concepts are well known. The next step in the definition of a flexible spinning space station control system should be the development of an integrated system concept. For example, actuator trade-offs have been considered in this study, but only relative to spinning mode requirements. While the specific actuators proposed in section VIII are compatible with nonspinning mode requirements, they may not be an optimum selection. Further trade-off

investigations, with increased emphasis on nonspinning mode requirements, are required to establish an optimum actuator configuration.

C. SUMMARY OF UNCONTROLLED VEHICLE CHARACTERISTICS

Equations of motion for a flexible vehicle of the type illustrated by figure 1 were generated and programmed for the digital computer. This program was used to establish the general dynamic characteristics of the space station, to determine the effect of the various configuration parameters on the vehicle dynamics, and to evaluate several alternate cable configurations.

As a result of this study, it was determined that the flexible vehicle would be similar to the rigid vehicle in many respects, but that structural flexibility would play an important role in some practical cases. The cable configuration used to couple the manned body to the empty booster stage was, of course, found to affect the structural flexibility. An eight-cable configuration (cf. figure 4) suggested by Langley Research Center personnel was found to be somewhat more desirable than the other cable configurations considered in the study. However, all of the cable configurations which were analyzed appeared satisfactory during both the operational spinning mode and the transition mode. No differences were discovered significant enough to dictate the use of a specific configuration to obtain adequate control.

D. SUMMARY OF CONTROL SYSTEM OPERATION

1. Operational Spinning Mode Control

A functional block diagram of the nominal stabilization and control system is shown in figure 2. The following paragraphs describe these functions.

The rate stabilization system is designed to damp undesirable transient motions of the vehicle. The nominal system has been sized to damp the dominant vehicle resonance to 10 percent of critical, and also damps the structural resonances to 1 percent of critical. Rate gyros are used to sense spurious motions of the manned body, and opposing torques are applied to the vehicles by the proper actuator. A two degree of freedom control moment gyro is used to provide the torques for damping angular velocities about axes normal to the spin vector. An inertia wheel damps the structural oscillations of the manned body about the spin axis. As discussed

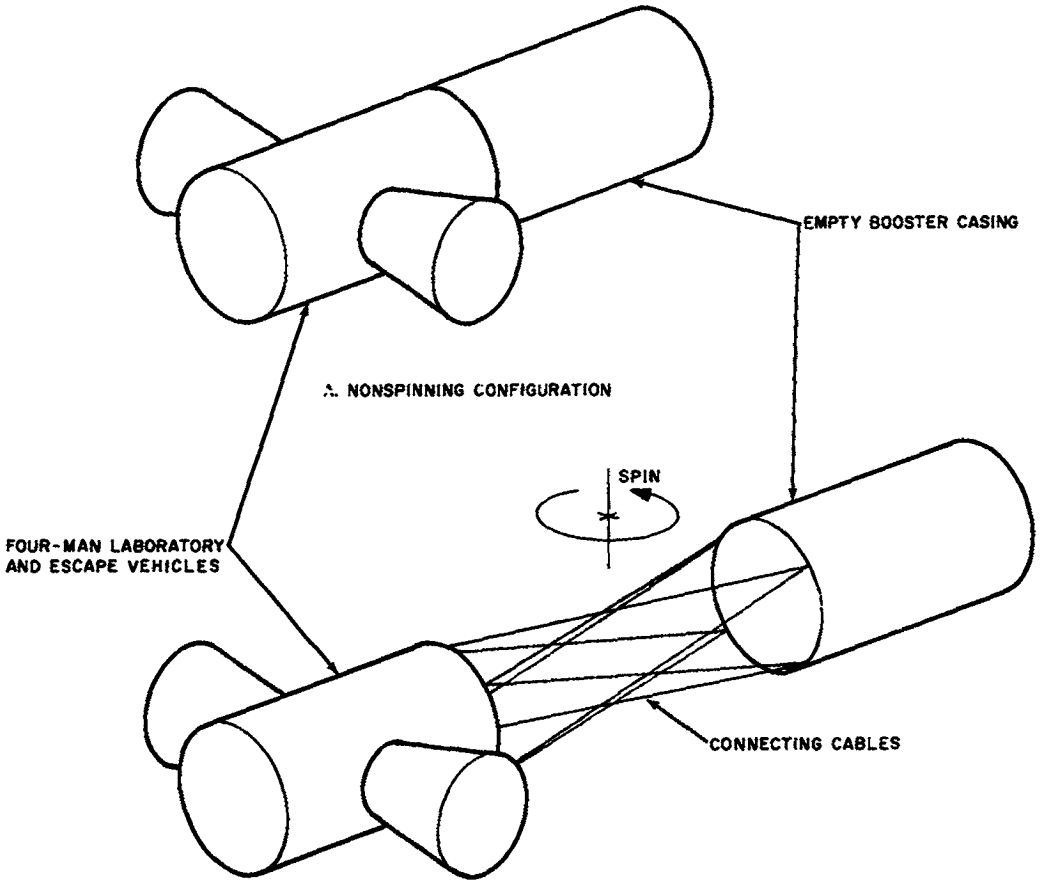

FIGURE I
TYPICAL STATION CONFIGURATION

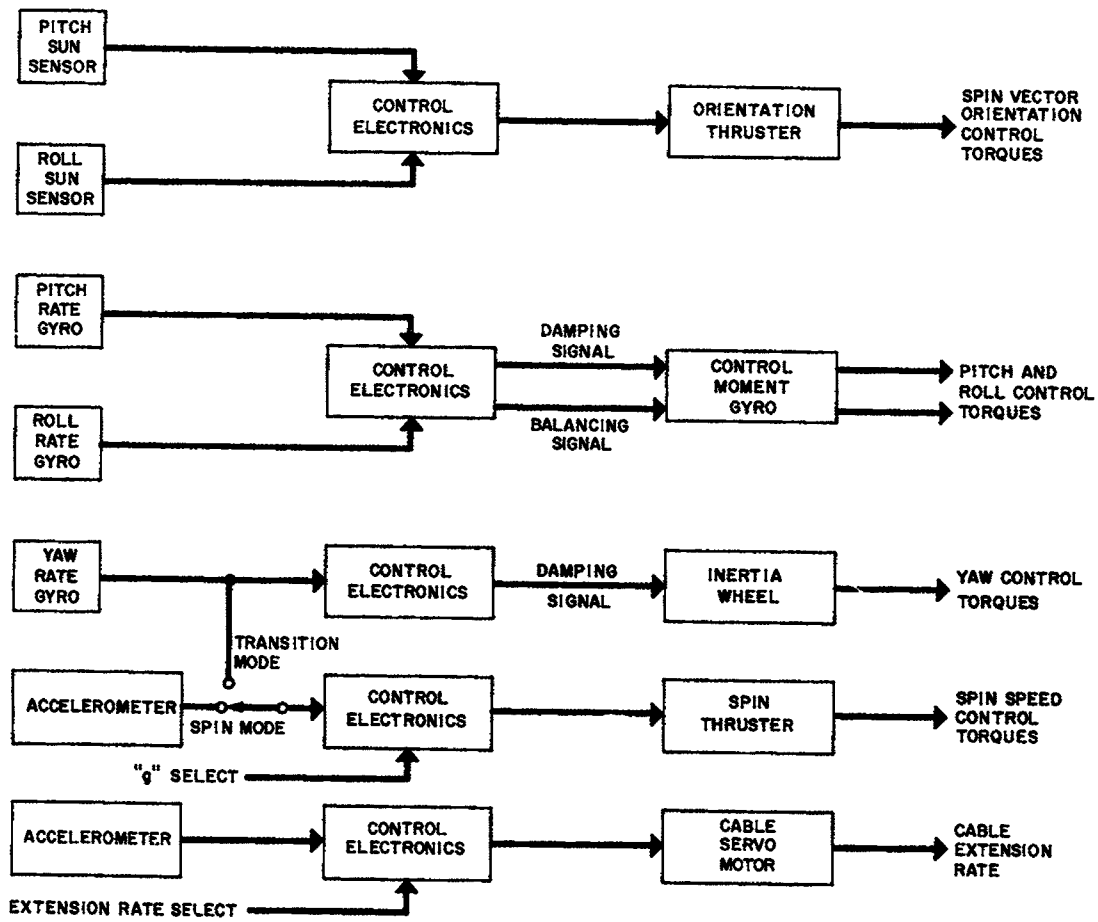

FIGURE 2
FUNCTIONAL BLOCK DIAGRAM OF
NOMINAL CONTROL SYSTEM

in section V, the control moment gyro appears to offer significant advantages relative to inertia wheels, reaction jets, or single degree of freedom gyros.

The damped vehicle tends to spin about its axis of major moment of inertia, which may not coincide with the space station geometric axis-the desired axis of rotation. The dynamic balancing system utilizes the same rate gyros and the same control moment gyro mentioned above to provide the torques required to make the vehicle spin about its geometric axis. In doing so, it compensates for dynamic imbalances which may arise because of crew motions inside the manned body.

The long term orientation of the space station spin vector (and geometric axis) is controlled by reaction jets. A solar alignment control system accurate to ±1/2 degree was synthesized to determine the response of the vehicle to orientation thrusts and to demonstrate feasibility. Sun sensors, reaction jets, and control logic comprise the orientation control system.

Artificial gravity level is maintained constant within ±2 percent of desired level (0.4g nominal) by means of reaction jets controlled by a suitably oriented accelerometer.

2. Transition Mode Control

The transition mode is typified by a continuous, and gross, change in vehicle dynamics, and by certain nonlinear phenomena which arise only during this mode of operation. As an example of the latter, it was found that cable slacking was not likely to occur during the operational spinning mode, but was almost certain to occur during the transition mode at low spin speeds and short cable lengths. Accordingly, a special analog simulation incorporating the relevant nonlinearities was employed for the transition mode control study.

The transition maneuver itself was designed to strike a reasonable compromise between propellant economy and vehicle rigidity. From the standpoint of propellant economy, it would be most desirable to completely extend the cables before thrusting to attain operational spin speed. This is not possible, however, since the centrifugal force due to spin is the only thing that keeps the cables taut and prevents the two vehicles from following separate independent trajectories.

A maneuver consisting of extension at a low spin speed (10 percent of operational speed), followed by a spin-up to final speed at full extension was finally selected. This maneuver required only six percent more propellant than would be required if all thrusting could be done at full extension. The rigidity of the vehicle was sufficient to keep attitude oscillations below three or four degrees during the five minute extension. The attitude oscillations were smaller during the ensuing 10 percent minute spin-up which completed the transition maneuver.

The transition mode control system consists of a spin speed controller and a cable extension rate controller. Reaction jets controlled by a rate gyro mounted in the manned body are used to control spin speed. The extension rate is controlled by an electric servo motor on the cable drum, which also provides the damping (tachometer feedback) which is needed to reduce cable slacking and associated "bounce" of the manned body as it hits the end of the cables.

E. SUMMARY OF CONTROL SYSTEM CHARACTERISTICS

As indicated above, the control system components include:

Qty	Item	Wt. Lbs	Vol. Cu ft	Power, Watts	
				Peak	Steady
1	3-axis rate gyro assembly	2.5	0.03	13	13
2	Sun sensors	1	-	-	-
1	Accelerometer	1	0.01	1	1
1	Control moment gyro (2 degree of freedom)	152	4.2	28	43
1	Inertia wheel	150	1.3	-	360
1	Cable servo motor	17	0.2	-	75
4	100 lb thrust reaction jets	18	-	-	54
1	Electronics assembly	11	0.25	20	25

The total weight of the nominal system is 355 lbs, excluding reaction jet plumbing and tankage, cable drum and gearing, wiring, displays, and manual controllers. Components required solely for nonspinning mode control are also excluded, but all of the actuators and some of the sensors listed above are compatible with nonspinning mode requirements.

Major propellant requirements for the spinning mode are as follows:

- 450 lbs of propellant per spin/despin cycle.
- 4500 lbs of propellant per year to maintain solar orientation.

These requirements assume that the reaction jets are mounted on the manned body. If booster-mounted jets are used, the amounts become 220 lbs and 2200 lbs respectively.

Variations in mission requirements or vehicle parameters will, of course, affect the weight of the control system. The results of several parametric studies have been summarized in section VIII. Section III describes the flexible vehicle control problem in some detail, and sections IV-VII present the study results in more detail.

Section III

DISCUSSION OF THE PROBLEM

A. MISSION ANALYSIS

1. Vehicle Description

The nominal vehicle configuration selected for study is shown in figure 3. It consists of two capsules connected by a number of flexible cables. One capsule is manned and the other is an empty booster casing. The two are spun about their common mass center so as to create an artificial gravity environment.

When launched, the two vehicles are joined together and must be extended and spun after arrival in orbit. The manned body launch weight, approximately 19,000 lbs, is within the capabilities of the Saturn C-1 launch vehicle.

The station is periodically despun and retracted to allow docking by an incoming resupply vehicle. A small unmanned rocket vehicle is, in this particular concept, used as a resupply vehicle. Two gemini capsules serve as crew emergency escape vehicles.

Variations in major vehicle parameters were considered in the study. Table 1 summarizes the range of spin speeds, separations, and inertia ratios which were investigated.

TABLE 1

VEHICLE PARAMETER RANGES

Cable Length	
Operational Spinning Mode	50; 100; 150 ft
Transition Mode	0-100 ft (Typical)

(Table continued on next page.)

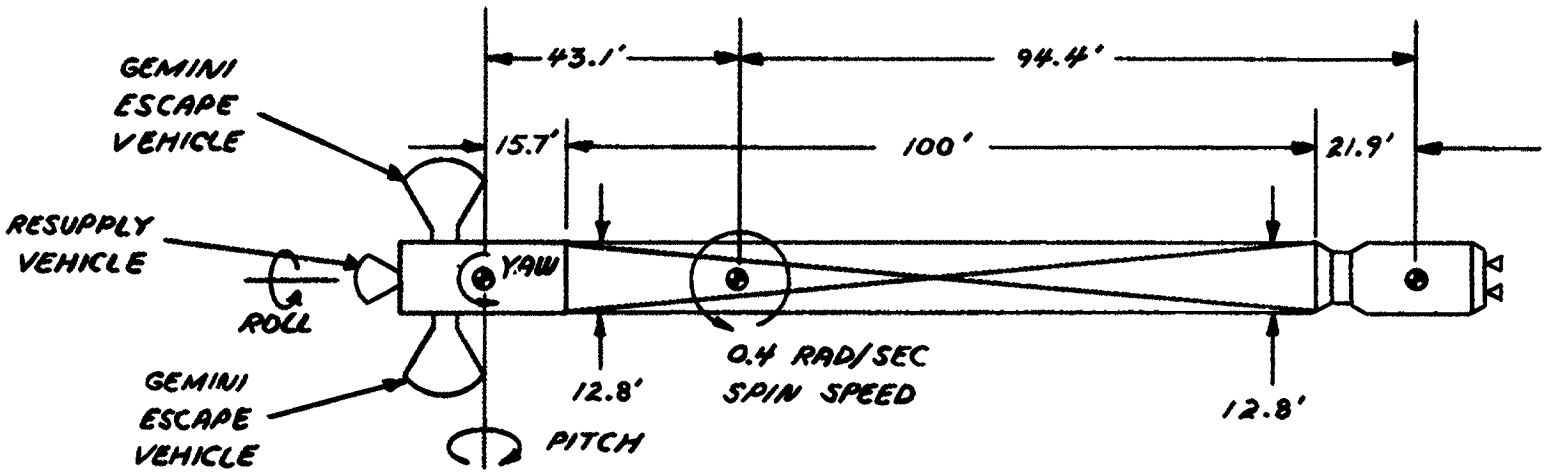

FIGURE 3 NOMINAL VEHICLE PARAMETERS

MANNED BODY

TOTAL MASS	$\equiv M_1$	1220 SLUGS
YAW INERTIA	$\equiv I_{13}$	173,000 SLUG FT^2
PITCH INERTIA	$\equiv I_{12}$	90,500 SLUG FT^2
ROLL INERTIA	$\equiv I_{11}$	103,000 SLUG FT^2

BOOSTER COUNTERWEIGHT

TOTAL MASS	$\equiv M_2$	557 SLUGS
YAW INERTIA	$\equiv I_{23}$	93,000 SLUG FT^2
PITCH INERTIA	$\equiv I_{22}$	73,000 SLUG FT^2
ROLL INERTIA	$\equiv I_{21}$	30,000 SLUG FT^2

TABLE 1 (Cont)

VEHICLE PARAMETER RANGES

Spin Speed	
Operational Spinning Mode	0.2; 0.4; 0.6 rad/sec
Transition Mode	0-0.4 rad/sec (Typical)
Inertia Ratio	
$(I_3 - I_2)/I_3$	0.0027; 0.0048; 0.0107

The inertia ratios tabulated in table 1 are the difference in the composite yaw and pitch inertias divided by the yaw inertia. The yaw inertia of the manned body was varied to change this ratio.

Five different cable configurations were analyzed. These configurations are shown in figure 4. A single cable, three cable, four cable, and two eight cable configurations are included. The eight crossed cable configuration has been treated as the nominal case.

2. Mission Description

A typical mission for this type of vehicle might include the following phases:

- Initial stabilization of the retracted station after orbital insertion.
- Acquisition of the sun and alignment of the retracted station.
- Angular acceleration and simultaneous cable deployment to reach the operational spinning condition.
- Spinning operation at a fixed spin speed and extension.
- Periodic deceleration and simultaneous cable retraction for resupply operations.
- Extended operation in the nonspinning state for, say, experimental observation.

Problems associated with the extension and retraction operations, called the transition mode hereafter, and with the operational spinning mode have been emphasized in this study. The nonspinning mode was also given brief attention in order to define mode switching requirements and to assure actuator compatibility.

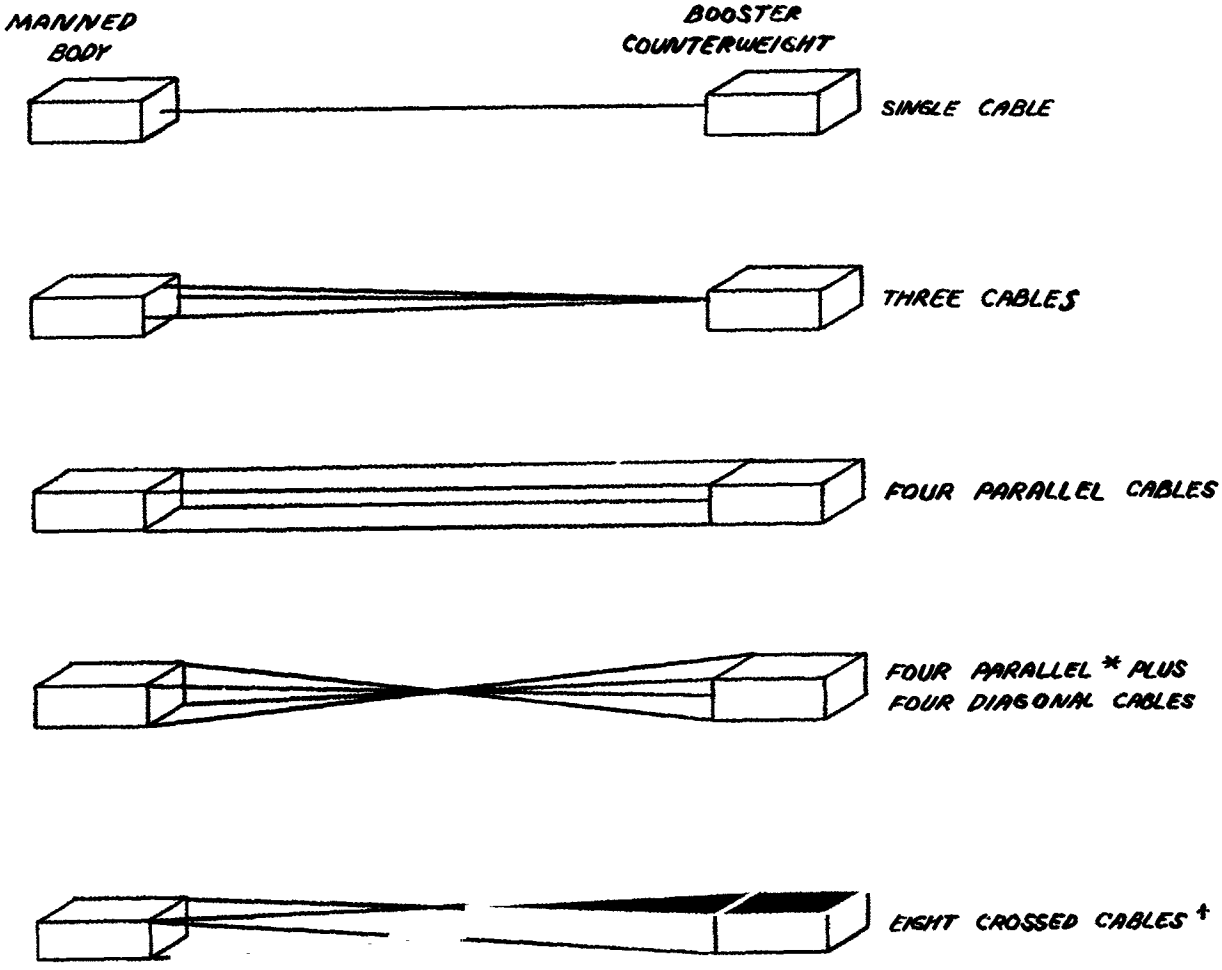

NOTE:

* PARALLEL CABLES (AS IN PRECEDING CONFIGURATION) OMITTED FOR CLARITY

\+ ONLY TWO SETS OF CROSSED CABLES SHOWN. VEHICLE IS SYMMETRICAL ABOUT CENTER PLANES

FIGURE 4 ALTERNATE CABLE CONFIGURATIONS

3. Control Requirements

a. Operational Spinning Mode

The control functions to be provided during the operational spinning mode can be summarized as follows:

- Rate stabilization
- Dynamic balancing
- Spin plane orientation
- Artificial gravity control

Table 2 summarizes the detailed control requirements. Very briefly, the rate stabilization requirement assures damping of the transient motions of the vehicle. However, if only this damping function were supplied, the vehicle would spin around its axis of maximum inertia rather than its geometric axis. The dynamic balancing requirement therefore has been added to force the geometric axis into alignment with the principal axis.* Thus, the undisturbed vehicle will spin steadily about the geometric axis. Spin plane orientation control is supplied to keep the spin vector (geometric axis) pointed in the desired direction, and artificial gravity control is supplied to maintain the desired level of artificial gravity.

The necessity for damping the structural resonances is not clear at this time, since the amplitudes of these oscillations and their associated accelerations are extremely small. It may be that the cables themselves will supply sufficient internal energy dissipation to provide this damping. However, uncertainties associated with the cable construction details, the actual dissipation capabilities of real cables, and the unknowns of the space environment preclude dependence on cable damping at this time. Accordingly, a modest one percent damping requirement has been imposed for structural damping on the control system.

---

*The dynamic balancing function can be performed either by shifting mass or by supplying the requisite compensatory torques. Torque balancing has been considered in this study.

TABLE 2

CONTROL REQUIREMENTS FOR THE OPERATIONAL SPINNING MODE

Function	Nominal Requirement	Range of Alternate Requirements
Rate Stabilization	Damp primary vehicle resonance to 10% of critical. Damp higher structural resonances to 1% of critical.	Damp primary vehicle resonance from 1% to 20% of critical.
Dynamic Balancing	Completely restore balance within three minutes after an internal mass shift.	Roll balancing only. No dynamic balancing.
Spin Plane Orientation	Maintain Solar Pointing to ± ½°.	-
Artificial Gravity Control	Maintain Gravity Level to ±2%.	-

A solar pointing requirement has been selected and conceptually implemented to illustrate the orientation control technique. In practice, other more specialized pointing requirements may be imposed and these would, of course, require additional sensors to define the desired axis of orientation. It should be mentioned that solar panel control could pose significant control problems in such cases. Since fixed panels may be employed in the solar-oriented case considered here, the solar panel control problem was not analyzed in detail and therefore is not discussed in this report.

b. Transition Mode

The control functions to be supplied during the transition mode include the following:

- Rate stabilization
- Cable rate control
- Spin speed control

Detailed control requirements to be associated with these functions were not available when this study was initiated. Accordingly, the transition mode control system was designed with the following general objectives in mind:

- Minimize transition propellant requirements.
- Assure vehicle stability.
- Keep vehicle attitude motions below a few degrees.

In discussing the transition mode control system, an attempt has been made to establish the trade-offs involved in meeting all of these objectives simultaneously, rather than to design to a single specific set of requirements.

Two types of transition maneuvers had to be considered. The first consists of the transition from the nonspinning state, for example, to the operational spinning state. The second consists of cable length changes at full spin speed. While the control systems employed for these two maneuvers are identical, some sizing penalty is involved in supplying the latter capability.

Problems associated with switching from the nonspinning mode to the transition mode, and from the spinning mode to the transition mode, have also been considered. Actuator and control logic switching functions have been provided where applicable.

Finally, an effort has been made to centralize all control equipment in the manned body. Thus, no control data exchange is required between the booster and the manned body. As discussed in section VI, a propellant penalty is imposed by such a procedure. However, there are no control problems associated with moving all or part of the control equipment to the booster, and this may be done if so desired. The operational trade-off existing between propellant economy, data transfer requirements, and equipment availability for maintenance is beyond the scope of this report.

4. Disturbance Levels

Only major disturbance inputs were considered in this study. These included the effects of dynamic imbalance due to crew motions, jet misalignment torques, and gravity gradient torques. Magnetic drag and aerodynamic forces were neglected, since they were not expected to be determining factors.

Estimated disturbance torques were established on the basis of:

- An imbalance equal to three, six-slug men located four feet outboard from the mass center, six feet out along the pitch axis, and six feet out along the yaw axis.

- A reaction jet misalignment of 0.05 radian on all jets.
- Gravity gradient torques averaged over one orbit at a time, and integrated over one year. Perfect solar alignment was assumed, and a low altitude equatorial orbit was considered.

The disturbances due to the imbalance and jet misalignment effects were summed arithmetically and applied as a step torque. Thus, both the magnitude of the disturbance input, and its rate of application, have been more than adequately estimated. The actuator sizing estimates are, therefore, conservative.

The average gravity gradient torque is computed in appendix G. A detailed torque-time history analysis was not attempted. The existing unknowns relative to the vehicle configuration and mission profile would have made such an effort meaningless. A similar remark applies to propellant consumption calculations, and only order of magnitude propellant consumption calculations have been performed.

B. STUDY APPROACH

The study performed to solve the problem outlined above included five major phases:

- Establishment of the characteristics of the uncontrolled vehicle
- Analysis of the operational spinning mode
- Analysis of the transition mode
- Definition of restrictions imposed by the nonspinning mode
- Generation of control system characteristics

A digital computer program comprised the major tool used to establish the uncontrolled vehicle characteristics. A number of analog computer programs were employed in analyzing the operational spinning mode and transition mode control problems. Related studies were drawn upon to define nonspinning mode control requirements. The results obtained from these five study efforts are discussed in the following sections of this report.

Section IV

CHARACTERISTICS OF THE UNCONTROLLED VEHICLE

A. ANALYSIS OF VEHICLE DYNAMICS

1. Discussion

The objectives of the uncontrolled vehicle analysis were threefold: first, to establish the general dynamic characteristics of this somewhat unusual vehicle; second, to determine the effect of configuration changes on these characteristics; and third, to evaluate and compare the several alternate cable configurations. The following paragraphs present the results of a digital computer program designed to meet these objectives. This section deals with the development of an adequate dynamic model, and discusses the restrictions imposed on the analytical results by the assumptions and simplifications used to obtain the model. Section IV.B summarizes the dominant response characteristics of the vehicle for each of the three control axes. Sections IV.C. and IV.D. present discussions of the vehicle transient response for the nominal and perturbed configurations respectively. A detailed analysis of the several alternate cable configurations is included.

2. Dynamic Model

The dynamic model employed in the analysis is shown in figure 5. The nomenclature employed here and throughout the report is summarized in appendix A. All vehicle motions are computed relative to the instantaneous mass center. This leads to a nine degree of freedom model. The angles φ and e_{ij}, as well as the perturbations in spin speed ($\dot{\psi}-\Omega_o$) and separation (x), were considered small quantities. The cables connecting M_1 and M_2 were assumed massless.

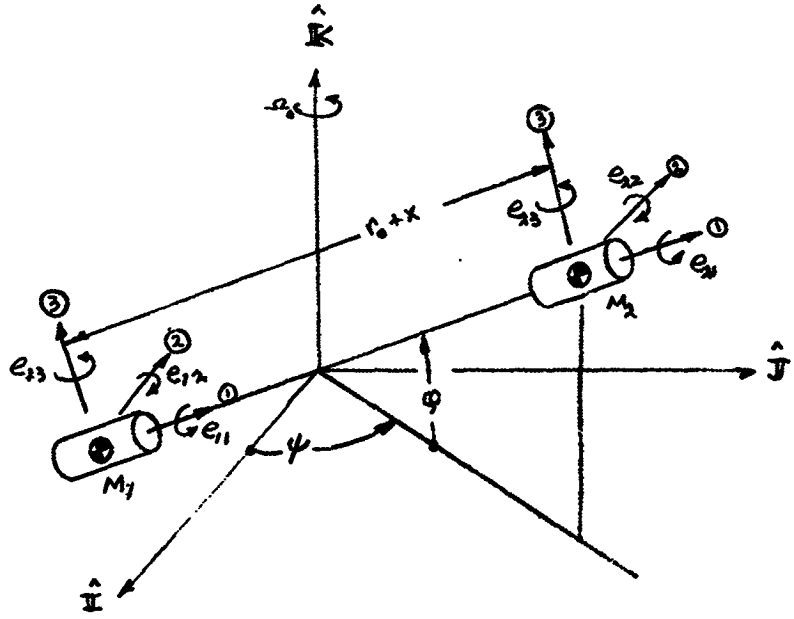

FIGURE 5 NINE-DEGREE-OF-FREEDOM VEHICLE MODEL

While the nine coordinates shown in figure 5 completely define the state of the vehicle at any instant in time, other coordinate angles are often of more interest. For example, the instantaneous spin plane pointing error does not appear explicitly in figure 5. As shown, the angular velocity of the composite station nominally lies along the $\hat{K}$ axis and the vehicle spins in the $(\hat{I},\hat{J})$ plane. Deviations from this nominal position must be computed in terms of φ and the ratio $\dot{\varphi}/\Omega_o$. The calculation is illustrated in figure 6.

Similarly, there are several measures of manned body orientation which may be of interest. The orientation of the manned body (M_1) relative to the line joining the mass centers, relative to the counterweight, relative to the instantaneous spin plane, and relative to inertial space has been expressed in terms of e_{ij} and φ, and tabulated in table 3. The angular velocities which would be sensed by appropriately oriented rate gyros on the manned body are also shown in the table.

TABLE 3

DEFINITION OF ORIENTATION ANGLES

1. Orientation Relative to Line Joining Mass Centers
   - Pitch Angle = e_{12}
   - Yaw Angle = e_{13}
2. Orientation Relative to Booster
   - Roll Angle = $e_{11} - e_{21}$
   - Pitch Angle = $e_{12} - e_{22}$
   - Yaw angle = $e_{13} - e_{23}$
3. Orientation Relative to Spin Plane
   - Roll Angle = $e_{11} - \dot{\varphi}/\Omega_o$
   - Pitch Angle = e_{12}
4. Orientation Relative to Inertially Fixed Axes
   - Roll Angle = e_{11}
   - Pitch Angle = $e_{12} - \varphi$
   - Yaw Angle = $e_{13} + \psi$

NOTE: Table continued on next page.

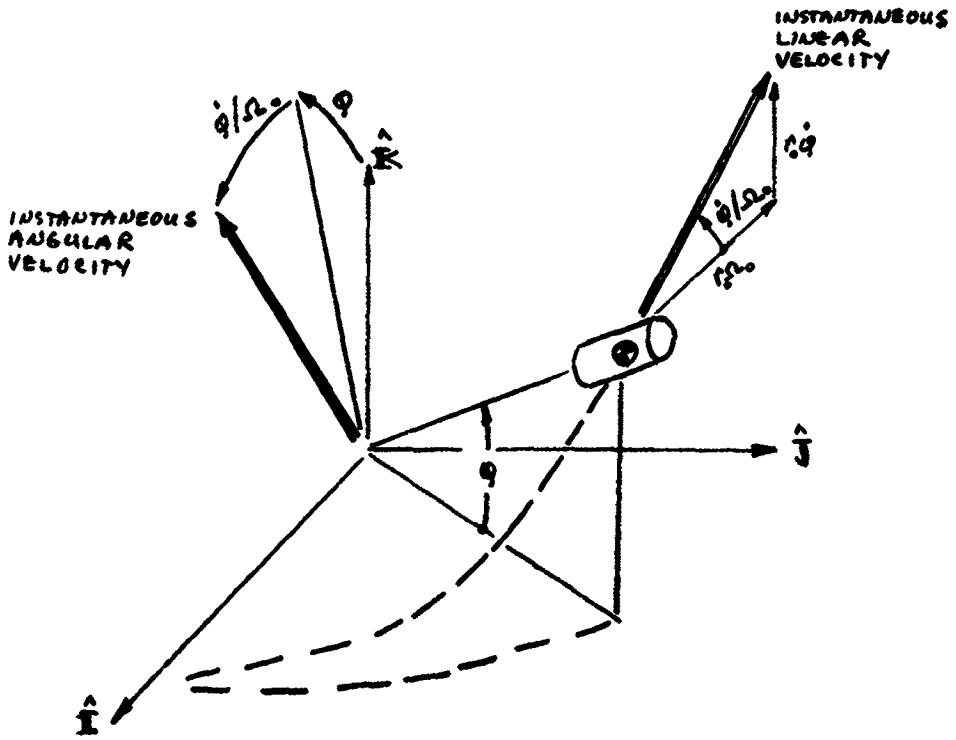

FIGURE 6 SPIN PLANE ORIENTATION MEASUREMENT

TABLE 3

DEFINITION OF ORIENTATION ANGLES (Cont)

5. Rate Gyro Signals

Roll Rate Gyro Signal = $\dot{e}_{11} + \Omega_o (\varphi - e_{12})$

Pitch Rate Gyro Signal = $\dot{e}_{12} - \dot{\varphi} + \Omega_o e_{11}$

Yaw Rate Gyro Signal = $\dot{e}_{13} + \dot{\psi}$

The angles e_{12} and e_{13} are defined as structural response motions of the manned body, since they would be zero in a rigid body. The angles e_{11} and φ are defined as the rigid body response motions. Clearly, the two types of motions interact, and the magnitude of e_{12}, for example, is affected by the magnitude of e_{11} and φ.

A detailed derivation of the equations of motion has been included in appendix B. The Lagrangian form of the equations of motion has been employed, rather than the Newtonian form, because of the advantages it offers relative to the computation of cable influence coefficients.

As indicated earlier, the equations of motion are based on small-perturbation approximations for both rotational and translational motions. Cross-products of inertia effects have been included, but only small imbalances may be considered without violating the small-angle approximations.

As in standard practice, the effects of cable flexibility have been included in the equations of motion by the use of cable influence coefficients, or spring gradients. Appendix C summarizes the calculation of influence coefficients for an arbitrarily located cable.

The influence coefficients are obtained by computing the strain energy stored in the flexible structure (cables) used to connect the manned body to its counterweight. It is interesting to note that the spin rotation displacement ψ and orientation rotation displacement φ cannot affect the strain energy stored in the cables. Thus there are no cable influence coefficients associated with the angles ψ and φ.

Other potential energy storage mechanisms have been neglected. These include, for example, gravity gradient forces.

Small angle approximations are introduced in the potential energy calculation, and a linear elastic structure is assumed. The latter assumption means, of course, that this model cannot be used to study the cable slacking problem. A nonlinear model is developed in section VI specifically for this purpose.

3. Applicability of Simplifications and Assumptions

The significant approximations stated above can be summarized as follows:

- Small response motions take place.
- No gravity gradient effects are present.
- Massless cables are employed.
- No cable slacking occurs.

The small response motion approximation will be justified after the fact by analyzing the response amplitudes obtained from the linearized model.

The importance of gravity gradient forces has been analyzed in other documents*. To summarize, it was found that the gravity gradient forces affected the vehicle dynamics only if the spin speed dropped near orbital frequency. At this point, the tidal separation forces become the same order of magnitude as the centrifugal force in the cable, and must therefore be considered in computing the vehicle's short period response.

While the gravity gradient has little effect on the vehicle's dynamic characteristics at higher spin speeds, the presence of the resulting low level torque cannot be entirely neglected. The major portion of the vehicle's propellant will be consumed in combatting the cumulative effect of this torque, which continually attempts to precess the vehicle's spin vector. Gravity gradient propellant calculations have been included in appendix G.

The document previously cited also considered the effect of cable mass on vehicle dynamics. Cable inertia could result in lateral cable motions. These, in turn, could conceivably have a significant effect on the attitude motions of the manned body because of transverse cable vibrations, or because of traveling wave disturbance propagation effects. It was found, however, that in the cases of interest the cable natural frequency was well separated from the space station attitude resonance. Thus the dynamic interaction of cable and attitude oscillations can be neglected.

- - - - - - -

*J.L. Keller and I.N. Hutchinson, "The Effect of Cable Dynamics and Gravity Gradient Forces on a Flexibly Coupled Space Station." Sperry Engineering Memorandum, July 1963.

It was also found that cable motions would have a negligible effect on attitude dynamics even if the resonances were close together, as long as the cable mass was very small relative to the vehicle mass, and some minimal damping was present in the cable. (The effects of attitude motions on the cable might be significant in this case however.) In any event, cable oscillations, or cable mass effects, can be neglected at the cable lengths of interest. They may assume importance in the 300-500 foot cable length regime.

Cable slacking phenomena impose the most significant limitations on the linearized vehicle They definitely restrict the applicability of this model to the operational spinning mode, where the spin speed is fairly high and cable extension fairly large. A numerical analysis of the cable slacking problem is presented in section IV.D.3.

4. Digital Computer Program Description

The equations of motion for the linearized nine degree of freedom model were programmed for a digital computer. The computer program was divided into two subroutines. In the first subroutine, the generalized cable influence coefficient equations developed in appendix C were applied to each cable of the configuration in question. Composite influence coefficients were then obtained by summing those for the individual cables.

In the second subroutine the equations of motion developed in appendix B were solved to find the vehicle frequency response. Both the magnitude and the phase angle of the vehicle response to a unit forcing function were computed at a specified frequency. Eighty-one transfer functions, corresponding to the nine response motions to each of the nine possible forcing functions, were obtained. The calculation was repeated for a number of forcing frequencies.

The frequency response data were plotted and used to compile information concerning static sensitivities and resonant frequencies. The peak response to transient disturbances was then estimated by constructing simplified analytical models from the frequency response plots, and solving for the response motions of these simpler models. These transient response estimates were substantiated by analog computer simulations of selected configurations.

Before proceeding to a detailed discussion of the attitude response characteristics of the vehicle, it should be mentioned that in

all cases considered herein, the resonance associated with translational motions of the two end masses was much higher than the other significant vehicle resonances. Accordingly, relative translational motions will be small during the operational spinning mode, and may be safely neglected for the remainder of the discussion.

B. GENERAL DYNAMIC CHARACTERISTICS

1. Primary Dynamic Effects

Motions of the flexibly coupled spinning space station are affected by both the rigid body properties of the vehicle and the flexibility of the structure used to connect the manned body to the counterweight. A brief description of these phenomena will prove helpful in subsequent discussions.

Two rigid body effects are important: wobble of the spin vector, and precession of the spin plane. In this discussion, wobble will include all periodic spin vector motions while precession will be limited to secular motions of the spin vector. Both of these effects are associated with the gyroscopic properties of the station.

For a rigid vehicle, the frequency of the wobbling motions is determined by the composite inertia distribution of the station, and is given by

$$\omega_o = \sqrt{\frac{(I_3 - I_1)(I_3 - I_2)}{I_1 I_2}}\,\Omega_o \qquad (1)$$

where I_3 is the spin, or yaw inertia, I_1 is the roll inertia, I_2 is the pitch inertia, and Ω_0 is the nominal spin speed. For the cases considered here, the flexibility of the connecting structure has some effect on this resonance, but equation (1) still gives a reasonable estimate of its value. This wobble resonance is the lowest of the several vehicle resonances, and therefore plays a dominant role in determining the gross dynamic characteristics of the vehicle.

Spin plane precession is worthy of special discussion because of the somewhat unusual form it takes in the coordinates defined in figures 5 and 6. The spin plane precession effect causes the angle φ to exhibit an undamped resonance at a forcing frequency equal to the spin speed. This resonance can be interpreted as follows: First, note from figure 6 that if

a constant spin plane pointing error exists, the angle φ oscillates as the manned body rises and falls relative to the $(\hat{\mathbf{i}},\hat{\mathbf{j}})$ reference plane. Thus, if the pointing error were steadily increased, φ would appear to undergo a divergent oscillation. A space-fixed torque would be required to maintain such a steady precession, and this torque would also appear to oscillate at spin speed relative to the rotating body axes. That is, a divergent oscillation of the angle φ is caused by application of a body referenced torque which oscillates at spin speed. This divergence represents steady precession of the spin plane under the influence of a space-fixed torque.

The resonant phenomena associated with vehicle flexibility are much more straightforward. They result from relative motions of the two end masses on the spring provided by the connecting cables. Oscillations in roll, pitch, yaw, and linear separation are all possible. These resonances will be damped by energy dissipated internally in the structure itself, although the exact value of such damping is hard to predict.

2. Yaw Response Characteristics

The nine degree of freedom equations indicate that within the linear approximation, the yaw axis of the spinning space station decouples from the pitch and roll axes. Thus the yaw response can be analyzed independently of the pitch and roll responses. The yaw frequency response of the nominal vehicle is shown in figure 7. Figure 3 and table 8 define the nominal vehicle configuration parameters.

Two resonances appear in figure 7, both of which are due to structural flexibility. The higher of the two is above the frequency range of interest, and is suppressed by the counterweight anti-resonance. This leads to the conclusion that in the operational spinning mode, the higher yaw resonance can be neglected.

The data of table 4 substantiate this conclusion. The yaw response to a unit impulse has been tabulated. It is apparent that the high frequency response can be neglected against the low frequency response.

TABLE 4

YAW RESPONSE TO UNIT IMPULSE FOR NOMINAL CONFIGURATION
(RESULTS IN 1 RAD/SEC INITIAL CONDITION ON $\dot{e}_{13}$)

$e_{13} = 0.48 \sin 2t + 0.015 \sin 3.6t$
$(e_{13}-e_{23}) = 0.66 \sin 2t - 0.08 \sin 3.6t$

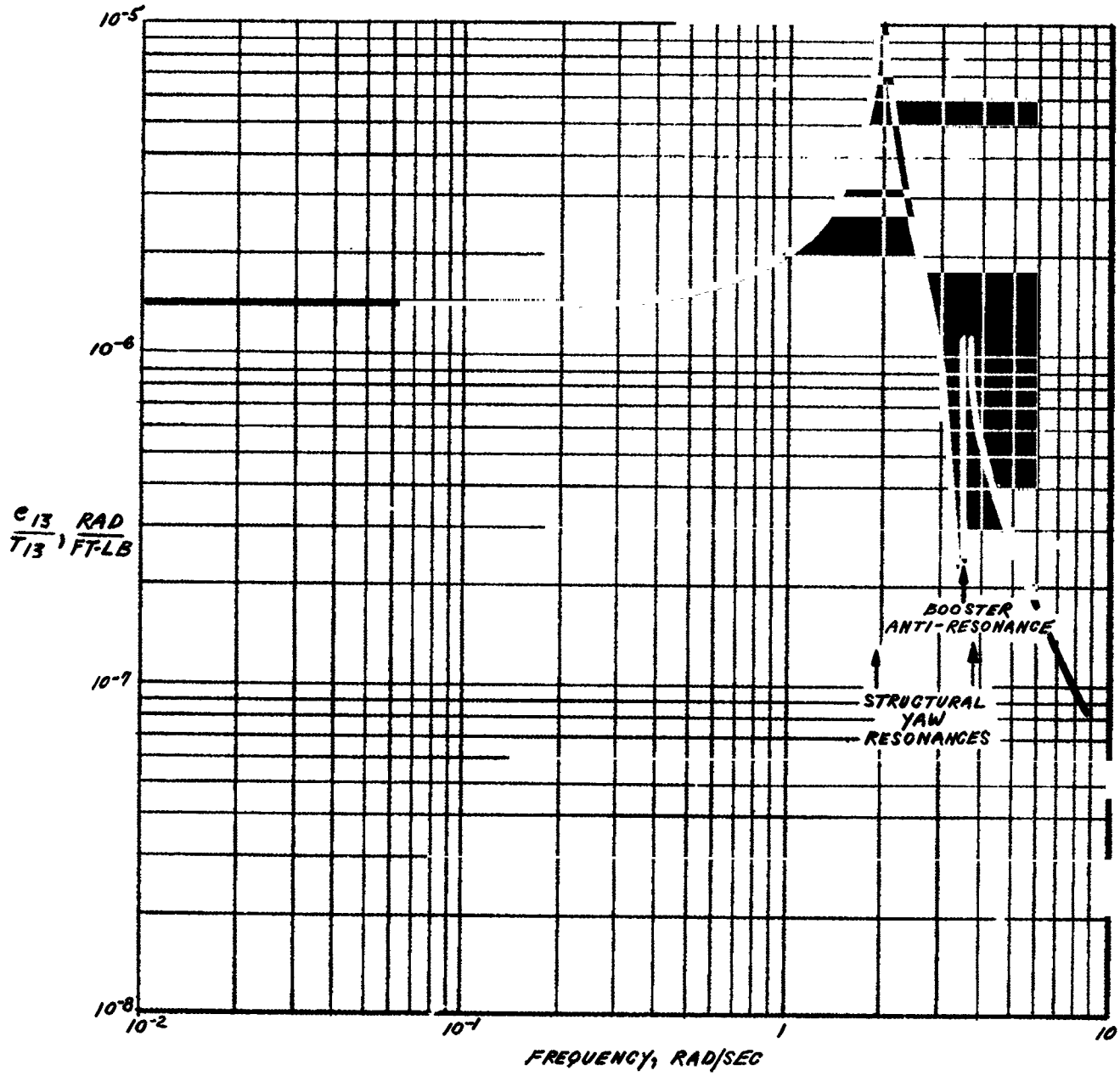

FIGURE 7 YAW–FREQUENCY RESPONSE OF NOMINAL VEHICLE

The table also indicates that the yaw angle e_{13} and the relative yaw angle $(e_{13}-e_{23})$ are the same order of magnitude. This was generally found to be the case.

In summary, the following conclusions may be stated:

- The yaw axis decouples from the pitch and roll axes.
- The higher of the two yaw resonances may be neglected in approximate calculations.
- Relative yaw motions of the manned body and the counterweight will be the same order of magnitude as the manned body motions.

3. Pitch Response Characteristics (Structural)

The structural pitch response of the nominal vehicle, e_{12}, is shown in figure 8. It is quite similar to the yaw response, except for the resonant/anti-resonant pair at the roll resonance. Neglecting this region for the moment, it is clear from figure 8, and consideration of the vehicle geometry, that the structural pitch and yaw characteristics will be qualitatively the same. Thus the conclusions drawn from analysis of the yaw axis also apply to the pitch axis. That is, the pitch fundamental will dominate the structural response, and relative pitching motions will be the same order of magnitude as the manned body motions.

Figure 8 indicates that a resonance exists at the roll resonance which is nearly cancelled by an anti-resonance. It should be mentioned that similar pairs must exist at the other roll resonance, and at spin speed, since the pitch and roll axes are gyroscopically cross-coupled. They do not appear in figure 8 because the cancellation is so nearly complete that the digital computer calculations, performed at a number of discrete, finely spaced frequencies, did not include a point near enough to the resonance to sense its presence. If plotted, they would appear as vertical lines exactly at the resonant frequencies.

The importance of such factors is best illustrated by an example. Neglecting the counterweight anti-resonance and the pitch structural harmonic, the response of the system illustrated by figure 8 to a torque impulse is:

$$e_{12} = K_0 \omega_{p_1} \left(\frac{\omega_{r_2}}{z}\right)^2 \left[\left(\frac{\omega_{p_1}^2 - z^2}{\omega_{p_1}^2 - \omega_{p_2}^2} \right) \sin \omega_{p_1} t + \left(\frac{\omega_{p_1}}{\omega_{r_2}} \right) \left(\frac{z^2 - \omega_{r_2}^2}{\omega_{p_1}^2 - \omega_{r_2}^2} \right) \sin \omega_{r_2} t \right] \qquad (2)$$

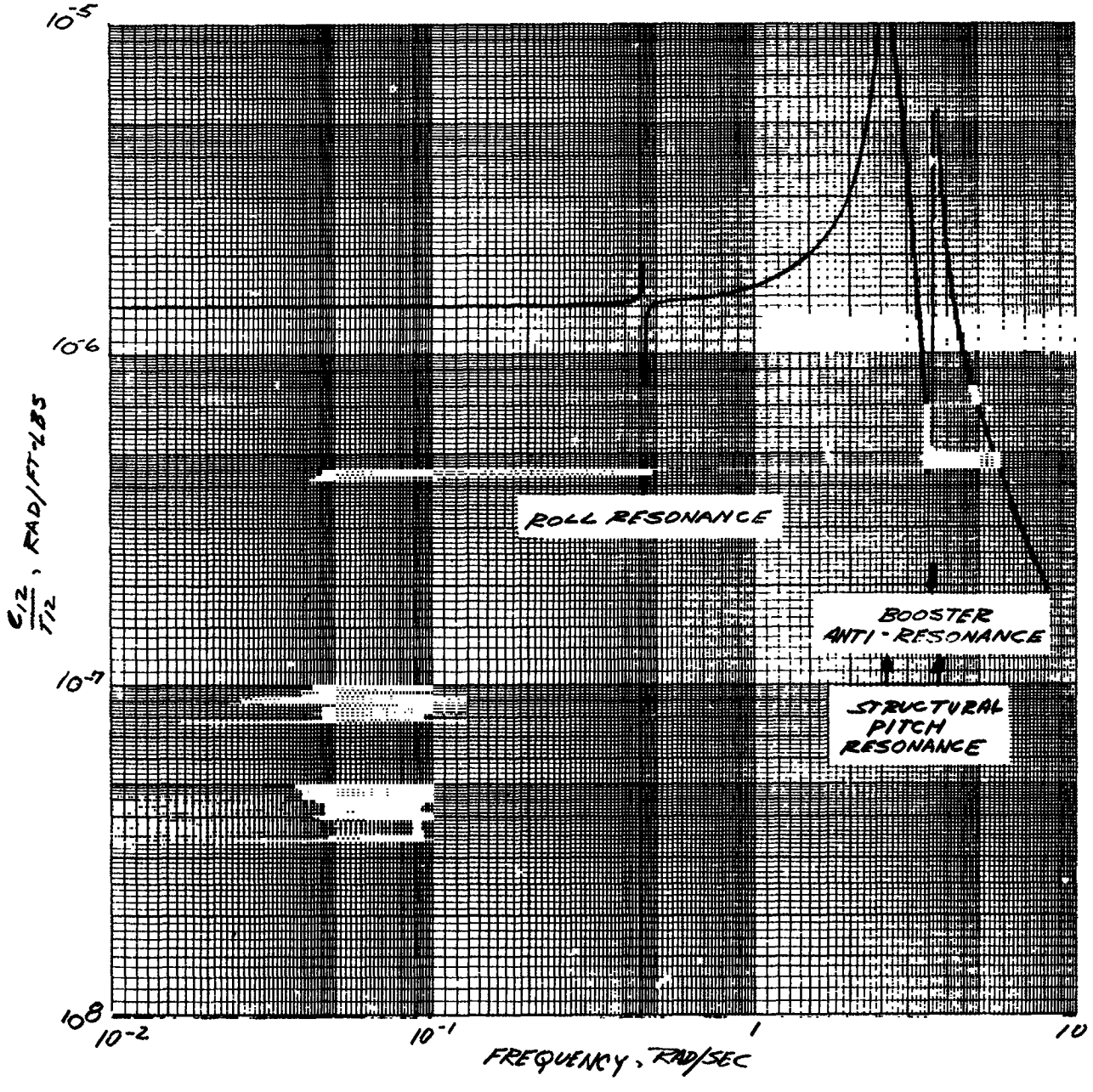

FIGURE 8 STRUCTURAL PITCH FREQUENCY RESPONSE OF NOMINAL VEHICLE

where

K_o = static gain = $1.4(10^{-6})$ rad/ft-lb

p_1 = pitch resonance = 2.7 rad/sec

r_2 = roll resonant frequency = 0.46 rad/sec

Z = anti-resonant frequency = $\Omega_o + \Delta\omega$

$T\Delta t$ = magnitude of impulse = 1 ft lb sec

For the case at hand, ω_{r_2} and Z are well below ω_{p_1}, and the expression reduces to

$$e_{12} \approx 3.6(10^{-6})[\sin 2.7t + .74\Delta\omega \sin .46t] \qquad (3)$$

From figure 8, a conservative estimate of the magnitude of $\Delta\omega$ is 0.01 rad/sec. In this case, the resonant/anti-resonant pair results in an oscillation whose magnitude is less than 0.8 percent of the structural oscillation itself. The resonance/anti-resonance pairs at the other natural frequencies are, as mentioned earlier, even closer together and thus would have an even smaller effect. It would appear, then, that all cross-coupling can be neglected in computing the structural pitch response to a pitch torque input.

The inertial pitch response, $(e_{12}-\varphi)$, is also of interest, and is shown in figure 9. The high frequency part of the plot is essentially the same as that of figure 8. This implies that spin plane motions, as measured by the angle, φ, will be small in this region. A more interesting phenomenon appears in the low frequency region. Here, the spin plane precession resonance appears, as would be expected, but there is also an anti-resonance at the roll natural frequency. As a result, the spin plane response (oscillation at spin speed of 0.4 rad/sec) is again found to be small relative to the structural response (oscillation at pitch resonance of 2.7 rad/sec). Table 5 illustrates the situation.

TABLE 5

APPROXIMATE PITCH RESPONSE TO A UNIT IMPULSE
(RESULTS IN $\dot{e}_{12}$ = 1 RAD/SEC AT T = 0)

$e_{12} = 0.37 \sin 2.7t$
$e_{12} - = 0.37 \sin 2.7t - 0.035$ in. $4t$

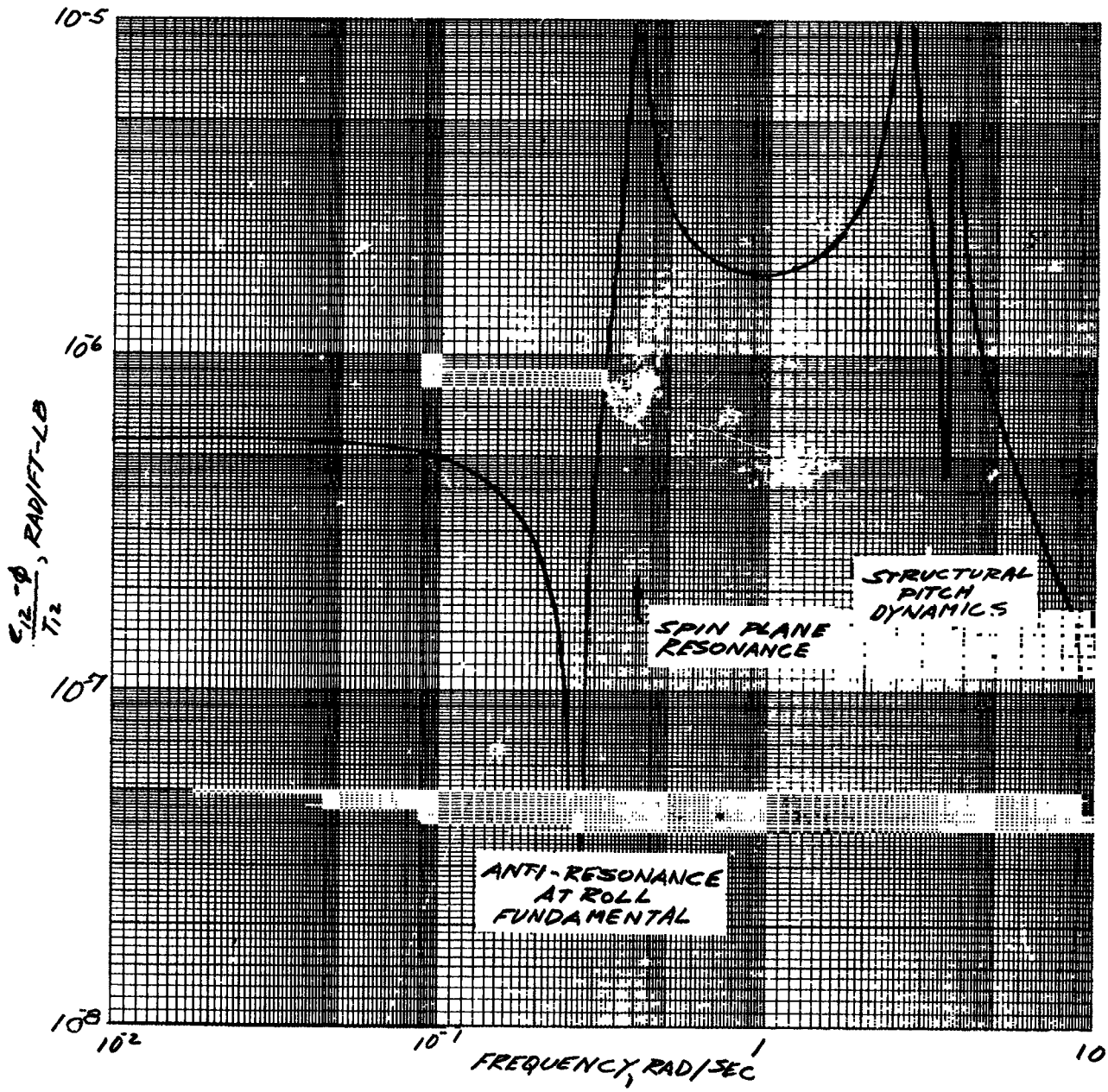

FIGURE 9 INERTIAL PITCH FREQUENCY RESPONSE OF NOMINAL VEHICLE

It would therefore appear that in evaluating the vehicle's pitch response, the following simplifications are in order:

- Spin plane motions can be neglected in approximate calculations.
- The higher of the two structural resonances may be neglected in approximate calculations.
- Relative pitching motions of the manned body and the counterweight will be the same order of magnitude as the manned body motions.

4. Roll Response Characteristics

The roll axis frequency response of the nominal vehicle is shown in figure 10. Perhaps its most striking characteristic is the high static sensitivity. It appears that the vehicle is much softer in roll than either pitch or yaw by a large margin. Thus, the key control problem during operational spinning operation is to keep the rolling motions of the vehicle within reasonable bounds. Having accomplished this objective, control of the remaining axes is straightforward.

In addition to the much larger static sensitivity, the roll axis differs from the pitch and yaw axes in that a significant amount of cross-coupling exists between structural dynamics and rigid body dynamics. This characteristic is peculiar to the vehicle considered herein, and does not appear to be an inherent characteristic of the broad class of cable coupled space stations. Other configurations analyzed in related studies exhibited little or no rigid body/structural cross-coupling on the roll axis.

Figure 10 shows two roll resonances. One appears at a frequency of 0.27 rad/sec, and the other appears at a frequency of 0.46 rad/sec. These represent the shifted values of the uncoupled roll structural resonance (0.396 rad/sec) which is computed as if the vehicle were not spinning, and the uncoupled wobble resonance (.32 rad/sec) which is computed as if the vehicle were rigid. The interaction between the structural dynamics and the rigid body dynamics is large enough in the nominal case to cause this shift.

Figures 11 and 12 provide some understanding of this behavior. In figure 11, the two roll resonances ($\omega_{r_1}, \omega_{r_2}$) have been plotted as a function of the uncoupled roll structural resonance ω_{r_o}. All frequencies have been normalized by dividing by the rigid body wobble resonance ω_o given in equation (1). If the uncoupled structural resonance is very low

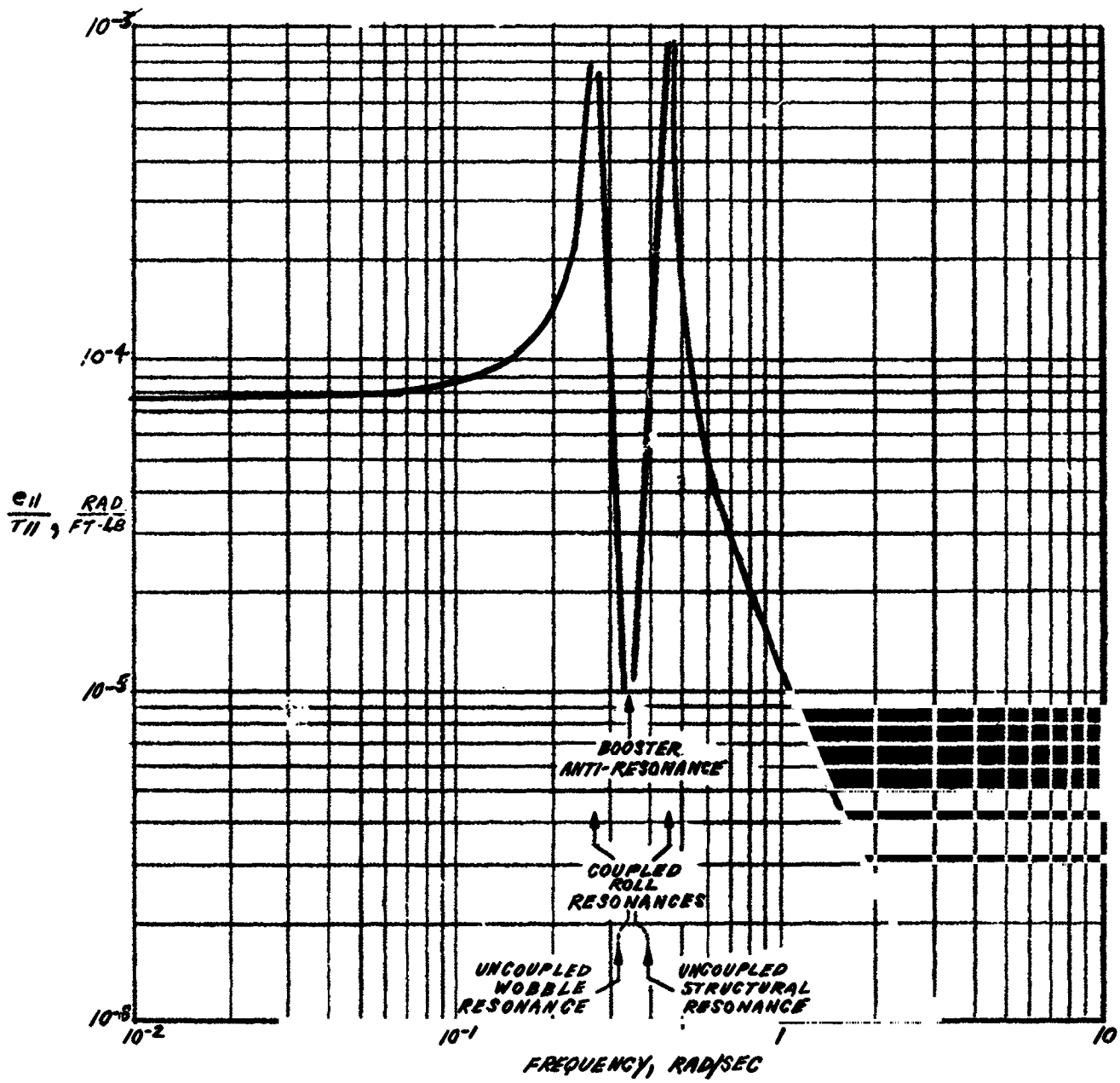

FIGURE 10 ROLL-FREQUENCY RESPONSE OF NOMINAL VEHICLE

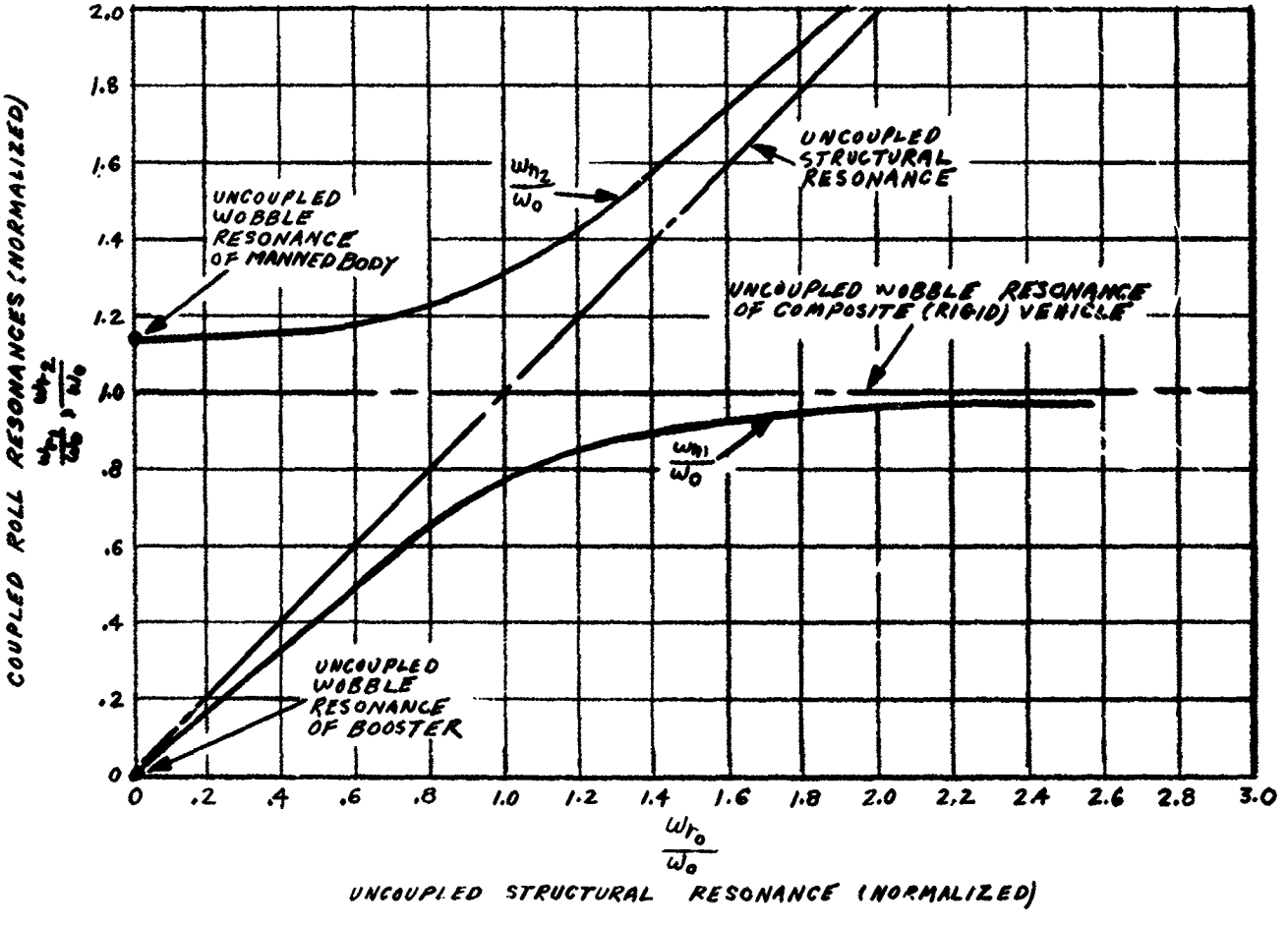

FIGURE 11 EFFECT OF STRUCTURAL RESONANCE ON ROLL AXIS DYNAMICS

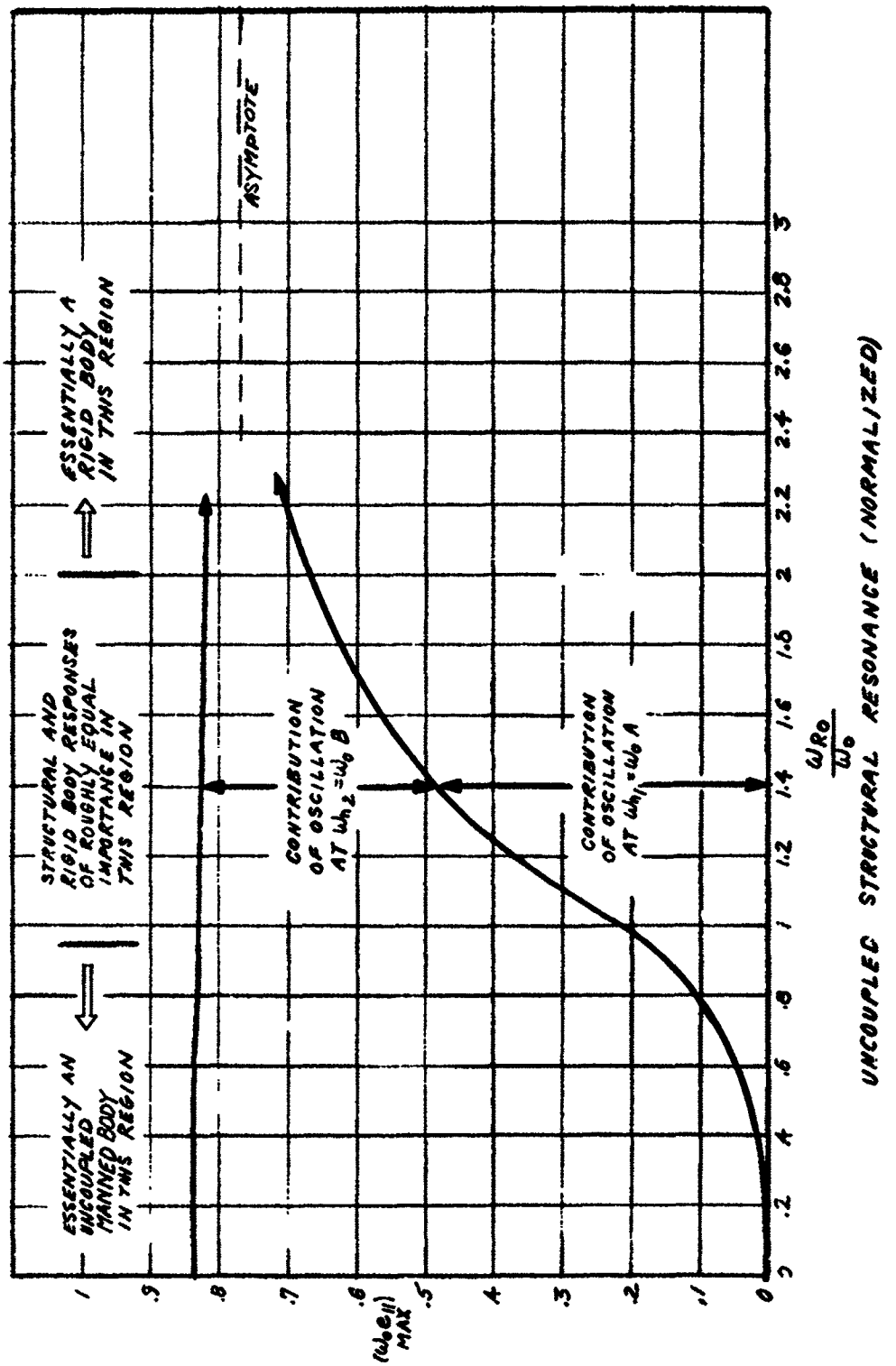

FIGURE 12 PEAK ROLL RESPONSE TO UNIT ROLL IMPULSE

(weak roll spring), the two roll resonances appear at the wobble frequencies of the individual bodies. (The wobble frequency of the booster is zero, since this vehicle is symmetric.) If the uncoupled structural resonance is very high (stiff roll spring), the two roll resonances shift to the rigid body wobble frequency and the uncoupled structural resonant frequency. In this case the structural and rigid body dynamics no longer interact. Rigid body phenomena will then dominate the response, since the wobble frequency is the lower of the two resonances. If the uncoupled structural resonance lies between these limiting values, the coupled resonances are as shown in the figure.

It appears from figure 11 that the uncoupling is fairly complete at frequency ratios such that the uncoupled structural resonance is about 2-3 times the rigid body wobble resonance. Figure 12 substantiates this conclusion. The peak response of the manned body to a unit impulse ($\dot{e}_{11}$ = 1 rad/sec) has been shown. Neglecting the spin plane motion, which will be small, the oscillation will be of the form

$$e_{11} = A \sin \omega_{r_1} t + B \sin \omega_{r_2} t \qquad (4)$$

where ω_{r_1} and ω_{r_2} are the resonant frequencies shown in figure 11. The peak response is thus

$$(e_{11})_{MAX} = A + B \qquad (5)$$

The values of $e_{11}\omega_o$, $A\omega_o$, and $B\omega_o$ are shown in figure 12 as a function of the uncoupled structural resonance. Again, it has been found expedient to introduce the rigid body wobble frequency, ω_o, as a normalizing factor.

Three important conclusions may be drawn from figure 12:

- The peak transient response is relatively insensitive to changes in the uncoupled structural resonance (roll spring stiffness). This is due to the fact that the roll inertia of the booster comprises only 25 percent of the total roll inertia.
- At low values of the roll structural resonance, say for $\omega_{r_o} < 0.8\,\omega_o$, the manned body responds essentially independently of the counterweight. That is, the transient oscillation is largely at the wobble resonance of the manned body alone, and the oscillation at the structural resonance is small.

- At high values of the roll structural resonance, say for $\omega_{r_o} > 2.5\omega_o$, the manned body responds as if the vehicle were rigid. That is, the transient oscillation is largely at the rigid body wobble resonance, and the oscillation at the structural resonance is small.

In the intermediate range, of course, the structural oscillation comprises a significant part of the total respons. of the manned body. It should be emphasized, however, that the peak total response is nearly independent of the uncoupled structural resonance.

One further comment appears in order: figures 11 and 12 apply to a vehicle having the roll inertia distribution of the nominal vehicle. If the inertia ratio I_{21}/I_{11} is decreased, for example, the wobble resonance of the composite station approaches that of the manned body. In this case, the curves of figure 11 would approach their asymptotes more closely, and the central range where structural effects assume significance would then become smaller. The converse is also true.

In the configurations of interest here, the ratio of the uncoupled roll structural resonance to the rigid body wobble resonance was such as to result in operation in the central portion of figure 11. The relatively broad range of frequency ratios for all configurations led to a practical difficulty: it was desirable to have a simple approximate model for use in preliminary actuator sizing calculations, but no single simple model was accurate for all configurations. For some, a rigid vehicle model would have provided sufficient accuracy. For others, structural effects would have to be included and this tended to complicate the calculations. Because of these difficulties, the analog computer was used to make the final control system parameter selection.

The conclusions to be drawn from the roll axis analysis are as follows:

- The roll axis is, by far, the softest of the three axes.
- The roll structural dynamics do, in some instances, have a significant effect on the vehicle response. Such situations can arise in cases of practical interest.

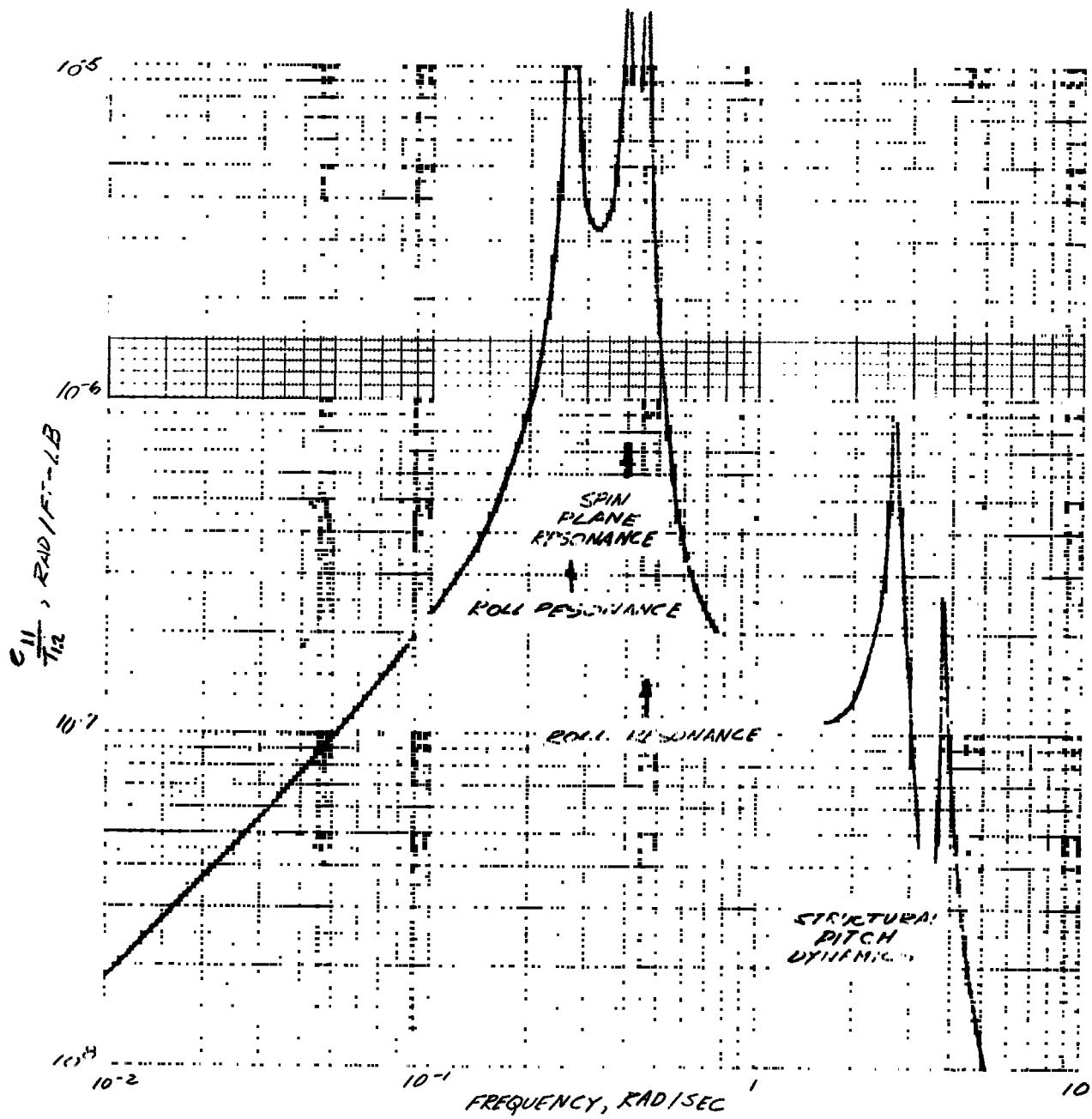

FIGURE 13 ROLL-FREQUENCY RESPONSE TO PITCH TORQUE FOR NOMINAL VEHICLE

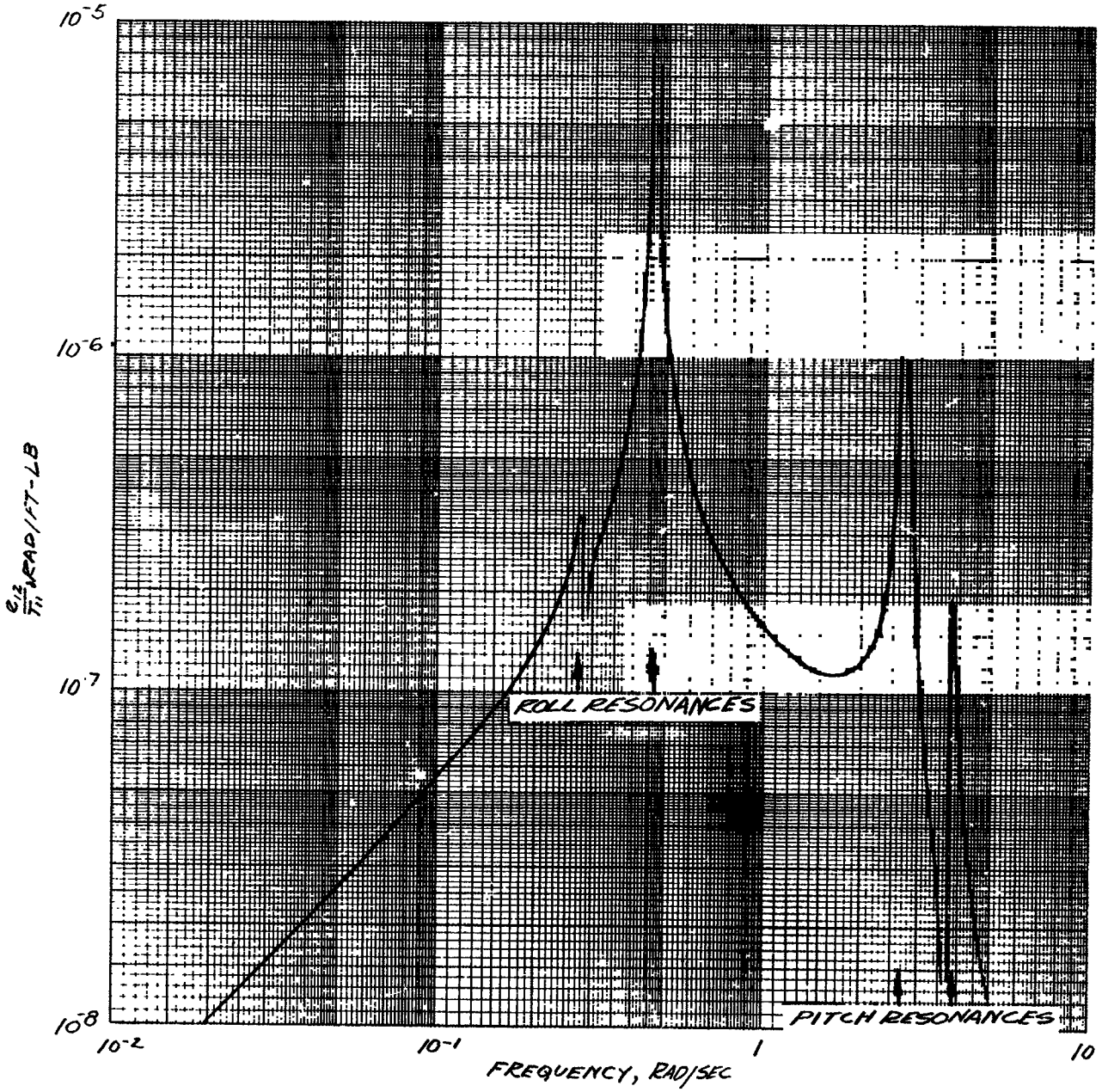

FIGURE 14 PITCH-FREQUENCY RESPONSE TO ROLL TORQUE FOR NOMINAL VEHICLE

5. Pitch/Roll Cross-Coupling Characteristics

The cross-coupling between the pitch and roll axes due to gyroscopic effects, is illustrated by figures 13 and 14. As noted on the figures, the dynamic characteristics of both axes affect the cross-coupled responses. At very low frequencies ($\omega < 0.1$ rad/sec), both responses exhibit the forms normal for gyroscopically cross-coupled systems. At higher frequencies, the pitch and roll resonances dominate the response. Table 6 shows the effects of cross-coupling on the vehicle motion.

TABLE 6

APPROXIMATE RESPONSE TO UNIT PITCH AND ROLL IMPULSES
(RESULTS IN 1 RAD/SEC INITIAL VELOCITIES IN PITCH AND ROLL RESPECTIVELY)

Response to pitch impulse
$e_{12} = 0.37 \sin 2.7t$
$e_{11} = 0.013 \left[\cos 0.27t - \cos 2.7t\right]$
Response to roll impulse
$e_{12} = 0.012 \left[\cos 0.46t - \cos 2.7t\right]$
$e_{11} = 1.3 \sin 0.27t + 1.4 \sin 0.46t$

Table 6 shows only approximate response motions. In general, there is an oscillation at each resonant frequency (two pitch, two roll, and one spin plane resonances) in both the pitch and roll motions. The smaller of these (10 percent of those in table 6) have been neglected. It should also be mentioned that the actual torque levels associated with the unit pitch and roll impulses are quite different. Roughly 10^6 ft-lb-sec is required to establish the initial condition $\dot{e}_{12} = 1$ rad/sec, while about 10^5 ft-lb-sec makes $\dot{e}_{11} = 1$ rad/sec. In any event, table 6 leads to the conclusion that the cross-coupled response is small relative to the motion of the excited axis.

C. RESPONSE OF NOMINAL VEHICLE

1. Summary of Dynamic Characteristics

The preceding discussion led to several conclusions. The most important of these are as follows:

- The roll axis is the softest of the three axes.
- The greatest coupling between rigid body phenomena and structural phenomena occurs on the roll axis. It can be important.
- The cross-coupling between the pitch, yaw, and roll axes is small.

It should be mentioned, however, that the rate gyro signals will be cross-coupled quite significantly. As indicated in table 3, the rate gyros do not measure $\dot{e}_{11}$ or $\dot{e}_{12}$, since they also sense components of spin speed as the vehicle rotates out of the spin plane. For example, table 3 shows that even if there was no pitching motion ($e_{12} = \varphi = 0$), the pitch rate gyro output would be $e_{11}\Omega_o$, which would still be the same order of magnitude as the roll rate gyro output $\dot{e}_{11}$.

2. Response to Typical Disturbance Inputs

The magnitude of the uncontrolled vehicle's response to typical disturbance torques is of some interest. Table 7 shows the vehicle response to equivalent static disturbance torques which represent a three man imbalance at the extremity of the vehicle. The relation between this physical cross-product of inertia disturbance and the equivalent static torque is established in appendix B, equation (B-27). The three torque components have been applied one at a time to allow easier interpretation of the results. In practice, all components would be applied simultaneously. Table 7 also assumes instantaneous application of the torques. In practice, the total imbalance would build up slowly so that somewhat smaller transient motions than indicated in the table can be expected.

The results shown in table 7 are as would be expected from the preceding discussion. The roll axis is certainly the most critical of the three axes, even though it experiences the smallest disturbance torque. In general, the correlation between peak response motions predicted by rigid body theory and those predicted by the more exact flexible body theory is good, but the dominant frequencies differ. The structural pitch and yaw motions are, of course, not predicted by the rigid body theory.

It should also be mentioned that the magnitude of these response motions appear to be compatible with the linearizing approximations introduced earlier. Other configurations exhibited larger response motions, but in general, the various angular deflections were always less than 10 degrees or 15 degrees.

TABLE 7

RESPONSE TO TYPICAL DISTURBANCE INPUTS

Disturbance Torque	Response of Nominal Vehicle							
	Yaw		Pitch		Roll		Spin Plane	
	Peak Motion (deg)	Dominant Freq. (rad/sec)	Peak Motion (deg)	Dominant Freq. (rad/sec)	Peak Motion (deg)	Dominant Freq. (rad/sec)	Peak Motion (deg)	Dominant Freq. (rad/sec)
Yaw Torque T_{13} = 813 ft. lbs.	0.13	2.0	--	--	--	--	--	--
Pitch Torque T_{12} = 813 ft. lbs.	--	--	0.13	2.6	0.025	0.27, 2.7	0.078	0.40
Roll Torque T_{11} = 10^4 ft. lbs.	--	--	0.0017	0.46, 2.7	0.92	0.27, 0.46	0.0013	0.27, 0.40

	Rigid Body Response			
Disturbance Torque	Roll		Spin Plane	
	Peak Motion (deg)	Dominant Freq. (rad/sec)	Peak Motion (deg)	Dominant Freq. (rad/sec)
Yaw Torque T_{13} = 813 ft. lbs.	--	--	--	--
Pitch Torque T_{12} = 813 ft. lbs.	0.097	0.31, 0.40	0.078	0.40
Roll Torque T_{11} = 10^4 ft. lbs.	0.92	0.31	0.0013	0.31, 0.40

D. PARAMETRIC ANALYSIS

1. Changes in Cable Configuration

The preceding paragraphs have established the general characteristics of the nominal vehicle. The next step is to investigate the effects of changes in vehicle parameters. Accordingly, a parametric analysis of these variables is presented in the following paragraphs.

The alternate cable configurations shown in figure 4 will be compared on an equal weight basis. Individual cables in the eight cable configuration, for example, will have one-eighth the cross-sectional area of the cable used in the single cable configuration. Table 8 lists the cable parameters employed in the analysis.

TABLE 8

CABLE PARAMETERS FOR OPERATION AT 0.4 R/SEC AND 100 FT.

Elasticity	2.1 (10^9) lbs/ft^2
Total Area	1.05 (10^{-3}) sq. ft.
Breaking Load	..6000 lbs.

The cable breaking load is twice the actual load carried by the cables when operating at 0.4 r/sec and 100 ft. The cable data were obtained from ANC-5, "Strength of Metal Aircraft Elements."

Changes in the cable configuration have their largest effect on the yaw and pitch axes of the vehicle. The peak yaw response to a unit impulse has been tabulated in table 9 for the several cable configurations in question.

TABLE 9

PEAK YAW RESPONSE TO UNIT IMPULSE FOR Ω_o = 0.4 RAD/SEC AND ℓ_u = 100 ft.
(RESULTS IN $\dot{e}_{13}$ = 1 RAD/SEC AT T = 0)

Cable Configuration	(e_{13}) max, rad.	(e_{13}-e_{23}) max, rad.
Single Cable	1.1	1.2
Three Cables	0.50	0.83
Four Parallel Cables	0.69	0.39

TABLE 9 (Cont)

PEAK YAW RESPONSE TO UNIT IMPULSE FOR Ω_o = 0.4 RAD/SEC AND ℓ_u = 100 ft. (RESULTS IN $\dot{e}_{13}$ = 1 RAD/SEC AT T = 0)

Cable Configuration	(e_{13}) max, rad.	$(e_{13}-e_{23})$ max, rad.
Four Parallel plus Four Diagonal Cables	0.52	0.77
Eight Crossed Cables	0.49	0.74

It is clear that the single cable configuration is considerably softer in yaw than the other, and that the four cable configuration is slightly softer than the three or eight cable configuration. It should be mentioned, however, that all configurations are stiff enough to be controllable. Further, all have resonant frequencies which are well separated from the critical roll axis resonant frequencies. Table 10 lists the yaw resonant frequencies of each configuration.

TABLE 10

YAW RESONANT FREQUENCIES FOR Ω = 0.4 RAD/SEC AND ℓ_u = 100 ft.

Cable Configuration	ω_{y_1} rad/sec	ω_{y_2} rad/sec
Single Cable	0.92	1.8
Three Cables	1.5	2.3
Four Parallel Cables	1.3	3.3
Four Parallel plus Four Diagonal Cables	2.0	3.6
Eight Crossed Cables	2.0	3.6

In view of the similarity between the pitch and yaw axes of the vehicle, the same conclusions developed above also apply to the pitch response.

Interestingly enough, the roll response of the vehicle is relatively insensitive to changes in the cable configuration. This is only true, however, for cases of the type considered here. The manned body is nonsymmetric and, therefore, exhibits gyroscopic stability, while the booster is symmetric and has no inherent stability.

The peak roll response to a unit impulse is shown in table 11. As would be expected from the discussion centered around figures 11 and 12, the differences in manned body response are small. There is considerable difference, of course, in the booster response motions.

TABLE 11

PEAK ROLL RESPONSE TO UNIT IMPULSE FOR Ω_o = 0.4 RAD/SEC AND ℓ_u = 100 ft.

Cable Configuration	(e_{11}) max, rad	$(e_{11}-e_{21})$ max, rad
Single Cable	3.2	3.2
Three Cables	3.2	3.2
Four Parallel Cables	2.6	5.5
Four Parallel plus Four Diagonal Cables	3.3	7.4
Eight Crossed Cables	2.6	5.3

Table 12 shows the resonant frequencies associated with the roll axis. The uncoupled structural resonance ω_{r_o} (computed neglecting gyroscopic stabilization effects), the ratio of this frequency to the rigid body wobble resonance ω_o, and the values of the coupled roll resonances are tabulated.

TABLE 12

ROLL RESONANT FREQUENCIES

Cable Configuration	ω_{r_o} (rad/sec)	ω_{r_o}/Ω_o	r_1 (rad/sec)	r_2 (rad/sec)	Comments
Single Cable	0	0	0	0.314	Booster uncoupled in roll
Three Cables	0	0	0	0.314	Booster uncoupled in roll
Four Cables	0.385	1.2	0.265	0.452	
Four Parallel plus Four Diagonal Cables	0.042	0.14	0.042	0.314	Booster uncoupled in roll
Eight Crossed Cables	0.396	1.3	0.268	0.459	

Summarizing, the data of tables 9 through 12 lead to the following conclusions:

- The single cable and four cable configurations are not as stiff in yaw or pitch as the others.
- The eight cable configuration which consists of four parallel plus four diagonal cables gives negligible torsional rigidity. It offers no significant advantages relative to the three cable configuration, for example.
- The (nominal) eight crossed cable configuration offers a slight advantage relative to the three cable configuration in that the peak response to a roll impulse is slightly lower. The peak response to an imbalance disturbance would be the same for both configurations, however.

Accordingly, it would appear that the eight crossed cable configuration was somewhat better than the others. However, the differences are not large, and all configurations are controllable. Thus the cable configuration selection can largely be based on extension/retraction mechanism implementation problems, and on reliability and fail-safe considerations. Such factors are beyond the scope of this report.

2. Changes in Inertia Distribution

The inertia difference (I_3-I_2) plays an important role in determining the response of the vehicle to, say, an imbalance disturbance. The effect of changes in inertia distribution can be estimated from rigid body theory, which states that

$$(e_{11})_{max} \approx \frac{2T}{(I_3 - I_2)} \text{ radians} \tag{6}$$

where T, the equivalent static disturbance torque, is given by

$$T = mab\Omega_o^2 \tag{7}$$

and (ab) is the product of the distances along the pitch and yaw axes from the mass center to the dynamic imbalance m. This approximation is valid, however, only for cases similar to those at hand, where the laboratory is nonsymmetric and the booster is symmetric. It also, of course, must be used only when small angle approximations are applicable.

3. Changes in Separation and Spin Speed

Changes in separation have some effect on the vehicle dynamics. Table 13 shows the yaw and roll resonant frequencies and static sensitivities for three values of separation. (The peak response to a step disturbance torque is proportional to the static sensitivity.) It appears from these results that the vehicle structural stiffness increases slightly with decreasing separation.

TABLE 13

EFFECT OF CABLE LENGTH ON DYNAMICS OF THE NOMINAL VEHICLE

Cable Length (ft)	Yaw Axis Dynamics			Roll Axis Dynamics		
	Static Sensitivity (rad/ft-lb)	Resonant Frequencies (rad/sec)		Static Sensitivity (rad/ft-lb)	Resonant Frequencies (rad/sec)	
		ω_{y_1}	ω_{y_2}		ω_{r_1}	ω_{r_2}
50	$7.54\ (10^{-7})$	2.6	5.6	$7.58\ (10^{-5})$	0.31	1.1
100 (nominal)	$1.40\ (10^{-6})$	2.0	3.6	$7.58\ (10^{-5})$	0.27	0.46
150	$1.81\ (10^{-6})$	1.8	3.1	$7.58\ (10^{-5})$	0.19	0.38

The effect of spin speed changes is illustrated by table 14. The yaw and roll axis dynamic parameters are tabulated for three values of spin speed. As would be expected, the rigidity of the vehicle increases as the spin speed increases, although the increase is not proportional.

TABLE 14

EFFECT OF SPIN SPEED CHANGES ON DYNAMICS OF THE NOMINAL VEHICLE

Spin Speed (rad/sec)	Yaw Axis Dynamics			Roll Axis Dynamics		
	Static Sensitivity (rad/ft-lb)	Resonant Frequencies (rad/sec)		Static Sensitivity (rad/ft-lb)	Resonant Frequencies (rad/sec)	
		ω_{y_1}	ω_{y_2}		ω_{r_1}	ω_{r_2}
0.2	$1.68\ (10^{-6})$	1.8	3.3	$3.04\ (10^{-4})$	0.16	0.40
0.4 (nominal)	$1.40\ (10^{-6})$	2.0	3.6	$7.58\ (10^{-5})$	0.27	0.46
0.6	$1.11\ (10^{-6})$	2.2	4.1	$3.70\ (10^{-5})$	0.32	0.58

The above data on spin speed and separation effects apply only to the nominal eight crossed cable configuration. This configuration is somewhat less sensitive to changes in spin speed and separation than the three or four cable configurations.

The angular rotation at which cable slacking occurs is also a function of spin speed and separation. Table 15 lists the relative roll angles (e_{11}-e_{21}) which cause the cables to go slack in the nominal, eight cable configuration.

TABLE 15

CABLE SLACKING LIMITS ON (e_{11}-e_{21}) FOR RELATIVE ROLL DEFLECTIONS

Spin Speed \ Cable Length	50 ft	100 ft	150 ft
0.2 r/sec	1.6°	5.1°	16°
0.4 r/sec	4.7°	19°	Large
0.6 r/sec	19°	Large	Large

Recall that typical roll deflections were on the order of 1 degree for the nominal vehicle. They were less than 15 degrees in all cases considered in the study. Thus, it does not appear that rolling motions large enough to slack the cables will occur during the spinning mode of operation.

The yaw slacking limits are shown in table 16. In a yawing motion, any of the cables can go slack. Referring to figure 3, which shows a spin plane projection of the nominal cable configuration, either the cables which cross the center line can go slack, or the cables whose projection on the spin plane runs parallel to the vehicle centerline can go slack. The first number in each column of table 16 is the slacking limit for the cables whose projection are parallel to the vehicle centerline. The second number is the crossing cable slacking limit. Different relative motions of the manned body and the counterweight are required to slack the crossing and parallel cables. The data in table 16 are based on a fundamental mode yaw oscillation, in which case e_{23} must be in a specific ratio to e_{13}. In this regard, recall from section IV.B.2 that the fundamental mode response dominated the yaw axis. Again, it appears that the spinning mode response motions will not be large enough to slack the cables.

TABLE 16

CABLE SLACKING LIMITS ON e_{13} FOR FUNDAMENTAL MODE YAW OSCILLATION

Spin Speed \ Cable Length	50 ft		100 ft		150 ft	
0.2 rad/sec	-	-	0.42°	1.10	-	-
0.4 rad/sec	0.76°	2.1°	1.8°	3.2°	5.3°	5.0°
0.6 rad/sec	-	-	7.6°	12°	-	-

At very low spin speeds and small extensions, the cable slacking limits drop low enough that almost any disturbance will slack the cable. For example, at a spin speed of 0.04 rad/sec and extension of 10 ft., the slacking limit for the parallel cables is about 0.0012 degree. In this case the linearized model breaks down, and alternate models must be devised.

The preceding discussion has established the gross characteristics of the flexible spinning space station. It was discovered that the flexible vehicle would be similar to the rigid vehicle, but that important differences might exist in some cases. It was also established that the linearizing approximations used in the dynamics analysis were valid for the operational spinning mode, but became questionable for the transistion mode. The following section of this report discusses the synthesis of a control system for use in the operational spinning mode. A linearized vehicle model which includes structural flexibility effects serves as the basis for this discussion. Section VI deals with the transition problem in some detail. The model used in that discussion reflects the appropriate nonlinear phenomena.

Section V

STABILIZATION AND CONTROL IN THE OPERATIONAL SPINNING MODE

A. INTRODUCTION

As discussed in section III, the control functions specified in table 2 can logically be assigned to the following subsystems:

- Rate stabilization subsystem
- Dynamic balancing subsystem
- Spin plane orientation subsystem
- Artificial gravity control subsystem

The objective of the control system study was to determine the feasibility of providing such functions, and to establish suitable values for all critical subsystem parameters. The control functions of section III were first translated into the control concepts noted in table 17. The performance of each subsystem was then evaluated for the nominal vehicle. Finally, the effect of changes in the station's inertia ratio, spin speed, and separation were investigated in order to determine the effect on the nominal control system.

TABLE 17

CONTROL CONCEPTS

Control Function	Control Requirements	Control Concept
Rate Stabilization	a. Damp roll resonance to 10% of critical. b. Damp structural resonances to 1% of critical.	1. Linear Control. Sensor-Body rate gyro. Actuator-control moment gyro for roll and pitch, inertia wheel for yaw. 2. On-off Control. Same system as linear except uses on-off torquers or reaction jets. 3. Hybrid Control. Combination of linear and on-off elements.
Dynamic Balance	Align the manned body's geometric axis with the spin axis.	1. Torque balance steady state imbalances or 2. Transfer mass to balance steady state imbalances
Spin Plane Orientation	Align spin vector to within 0.5° of sun line.	Apply space-referenced precession torques thru logical control of pitch reaction jets.
Spin Speed Control	Maintain artificial gravity to within 2% of selected reference.	Fire spin jets when gravity error exceeds 2% of reference thru use of body accelerometer.

Note: All control assumed within the manned body.

Table 18 presents a summary of the vehicle configurations evaluated in the study. For purposes of facilitating the following discussion, each vehicle configuration is identified by a roman numeral as indicated in the table.

TABLE 18

STATION CONFIGURATIONS

Station Identification	Inertia Ratio	Spin Speed Rad/Sec	Cable Length feet	Cable Configuration
I (Nominal	0.0107	0.4	100	8 crossed
II (Inertia Ratio)	0.0048	0.4	100	8 crossed
III	0.0027	0.4	100	8 crossed
IV (Spin Speed)	0.0107	0.2	100	8 crossed
V	0.0107	0.6	100	8 crossed
VI (Separation)	0.00585	0.4	150	8 crossed

The stabilization and control studies utilized seven degree of freedom linear equations of motion to represent the vehicle's dynamics. The nine degree of freedom model discussed in appendix B was reduced to a seven degree of freedom model by assuming constant spin speed and separation.

Examination of these equations of motion show that the station's yaw (spin) axis is uncoupled from the other two axes. This allows the control problem to be divided into two areas: a two degree of freedom vehicle for spin axis stabilization and control and a five degree of freedom vehicle for roll and pitch axis control. Analysis of the two degree of freedom model is relatively straight-forward and can be handled by suitable analytical techniques. Analysis of the five degree of freedom model is more complex and control system evaluation was accomplished through the use of an analog computer.

To evaluate the controlled vehicle's response, estimates of manned body disturbances were made. In the spinning mode two sources of disturbance inputs were considered; steady torques resulting from crew motion within the manned body, and impulsive torques produced by spin or orientation reaction jet misalignment.

The estimated disturbance levels are presented in table 19 by vehicle configuration. The jet disturbances, based on 100-pound thrust jets, are listed as steady torques in the table. The disturbance totals, the sum of the two steady torques, were used in the study to evaluate and size the rate stabilization system. This was done to eliminate the jet on-time variable and results in a conservative design. Only the steady torques (dynamic imbalance) due to crew motion were considered when evaluating the dynamic balancing subsystem.

TABLE 19

ESTIMATED DISTURBANCES

Manned Body Disturbance	Vehicle Configuration					
	I (Nominal)	II	III	IV	V	VI
Roll-Crew Motion	104	104	104	26	234	104
Jet Misalignment	37	37	37	37	37	37
TOTAL	141	141	141	63	271	141
Pitch-Crew Motion	813	813	813	203	1830	1180
Jet Misalignment	20	20	20	20	20	20
TOTAL	833	833	833	223	1850	1200
Yaw-Crew Motion	813	813	813	203	1830	1180
Spin Jet	332	332	332	332	332	359
TOTAL	1145	1145	1145	535	2162	1539

Note: All disturbances are in foot-pounds.

The following discussion, presented on a control subsystem (function) basis, establishes the nominal control configuration and demonstrates its performance. In addition, parametric analyses of the rate stabilization subsystem are presented showing the effect which changes in the damping specification and the vehicle configuration have on the nominal system.

B. RATE STABILIZATION SUBSYSTEM

1. Actuator Considerations

The rate stabilization control concepts, presented in table 17, suggest several alternate methods for applying control torques. The actuating or torquing devices considered in this study were the following:

- Two-degree-of-freedom control moment gyro
- Single-degree-of-freedom control moment gyros
- Inertia wheels
- Reaction jets

Appendix D contains a trade-off analysis which concludes that the two degree of freedom control moment gyro has characteristics that are generally more favorable than the other actuators for roll and pitch torquing.

Two single-degree-of-freedom gyros also could provide the roll and pitch damping torques. However, they would have a combined angular momentum equal to twice that of the two-degree-of-freedom gyro. The two-degree-of-freedom gyro therefore has both a weight and power advantage. This conclusion is predicated on a requirement for pitch structural damping. In the event that pitch structural damping is not required, the two-degree-of-freedom gyro could be replaced by one single-degree-of-freedom gyro of equal angular momentum. However, no pitch control torques would then be available for the non-spinning mode.

Inertia wheels were not selected because, as shown in the appendix D, the peak torquer power required for the inertia wheel system is three orders of magnitude higher than that required for the control moment gyro. The servo size (14 hp) required with inertia wheels appears impractical. The reason for the power discrepancy becomes apparent when it is considered that the inertia wheel must be torqued at wheel speed, while the gyro will be torqued at gimbal precession rates, which are very low in comparison with the inertia wheel rotational speeds.

The jet system appears more competitive with the control moment gyro. Here the comparison must be on a weight basis. The jet system weight is predominately propellant, and the amount of propellant required for damping is a function of disturbance frequency, disturbance amplitude, and mission life. Analog computer results indicate that the gyro enjoys a weight advantage if more than thirty peak disturbances are to be damped. In this study it has been assumed that long missions are of interest and that the number of disturbances will exceed thirty. It should also be noted that efficient dynamic torque balancing cannot be provided by jets.

The manned capsule yaw axis, being essentially parallel with the space station spin axis, did not have the same actuator problems as the

pitch and roll axes. Therefore the relative advantages of one torquing device over the other was not as clear cut as for the pitch and roll axes. For purposes of this study, an inertia wheel has been selected as the yaw axis actuator. Other actuating devices, in particular certain combinations of control moment gyros, may prove more desirable. Selection of the optimum actuator configuration requires detailed analysis of the nonspinning mode control problem, which is beyond the scope of this report.

2. Nominal Rate Stabilization Subsystem

a. Description

The foregoing discussion concluded that a two-degree-of-freedom control moment gyro should be employed to provide the damping torque for the roll and pitch axes and an inertia wheel to damp the yaw axis. The remaining alternatives presented in table 17 consisted of using on-off vs proportional torquing of the gyro and inertia wheel. Linear torquing has been selected for the control moment gyro since the control electronics are relatively simple for the low torquer power required (approximately 30 watts), and since dynamic torque balancing requires a linear torquing capability. The inertia wheel is controlled in an on-off fashion in order to eliminate the complexity associated with providing a servo amplifier having a peak power of approximately 360 watts.

A functional block diagram of the rate stabilization (wobble damping) system is presented in figure 15.

The body mounted rate gyros sense the inertial angular velocities induced by disturbances on the vehicle, and the torquers apply opposing proportional torques. The reaction torque from the torquers is absorbed by the control moment gyro. As described below, gyro damping and centering (i.e., unloading) is provided by the torquer back EMF.

The control moment gyro equations of motion, presented in appendix D, indicate that the gyro will act as an undamped oscillator in response to control torque inputs. Therefore, compensation is required to provide some gyro damping. As indicated on the block diagram, the back EMF characteristics of the torque motors will supply the required gyro damping. In this case the actual torques on the gyro are related to the commanded torques by:

$$T_I = T_{IC} - K_V \dot{\alpha}_T$$
$$T_O = T_{OC} - K_V \dot{\beta}_T \qquad (8)$$

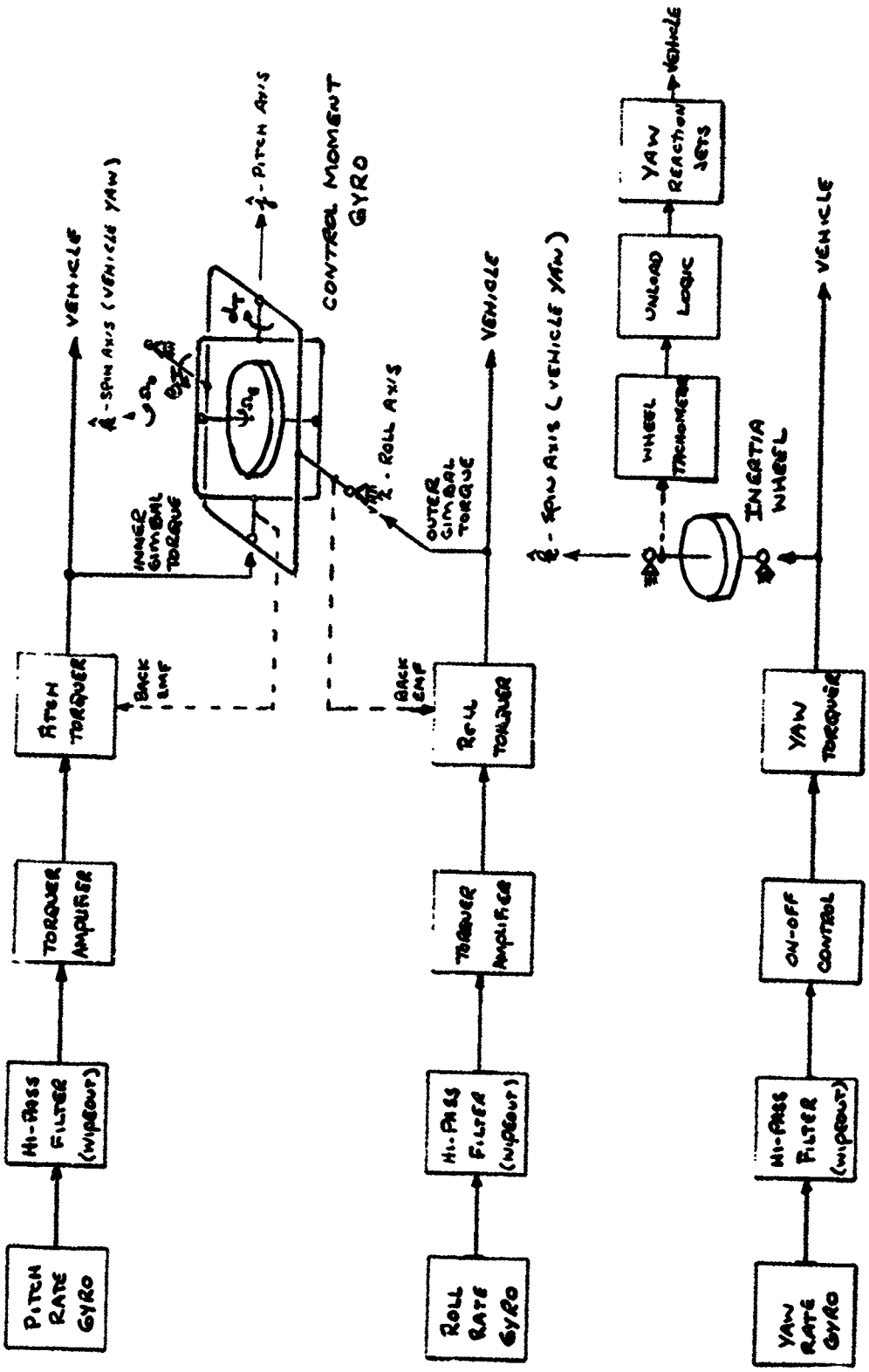

FIGURE 15 RATE STABILIZATION SUBSYSTEM BLOCK DIAGRAM

where T_{IC} and T_{OC} are the commanded torques on the inner and outer gimbals, α_T and β_T are the inner and outer gimbal angles, and K_V represents the slope of the torque motor torque-speed curve.

Since the space station is spinning and the gyro is viscously coupled to the station by the damping torques, $K_V \dot{\alpha}_T$ and $K_V \dot{\beta}_T$, the gyro will precess into alignment with the space station spin axis in the absence of input signals. This unloads the gyro and assures that full gyro capability will be available to damp subsequent transients. The angular momentum due to the initial disturbance is transferred back into the space station. The rate of transfer is slow enough so that the induced wobble rates are insignificant. However, a small station orientation error will result.

An estimate of the magnitude of this error is obtained by noting that the maximum angular momentum that can be absorbed by the gyro is equal to the rotor angular momentum, H. Since the vehicle angular momentum is $I_3 \Omega_0$, a rotation of the vehicle spin plane through an angle

$$\varphi \approx \frac{H}{I_3 \Omega_0} \quad \text{radians} \qquad (9)$$

is required to transfer all the absorbed angular momentum back into the vehicle. For the nominal vehicle this amounts to an error of 0.005 degree.

Returning to consideration of figure 15, the need for shaping the rate gyro signals with high pass filters (wipeout networks) is as follows:

- The yaw wipeout eliminates the steady state spin speed signal. The yaw damper then operates only on the transient signals due structural motions.
- The pitch wipeout reduces the component of spin speed sensed by the pitch rate gyro when the vehicle rolls. If this low frequency component were not attenuated by the pitch axis wipeout, it would saturate the pitch torquer and little structural damping would be obtained.
- The roll wipeout has been included to eliminate the effect of rate gyro misalignment. Its frequency characteristics were selected to make it ineffective at the vehicle roll resonance.

b. Performance

The preceding paragraphs established a nominal rate stabilization control subsystem. The following discussion establishes suitable control parameters for this subsystem and demonstrates its performance. The performance evaluation was accomplished by employing an analog computer. The vehicle was simulated using a seven degree of freedom model. The control system of figure 15 was simulated using the rate gyro equations shown in table 3 and the control moment gyro equations contained in appendix D.

The roll and pitch rate stabilization parameters considered in the analog computer were:

- Rate gain
- Wipeout time constant
- Control moment gyro angular momentum
- Control moment gyro gimbal damping
- Maximum control torque

The roll wipeout break frequency was set at one-quarter of the dominant roll resonant frequency, and the pitch wipeout break frequency was set at one-quarter of the pitch structural resonance. Values for the control moment gyro angular momentum and gimbal damping gain were set at reasonable calculated values for computer simulation and then kept constant. The rate gains were then varied to determine the effect on vehicle response, gyro response and maximum control torques.

The roll rate gain was varied until the vehicle roll response satisfied the specified damping requirement of 10 percent of critical. The gyro gimbal angles were noted and the pitch rate gain adjusted until the inner and outer gimbal angles were equal. In essence, the gyro was sized to handle the peak roll transient, and the pitch structural damping was then maximized consistent with the gyro capacity. It should be noted that this rate stabilization system is designed to damp the body axis rates to zero and does not attempt to eliminate the coning angle resulting from steady disturbance torques. For this reason, the peak control torques can be considerably smaller than the disturbance torques. Elimination of the coming angle requires a larger gyro, and control torques equal to the steady disturbance torques. It is discussed in the section on dynamic balancing (section V paragraph c). The control parameters which resulted,

representative of the nominal system, are presented in table 20. In this table, the gyro angular momentum has been scaled to give peak gimbal angles of one radian. The yaw damper gain was selected to give a yaw structural damping ratio of 1 percent of critical. The performance of this system is summarized in table 21.

TABLE 20

NOMINAL RATE STABILIZATION SYSTEM PARAMETERS

Parameter	Value
Roll rate gain	8000 Ft-lb/Rad/Sec
Pitch rate gain	5000 Ft-lb/Rad/Sec
Yaw rate gain	7000 Ft-lb/Rad/Sec
Roll wipeout time constant	13 Sec
Pitch wipeout time constant	1.5 Sec
Yaw wipeout time constant	2 Sec
Gyro angular momentum	47 Slug-Ft^2/Sec
Gyro gimbal damping	50 Ft-lb/Rad/Sec
Maximum roll control torque**	24 Ft-lb
Maximum pitch control torque**	24 Ft-lb
Maximum yaw control torque	15 Ft-lb

*This value of angular momentum has been scaled to produce peak gimbal angles of 1 radian for the disturbance torques noted in table 19.

**The peak control torques are based on the maximum disturbances noted in table 19.

TABLE 21

RESPONSE OF CONTROLLED VEHICLE TO STEP DISTURBANCE INPUTS

	Roll	Pitch	Yaw
Peak acceleration-	0.12°/Sec^2	0.56°/Sec^2	0.38°/Sec^2
Peak angular velocity -	0.14°/Sec	0.50°/Sec	0.18°/Sec + spin speed
Steady state angular velocity -	0.02°/Sec	0.24°/Sec	Spin speed
Peak angle -	0.90°	0.10°	0.10°
Steady state angle -	0.60°	0.06°	0.05°

Notes: 1. Disturbance inputs:
Roll - 141 Ft-lb
Pitch - 833 Ft-lb
Yaw - 1145 Ft-lb

2. Damping ratios:
Primary Resonance - 0.1
Pitch structure - 0.04
Yaw structure - 0.01

Figure 16 is a computer record demonstrating the performance of the rate stabilization system. In this record, however, the control parameters were different from those listed in table 20. The gyro angular momentum is 160 slug-ft^2/sec and the pitch gain had not been optimized. In addition, the applied steady disturbance torques are larger than indicated in table 19. The larger disturbance torques reflect the use of 400 pound thrust reaction jets for spin-up during early simulations. However, since the spin-up study later indicated 100 pound jets would be satisfactory, the smaller disturbance values of table 19 were used to establish the nominal control system parmeters. The parametric discussion that follows will cover the effect of changing disturbance levels.

3. Parametric Analysis

a. General

The parameter changes considered in this study fall into two basic categories: control system performance parameters and vehicle configuration parameters. The performance parameters considered in the investigation were damping specification and disturbance input magnitude. The vehicle configuration parameters considered were inertia ratio, spin speed, and separation. These performance and vehicle parameters were changed one at a time and the effect of each on the control system was determined. The control parameters included control moment gyro angular momentum, peak control torques, rate gains, and wipeout time constants. Each of the parameter changes is treated separately below.

b. Effect of Damping Specification

The nominal roll and pitch rate stabilization system was designed to provide a damping ratio of 10 percent of critical. The damping factor provided by the roll stabilization system is directly proportional to roll rate gain. The effect of pitch rate gain on the primary roll resonance is negligible, because of the weak pitch/roll cross-coupling existing in this type of vehicle. Thus if the damping specification is doubled, the roll rate gain doubles. Doubling the roll rate gain doubles the gyro angular momentum and the peak roll torque. For purposes of illustration, four different damping requirements were assumed and their effects on the control system are summarized in table 22.

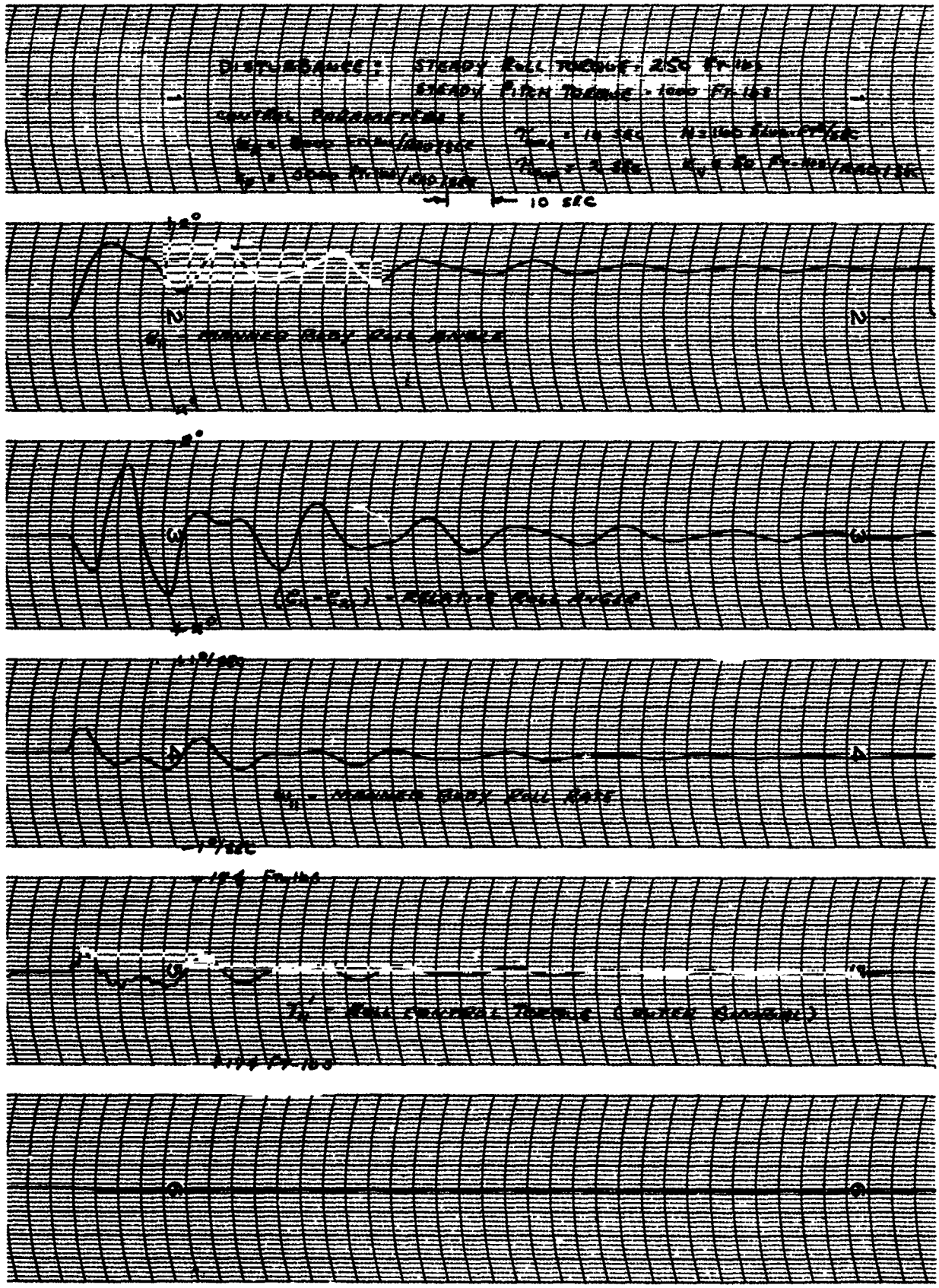
Disturbance: Steady Roll Moment, 250 Ft-lbs
Steady Pitch Moment - 1000 Ft-lbs
Control Parameters:
10 sec
Measured Body Roll Angle
Measured Body Roll Rate
Roll Control Moment (Output Signal)

16-1

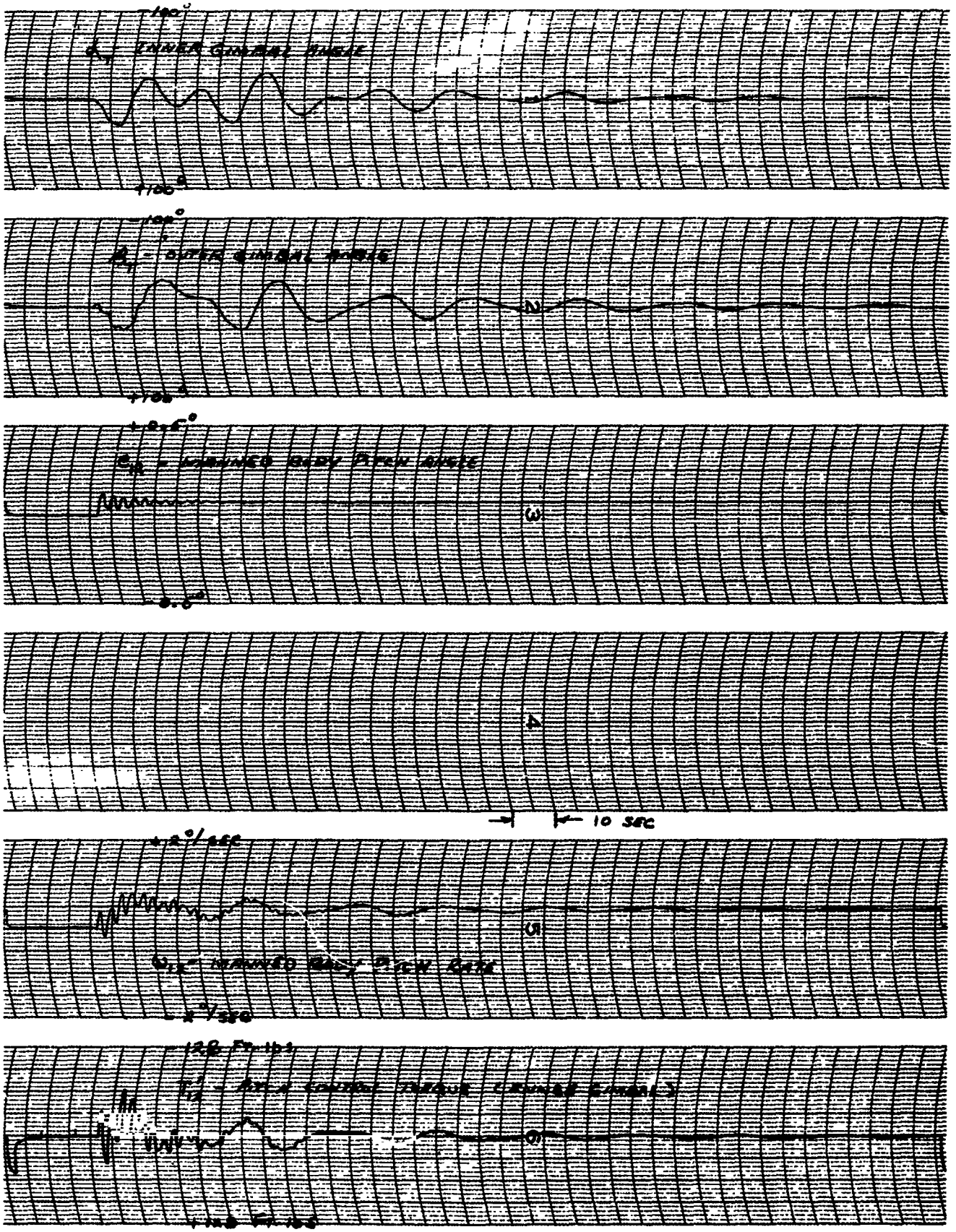

FIGURE 16
RATE STABILIZATION SYSTEM PERFORMANCE

TABLE 22

EFFECT OF DAMPING SPECIFICATION

Damping Ratio	Roll Rate Gain K_R	Gyro Angular Momentum H	Peak Roll Torque	Roll Wipeout Time Constant
1%	800	5	2	13
5%	4000	23	12	13
10%	8000	47	24	13
20%	16000	94	48	13

c. Effect of Disturbance Level

The disturbance levels noted in table 19 were based on a three-man imbalance and a 100-pound jet misalignment of .05 radian. The totals of these disturbances were used to size the nominal control system. For the nominal vehicle configuration, gyro size and peak torque requirements approximately scale in direct proportion to the total disturbance level. This approximation neglects the effects of vehicle motions on the gyro, and thus holds only for cases where the vehicle motions are small. However, if the inertia ratio is low, such as is the case for configuration III, the gyroscopic restraint of the manned body's roll attitude is much reduced and significant vehicle roll deflection results from input disturbances. If no control torque is applied to the gyro when the vehicle is disturbed, the gyro gimbal angle will be identical to the angle through which the vehicle rotates. The gyro capacity available for damping is reduced accordingly. Therefore, when sizing the gyro for peak gimbal angles of one radian, the allowable gimbal deflection due to applied control torque must be equal to one radian less the vehicle motion. For configuration III the peak vehicle roll angle for the specified total roll disturbance of table 19 (141 ft-lb) is approximately five degrees. Thus, the maximum gimbal angle produced by the control torques must be limited to approximately 52 degrees.

This effect is illustrated in the curves of figure 17, where vehicle configurations I and III are compared. The curves show peak gyro gimbal angle versus gyro angular momentum for a fixed disturbance level. It is apparent that vehicle rotation becomes more significant is sizing the gyro as the inertia ratio decreases. Further decreases in the inertia ratio would result in vehicle rotations accounting for a large percentage of the total gimbal angle. Figure 18, a plot of peak roll angle versus

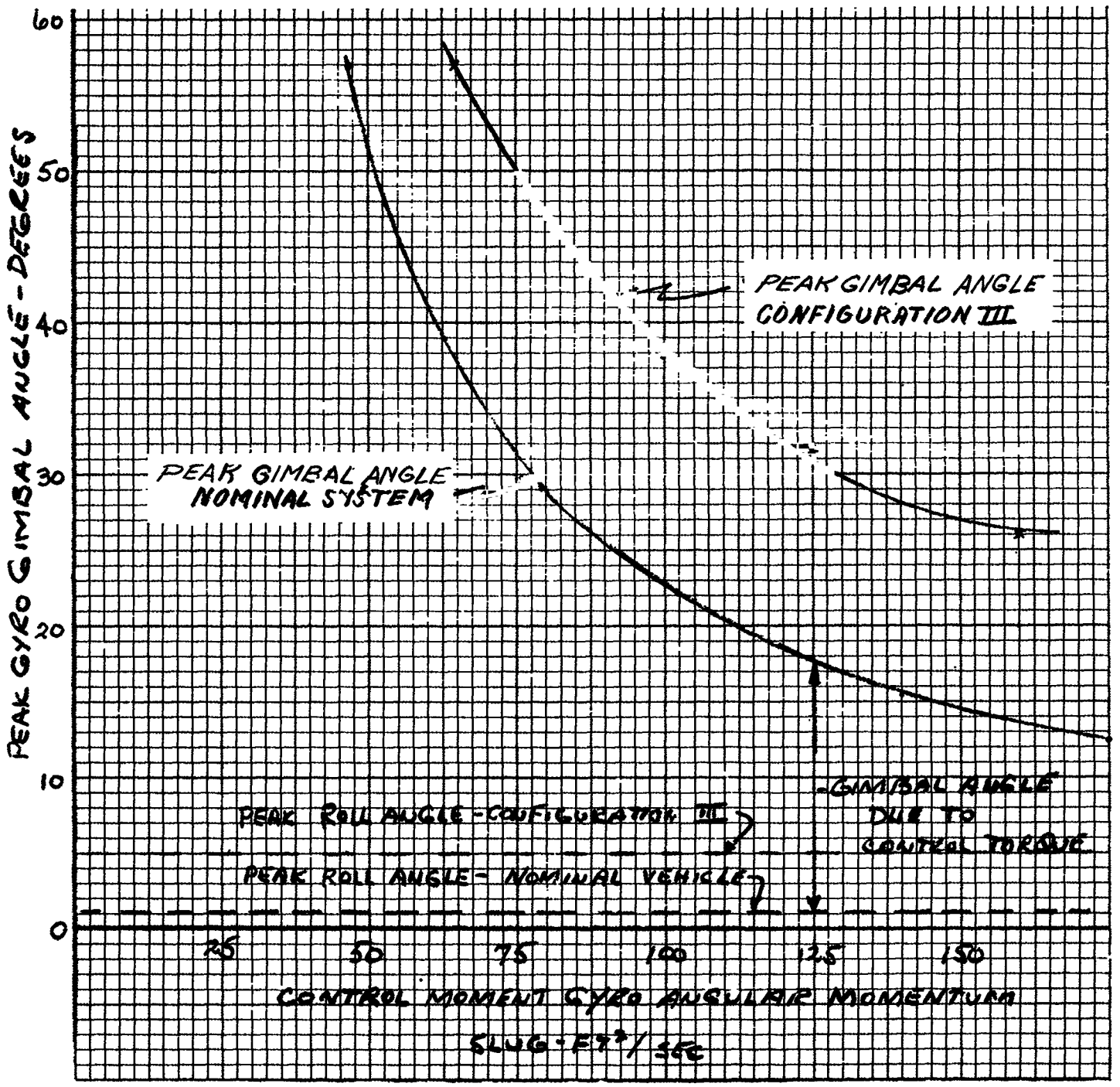

FIGURE 17 PEAK GIMBAL ANGLE VS CONTROL MOMENT GYRO ANGULAR MOMENTUM FOR DISTURBANCE TORQUE OF 141 FT-LBS

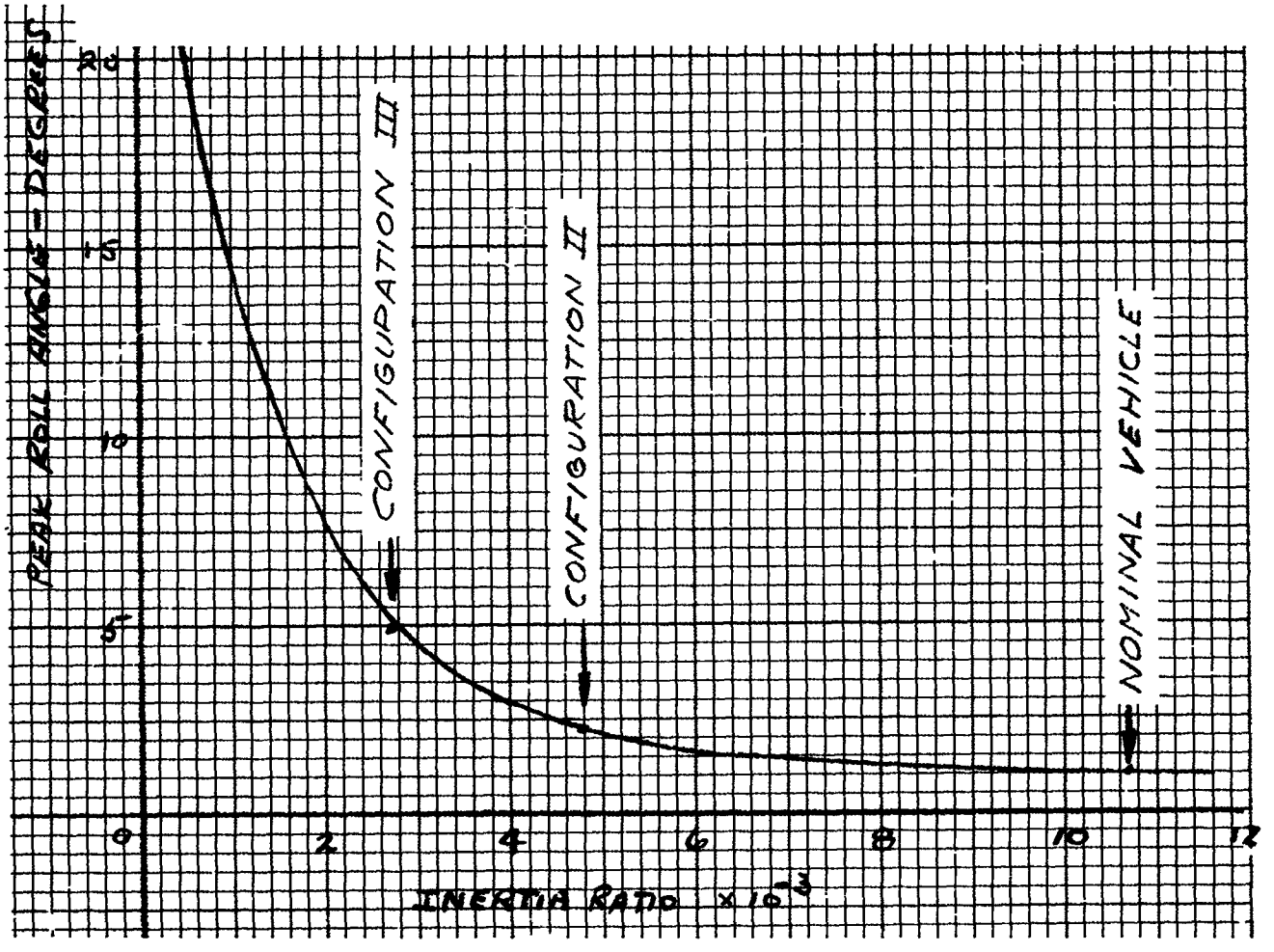

FIGURE 18 PEAK ROLL ANGLE VS INERTIA RATIO FOR STEADY DISTURBANCE TORQUE IN ROLL OF 141 FT-LBS

inertia ratio for a constant disturbance torque, shows that vehicle angles reach 20 degrees when the inertia ratio is lowered by a factor of five from that of configuration III.

d. Effect of Inertia Ratio

The total vehicle yaw and pitch moments of inertia, I_3 and I_2, determine the inertial roll restraint. As noted above, vehicle inertia ratio $(I_3-I_2)/I_3$ has a significant effect on control moment gyro size. In fact this is the most significant vehicle parameter because the vehicle's dominant resonant frequency, the roll resonance, is a function of this ratio. In this study three different inertia ratios were considered. Table 23 summarizes analog computer results showing the effect which vehicle inertia ratio has on the control system parameters. The control criteria for each case was a damping ratio of 10 percent of critical. Note that the rate gain, wipeout time constants, and the control moment gyro angular momentum all vary as a function of inertia ratio.

TABLE 23

EFFECT OF INERTIA RATIO

Vehicle Configuration	Inertia Ratio -	Roll Rate Gain Ft-lbs/Rad/Sec	Wipeout Time Constant Sec	Peak Torque Ft-lbs	Gyro Angular Momentum Slug-ft^2/Sec
I (Nominal)	0.0107	8000	13	24	47
II	0.0048	5400	19	24	53
III	0.0027	4000	27	24	64

e. Effect of Spin Speed and Separation

In this study three spin speeds and two separations were considered. Spin speed and separation are operating parameters as distinct from the vehicle physical parameters such as inertia ratio. Under normal operating conditions, spin speed and separation will change, whereas the physical parameters will essentially be fixed by design. In this regard, control system gain switching as a function of spin speed and/or separation might be necessary, and the gyro must be sized for the worst case.

Table 24 presents analog computer results showing the effect on the control parameters of several spin speeds and separations. The control parameters change with spin speed because the roll resonant frequency is

directly proportional to spin speed. Changing the cable length from 100 feet to 150 feet did not effect the control parameters because the roll resonant frequency does not shift very much.

TABLE 24

EFFECT OF SPIN SPEED AND SEPARATION

Configuration	Spin Speed Rad/Sec	Cable Length Feet	Roll Rate Gain Ft-lbs/Rad/Sec	Wipeout Time Constant Sec	Peak Roll Torque Ft/lbs	Control Moment Gyro Angular Momentum Slug-ft^2/Sec
I (Nominal)	0.4	100	8000	13	24	47
IV	0.2	100	4000	27	12	60
V	0.6	100	12000	9	36	38
VI	0.4	150	8000	13	24	47

C. DYNAMIC BALANCE SUBSYSTEM

1. General

In section III a requirement for dynamic balancing of the manned body was established. The most severe imbalance will occur when three men are located at the furthest point from the manned body mass center. The resulting cross-product of inertia disturbance can be represented by equivalent static disturbance torques. Estimates of these torques are noted in table 19. The magnitude of the steady state angular deflection resulting from application of these torques to each of the vehicle configurationts considered is presented in table 25. The steady state angles are those remaining after the rate stabilization system has damped the transient. Comparison with table 7 indicates that the steady state angles are about one-half of the peak transient. The steady state roll errors are considerably larger than the pitch and yaw errors because the gyroscopic roll restraint is much softer than the pitch and yaw structural restraints.

TABLE 25

STEADY STATE VEHICLE RESPONSE
TO DYNAMIC IMBALANCE

Configuration	Disturbance Torques (Ft-lb)			Steady State Angular Error-Degrees		
	T_{11}	T_{11}	T_{11}	e_{11}	e_{12}	e_{13}
I (Nominal)	104	813	813	0.45	.06	.06
II	104	813	813	0.85	.06	.06
III	104	813	813	2.0	.06	.06
IV	26	203	203	0.45	.07	.07
V	234	1830	1830	0.45	.05	.05
VI	104	1180	1180	0.45	.08	.08

Table 17 notes two control systems that could eliminate the steady state angular errors caused by dynamic imbalance: A torque balance system or a mass balance system. Although both of these systems could satisfy the control requirement, this study considered only the torque balance system. The mass balance system would either require large mass transfer within the manned body or mass control external to the body. Neither of these appear attractive.

In the torque balancing system, torques must be developed that are equal in magnitude and opposite in direction to the equivalent static disturbances noted in table 25. The required torque is constant in magnitude and spins with the vehicle. The control moment gyro can be used to apply such torques. If the gyro has a fixed gimbal angle, so that it is not aligned with the spin axis, a precession torque is required to keep the gyro turning with the station. This precession torque is fixed in magnitude and rotates with the vehicle. Thus dynamic balance can be obtained by making the precession torque equal in magnitude and opposite in direction to the equivalent disturbance torque.

From Appendix D, the linearized equations for the control moment gyro are:

$$T_o = H\left[\dot{\alpha}_T + \omega_{12} + \Omega_o \beta_T\right]$$

$$T_I = H\left[-\dot{\beta}_T - \omega_{11} + \Omega_o \alpha_T\right] \qquad (10)$$

where α_T and β_T are the gyro gimbal angles, T_o and T_I are the torques on the gyro, and H is the gyro angular momentum. Neglecting the effects of vehicle motions ($\omega_{11} = \omega_{12} = 0$), and assuming fixed gimbal angles, these equations reduce to:

$$T_o \propto H \Omega_o \beta_T$$

$$T_I \propto H \Omega_o \alpha_T \qquad (11)$$

For the nominal vehicle configuration the gyro angular momentums required to balance the steady disturbances are as follows if a limiting gimbal angle of one radian is assumed:

$$H = 260 \text{ slug ft}^2/\text{sec} \quad \text{in Roll}$$

$$H = 2030 \text{ slug ft}^2/\text{sec} \quad \text{in Pitch} \qquad (12)$$

The data in table 25 indicate that the pitch angles due to dynamic imbalance would be approximately 0.06 degree, while roll angles of 0.45 degree to 2 degrees would result. It would appear that the improved pointing accuracy obtained by balancing the pitch axis does not justify the order of magnitude increase in gyro size required to do so. It was therefore concluded that for the configurations studied, only roll balancing would be provided.

2. Description

A block diagram of the roll balance system is shown in figure 19. The steady state component of the pitch rate gyro signal is used as a measure of the roll imbalance. The pitch rate gyro equation, shown in table 3 is:

$$\omega_{12} = \dot{e}_{12} - \dot{\varphi} + \Omega_o e_{11} \qquad (13)$$

In the steady state this equation reduces to:

$$\omega_{12_{SS}} = \Omega_o e_{11} \qquad (14)$$

where e_{11} is the manned vehicle roll error. The torque balance system generates a torque proportional to the integral of the steady state pitch gyro output (i.e., $T_{balance} = -K_I \int \omega_{12}\, dt$) which drives the imbalance error to zero.

3. Performance

The dynamic balance system is relatively independent of vehicle dynamics provided the balance integral gain is suitably selected. Making this gain too high will obviously affect the rate stabilization system. This gain should be selected such that the time to integrate the imbalance to zero (i.e., develop enough torque to compensate for the imbalance) should be greater than:

$$\text{Time to Balance} = (6)\left(\frac{2\pi}{\omega_r}\right) \text{ sec} \qquad (15)$$

for the worst imbalance, where ω_r is the dominant roll resonant frequency. This assures that transient motions will have disappeared before balance is reached.

With the time to balance established, the integral gain is only a function of imbalance torque. For the nominal configuration the time to balance should be greater than two minutes. The roll disturbance of

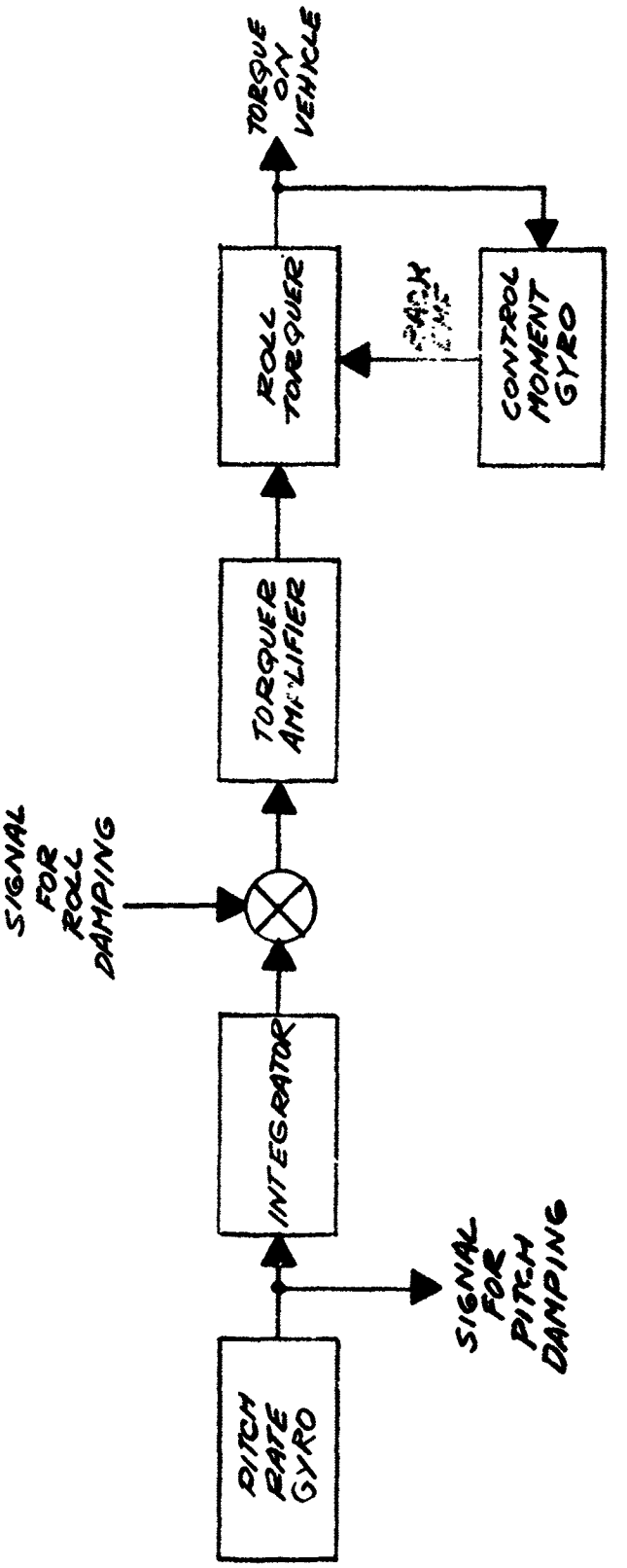

FIGURE 19 ROLL TORQUE BALANCING SYSTEM BLOCK DIAGRAM

104 ft-lb. produces a steady pitch rate of 0.24°/sec (from table 21). Therefore, the balance gain should be:

$$K_I = \frac{T_u}{(\omega_{12})_{ss}(\text{TIME})} = 210 \frac{\text{ft lbs}}{\text{sec}} \Big/ \frac{\text{RAD}}{\text{sec}} \qquad (16)$$

Figure 20 is a computer record showing the dynamic balance system functioning in the nominal vehicle. This record was taken with a 250 ft-lb disturbance instead of the nominal 104 ft-lb disturbance. The integral gain used for the computer run was 500 ft-lbs/sec/rad/sec. It can be seen that the response is well behaved, with a time to balance of approximately three minutes.

As noted above, the nominal dynamic balance system would require a gyro having an angular momentum of 260 slug ft/sec to fully balance the 104 ft-lb imbalance torque. It should be noted that a roll torquer capability of 104 ft-lb is required.

D. SPIN PLANE ORIENTATION SUBSYSTEM

1. General

For purposes of evaluation, it was assumed that the orientation control system was required to align the station's spin axis so that it pointed within 0.5 degree of the sun. Although directly concerned with sun orientation, the study results can be extended to include other references.

As discussed in section IV, the long-term response of the damped vehicle is equivalent to that of a gyroscope. Thus orientation torques must be applied in a manner that cause the vehicle to precess to the desired position. Figure 21 (a) shows the orientation control concept used for sun orientation. As shown, the pitch reaction jets must be fired as the roll error passes through its peak. As indicated by figure 21 (b), this means that each jet is pulsed as it passes the point furthest from the desired space-fixed torquing axis, or where it has the longest possible effective moment arm. The pulse width should be as short as possible, consistent with the desired maneuvering speed and minimum thrust impulse constraints.

It should be noted that thrusting on the booster to control orientation would require approximately half as much propellant as thrusting on the manned body because of the longer moment arm relative to the common

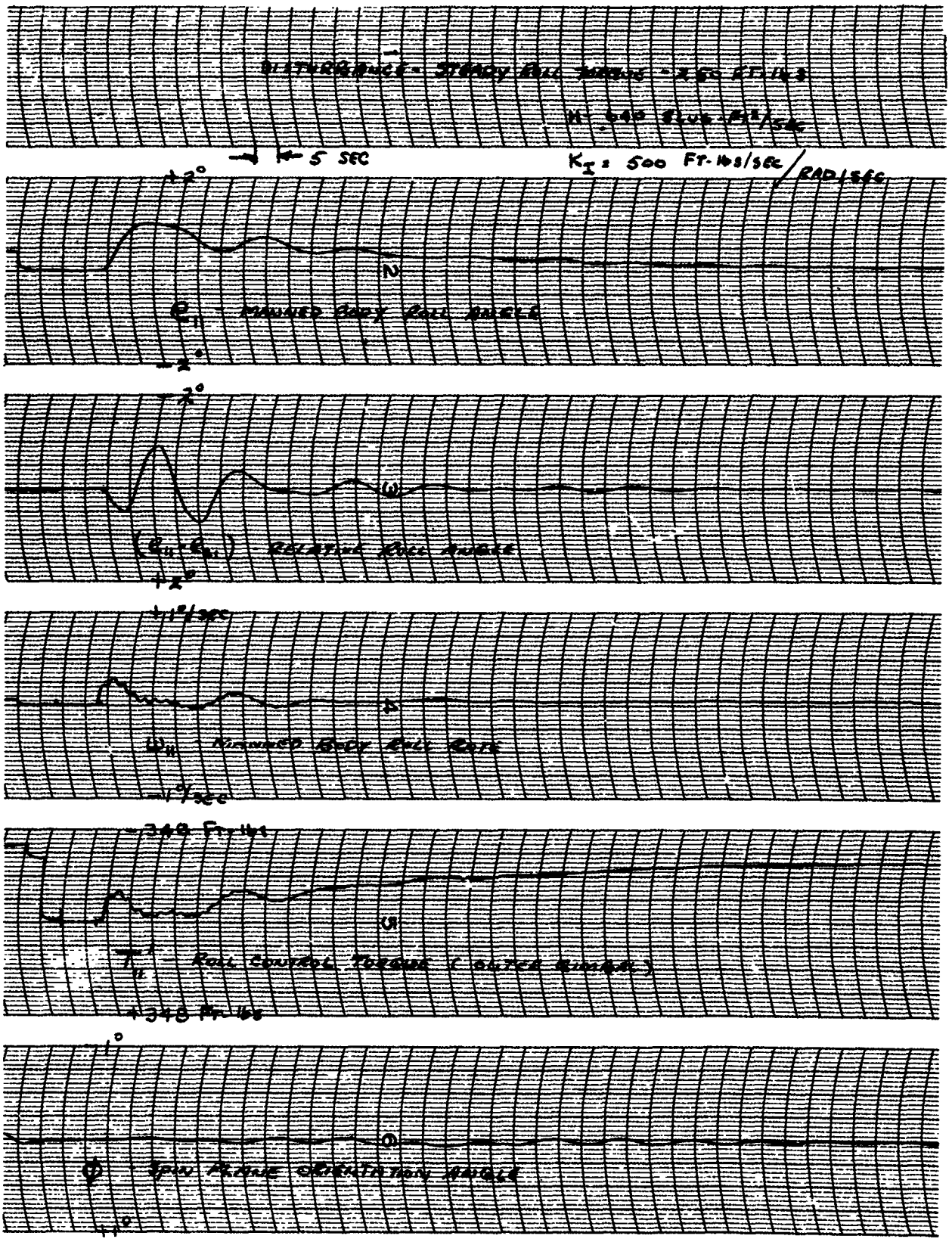
DISTURBANCE - STEADY ROLL MOMENT = 250 FT-LBS
K_I = 500 FT-LBS/SEC / RAD/SEC
5 SEC
+2°
ϕ_{II} - MEASURED BODY ROLL ANGLE
-2°
+2°
$(\phi_{II} - \phi_{III})$ RELATIVE ROLL ANGLE
+2°
+1°/SEC
ω_{II} MEASURED BODY ROLL RATE
-1°/SEC
-340 FT-LBS
T_{II} ROLL CONTROL TORQUE (CLOSED LOOP)
+340 FT-LBS
1°
ϕ - SPIN PLANE ORIENTATION ANGLE
-1°

20-1

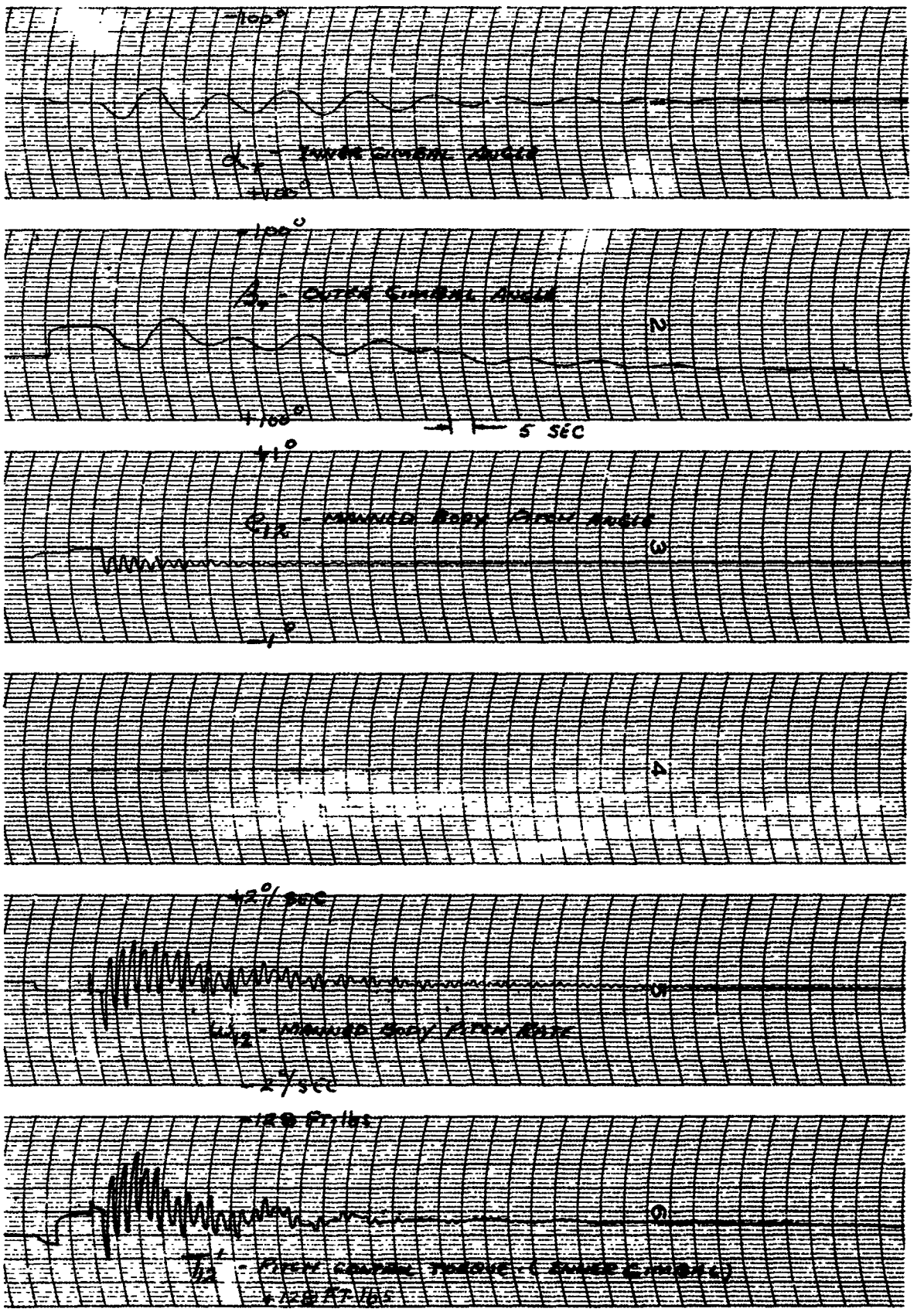

FIGURE 20 -2
ROLL TORQUE BALANCING SYSTEM PERFORMANCE

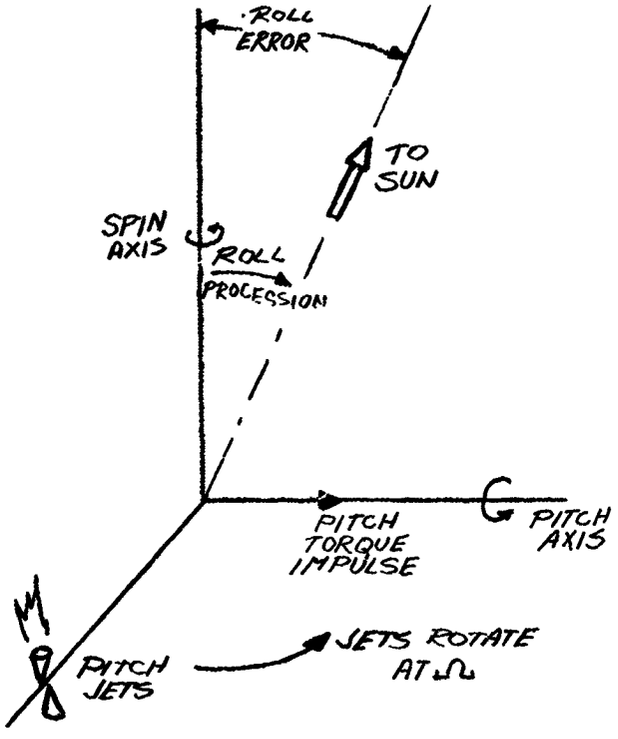

(a) PULSE PITCH JET WHEN ROLL ERROR IS AT MAXIMUM

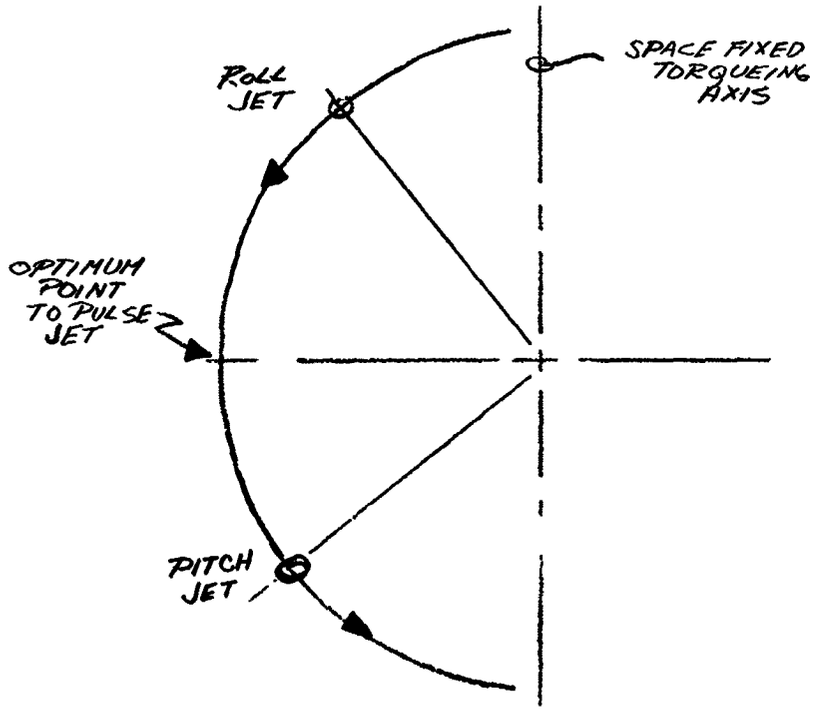

(b) PULSE JET AT MAXIMUM EFFECTIVE MOMENT ARM

FIGURE 21 ORIENTATION CONTROL CONCEPT

center of mass. The general conclusions of this study apply in either case, although only the manned body jet system was simulated.

2. Description

The detection of spin plane errors is best accomplished by use of a pitch error sensor mounted on the manned body. The vehicle pitch axis is structurally quite rigid, while the roll axis is relatively soft. Thus, a pitch error detector will essentially see only spin plane orientation errors. A roll error detector would see both spin plane errors and relative roll deflections.

As mentioned earlier, the pitch reaction jets must be fired when the roll spin plane error passes through its peak, i.e., 90 degrees of spin rotation after the pitch error peak has occurred. Thus a roll sensor appears most suitable for timing the pulses.

Accordingly, a system has been devised in which:

- A pitch error detector is used to determine whether or not the spin plane pointing error is greater than 0.5 degrees.
- The same pitch error detector is used to determine whether the positive or negative pitch jet should be fired.
- A roll error detector is used to turn the pitch jets on and off.

The logic functions described above have been conceptually implented by the use of body mounted, on-off sun sensors. No moving parts are required, and most of the required logic has been obtained by the use of suitable sensor masks.

Figure 22 shows the sun sensor masking concept. Each sensor (pitch and roll) has two apertures and two sensitive elements. Both sensors are rigidly attached to the manned body. If the manned body pitches relative to the sun, the sun will shine through one of the two wedge-shaped apertures on the pitch sensor and the corresponding sensitive element will be activated. The roll sensor will not be activated by this pitching motion.

The wedge shaped apertures are truncated; the size of the truncated portion determines the sensor threshold, as illustrated in the figure.

The vehicle is spinning, and as discussed earlier in section IV paragraph A, a spin plane pointing error appears first as a pitch error, then as a roll error. Thus each of the four sensitive elements will be

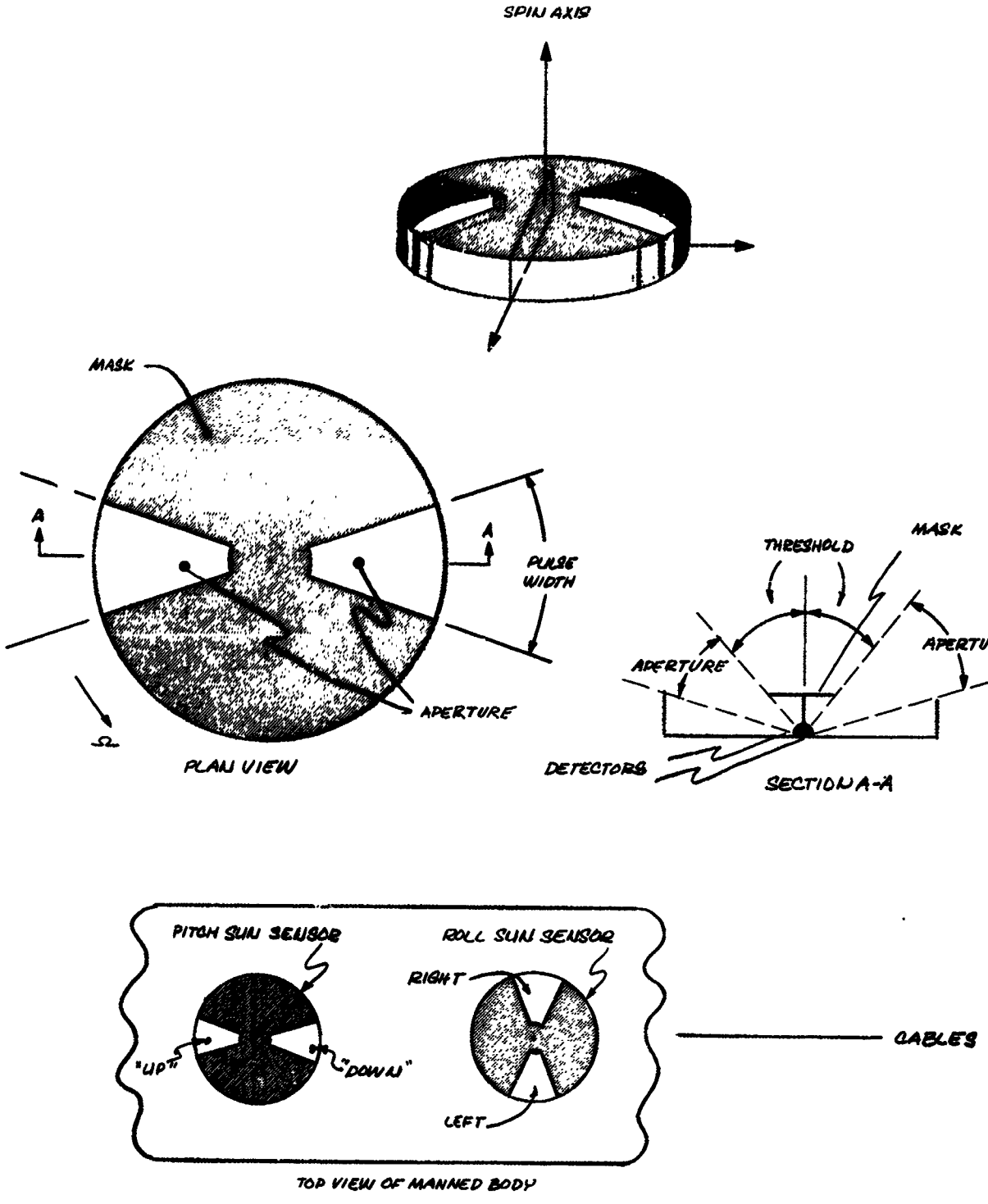

FIGURE 22 SUN SENSOR MASKING CONCEPT

activated in turn. The time they remain activated is detcrmined by the wedge angle and the spin speed. They will remain activated for a fixed fraction of each spin rotation, regardless of the spin speed.

The output of the pitch sensor is a series of positive and negative pulses of fixed magnitude and width. The roll sensor output will consist of a train of positive pulses (no polarity information is required) delayed by one quarter vehicle revolution relative to the pitch pulses. The roll pulse train is used only for timing the pitch jet impulses.

These sensors are incorporated into a spin plane orientation subsystem as shown in the block diagram of figure 23. This subsystem operates as follows: Suppose a spin plane error exceeding the threshold exists, and the pitch sensor "up" error detector is activated. One quarter of a spin cycle later, the spin plane error will also produce an output from the "right" roll sensor. The presence of both error signals at the "AND" gate will fire the "UP" correction jet. Since these signals do not occur simultaneously, the pitch error must be "remembered" for a time equivalent to a minimum of 90 degrees and a maximum of 270 degrees of rotation. This "memory" is provided by the low pass filters shown in figure 23.

The jet will fire for a length of time (pulse width) proportional to the aperture angle on the roll sensor. This angle has been set so that the roll detector has an output for 20 degrees of vehicle rotation. The pulse will be centered on the ideal location for impulsive thrusting. This pulse width (one eighteenth the time for one spin cycle) is short enough that the resultant propellant efficiency approaches that of an impulsive system.

The above discussion tacitly assumed that the vehicle had not rolled relative to the spin plane. For the nominal vehicle, it can be shown that rolling motions will affect the efficiency of the reorientation maneuver by a few percent. The system will, however, still operate satisfactorily.

3. Performance

The spin plane orientation system was simulated on an analog computer and its performance was evaluated. A spin plane misalignment error of five degrees was assumed as an initial condition. The spin plane orientation system was turned on, with the rate stabilization system operating. As shown in the computer record of figure 24, no instabilities were

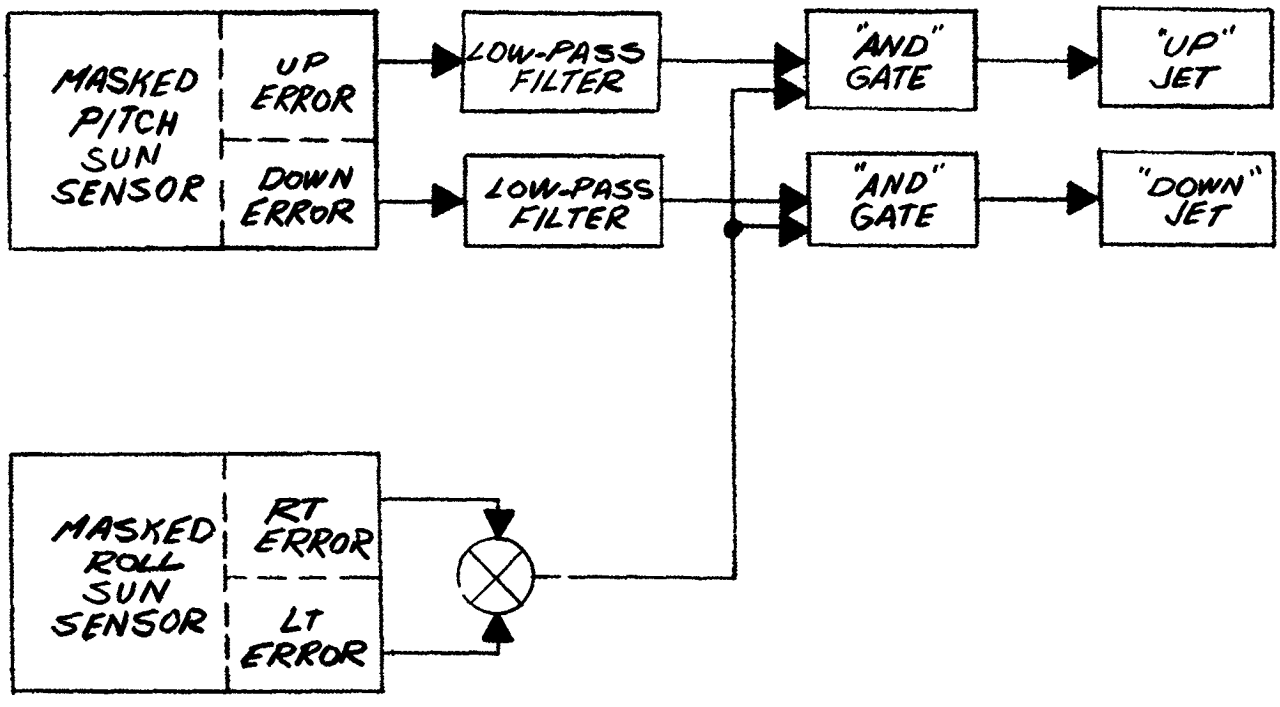

FIGURE 23 SPIN PLANE ORIENTATION SYSTEM BLOCK DIAGRAM

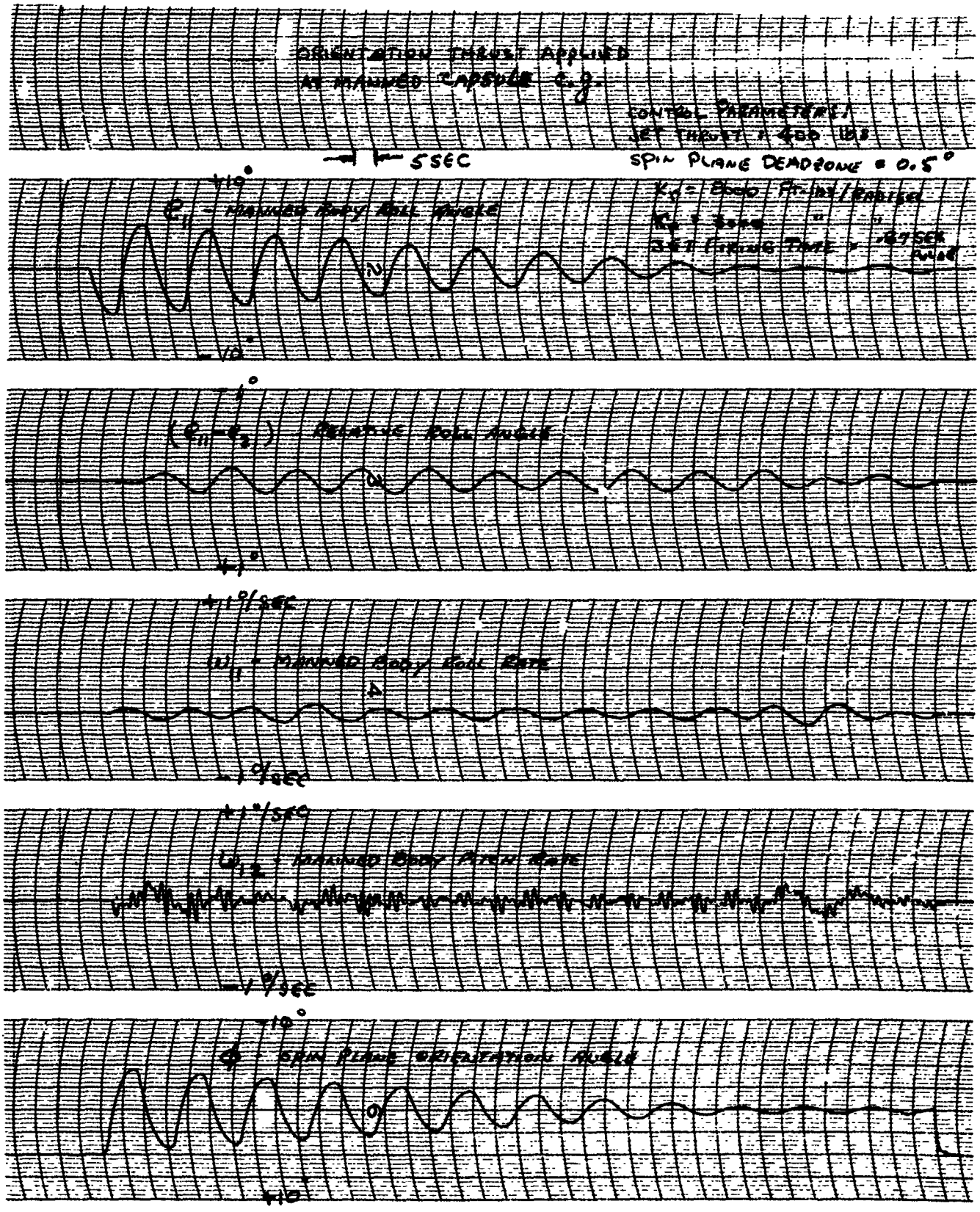
ORIENTATION THRUST APPLIED
AT MANNED CAPSULE C.G.
CONTROL PARAMETERS:
JET THRUST = 400 LBS
SPIN PLANE DEADBAND = 0.5°
5 SEC
+10°
ϕ_{II} - MANNED BODY ROLL ANGLE
K_d = 2000 FT-LBS/RADIAN
K_p = 3000 " "
3 & 4 FIRING TIME = .07 SEC
PULSE
-10°
+1°
$(\phi_{III}-\phi_{II})$ RELATIVE ROLL ANGLE
-1°
+1°/SEC
ω_{II} - MANNED BODY ROLL RATE
-1°/SEC
+1°/SEC
ω_{III} - MANNED BODY PITCH RATE
-1°/SEC
+10°
ϕ SPIN PLANE ORIENTATION ANGLE
-10°

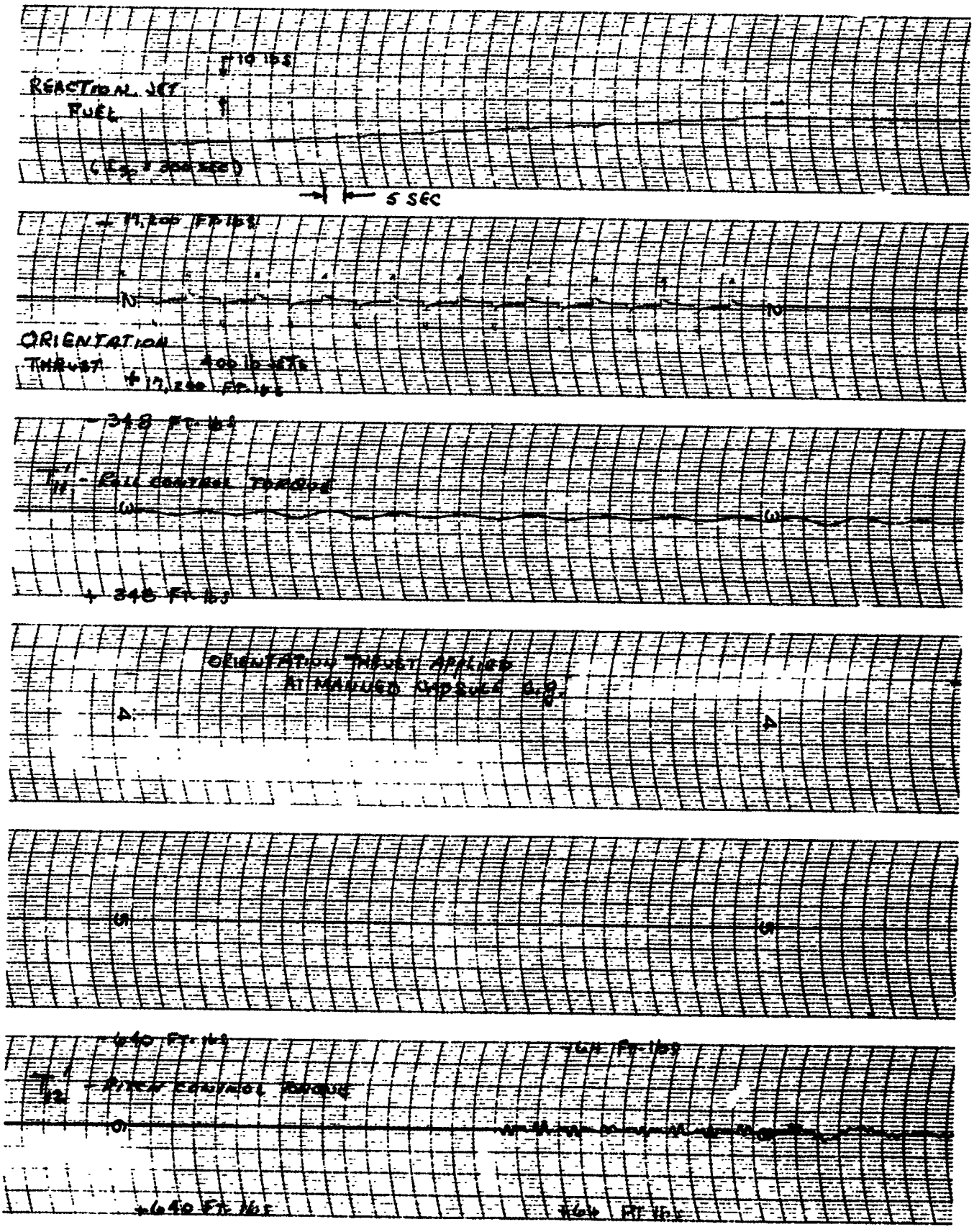

FIGURE 24 -2
ORIENTATION CONTROL SYSTEM PERFORMANCE

induced and the spin plane error (θ) was reduced to within the deadzone of 0.5 degree in less than 3 minutes. The system illustrated by figure 24 employed 400 pound thrust reaction jets. Reducing the jet thrust to 100 pounds would lengthen the time to complete the reorientation by a factor of four. No other significant performance changes would occur. The computer record indicates the system required 16 pounds of reaction jet juel (I_{sp} = 300 sec) to correct the initial misalignment. The theoretical minimum fuel required to make a 4.5 degree correction is 18 pounds. The 2 pound discrepancy is attributable to simulation and recording inaccuracy.

E. ARTIFICIAL GRAVITY CONTROL SUBSYSTEM

1. General

The gravity control system is required to maintain artificial gravity within 2 percent of the selected value in the operational spinning mode. This control function does not introduce any new or peculiar control problems. A brief discussion follows.

2. Description

Figure 25 presents a block diagram of the gravity control system. The station's centripetal acceleration is measured by a body mounted accelerometer and compared to a manually selected artificial gravity reference. When the station's centripetal acceleration differs from the selected reference level by more than 2 percent the threshold is exceeded and the spin jets fired. The station's spin speed is adjusted until the gravity level is within the threshold. A low pass filter is included to prevent "nuisance" spin jet actuation.

3. Performance.

The gravity control system's operation is not critical and its performance should satisfy the established control requirements.

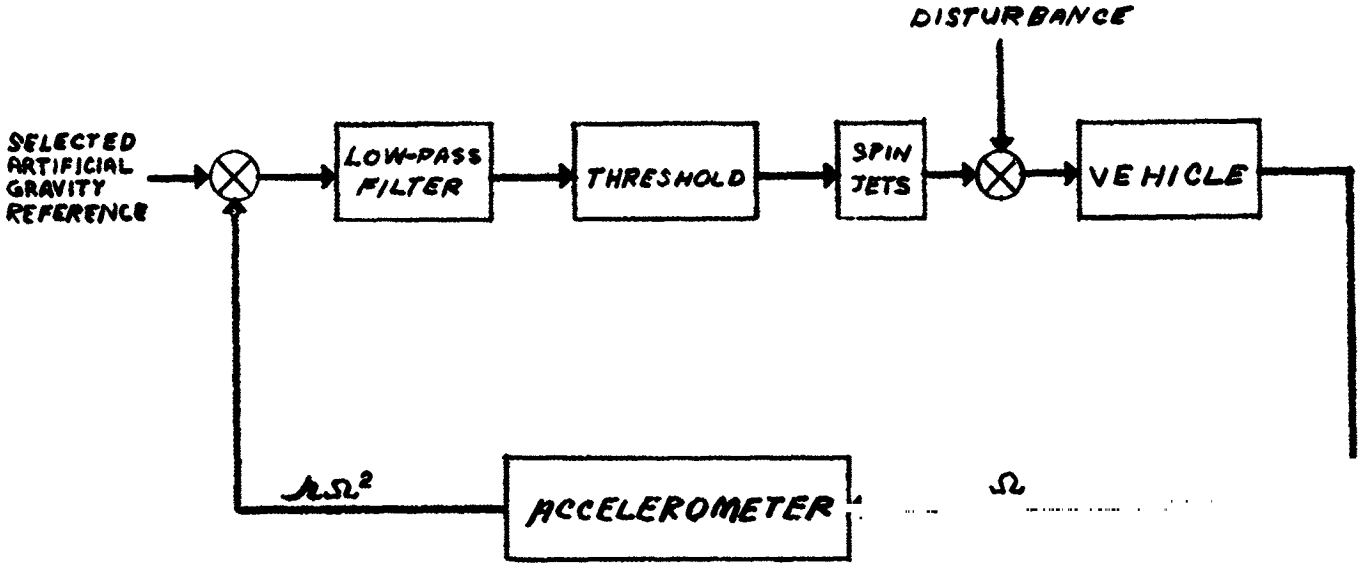

FIGURE 25 SPIN SPEED CONTPOL SYSTEM BLOCK DIAGRAM

SECTION VI

STABILIZATION AND CONTROL DURING TRANSITION MODE

A. DISCUSSION

The transition mode control problem is characterized by a continuous change in vehicle dynamics, and by certain nonlinear phenomena which arise only during this mode of operation. Cable slacking is an important example of the latter. Accordingly, a special nonlinear simulation was developed to study the transition mode control problem.

Mission considerations also affect the design of the transition mode maneuver and, therefore, the design of the control system itself. A reasonable compromise between propellant economy, maneuver time, and vehicle stability must be obtained. The following section considers the selection of a transition maneuver. Paragraph C of this section describes the vehicle dynamics and the computer simulation in some detail. The control system, its performance, and the effect of changes in maneuver parameters on the performance, are discussed in paragraphs D and E.

B. SELECTION OF A TRANSITION MANEUVER

In undertaking the synthesis of a control system for the extension and retraction maneuver, the first requirement was to define the manner of the maneuver. No restrictions or criteria had been established for this study, other than the specification of a nominal operational spinning state. In this state, the spin speed is 0.4 rad/sec and the cable length is 100 ft. The initial problem was, therefore, the definition of a desirable transition maneuver, taking into account the following factors that were considered to be of primary importance:

- Minimization of propellant required for the transition.
- Simplicity of control.
- Dynamic performance during transition.

The nominal transition profile that was established as meeting the requirements imposed by these factors is shown in figure 26, in which spin speed is plotted as a function of separation.

In selecting the particular transition profile defined by figure 26, the initial consideration was propellant economy. Since the effective moment arm of a thruster mounted on one of the vehicle's rigid bodies increases with vehicle separation, it can be appreciated that the transition from the nonspinning state to a spinning state can be most economically performed by making the speed change at the largest possible separation. However, some minimum spin speed must always be maintained to keep the cables taut. The objective of the trade-off, then, is to select a spin speed vs separation program which minimizes propellant consumption subject to the constraint that it provide reasonable vehicle rigidity at all times.

Appendix F contains an exact development of the spin impulse requirements for the general case of transition profiles that involve a linear variation of spin speed with separation. Equations (F-8) and (F-9) show that, for a given minimum spin speed during extension or retraction, the impulse requirement for the total transition is minimized by maintaining spin speed constant during extension or retraction. The resulting spin impulse requirements for the vehicle under consideration are shown in figure 27 as a function of the spin speed during extension or retraction. The cases of spin thrusters located at the mass center of the manned body and four feet further outboard are illustrated. It can be seen from this plot that the selection of the nominal extension/retraction spin speed of 0.04 rad/sec requires only 6.4 percent more impulse than the absolute minimum of 63,600 lb-sec. If this nominal spin speed is changed, the impulse increment with respect to the absolute minimum will change in proportion.

Figure 27 also shows the spin impulse required if the spin thruster is mounted on the booster. A longer effective moment arm is available in this case, and the impulse requirements are reduced correspondingly. There is no conceptual difference in mounting the jets on the booster or the manned body, and only the manned body mounting will be considered for the remainder of the discussion.

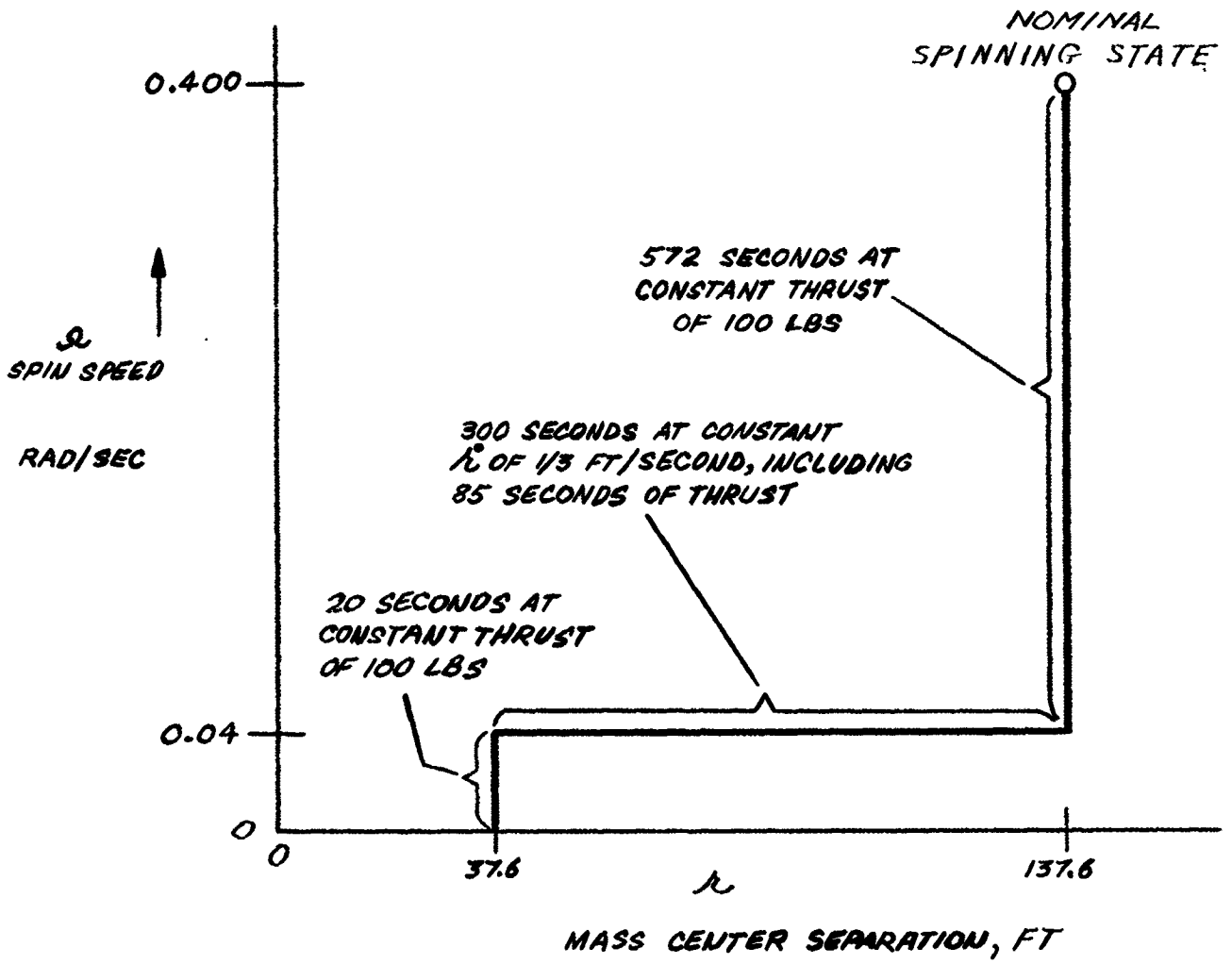

MINIMUM TOTAL TRANSITION TIME IS 892 SECONDS,
INCLUDING 677 SECONDS OF THRUST

FIGURE 26 NOMINAL TRANSITION PROFILE FOR
EXTENSION – RETRACTION MANEUVER

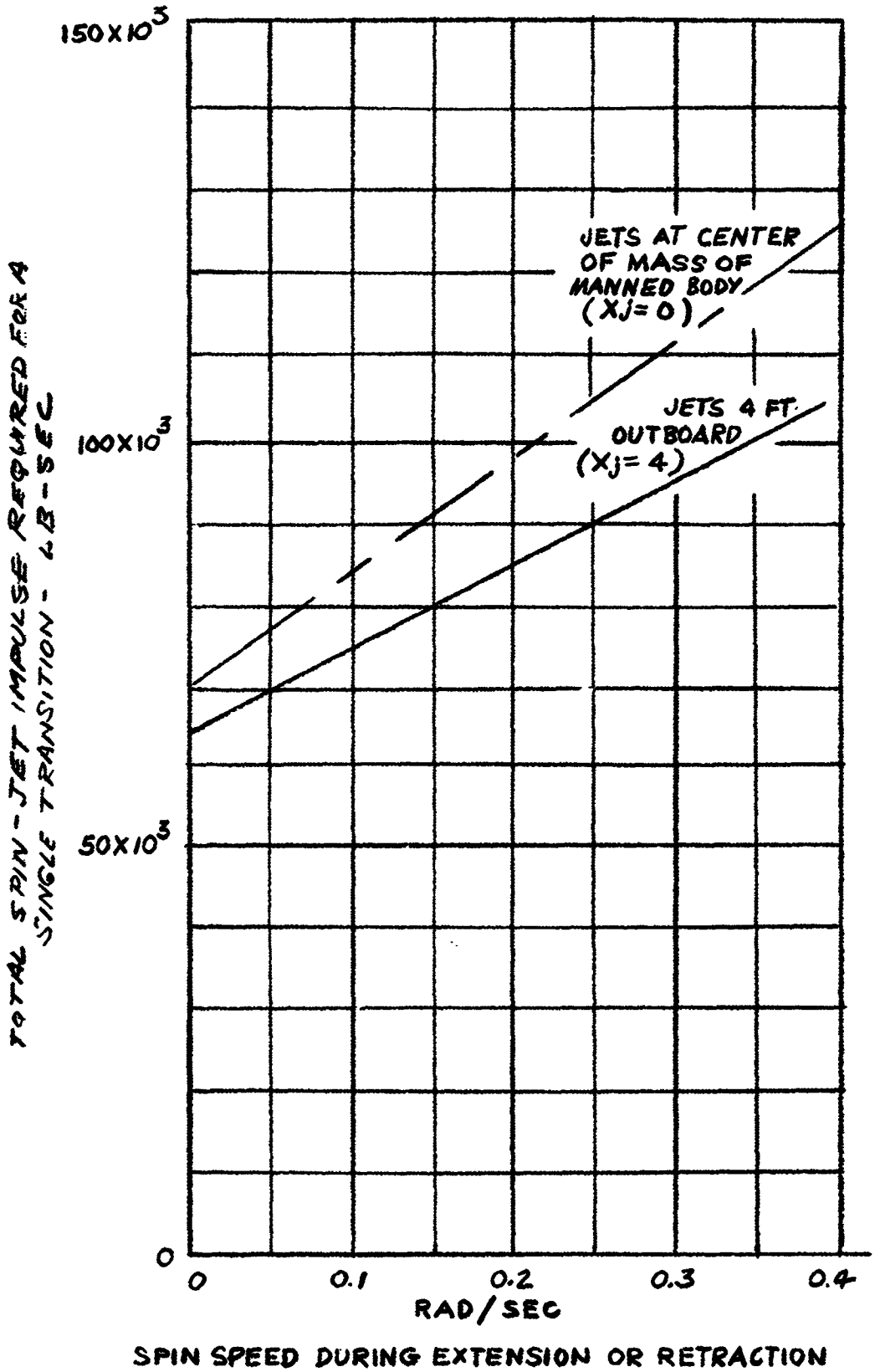

FIGURE 27 TOTAL SPIN–JET IMPULSE REQUIRED FOR A SINGLE TRANSITION VS SPIN SPEED DURING EXTENSION OR RETRACTION

The time required to complete each segment of the nominal transition maneuver has been shown on figure 26. The total transition time shown in figure 26 is slightly less than 15 minutes, of which 5 minutes is spent extending or retracting. It might be considered desirable to reduce the transition time to something on the order of 9 or 10 minutes so that the maneuver could be performed while passing over the continental U.S. This would allow continuous tracking and voice communication. This could be achieved simply by increasing the thruster size so as to reduce the time spent in the constant thrust segments of the transition. A 200 lb thruster would make the over-all time just less than 10 minutes. No significant control problems would be encountered in using the larger thruster.

It should be noted that since the maximum power output required of the cable motor for the nominal extension rate of 1/3 fps is about 0.06 hp, it would be feasible to consider manual operation of the cable deployment mechanism. Higher extension rates might require more power than could be delivered by a human operator.

In summary, then, the following nominal transition maneuver has been selected: The cables will be extended from 0 to 100 ft lengths at a fixed rate, while the spin speed is maintained constant at 0.04 rad/sec. After the vehicle reaches the 100 ft cable length condition, it will be spun to its nominal operational spin speed of 0.4 rad/sec. This maneuver requires only 6 percent more propellant than the absolute minimum, and is within the power delivery capabilities of a human operator.

C. VEHICLE DYNAMICS

1. Dynamic Model

Before proceeding to a discussion of the control system required to implement the transition maneuver, it is necessary to establish the dynamic characteristics of the vehicle in some detail. The dynamics of this nine degree of freedom vehicle during the extension/retraction maneuver are quite complex. Preliminary studies indicated, however, that considerable simplifications could be introduced in the cases of interest here. More specifically, it was found possible to simulate the dynamic effects of primary importance with a four degree of freedom model, and to approximate the cable slacking phenomena with simplified equations.

The ultimate dynamic representation of the vehicle was the four degree of freedom, two dimensional model (restricted to the spin plane) that is illustrated in figure 28. The equations that were developed for this model are presented in appendix E.

The four degrees of freedom were separation, spin speed, and the yaw rotation of each body. Cable slacking could occur either because relative rotations were large enough to relax one cable completely, or because the capsules moved toward one another far enough to slack all cables.

A four cable configuration has been illustrated in figure 28. The cable configuration consists of four parallel cables, symmetrically located between the principal axes so that two of the cables are superimposed on the other two when projected into the spin plane. Obviously, the cable configuration simulated here could equally well be assumed to be a bifilar arrangement with the two cables in the spin plane.

The four cable configuration was selected as typical of those in figure 4. It is somewhat less stiff than the eight cable configuration, and stiffer than the single cable configuration. Preliminary simulations of the single cable configuration were also performed. As would be expected, the yawing motions of the vehicles were approximately three times as large as those obtained with the four cable configuration. The response motions were qualitatively similar, however.

The four degree of freedom spin plane model cannot, of course, predict the pitching and rolling motions of the vehicle. However, only second order coupling exists between the spin plane degrees of freedom and the others. Since disturbances during extension are much greater among the spin plane variables than the others, it was felt that the achievement of acceptable yaw performance would be an adequate measure of success in overcoming vehicle control problems.

Preliminary simulations, including simulation of an eight degree of freedom model which neglected cable slacking, substantiated this position. No pitch or roll excitation due to dynamic changes in these axes were encountered. Other simulations indicated that the jet-induced disturbances of the roll and pitch axes could be neglected for purposes of this study.

2. Cable Slacking Effects

The cable slacking phenomena were simulated by treating each cable as if it were a linear spring when in tension, and assuming that it could

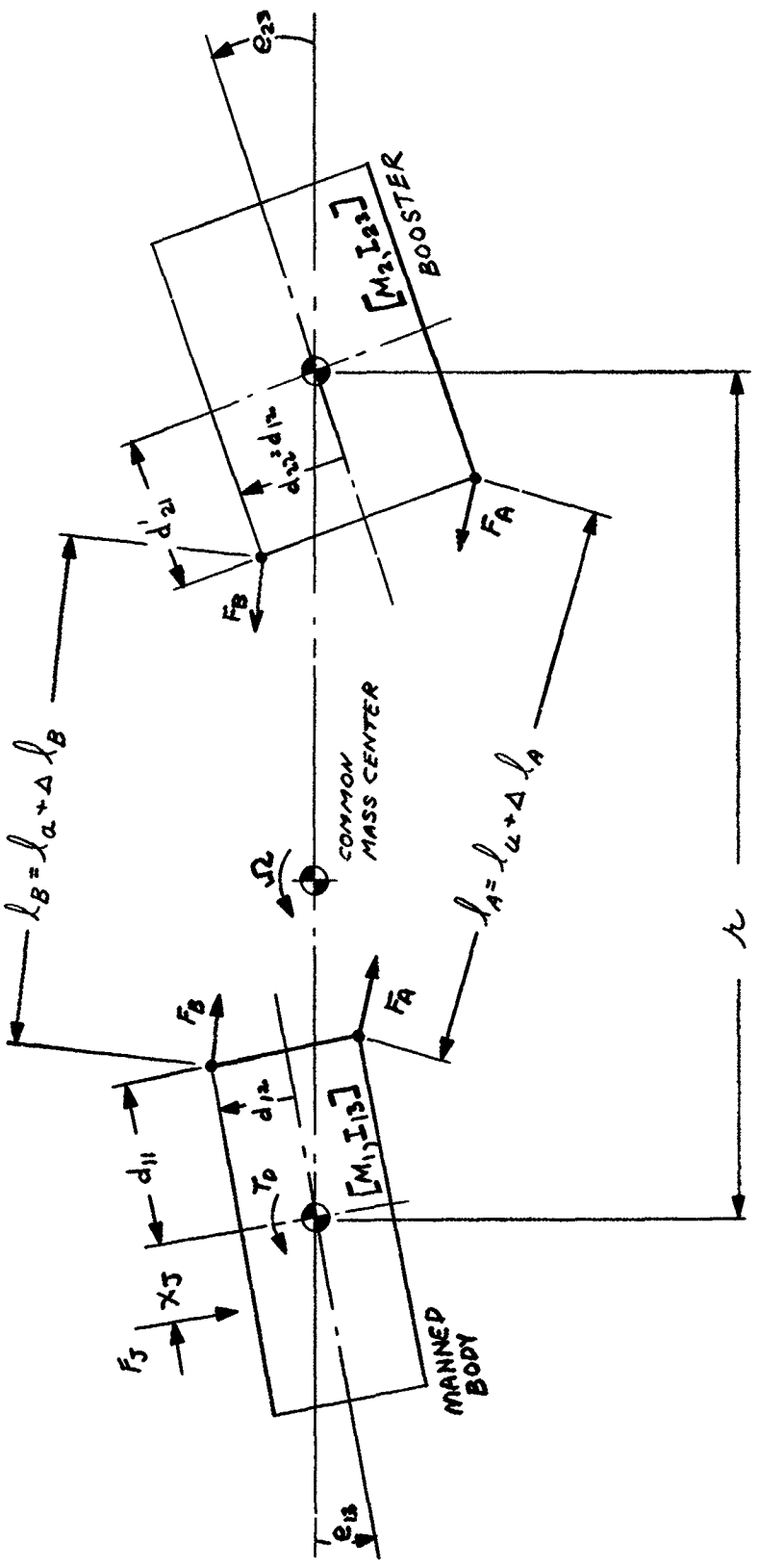

FIGURE 28 EXTENSION/RETRACTION MODEL

support no compressive load. Each cable pair was simulated independently, having a force proportional to elongation when stretched, and supporting no force when slack. A real flexible wire cable would undoubtedly exhibit more nonlinear and less abrupt changes in spring gradient as the tension was decreased to zero. The simulation was therefore probably conservative in its computation of longitudinal cable transients.

In addition, appendix E discusses several simplifications that were made in order to facilitate the computation of the torques exerted by the cables on the manned body and the booster. In general, these simplifications involved assumptions as to the dynamic behavior of the vehicle which were subsequently validated by the results of the analog computer study.

D. CONTROL SYSTEM SYNTHESIS

1. System Analysis

Several problem areas that have a significant effect upon the selection of control system parameters have been identified. These areas are as follow:

- A minimum thruster size is established by the requirement that the extension or retraction be accomplished at constant spin speed. In order to permit this, the rate of change of angular momentum due to operation of the thruster must be greater than that due to the rate of retraction or extension. This relationship can be expressed as:

$$F_J \geq 2M_1 \Omega \dot{r} \qquad (17)$$

where

F_J = spin jet thrust magnitude

M_1 = mass of manned body

Ω = spin speed

$\dot{r}$ = extension rate

This thrust level limit must be computed from the spin speed actually required to operate the rate threshold. The limiting thrust values computed for the nominal control system are +29.3 lb for extension and -35.8 lb for retraction, the difference being

due to the finite threshold level in the jet switching logic. The retraction case is therefore critical in sizing the thruster and especially critical from the stability standpoint. The use of an undersize thruster during retraction would cause the spin speed to diverge steadily. In extending, the undersize thruster would reduce spin speed until equation (17) was satisfied. Several values of thrust were considered in this study. Numerical data relating yaw amplitude to thrust level are presented in section VI paragraph E.

- Thruster location is also of extreme importance. If placed too close to the manned body mass center, an unstable oscillation may develop. This behavior and the criteria for avoiding it are discussed quantitatively in section VI paragraph E below. If the thruster is located further from the center of mass than required for stability, the result will be an increase in the manned body and booster yaw angles excited during the transition.
- The longitudinal cable force transients must be damped in order to avoid complex motions of the rigid bodies. In the absence of damping, the cables will nearly always be slack, except for occasional large transient forces as the bodies rebound from the slacking limit. Slacking will tend to occur if an irreversible cable deployment mechanism is used which gives truly constant cable extension rate. As described in the next section, the cable motor torque-speed characteristic can be used effectively to damp these longitudinal transients.

2. Description of Nominal System

Figure 29 shows a transfer function block diagram of the nominal system. It includes a spin control system and a cable control system. The spin control system consists of a rate gyro mounted on the manned body, a threshold detector, and spin thrusters (reaction jets) mounted on the manned body. The cable control system consists of a servo motor driving the cable drum, a tachometer to provide rate feedback signals, and control electronics.

To perform an extension maneuver, the spin speed controller is activated and the vehicle is spun up to 0.04 rad/sec. The cable rate controller is then activated, and cable begins to pay out as the centrifugal force pulls the cable off the drum. Neglecting transients for the moment,

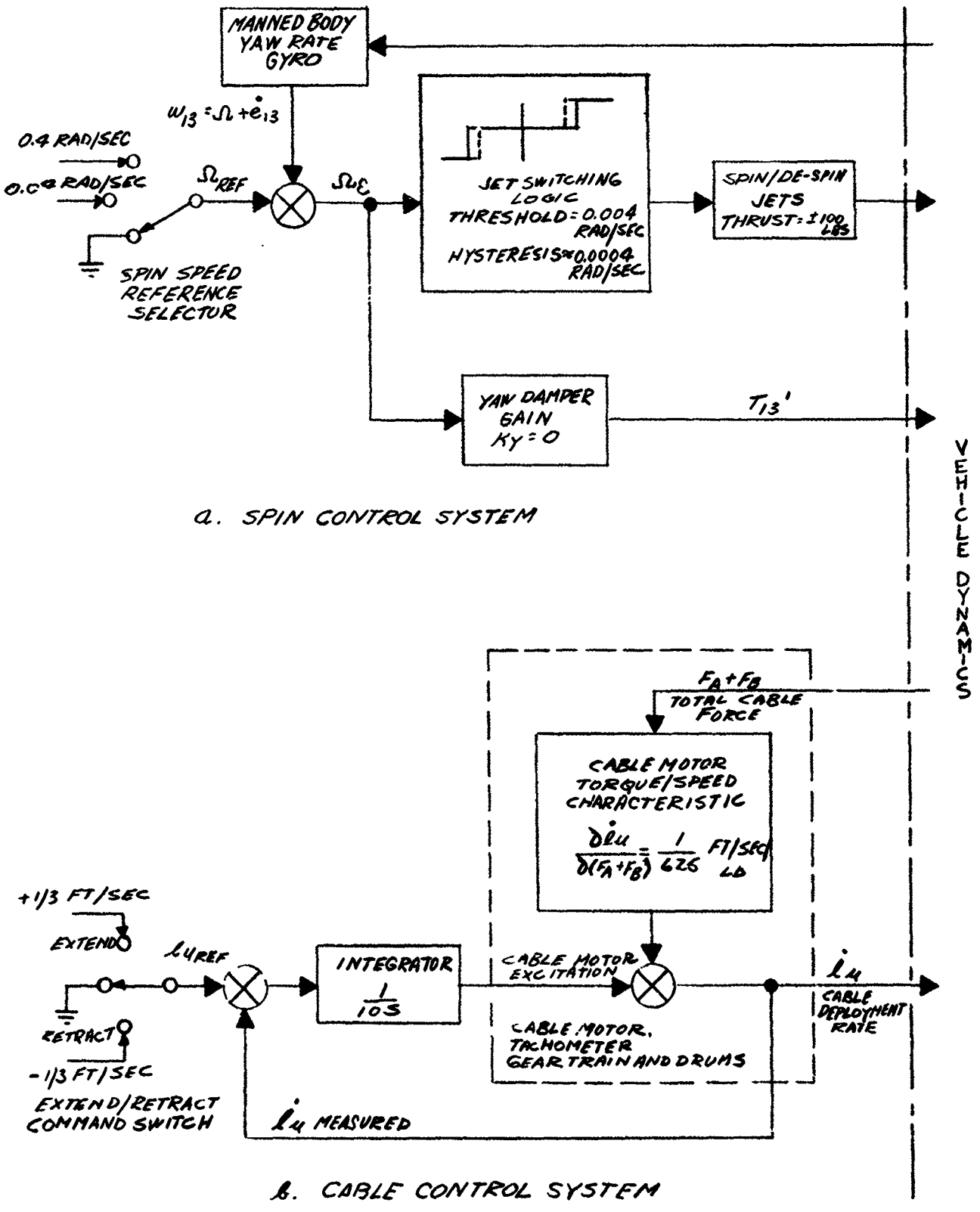

FIGURE 29 NOMINAL TRANSITION CONTROL SYSTEM USED IN ANALOG COMPUTER STUDY

the spin speed is held constant during the entire extension maneuver. As the cable extension increases, the centrifugal force builds up, and attempts to pull cable off faster. However, the integrated speed error signal which is applied to the cable servo motor also builds up so that the motor bias torque increases. The net result is that the long term cable extension rate holds nearly constant. Damping of the longitudinal cable force transients (due, for example, to cable slacking) is provided by the back EMF characteristics of the motor. Alternatively, tachometer feedback can be employed to provide short term damping.

During the analog computer program, the spin speed reference selector and extend/retract command switches shown in figure 29 were manually operated. In a real control system a number of interlock functions would presumably be provided for safety and possibly for automatic sequencing. With this change, it is believed that the control system of figure 29 will adequately fulfill the transition maneuver requirements.

3. Performance of Nominal System

Typical vehicle behavior with the nominal control system during the extension phase of the transition is illustrated by figure 30, which presents time histories of several variables in a typical analog computer run. This run started with an initial condition of 0.04 rad/sec spin speed and zero vehicle separation. (It has been assumed that the mating mechanism requires a cable length of two feet at zero separation.) The 1/3 ft/sec extension rate command was initiated and terminated manually. Note that cable slacking phenomena exist for a short period at the beginning of the extension, after which cable force variations are quite well behaved. Since the relative yaw angle between booster and manned body is small, the two bodies remain almost parallel. The maximum yaw amplitudes are less than 3.5 degrees. The vehicle exhibited similar response motion during the retraction maneuver.

As discussed earlier, the system parameters most sensitive to variation from the nominal values are:

- Thruster location.
- Thruster size and cable extension rate.
- Spin speed and spin speed threshold.
- Cable damper parameters.

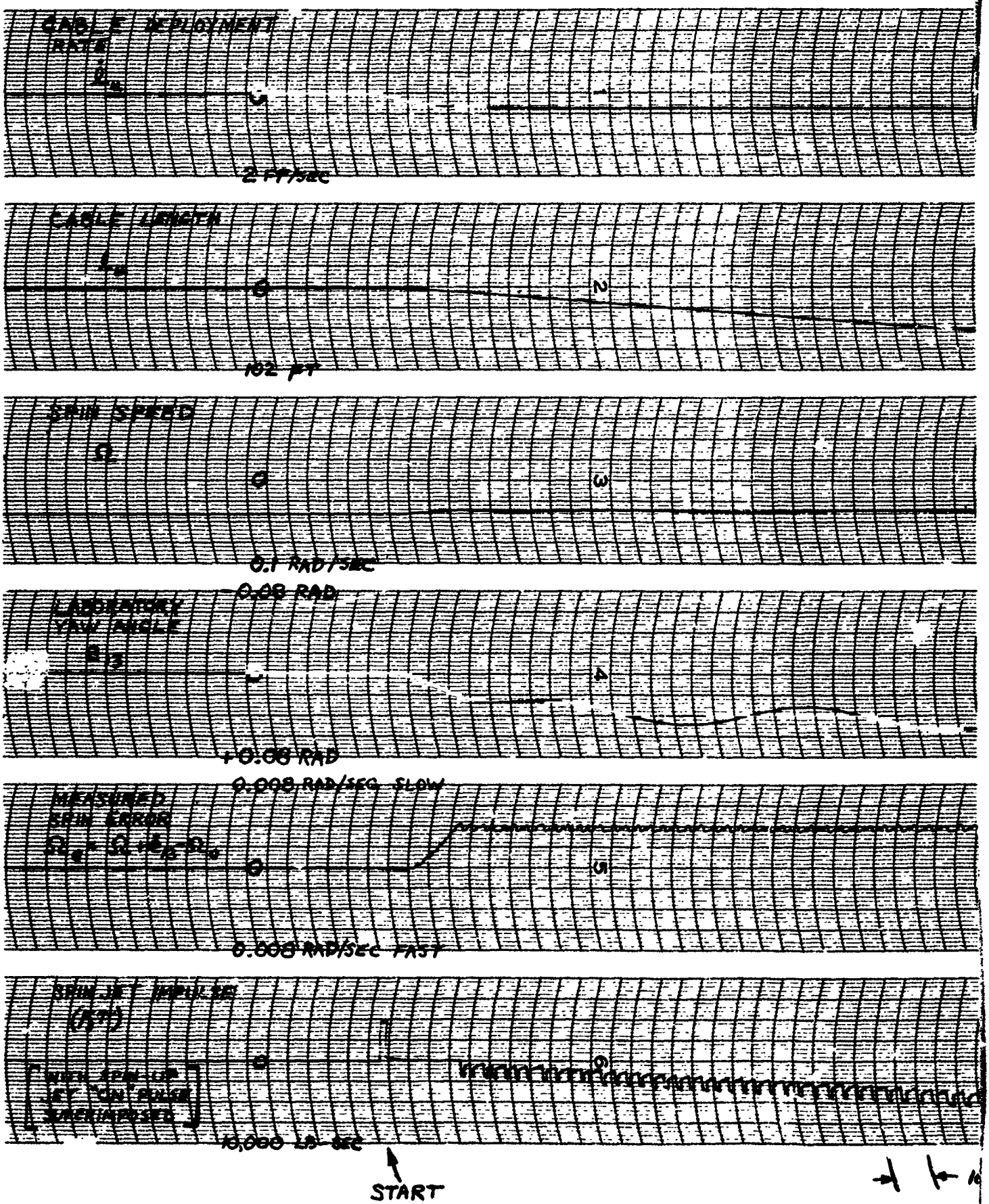
CABLE DEPLOYMENT RATE
$\dot{\ell}_{cable}$
2 FT/SEC
CABLE LENGTH
ℓ_{cable}
102 FT
SPIN SPEED
Ω
0.1 RAD/SEC
0.08 RAD
LAUNCHER YAW ANGLE
β_{12}
+0.08 RAD
0.008 RAD/SEC SLOW
MEASURED SPIN ERROR
$\Omega_{meas} = \Omega_{actual} - \Omega_{desired}$
0.008 RAD/SEC FAST
SPIN JET IMPULSE (ΔT)
(WHEN SPIN-UP JET "ON" PULSE SUPERIMPOSED)
10,000 LB-SEC
START
t
1
2
3
4
5
6

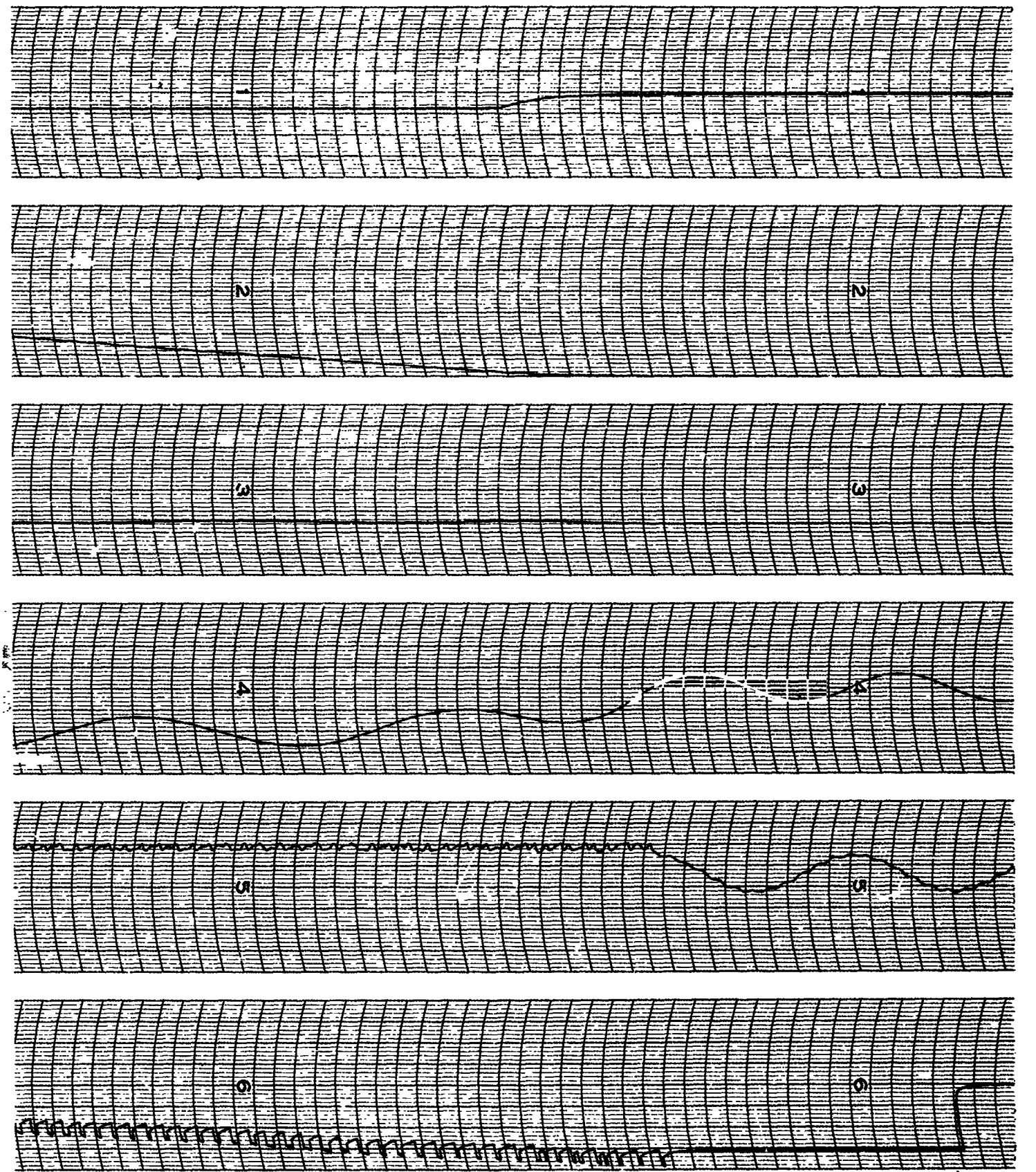

1 SEC

RESET IMPULSE

START

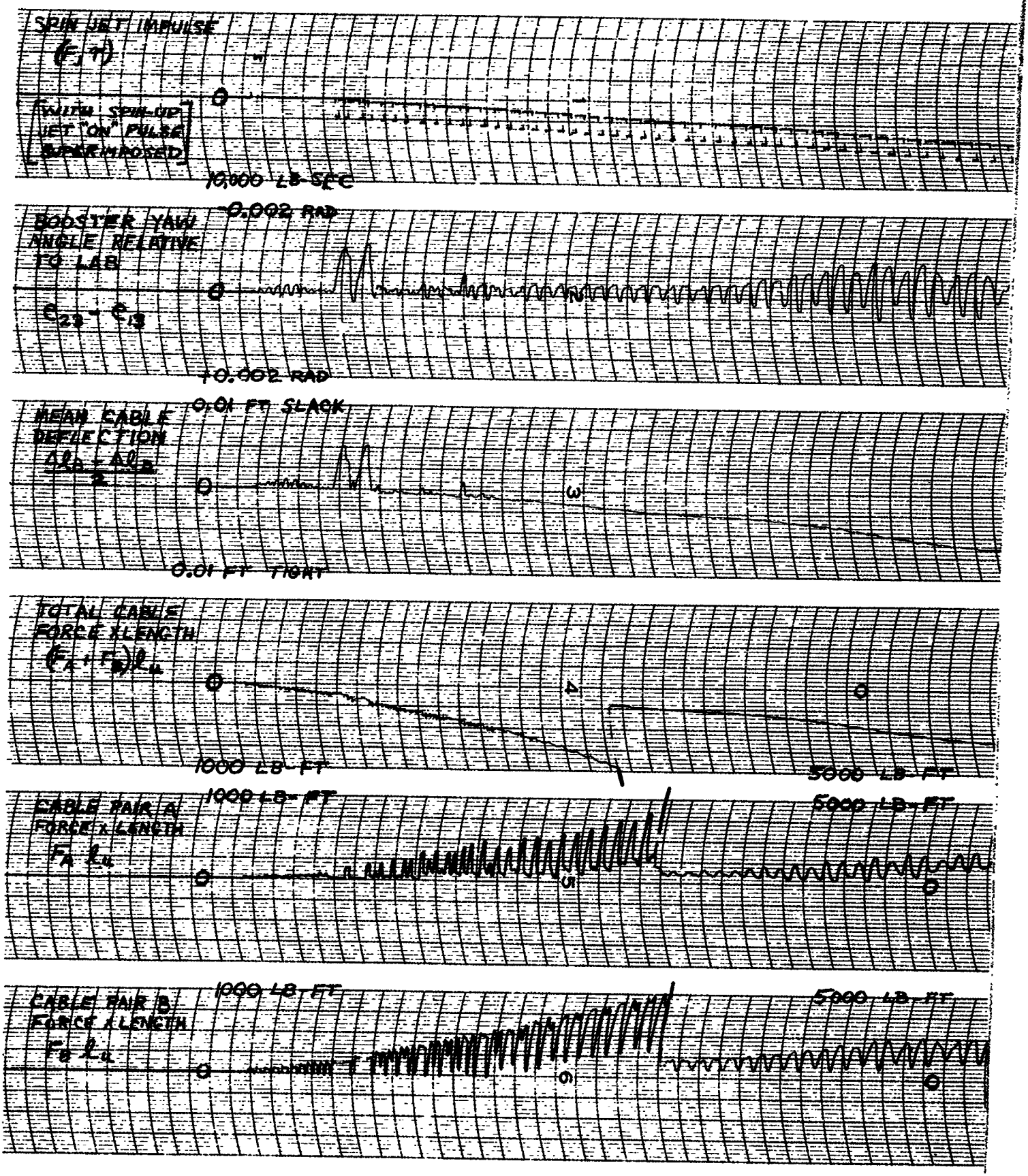

NOTE:
THESE ARE SIMULTANEOUS RECORDS.
THE SPIN-JET IMPULSE CHANNELS MAY BE USED FOR CORRELATING THE TIME SCALES

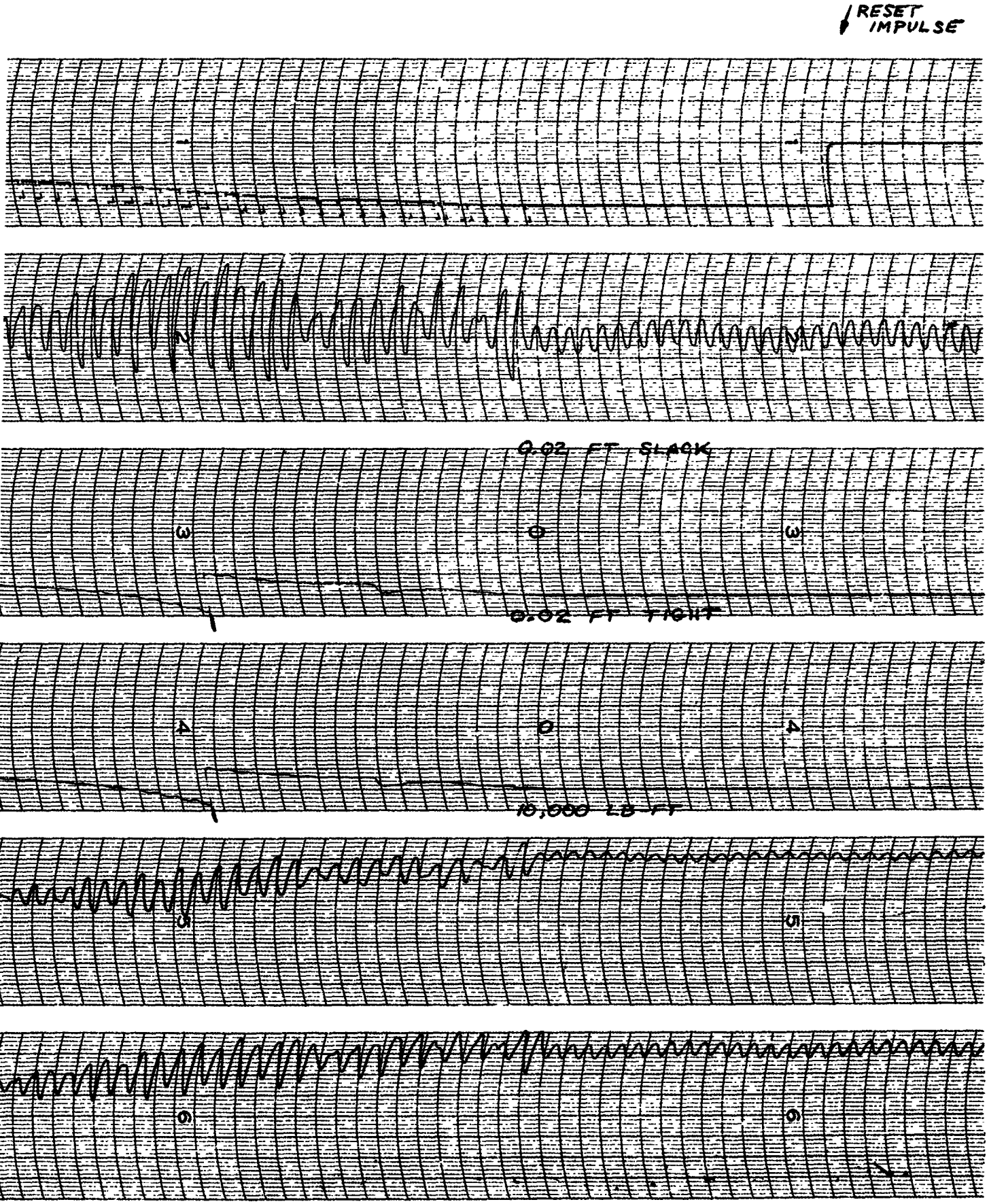

FIGURE 30 TRANSITION CONTROL SYSTEM PERFORMANCE

The following paragraphs discuss the quantitative effect of variations in each of these.

E. PARAMETRIC ANALYSIS

1. Effect of Variations in Thruster Location and Yaw Damper Gain

Computer results indicate that a spin speed instability can exist and that locating the thrusters outboard of the manned body center of mass will improve the stability. Alternatively, a yaw damper could be used to stabilize the vehicle. In order to better understand this instability, the dynamics of a similar linear system were studied. The following assumptions were made in order to simplify the analysis:

- The analysis was limited to consideration of the two yaw degrees of freedom, and the spin speed degree of freedom.
- Thruster force was assumed to be proportional to the manned body rate gyro signal, that is:

$$F_T = K_F \left[\Omega_{REF} - (\Omega + \dot{e}_{13}) \right] \qquad (18)$$

  where K_F is a constant.
- A linear yaw damper acting on the manned body was assumed such that the damper torque output was:

$$T_{13}' = K_Y \left[\Omega_{REF} - (\Omega + \dot{e}_{13}) \right] \qquad (19)$$

- Two limiting cases were considered to determine the effects of cable slacking on the stability limit. In the first, it was assumed that the cables were so stiff that the manned body and booster were coupled by pin-jointed struts in yaw. This represents the situation when no cable slacking occurs. In the second case, it was assumed that the booster exerted no moment on the manned body. These two cases will be referred to as the fully coupled and zero coupled cases respectively.

Application of these assumptions to the equations of motion given in appendix E yields a third order characteristic equation for each coupling case. By employing Routh's stability criteria, the following conditions on

thruster offset distance are obtained for system stability. They have been evaluated for the critical case of zero vehicle separation, at which point the cables are two feet long.

- For the fully coupled case the stability limit on jet offset, X_J, is:

$$X_J \geq \frac{I_{13}+I_{23}}{M_1 r} - \frac{K_Y}{K_F} \qquad (20)$$

$$X_J \geq 5.38 - \frac{K_Y}{K_F} \quad FT$$

- For the zero coupled case the stability limit is:

$$X_J \geq \frac{I_{13}}{M_1 r} - \frac{K_Y}{K_F}$$

$$X_J \geq 3.78 - \frac{K_Y}{K_F} \quad FT \qquad (21)$$

An attempt to correlate these theoretical stability limits with analog computer results can be made if the thruster gain K_F can be evaluated for the actual control system. This has been done by assuming that the effective gain was that at the threshold:

$$K_f = \frac{\text{Thruster Force Level}}{\text{Switching Logic Threshold}} = \frac{100}{0.004} = 25{,}000 \ \frac{LB}{rad/sec} \qquad (22)$$

The theoretical stability limit and the computer results are plotted in figure 31. It can be seen that the zero coupled case closely represents the actual results. This is probably due to the fact that the fully coupled approximation is valid only until cable slacking occurs, after which the zero coupled case is a better model. Since at low extension cable slacking occurs after very small yaw oscillations, the range where full coupling is obtained can be neglected. It appears, then, that a stability limit does exist relative to spin thruster location, and that this stability limit can be predicted by simplified linear analysis.

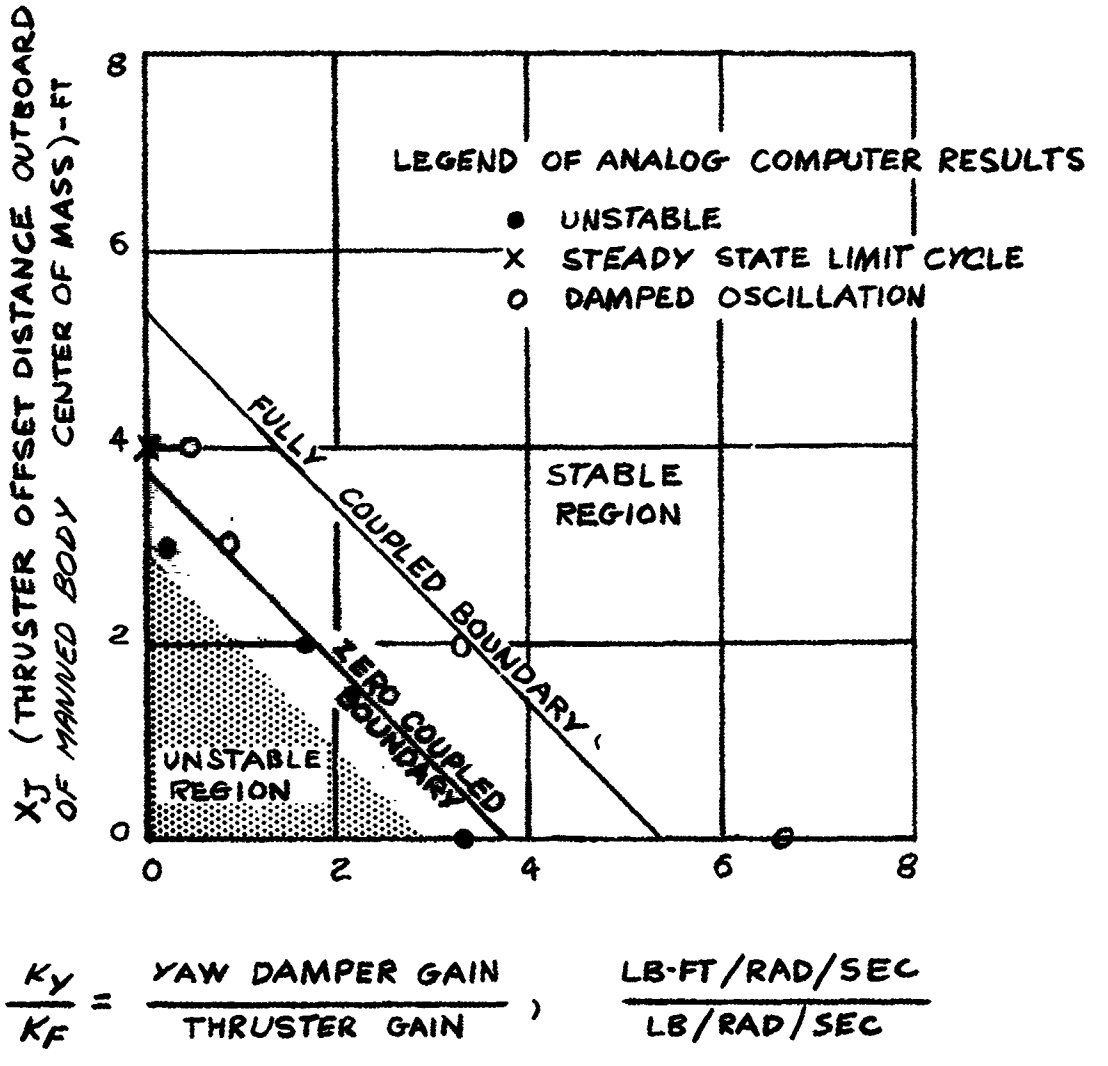

FIGURE 31 EFFECTS OF THRUSTER LOCATION AND YAW DAMPER GAIN ON SYSTEM STABILITY

Computer results also indicate that it is undesirable to locate the jet too far outboard, even though the system is stable in this instance, because the peak yawing angles become quite large. Table 26 shows the relationship between peak response angle and thruster location.

TABLE 26

EFFECT OF JET LOCATION ON PEAK MANNED BODY YAW ANGLE

Jet Distance Outboard of Mass Center (ft)	Manned Body Peak Yaw Angle In Extension (degrees)	Comment
4	3.4	Vehicle unstable for jet located less than 4 ft from mass center.
8	5.7	

As indicated by the linearized analysis, the vehicle can also be stabilized by increasing the yaw damper gain. However, an extremely large yaw damper would be required to have any effect, and therefore, this does not appear to be a feasible method of improving stability. It is much easier to move the jet.

2. Effect of Variations in Thruster Size and Extension Rate

Computer results indicate that thruster size has little effect upon extension/retraction performance unless the lower limit specified in equation (17) is exceeded. Table 27 shows the effect of changing the thruster size in the nominal system.

TABLE 27

EFFECT OF THRUSTER SIZE ON MANNED BODY YAW ANGLE

Thruster Size (lb)	Peak Yaw Angle in Extension (degrees)	Comment
25*	2.3	*The 25 lb thruster produces divergent spin speed behavior in retraction.
50	2.7	
100	3.4	
200	3.7	

Thruster size is interdependent with extension rate since the thruster lower stability limit is proportional to extension rate. The major effect of extension rate on performance is seen in the yawing amplitudes. The

computer results indicate that the yaw of each body is approximately proportional to extension rate. If the linear system analysis described in previous paragraph 1 is extended by assuming that:

- Yaw damper gain, $K_y = 0$ (23)
- Thruster offset distance, $X_J = \dfrac{I_{13} + I_{23}}{M_1 r}$ (24)

a solution for the peak yaw angle resulting from a step disturbance in extension rate can be obtained as:

$$\left(\frac{e_{13}}{\dot{r}}\right)_{MAX} = \frac{4(r - d_{11} - d_{21}')}{\Omega r (d_{11} + d_{21}')\left(1 + \frac{M_T r^2}{I_{13} + I_{23}}\right)} \qquad (25)$$

From this equation, the ratio of peak yaw angle to extension rate was evaluated for the nominal system and is shown in figure 32 as a function of vehicle separation. Data points for yaw peaks from computer records for both the nominal extension rate and for a slower rate are plotted in this figure. The correlation of these points with the linear analysis (the lower curve of figure 32) becomes poorer as separation increases. This is probably due to the fact that the computer results are for a system with a fixed four foot thruster offset while the linear analysis implies a thruster offset that decreases with separation (see equation (24)). In order to see this effect, the linear analysis values were multiplied by a correction factor:

$$\frac{\text{COMPUTER } X_J}{\text{ANALYSIS } X_J} = \frac{4 M_1 r}{I_{13} + I_{23}} \qquad (26)$$

The results are plotted as the upper curve of figure 32, which follows the shape of the computer data very well and provides a conservative estimate of the peak yaw angle.

It should be noted, in discussing thruster size and extension rate effects, that if the thruster were located at the center of mass of the laboratory, and the thrust level precisely met the limit of equation (17), that is, if

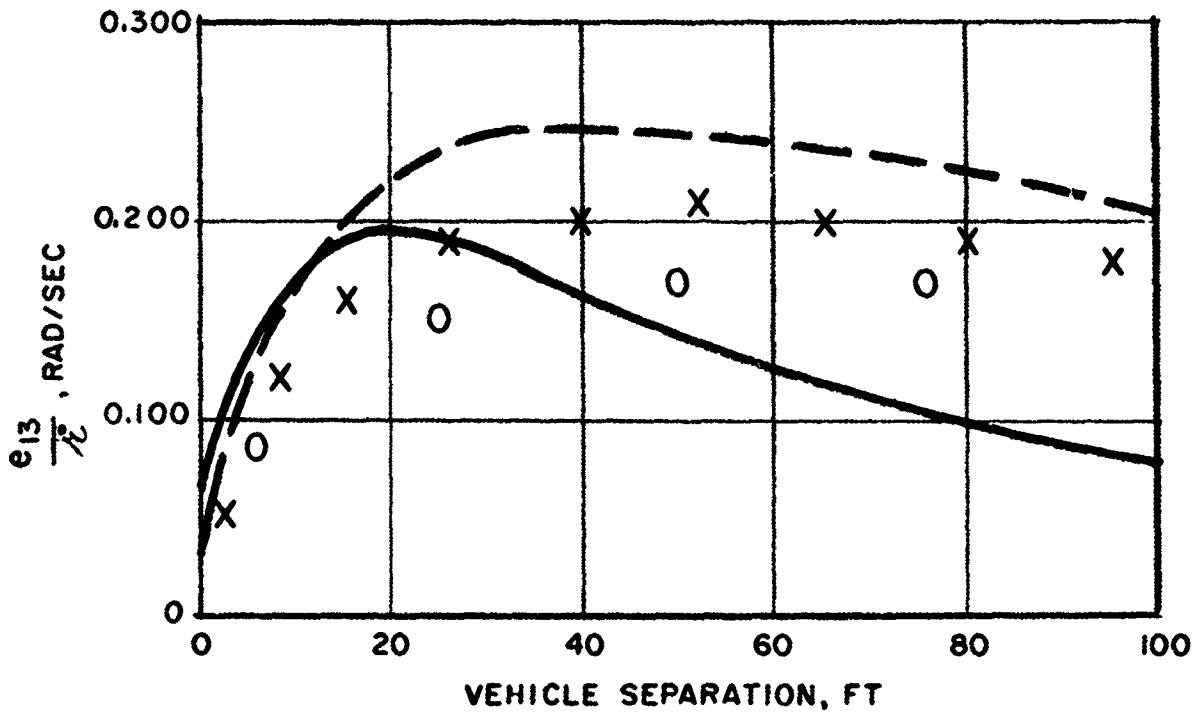

LEGEND:

——— PEAK $e_{13}/\dot{r}$ (FROM LINEAR THEORY THRUSTER AT FULLY COUPLED STABILITY BOUNDARY)

– – – [PEAK $e_{13}/\dot{r}$] x $\left(\frac{4 M i r}{I_{13}+I_{23}}\right)$

O — COMPUTER DATA AT 1/3 FPS EXTENSION (NOMINAL)

X — COMPUTER DATA AT 1/6 FPS EXTENSION

FIGURE 32 EFFECT OF EXTENSION RATE VARIATION

$$F_J = 2M_1 \Omega \dot{r} \qquad (27)$$

then extension and retraction could theoretically be performed without yaw disturbances or changes in spin speed. However, the problems inherent in computing and generating the required thruster force level make this approach to transition control impractical.

3. Effect of Variations in Spin Speed and Spin Speed Threshold

There would be two major effects of varying the spin speed reference level used during the extension or retraction phase of the transition. First, the impulse requirements would change linearly, as shown in figure 27. Second, the peak yaw angle would vary inversely with spin speed as indicated by equation (25).

The spin speed threshold also has a minor effect on yawing performance, since the actual average spin speed during extension or retraction differs from the nominal setting by the threshold value. The average speed is lower than nominal during extension and higher during retraction. If a yaw damper were being used to meet the stability requirements shown in figure 31, then the threshold level would presumably affect the stability by changing the effective thruster gain. Since this was not the case with the nominal system, the only effects detected in the computer results were the small changes in yawing performance.

4. Effect of Variation in Cable Damper Parameters

Variation of the cable motor torque-speed characteristic shown in figure 29 produces a proportional change in longitudinal cable force damping. The damping ratio can be expressed as:

$$\zeta_c = \frac{\partial \dot{l}_\mu}{\partial F} \sqrt{\frac{k M_T}{2 l_\mu}} \qquad (28)$$

For the nominal system this can be evaluated as:

$$\zeta_c = \frac{11.1}{\sqrt{l_\mu}}$$

$$\zeta_c = \begin{matrix} 7.85 & \text{fully retracted} \\ 1.10 & \text{fully extended} \end{matrix} \qquad (29)$$

Note that the longitudinal cable oscillations will be overdamped throughout the maneuver whenever the cables are taut. This means, for example, that if the vehicle hits the end of slack cables it will not rebound and cause the cables to go slack again. Thus the motor torque speed characteristic serves to cushion cable bounce effects.

The integral feedback loop around the cable motor that is shown in figure 29 serves to maintain the average cable rate equal to the commanded rate. It also smooths the step cable rate command which initiates an extension maneuver so that the cables do not initially go slack. In order to prevent initial slacking, the initial acceleration of the cable motor should be less than the relative acceleration of the two bodies which would occur if the cables slacked. This imposes a restriction on the integrator gain of the system:

$$\text{INTEGRATOR GAIN}, \frac{1}{\tau} < \frac{r\Omega^2}{\text{I.F.}}$$

or, at minimum separation,

$$\frac{1}{\tau} < 0.18 \quad \text{sec}^{-1} \qquad (30)$$

F. CONCLUSIONS

It has been demonstrated that extension and retraction of the cable-coupled space station are feasible. State of the art components can be used in the transition control system, and no insurmountable problems appear to exist. There is considerable leeway in the selection of maneuver parameters such as spin speed and extension rate, and in the selection of control system parameters such as thruster size and jet location. Although stability limits exist, these can be predicted by simplified analysis, and alleviated by proper control system design.

Section VII

COMPATIBILITY WITH NONSPINNING MODE CONTROL

A. INTRODUCTION

It is expected that a significant portion of the mission of a cable-coupled space station will be spent in a retracted, nonspinning condition. It is obvious, therefore, that nonspinning configuration control requirements will be a significant factor in the design of the vehicle control system. However, the degree of influence on the control system depends on the exact vehicle configuration, the orientation of the vehicle in orbit, and the specific maneuvering control required in the nonspinning mode. Although the scope of the study did not include detailed consideration of nonspinning mode requirements, a preliminary evaluation was made. It was concluded that the control concepts adopted for the spinning mode will be basically compatible with zero-g control requirements, but that, in general, different sensing equipment will be needed. The same actuators can be employed in both modes. However, the actuator sizing requirements for nonspinning control depend strongly on mission definition. Accordingly, no general conclusion can be stated regarding the suitability of the actuators sized for use in the spinning mode.

For a mission such as that of the Manned Orbiting Laboratory (MOL), the nonspinning control requirements are not particularly stringent. Pointing accuracy tighter than about 0.5 degree is not likely to be specified, although if military missions are incorporated, more accurate pointing may be desirable. The most rapid dynamic response could quite possibly be required in the docking phase, assuming cooperative procedures are adopted. Even here, it is unlikely that response times shorter than about a minute or maneuvering rates higher than about 0.05 degree per second would be required.

A key factor in achieving control efficiency in the nonspinning mode is the selection of a vehicle orientation that minimizes disturbance torques. These disturbances—mainly gravity gradient and aerodynamic effects—can be very significant. In fact, they will determine the size of the control system actuators if certain vehicle orientations are employed.

B. ACTUATOR SIZING CONSIDERATIONS

Two possible orientations illustrate the range of disturbance effects which might be encountered. The first of these, solar orientation, has the desirable feature of allowing the solar panels to remain fixed with respect to the vehicle body. A negligible amount of propellant is expended in tracking the sun line motion in inertial space in this case, but the amount of propellant required to overcome gravity gradient and aerodynamic torques is quite large.

The other orientation used for illustration is what has been termed "belly down." Here, the long vehicle axis is held in the orbital plane and aligned with the local horizontal. Such an orientation minimizes disturbing torques. Gravity gradient torques are essentially zero, provided the oriented axes are principal axes. In the "belly-down" orientation, aerodynamic torques are small but not quite zero. The solar panels will produce cyclic aerodynamic torques of magnitudes depending on their area, angle-of-attack, and location with respect to the vehicle mass center. The vehicle body itself will also experience some cyclic torques caused by variation in angle-of-attack as a result of the rotation of the earth's atmosphere relative to the orbital plane. However, for this orientation, aerodynamic torques are really only significant at the lower orbital altitudes and can be minimized by appropriate vehicle design.

Appendix H summarizes the effects of gravity gradient torques acting on a solar-oriented nonspinning vehicle. Momentum storage requirements, evaluated for the most demanding conditions, are seen to be quite significant. In fact, if this orientation were adopted, these storage requirements, which exceed the spinning mode demands, would size the control actuators.

The effect of aerodynamic torques on a solar oriented vehicle is also considered in Appendix H. These are a direct function of the vehicle configuration and will be influenced by size and mounting arrangements of external equipment, such as solar panels. The computations of

Appendix H, which are based on an idealized, cylindrical vehicle, indicate that the momentum storage capacity required to overcome aerodynamic torques is comparable to the gravity gradient requirements. Thus it can be seen that if the nonspinning vehicle is solar-oriented, nonspinning mode requirements will probably size the control actuators.

As stated earlier, gravity gradient and aerodynamic torques will be small in the "belly-down" orientation. However, significant momentum storage capacity may still be required to maneuver the vehicle. Due to the large vehicle inertias, even relatively modest maneuvering rates require considerable angular momentum storage capacity. For example, a maneuvering rate of 0.05 degree per second requires as much storage capacity as do the major disturbances in the solar orientation (Appendix H). A tradeoff of maneuvering control concepts will be needed after all mission requirements are assembled to determine the best division of control between momentum storage devices and reaction jets. If maneuvers are infrequent enough, it may prove more efficient to use reaction jet control for all but the slowest maneuvers.

C. ACTUATOR COMPATIBILITY

The combination of a two degree of freedom control moment gyro for pitch and roll and a reaction wheel for yaw, as recommended for the spinning mode, can also furnish satisfactory nonspinning control. This arrangement permits alignment of the nominal gyro spin axis and the reaction wheel spin axis normal to the orbital plane if a "belly down" orientation is used and thus avoids the continuous interchange of angular momentum required with orthogonal inertia wheel systems.

In the nonspinning mode, a single control moment gyro has the disadvantage of producing cross-coupling into the reaction wheel axis whenever the gyro is precessed off null. Since added reaction wheel storage capacity would be needed to counteract this cross-coupling effect, a better scheme might be to use two smaller control moment gyros spinning in opposition to cancel the cross-coupling torques. Further study is needed to determine whether resultant improved performance justifies the extra complexity associated with a dual gyro approach.

If a "belly-down" orientation is employed and the vehicle is designed to minimize aerodynamic disturbances, momentum storage required for adequate zero-g control will be small, and the storage devices will be sized by spinning mode control demands. Other nonspinning orientations,

such as solar pointing, call for momentum storage capacities exceeding those of the spinning mode control system.

D. SENSOR COMPATIBILITY

If the same attitude rate sensor are to be employed for both spinning and nonspinning stabilization, a large dynamic range will be required. The nonspinning rate sensors must be of a moderate inertial quality and be able to sense rates below 0.001 degree per second whereas autopilot grade rate gyros satisfy the spinning-mode performance requirements. Even though it is possible to build a gyro with the necessary range, it might prove better to use separate sensors for the two functions, especially in the yaw axis where the gyro range must be adequate to cover the maximum spin speed.

Several additional control sensors will be needed for zero-g orientation measurements. These include earth horizon and orbit plane sensors for the "belly-down" orientation and a sun sensor for the solar orientation. Other supplementary, special-purpose sensors may be needed for initial acquisition of the appropriate references. As the control system design progresses, it may be advantageous to combine orientation sensing functions for both spinning and nonspinning modes into single instruments; however, for the present, the divergence in sensor characteristics makes it desirable to consider the sensors to be separate.

SECTION VIII

CONTROL SYSTEM DESCRIPTION

A. INTRODUCTION

The preceding sections of this report have developed control techniques applicable to the spinning modes of the flexible, spinning space station. This section shows how the individual subsystems fit together into a control system. In keeping with the emphasis of the study, nonspinning control problems are considered only to the extent of insuring equipment compatibility.

Weight, volume and power estimates are presented for the nominal system. The effect of changes in control system performance specifications, and in vehicle and mission parameters, are also presented.

B. SYSTEM OPERATION

Figure 33 shows the control system block diagram for the spinning modes of operation. The spin mode control functions include extension/retraction, spin control, rate stabilization, dynamic balancing, and spin plane orientation.

For purposes of illustration, all switches shown in figure 33 are considered to be manually operated. In general, mission mode selection will be a manual function and all gain changes and subsystem switching can be interlocked with the mode selection. Figure 33 is drawn with all switches in the spin mode position. Switch positions are labeled according to the three basic modes of spin, nonspin, and extend/retract (transition). Unlabeled positions refer to modes not indicated in the labeled positions.

Prior to initiating a transition from the nonspinning mode to the spinning mode, the space station is oriented so that the yaw axis is aligned

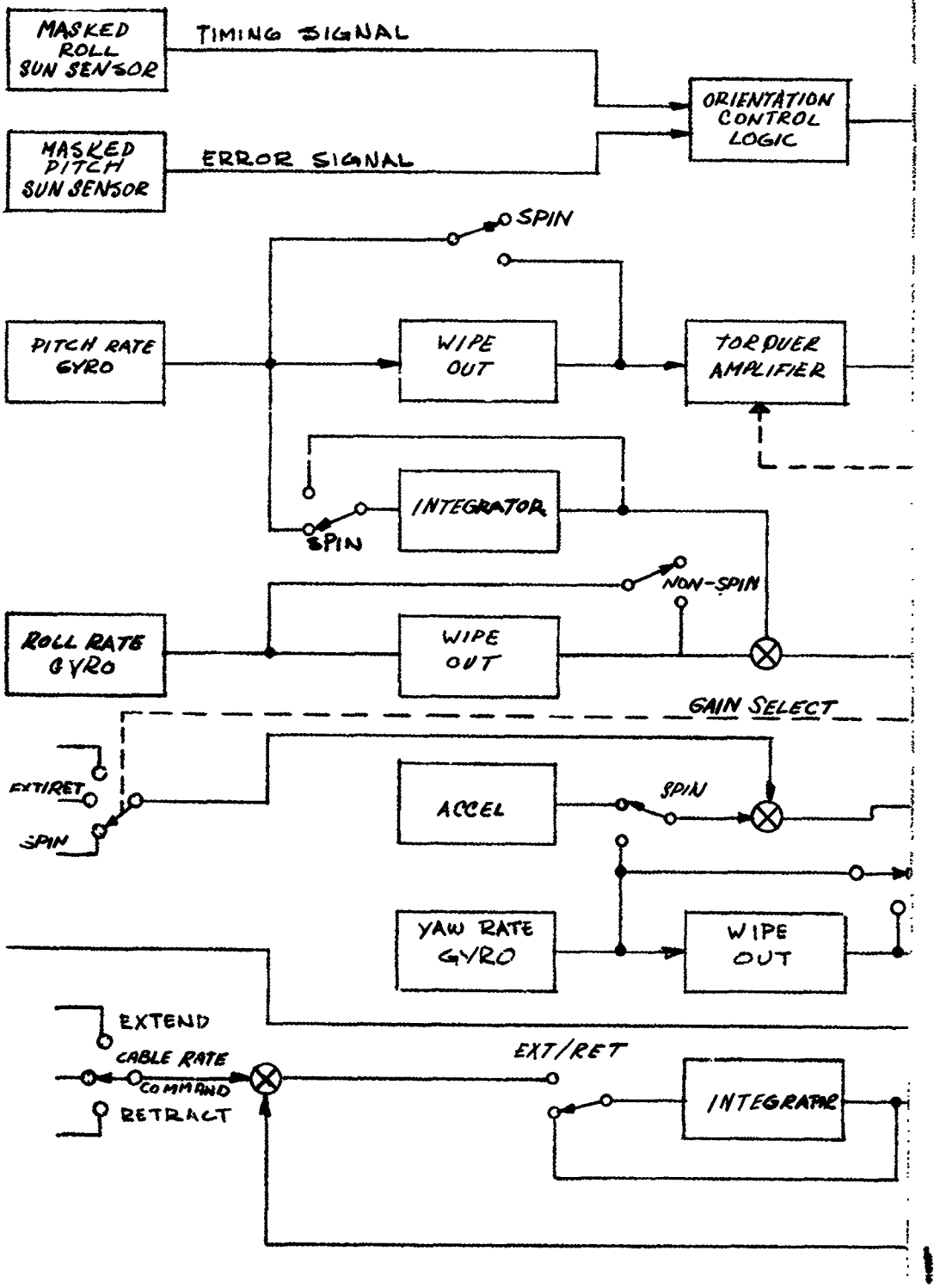
MASKED ROLL SUN SENSOR
TIMING SIGNAL
ORIENTATION CONTROL LOGIC
MASKED PITCH SUN SENSOR
ERROR SIGNAL
SPIN
PITCH RATE GYRO
WIPE OUT
TORQUER AMPLIFIER
INTEGRATOR
SPIN
NON-SPIN
ROLL RATE GYRO
WIPE OUT
GAIN SELECT
EXT/RET
SPIN
ACCEL
SPIN
YAW RATE GYRO
WIPE OUT
EXTEND
CABLE RATE COMMAND
RETRACT
EXT/RET
INTEGRATOR

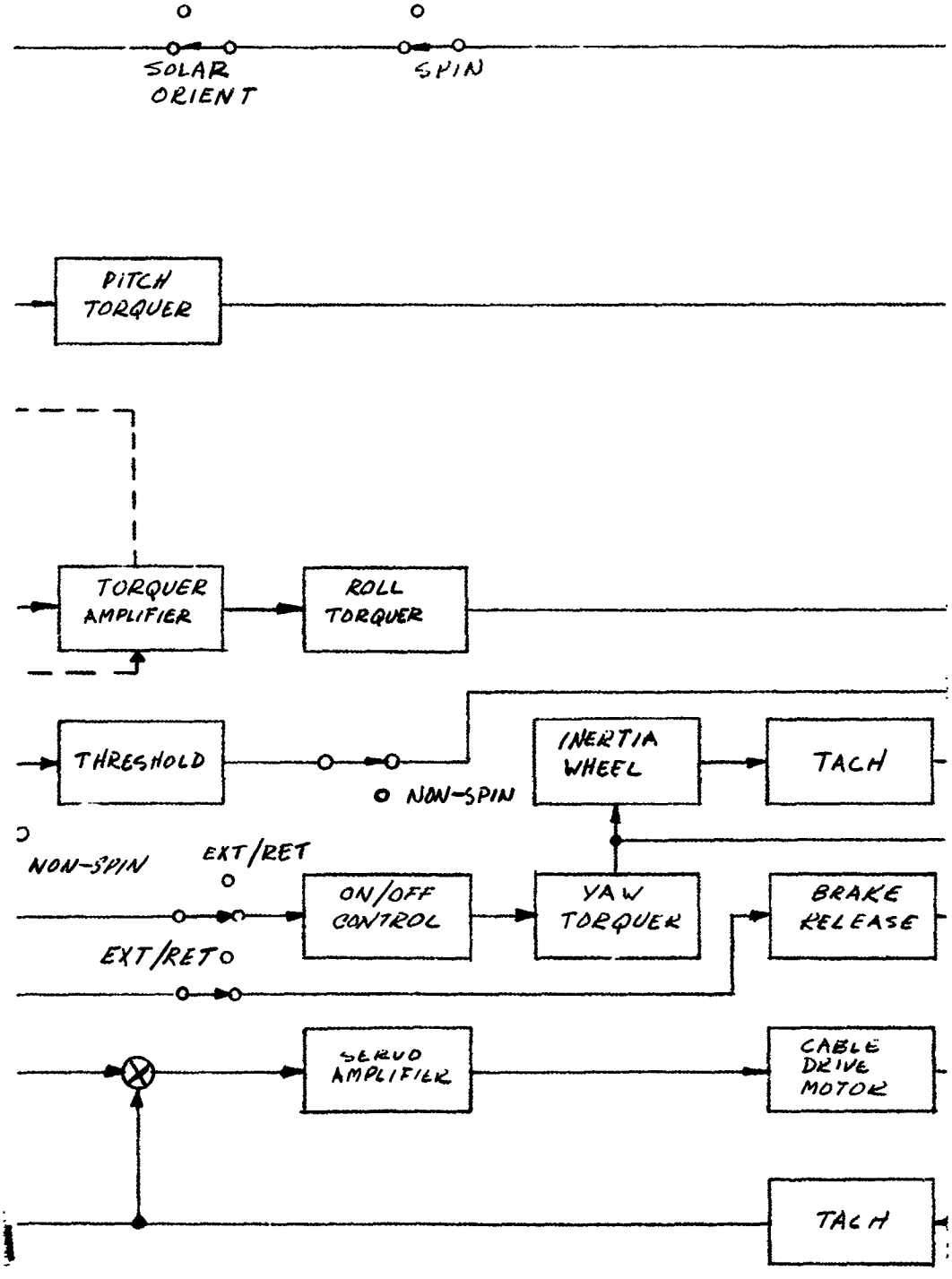
SOLAR ORIENT
SPIN
PITCH TORQUER
TORQUER AMPLIFIER
ROLL TORQUER
THRESHOLD
NON-SPIN
INERTIA WHEEL
TACH
NON-SPIN
EXT/RET
ON/OFF CONTROL
YAW TORQUER
BRAKE RELEASE
EXT/RET
SERVO AMPLIFIER
CABLE DRIVE MOTOR
TACH

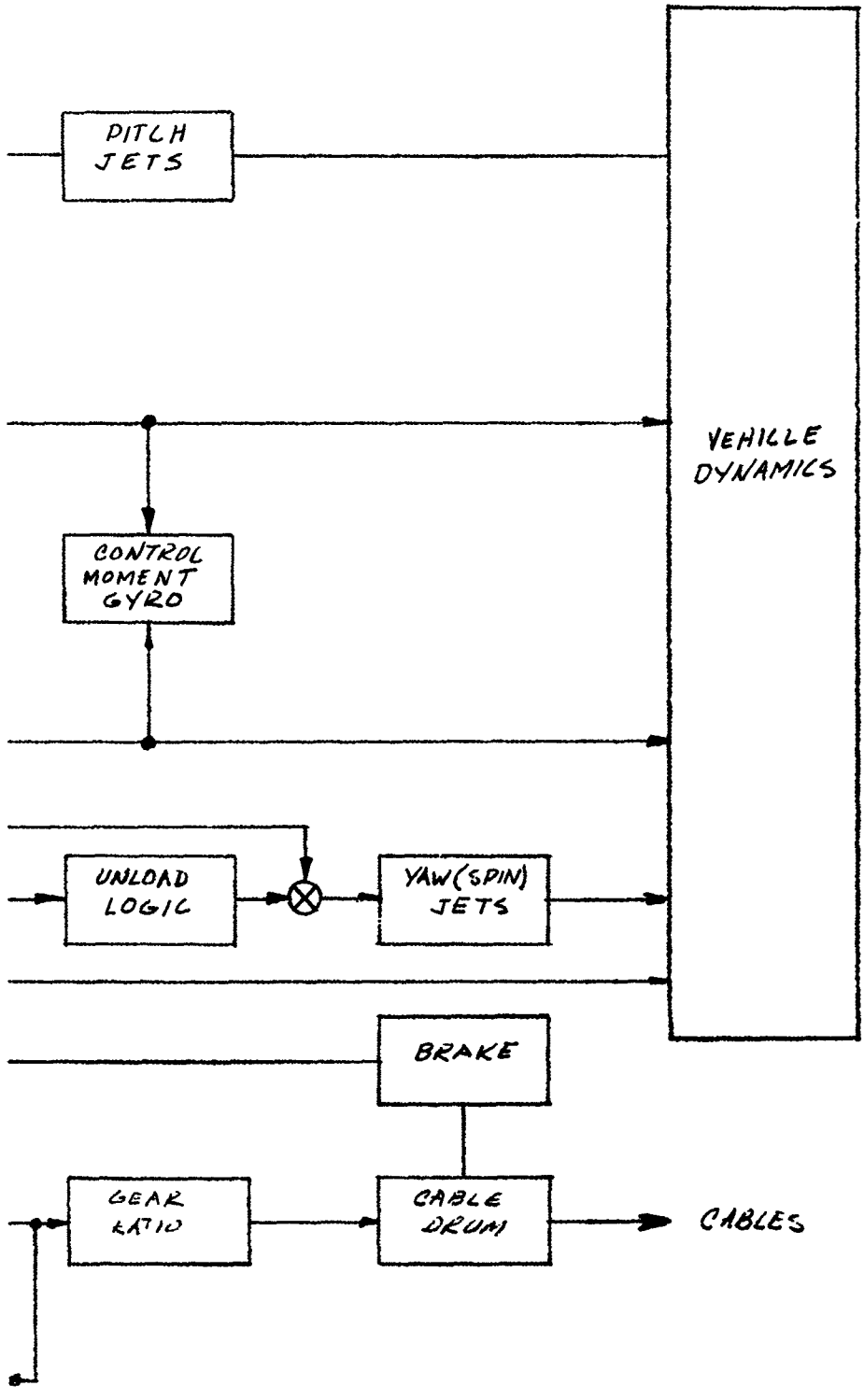

FIGURE 33
CONTROL SYSTEM
BLOCK DIAGRAM - SPIN MODES

with the sun line. The orientation control system is then disabled until the completion of transition.

Transition is initiated by placing the spin speed command switch in the extend/retract position. The spin speed command signal is compared to the output of the yaw rate gyro to develop a spin speed error signal for controlling the spin jets. During this phase of the transition maneuver (before the capsules are separated), the cable drum is locked. The yaw torquer is also disconnected so that all required yaw damping is obtained by the actions of the spin jets as described in section VI. The pitch and roll rate stabilization system operates as described in section V but at reduced gains. These damper gains are set by the position of the spin speed command switch.

When the transition spin speed has been attained, the cable drum brake is released and the cable rate command signal is inserted. Extension then proceeds at a constant rate while the spin control system continues to maintain the transition spin speed. When the cable extension reaches 97 feet, the cable rate command is switched to zero. Extension then continues to 100 feet because of the integration loop time constant, thereby bringing the extension rate smoothly to zero. When extension is complete, the cable drum is again locked, and the spin speed selection switch is placed in the spin position. The spin speed control system then completes the transition by causing the spin jets to fire until the final spin speed is attained. The pitch and roll rate stabilization gains are also adjusted by the spin speed selector.

Upon activation of the operational spinning mode, an accelerometer is substituted for the yaw rate gyro as a spin speed reference. The accelerometer is used as a spin speed reference because gravity level rather than spin speed is the parameter to be controlled. The yaw rate gyro is connected to the yaw torquer via a wipeout network in order to provide yaw structural damping.

Depending upon specific mission requirements, the dynamic balance system and the orientation control system may be engaged at any time during the operational spinning mode.

The transition from spin to nonspin is the reverse of the procedure described above.

C. NOMINAL SYSTEM COMPONENT COMPLEMENT

Table 28 lists the sensors and actuators required for control of the spinning vehicle, and indicates the functions these components would perform in the nonspinning mode of operation. One of the study objectives was to insure compatibility of the spinning and nonspinning mode control systems. This table shows that the nominal system satisfies this objective. The major components required for the nonspinning mode, but not shown in figure 23 or table 28, include attitude sensors, roll jets, and control moment gyro unloading logic.

The control system components required for the transition and operational spinning modes are listed in table 29. The noted quantities comprise a single system with no provision for redundancy. This table also presents the significant characteristics of each component. Weight, size and power estimates are tabulated. These estimates are, of course, subject to revision when firm system requirements are established. The following system totals result:

Weight--355 pounds

Volume--6.1 cubic feet

Steady Power--68 watts

Peak Power--577 watts

In addition to the component physical characteristics, the table indicates component performance characteristics. In general these characteristics are self-explanatory. However, some comment relative to the control moment gyro, inertia wheel and cable drive motor are in order. First, recall from section V that the angular momentum of the control moment gyro was determined by the roll dynamic balancing requirements. The effect on the control moment gyro (and on the system) of changing the roll balance requirements (either by elimination or by reduction of the required accuracy) is covered in the parametric discussion below.

The specified inertia wheel is sized to provide a structural yaw damping ratio in the operational spinning mode of approximately 1 percent of critical. Relaxing this damping requirement would reduce the size of the inertia wheel required in the spinning mode. However, a yaw inertia wheel of comparable size is required for vehicle control in the nonspinning mode.

TABLE 28

COMPONENT FUNCTIONS

Component	Spinning Modes	Nonspinning Mode
SENSORS		
a) 3-axis rate gyro ass'y	Damping and balance	Damping
b) Masked sun sensors	Pitch axis--orientation error	Possible use for initial acquisition
	Roll axis--firing time	
c) Accelerometer	Gravity level--quiescent spin mode	----
ACTUATORS		
a) Control moment gyro	Damp pitch and roll axes	Attitude control
	Balance roll axis	
b) Inertia wheel	Damp yaw axis	Attitude control
c) Cable drive motor	Control cable extension	----
d) Orientation jets	Orientation control	Pitch attitude control--unload cmg
e) Spin jets	Spin/despin, unload I.W.	Yaw attitude control--unload I.W.

TABLE 29

COMPONENT CHARACTERISTICS FOR NOMINAL SYSTEM

Qty	Component	Wt (lb)	Vol (ft^3)	Power (watts) S.S	Power (watts) Max	Comments
1	3-Axis rate gyro	2.5	.03	13	13	Roll and pitch: .01°/sec thresh., 2°/sec range. Yaw: .02°/sec thresh., 40°/sec.
2	Masked sun sensor	1	-	-	-	Externally mounted, on-off, dual ±10° aperture, 1/2° threshold
1	Accelerometer	1	.01	1	1	Range 0-1g, resolution ±.001g
1	Control moment gyro	152	4.2	28	43	H = 250 slug ft^2/sec. T_{max} = 108 ft-lb. Sized for roll balance. rotor speed = 4000 rpm, max gimbal angle = 60°
1	Inertia wheel	150	1.3	-	360	Max. wheel speed = 9500 rpm, Inertia = 1 slug ft^2, Radius = .7 ft, T_{max} = 15 ft-lb, on-off torque drive.
1	Cable drive motor	17	.2	-	75	1000:1 gear reduction to drum (1 ft rad.) sized for extension at 1/3 fps at Ω_s = .04 rad/sec
4	Reaction jets	18	-	-	54	100 lb jets located 4' beyond C.G. (manned body).
1	Control electronics assembly	11	.25	20	25	Includes: 2 torquer amps, 1 on-off servo amp, 1 linear servo amp, 3 wipeout networks, 2 electro-mechanical integrators, ac power converter, signal and power control logic
1	Engage panel	2.5	.11	6	6	Manual mode select
	TOTALS	355	6.1	68	577	Not included: Primary power source, jet tankage and plumbing, propellant, cable drum ass'y, slip ring, manual controllers, displays, nonspin components (except as req'd for spin modes)
						Note: Propellant requirements include 4500 lb/year of solar pointing and gravity gradient (equatorial, low altitude orbit) 450 lb per spin-despin cycle

The cable drive motor listed in the table is sized to provide a cable extension rate of 0.33 ft/sec at a spin speed of 0.04 rad/sec. In some cases, it may be desirable to extend or retract at full spin speed. Cable extension at these higher spin speeds would require additional servo torque. Additional torque could be obtained without materially affecting motor size by changing the gear ratio, but the extension rate would be reduced by the gear ratio. However, this might result in undesirably low extension rates. The other alternative is to use a larger motor. A definite mission, with clearly defined operating modes, must be established before selecting the specific cable drive motor characteristics.

D. PROPELLANT REQUIREMENTS

During the transition and operational spinning modes, reaction jet propellant is expended to do the following:

- Spin-up and despin.
- Maintain solar orientation.
- Unload yaw inertia wheel.
- Maintain spin speed and orbit.

It was shown in section VI that a complete transition cycle (spin plus despin) requires 450 pounds of propellant assuming a specific impulse (Isp) of 300 seconds. The total propellant required for a particular mission will depend, of course, on the number of spin/despin cycles to be performed.

It is estimated that 4500 pounds of propellant would be required to maintain solar orientation for a one year mission in the operational spinning configuration. (See appendix G.) The major portion of this propellant expenditure was due to the gravity gradient disturbance torque anticipated for an equatorial orbit.

Propellant estimates were not made for the inertia wheel unloading and spin and orbit correction requirements. These are predominantly functions of the mission, and are essentially independent of control system implementation. At the time of this study, the space station mission had not been defined well enough to permit meaningful estimates.

It should be mentioned that magnetic torquing does not appear suited to the subject space station. The station geometry is such that a magnetic coil of sufficient area cannot easily be implemented.

E. PARAMETRIC ANALYSES

The component characteristics specified in table 29 were based on spinning mode control requirements as they apply to the nominal vehicle. The parametric analysis presented below establishes the effect which changes in control requirements and vehicle configuration have on the control moment gyro. It should be noted, however, that the results of this study pertain to the spinning mode and may become irrelevant if the nonspinning mode requirements are such as to be the basis for the gyro design.

1. Effect of Dynamic Balance Specification on Control Moment Gyro Size

As noted in section VIII paragraph C, the gyro characteristics presented in table 29 were based on providing complete roll imbalance compensation (i.e., the vehicle should have no steady state roll error). It was shown in section V that the maximum steady state roll error resulting from crew motions for the nominal station was approximately 0.5 degree. It is apparent that if the balance specification is relaxed to permit steady state roll errors of 0.5 degree or less, the control moment gyro capability could be much reduced. For the nominal case, the rate stabilization requirement would then size the gyro, and the gyro weight, for instance, would be reduced from 152 pounds to 48 pounds.

Figure 34 presents curves relating gyro weight to roll balance accuracy requirements for the three inertia ratio configurations considered in section V. The gyro weight is presented as equivalent weight. This is the sum of the gyro weight and its associated rotor power supply. As noted on the figure, the equivalent weight is approximately 30 percent higher than the physical weight. This assumes a gyro design based on minimum equivalent weight, i.e., the rotor power has been represented by power supply weight, and the rotor wheel speed and geometry have been selected to minimize the sum of gyro weight and power supply weight. It should be noted that the zero gyro weight point on figure 34 refers to balancing capability only. Rate stabilization capability must still be provided.

2. Effect of Vehicle Inertia Ratio on Control Moment Gyro Size

The effect of vehicle inertia ratio on the control moment gyro was estimated by assuming that the gyro characteristics are determined by the rate stabilization requirements above (i.e., no roll balancing). Section V showed how the gyro angular momentum requirements varied as a function of inertia ratio. These angular momentum requirements were

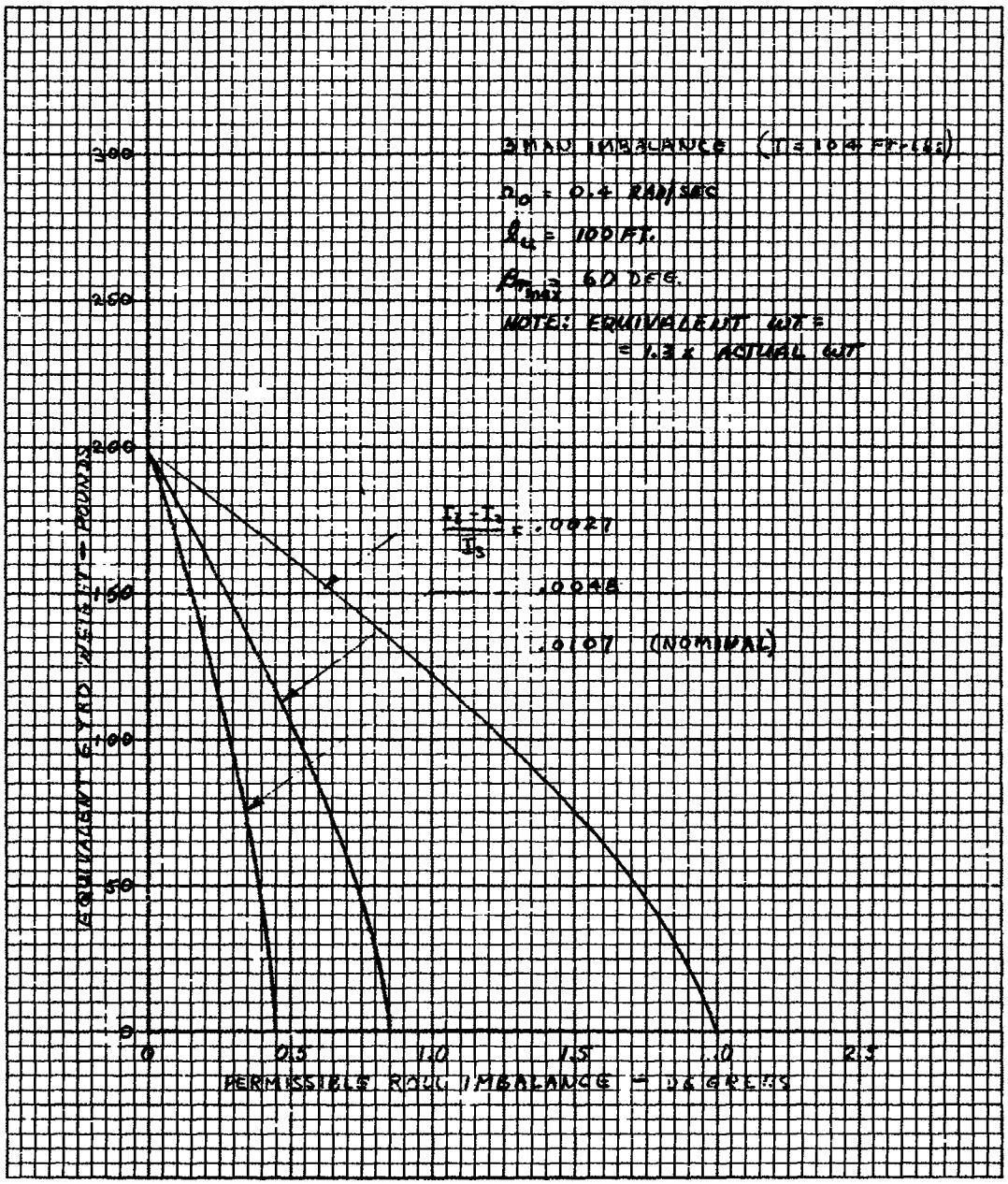

FIGURE 34 GYRO WEIGHT VS
ROLL DYNAMIC BALANCE SPECIFICATION

translated into component weight, volume and power as presented in table 30. This table indicates that the gyro characteristics are relatively insensitive to inertia ratio.

3. Effect of Spin Speed on Control Moment Gyro Size

Table 31 presents control moment gyro weight, volume and power for three spin speeds. Since spin speed may vary throughout the mission, the gyro must be sized to handle the entire range of anticipated spin speeds. The data in the table assume a configuration with a constant separation of 100 feet and an inertia ratio of .0107 (nominal). It should be noted that the largest gyro of table 31 is still much smaller than that required to provide roll balancing. Preliminary results indicate that a gyro sized to provide a roll balance capability is more than adequate for rate stabilization during the low spin speed transition maneuver.

4. Effect of Damping Specification on Control Moment Gyro Size

The curves of figure 35 show control moment gyro characteristics as a function of damping specification. A damping range of 1 to 20 percent of critical is shown. This figure indicates that a damping ratio of approximately 10 percent (selected for the nominal system) is at the knee of the peak power curve. Thus a significant power penalty is imposed by higher damping requirements. Other characteristics are not affected as severely.

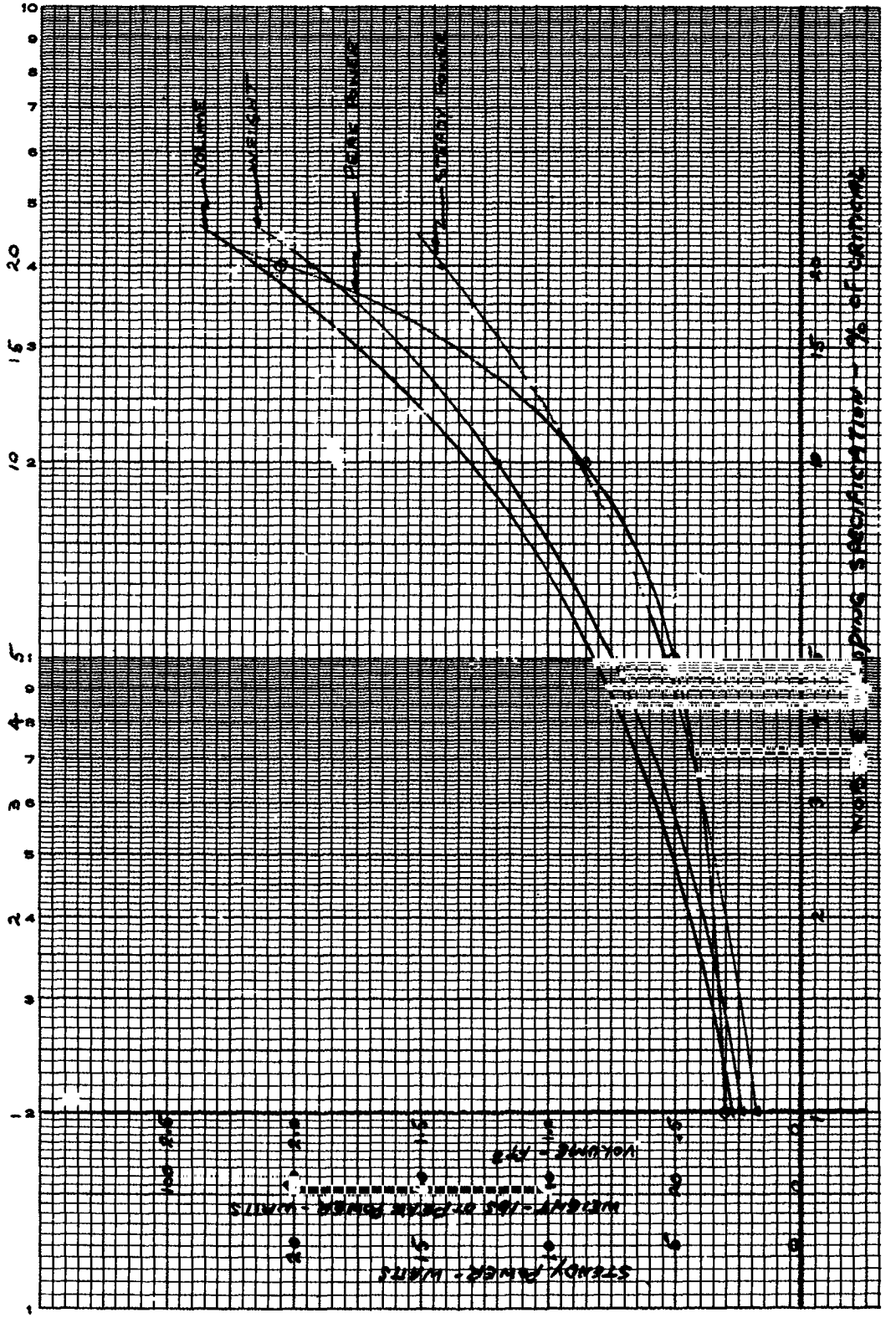

FIGURE 35 GYRO CHARACTERISTICS VS
WOBBLE DAMPING SPECIFICATION

TABLE 30

EFFECT OF INERTIA RATIO ON CONTROL MOMENT GYRO REQUIRED FOR RATE STABILIZATION

Inertia Ratio	Control Moment Gyro Characteristics				
	H (slug-ft^2/sec)	Weight (lb)	Volume (ft^3)	Steady Power (watts)	Peak Power (watts)
.0107 (Nominal)	47	48	1.3	8.8	35
.0048	53	52	1.4	9.6	34
.0027	64	59	1.6	10.9	33

Note: Spin speed = 0.4 rad/sec
Separation = 100 feet

TABLE 31

EFFECT OF SPIN SPEED ON CONTROL MOMENT GYRO REQUIRED FOR RATE STABILIZATION

Spin Speed (rad/sec)	Control Moment Gyro Characteristics				
	H (slug-ft^2/sec)	Weight (lb)	Volume (ft^3)	Steady Power (watts)	Peak Power (watts)
0.2	60	57	1.6	10.4	22
0.4 (nominal)	47	48	1.3	8.8	34
0.6	38	41	1.1	7.6	62

Note: Separation = 100 feet
Inertia ratio = .0107

Section IX

CONCLUSIONS AND RECOMMENDATIONS

A. CONCLUSIONS

The stabilization and control study of flexible spinning vehicles has established that:

- The dynamics of flexibly coupled vehicles are relatively insensitive to cable configuration. A broad range of configurations is adequate from a controls viewpoint, although an eight crossed cable configuration appears somewhat more favorable than the others.
- Extension and retraction of the cabled vehicle can be readily performed, and only slightly more (6 percent) propellant is required to spin the flexible vehicle than would be required to spin a rigid vehicle.
- The stabilization and control functions can be provided with state of the art components of reasonable size, weight, and power.
- The only unique component required in the control system is a large two degree of freedom control moment gyro. The development of this gyro is well within the state of the art.

B. RECOMMENDATIONS

As a result of this study, several areas requiring further investigation have been identified. These can be divided into categories concerned with:

- Broadening the study scope to include alternate vehicle configurations and mission requirements.

- Generation of simplified analytical rules for use in sizing components for specific missions.
- Definition of a nonspinning mode control systems, integration of spinning and nonspinning mode control systems, and implementation of the resulting system.

The specific items recommended in the first category for follow-on effort are as follows:

1. Analyze vehicles with configurations differing significantly from the nominal vehicle defined in this study. This would include, for example, vehicles having no inherent roll stability; vehicles having an asymmetric booster and/or cable configuration; and vehicles operating at larger (5000 ft) extensions.
2. Analyze alternate pointing requirements. This would include analysis of nonsolar referenced orientations, and the associated solar panel control problem. Further analysis of the solar orientation control problem is also desirable for vehicles having low roll stability, since interactions between the balancing system and the orientation control system are probable in such cases. With regard to the latter possibility, the feasibility of roll attitude control (as opposed to rate stabilization) should also be investigated. Finally, further analysis of the solar pointing system with the objective of trading off pointing accuracy for propellant efficiency is recommended.

The second category, model generation, includes the following recommended work items:

1. A detailed analysis of the nonlinear effects present in the cable coupled vehicle is required prior to development of simplified dynamic models. The nonlinear effects of large angle rotations of the cable structure should be studied in order to better define the region where linearizing approximations are valid. Similarily, a more detailed investigation of the effect which cable slacking has on the pitch and roll axis response during transition is desirable, since only the most critical axis (yaw) was analyzed in detail in this study.
2. Develop generalized actuator sizing laws applicable over a broad range of vehicle/mission parameters.

3. Develop a comprehensive analytical model for use in transition performance predictions.

In the third category, control system definition, the following work items are recommended:

1. Extend the nonspinning mode analysis to include initial stabilization and alignment, docking, and maneuvering requirements.
2. Perform actuator trade-off analyses, placing increased emphasis on the nonspinning mode requirements.
3. Establish detailed performance specifications for the mating devices used to couple the manned body to the boaster. This would include definition of the allowable transients imparted by such a mechanism at the initiation of an extension maneuver, and definition of the maximum terminal errors and error rates.
4. Investigate the feasibility of providing an enhanced energy dissipation capability in the cables themselves in order to obtain passive damping of the structural resonances.
5. Establish philosophy and design criteria for reliability, crew safety, emergency control, and abort procedures. Establish a manual control and display concept.
6. Initiate control moment gyro design studies.

APPENDIX A

NOMENCLATURE

A. CO-ORDINATE SYSTEMS

$(\hat{\mathbb{I}}, \hat{\mathbb{J}}, \hat{\mathbb{K}})$	Inertially fixed unit triad (figure B-1)
$(\hat{i}, \hat{j}, \hat{k})$	Reference triad aligned with vehicle mass centers (figure B-1)
$(\hat{i}_1, \hat{j}_1, \hat{k}_1)$	Body axes of vehicle No. 1 (figure B-3)
$(\hat{i}_2, \hat{j}_2, \hat{k}_2)$	Body axes of vehicle No. 2 (figure B-3)
$\hat{j}_1'$	Axis of rotation for e_{12}, including "order of rotation" effects
$\hat{k}_1''$	Axis of rotation for e_{13}, including "order of rotation" effects
$(\hat{d}, \hat{n}, \hat{a})$	Local geocentric unit triad (figure G-3)
$\hat{i}^*$	$\hat{d} \times \hat{k}$
$\hat{j}^*$	$\hat{k} \times \hat{i}^*$
$(\hat{S}_1, \hat{S}_2, \hat{S}_3)$	Sun-referenced unit triad (figure G-3)

B. LINEAR AND ANGULAR POSITION

e_{ij}	Small rotation of body i about axis j
δ_{ij}	Pointing error of vehicle i about axis j
ψ	Spin angle
ϕ	Orientation angle
$\theta_{1,\,2}$	Angles locating local vertical in body axes

i	Orbital inclination relative to ecliptic
λ	Position of vehicle in orbit
μ	Position of sun in ecliptic
Ω	Position of ascending node in ecliptic
α	Angle of attack
q_j	Generalized co-ordinate
δq_j	Virtual change in q_j
$\delta \vec{x}_i$	Virtual displacement of body i
$\delta \vec{\gamma}_i$	Virtual rotation of body i
r	Mass center separation
r_o	Nominal value of r
x	Perturbation in r
$\{y\}$	Vector form of system co-ordinates
$\vec{R}$	Vehicle mass center position relative to center of earth
(ξ, η, ζ)	Components of $\vec{R}$ along $(\hat{i}, \hat{j}, \hat{k})$
$\vec{\rho}$	Position of differential mass element relative to vehicle mass center
$\vec{\rho}_T$	$\vec{R} + \vec{\rho}$

C. LINEAR AND ANGULAR VELOCITIES

Ω	Spin speed (equals $\dot{\psi}$)
Ω_o	Nominal value of Ω
ω_{ij}	Inertial angular velocity of vehicle i about body axis j
ω'_{i3}	Perturbation in inertial angular velocity of vehicle i about body axis $3 = (\omega_{i3} - \Omega_o)$
ω_a, ω_b	Inertia wheel speeds
ω_g	Gyro wheel speed
ω_e	Orbital angular velocity

V	Orbital linear velocity
$\vec{\omega}_i$	Inertial angular velocity of vehicle i
$\vec{V}_i$	Linear velocity of vehicle i relative to the common mass center

D. FORCES AND MOMENTS

Tij	Torque about mass center of body i, around axis j
Ti′j	Control torque
Fij	Force through mass center of body i, directed along axis j
Q_j	Generalized force (also written Qx, Q4, Qq, Q_{e11}, . . ., Q_{e23})
Fr	Equivalent radial force
T_α	Equivalent spin torque
T_φ	Equivalent orientation torque
$F_{A,\ B}$	Tension force in cables A and B, respectively
T	Total centrifugal tension
F_J	Jet thrust
D	Drag force
$(T_O,\ T_I)$	Outer and inner gimbal torques on two-degree-of-freedom gyro
$(T_{OC},\ T_{IC})$	Commanded gimbal torques
$\mathcal{J}_1, \mathcal{J}_2, \mathcal{J}_3$	Gravity gradient impulsive torque components (nonspinning mode)
$T\Delta t$	Impulsive torque magnitude
(Tr, Tp)	Total torques on roll and pitch axes of single-degree-of-freedom gyros or inertia wheels
(Tra, b, Tpa, b)	Torques on individual single-degree-of-freedom gyros, or inertia wheels, a and b respectively
$(T_\xi,\ T_\eta,\ T_\zeta)$	$(\hat{i},\ \hat{j},\ \hat{k})$ components of gravity gradient torque
{fo}	Imbalance torques due to cross-products of inertia

$\{f_o\}$	Disturbance torques
$\vec{T}_i$	Torque about mass center of body i
$\vec{F}_i$	Force through mass center of body i
$d\vec{f}$	Differential force vector
$d\vec{T}g$	Differential gravity gradient torque
$\vec{T}g$	Gravity gradient torque
$\vec{T}av$	Average (one orbit) value of $\vec{T}g$
$\vec{T}_s$	Precession torque required to maintain solar orientation
$\vec{T}_c$	$\vec{T}_s - \vec{T}g$

E. ENERGY

T	Kinetic energy
T_{vi}	Translational kinetic energy of body i
T_{Ri}	Rotational kinetic energy of body i
V	Potential energy
L	Lagrangian (T - V)
δW	Work done in virtual displacement

F. VEHICLE PARAMETERS

M_i	Mass of body i
$\bar{M}$	$M_1 + M_2$
M_T	$\frac{M_1 M_2}{M_1 + M_2}$
dm	Differential mass element
m	Mass imbalance
I_1, I_2, I_3	Total vehicle moment of inertia about axes $(\hat{i}, \hat{j}, \hat{k})$
I_{ij}	Moment of inertia of body i about axis j

J_i, K_i, L_i	Cross-products of inertia of body i
H_V	Vehicle angular momentum
d_1, d_2	Distance from body centers of mass to composite center of mass (nonspinning mode)
c_1, c_2, c_3, c_4	Vehicle dimensions for nonspinning aerodynamic model
$[M]$, $[C]$, $[K]$	Data matrices
k_{ij}^*	Cable influence coefficients
c_{ij}^*	Cable damping factors
ω_o	Rigid body wobble frequency
ω_{ro}	Uncoupled roll structural resonant frequency
ω_{r1}, ω_{r2}	Roll resonant frequencies
ω_{p1}, ω_{p2}	Pitch structural resonant frequencies
ω_{y1}, ω_{y2}	Yaw structural resonant frequencies
z	Anti-resonant frequency
k_o	Vehicle static gain

G. CONTROL PARAMETERS

$(\alpha_{ij}, \beta_{ij}, \gamma_{ij})$	Control gain settings
(k_R, k_P, k_Y)	Rate stabilization gains (roll, pitch, yaw)
k_V	Control moment gyro gimbal damping gain
k_I	Roll balance gain
T_r, T_p, T_y	Wipeout time constants (roll, pitch, yaw)
ζ	Damping ratio
H	Angular momentum, two-degree-of-freedom gyro
h_a, h_b	Angular momentum, single-degree-of-freedom gyros
h_T	$h_a + h_b$
Iw	Moment of inertia, inertia wheel
Ig	Moment of inertia, gyro wheel

P_a, P_b	Peak inertia wheel servo power
P_g	Peak torquer power, two-degree-of-freedom gyro (each torquer)
I_{SP}	Specific impulse of reaction jet propellant
W	Propellant weight
X_J	Distance from center of mass of manned body to spin jet centerline
r_1^*	Distance from center of mass of station to orientation jet centerline
α_T, β_T	Gyro gimbal angles (two-degree-of-freedom)
α_s, β_s	Gyro gimbal angles (single-degree-of-freedom)

H. CABLE PARAMETERS

$\vec{\ell}$	Cable length vector
ℓ	Magnitude of $\vec{\ell}$
ℓ_a	Unstretched magnitude of $\vec{\ell}$
ℓ_A, ℓ_B	Length of cables A and cables B
$\Delta\ell_A$, $\Delta\ell_B$	Change in length of cables A and B
ℓ_1, ℓ_2, ℓ_3	Components of unstretched $\vec{\ell}$
x_o	Cable stretch due to centrifugal force alone
ℓ_1^*	$\ell_1 + x_o$
ℓ_1^{**}	$\ell_1 + \frac{x_o}{2}$
Δ_1, Δ_2, Δ_3	Components of total cable stretch
k	Stiffness per unit length of two parallel cables
$\vec{d_i}$	Position of cable attachment point relative to mass center of body i
d_{ij}	Components of $\vec{d_i}$
d_{21}'	$- d_{21}$
A	Cross-sectional area of a cable
E	Cable modulus of elasticity

I. MISCELLANEOUS CONSTANTS

T_w	Vehicle skin temperature
T_∞	Free stream temperature
S_∞	Molecular speed ratio
C_D^*	Aerodynamic drag coefficient
q	Dynamic pressure
ρ^*	Atmospheric density
R_o	Radius of earth
g_o	Acceleration of gravity at earth's surface
a, b	Arbitrary constants
K_{T1}, K_{T2}, K_{T3}	Arbitrary constants
A, B	Arbitrary constants

J. OPERATORS

$( )_{min}$	Minimum value of $( )$
$( )_{max}$	Maximum value of $( )$
$( )_{ss}$	Steady state value of $( )$
$\dot{( )}$	Derivative of $( )$ with respect to time
$\ddot{( )}$	Derivative of $\dot{( )}$ with respect to time
$\lvert ( ) \rvert$	Magnitude of $( )$
$>>$	Much greater than

APPENDIX B

DERIVATION OF LINEARIZED EQUATIONS OF MOTION FOR NINE-DEGREE-OF-FREEDOM CABLE-COUPLED SPACE STATION

A. DISCUSSION

This appendix summarizes a derivation of the equations of motion for a nine-degree-of-freedom model of the cable-coupled space station. Small disturbances are assumed, and cable-inertia effects are neglected.

Lagrange's method is used to derive the equations of motion. The kinetic energy, T, the potential energy, V, and the Lagrangian L = T-V are first computed. The equations of motion are then obtained from

$$\frac{d}{dt}\left(\frac{\partial L}{\partial \dot{q}_j}\right) - \frac{\partial L}{\partial q_j} = Q_j \qquad , \; j = 1, \ldots N \tag{B-1}$$

where the q_j's are the generalized coordinates of the system. The Q_j's are generalized forces, and must be evaluated by computing the work done, δw, by the external forces in an arbitrary displacement of the system:

$$\delta W = \sum_{j=1}^{N} Q_j \delta q_j \tag{B-2}$$

The Lagrangian formulation has been used because of its advantages relative to the calculation of cable restoring forces.

The first step in the derivation is to define the coordinate systems and explicitly state the small-angle assumptions and other approximations used to simplify the problem. Figure B-1 shows a sketch of the cable-coupled vehicle. As noted, $(\mathbf{I}, \mathbf{J}, \mathbf{K})$ are inertially fixed unit vectors, $(\hat{i}, \hat{j}, \hat{k})$ is a reference triad located at the common mass-center,

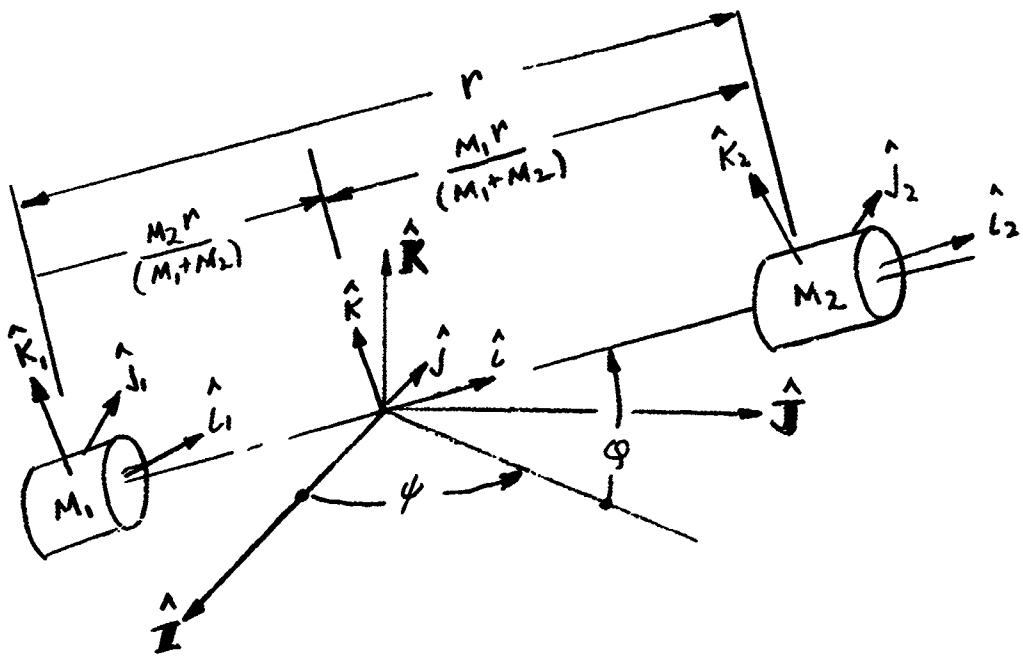

$(\hat{\mathbf{I}}, \hat{\mathbf{J}}, \hat{\mathbf{K}})$ ≡ INERTIALLY FIXED

$(\hat{\imath}, \hat{\jmath}, \hat{k})$ ≡ REFERENCE SYSTEM, WITH $\hat{\imath}$ POINTING FROM VEHICLE #1 TO VEHICLE #2 AND $\hat{\jmath}$ IN THE $(\hat{\mathbf{I}}, \hat{\mathbf{J}})$ PLANE

$(\hat{\imath}_1, \hat{\jmath}_1, \hat{k}_1)$ ≡ BODY AXES OF VEHICLE #1, NOMINALLY ALIGNED WITH $(\hat{\imath}, \hat{\jmath}, \hat{k})$

$(\hat{\imath}_2, \hat{\jmath}_2, \hat{k}_2)$ ≡ BODY AXES OF VEHICLE #2, NOMINALLY ALIGNED WITH $(\hat{\imath}, \hat{\jmath}, \hat{k})$

FIGURE B-1 DEFINITION SKETCH OF CABLE-COUPLED VEHICLE COORDINATE SYSTEMS

and ($\hat{i}_1$, $\hat{j}_1$, $\hat{k}_1$) are body axes (not necessarily principal axes) of vehicle no. 1. In figure B-1, it will be assumed that

$$r = r_c + x \quad , \quad r_c \text{ (constant)} >> x$$
$$\varphi << 1$$

The angle ψ will be considered large.

In addition to the above approximations, the common mass-center of the two vehicles will be assumed fixed in inertial space, and the inertia of the cables coupling vehicle no. 1 to vehicle no. 2 will be neglected. Finally, the misalignments existing between the reference triad ($\hat{i}$, $\hat{j}$, $\hat{k}$) and the body axes ($\hat{i}_1$, $\hat{j}_1$, $\hat{k}_1$) and ($\hat{i}_2$, $\hat{j}_2$, $\hat{k}_2$) will be assumed small angles.

B. CO-ORDINATE CONVERSIONS

Figure B-2 illustrates the transformation from the inertial axes $(\mathbb{I}, \mathbb{J}, \mathbb{K})$ to the reference axes ($\hat{i}$, $\hat{j}$, $\hat{k}$). The transformation has been simplified by introducing the small angle approximations

$$\sin\varphi \approx \varphi$$
$$\cos\varphi \approx 1 - \varphi^2/2$$

All second-order terms have been retained. This is necessary in the intermediate steps of this energy-based formulation of the equations of motion. Only first-order terms will be retained in the final equations of motion.

Figure B-3 shows the transformation from reference axes to vehicle body axes. Again, small-angle approximations have been introduced and second-order terms have been retained.

It is clear from figures B-2 and B-3 that the angular velocity of vehicle no. 1 is

$$\vec{\omega}_1 = \dot{\psi}\hat{K} - \dot{\varphi}\hat{j} + \dot{e}_{11}\hat{i}_1 + \dot{e}_{12}\hat{j}_1' + \dot{e}_{13}\hat{k}_1'' \qquad (B\text{-}3)$$

The unit vectors $\hat{j}_1'$ and $\hat{k}_1''$ define the axes used for the angular rotations, e_{12} and e_{13}. Since second-order terms are being retained, the order of rotation is important, and these axes must be defined in detail:

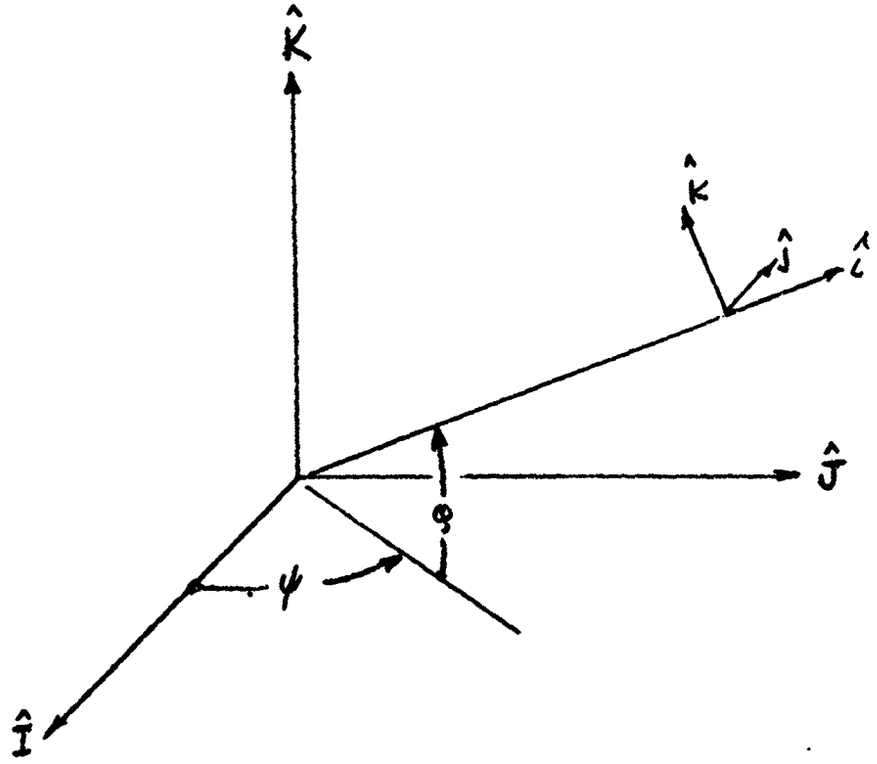

$$\begin{Bmatrix} \hat{I} \\ \hat{J} \\ \hat{K} \end{Bmatrix} = \begin{bmatrix} (1-\frac{\varphi^2}{2})\cos\psi & -\sin\psi & -\varphi\cos\psi \\ (1-\frac{\varphi^2}{2})\sin\psi & \cos\psi & -\varphi\sin\psi \\ \varphi & 0 & (1-\varphi^2/2) \end{bmatrix} \begin{Bmatrix} \hat{i} \\ \hat{j} \\ \hat{k} \end{Bmatrix}$$

FIGURE B-2 TRANSFORMATION FROM REFERENCE AXES ($\hat{i},\hat{j},\hat{k}$) TO INERTIAL AXES ($\hat{I},\hat{J},\hat{K}$)

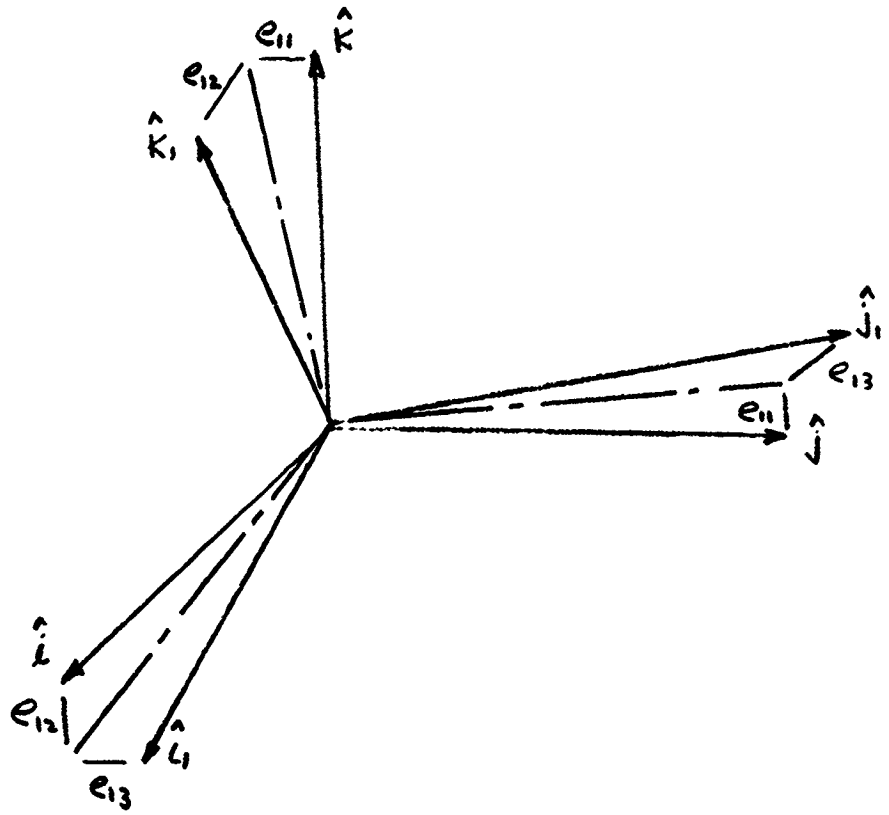

$$\begin{Bmatrix} \hat{i} \\ \hat{j} \\ \hat{k} \end{Bmatrix} = \begin{bmatrix} \cos e_{13} & -\sin e_{13} & 0 \\ \sin e_{13} & \cos e_{13} & 0 \\ 0 & 0 & 1 \end{bmatrix} \begin{bmatrix} \cos e_{12} & 0 & \sin e_{12} \\ 0 & 1 & 0 \\ -\sin e_{12} & 0 & \cos e_{12} \end{bmatrix} \begin{bmatrix} 1 & 0 & 0 \\ 0 & \cos e_{11} & -\sin e_{11} \\ 0 & \sin e_{11} & \cos e_{11} \end{bmatrix} \begin{Bmatrix} \hat{i}_1 \\ \hat{j}_1 \\ \hat{k}_1 \end{Bmatrix}$$

RETAINING ONLY SECOND ORDER TERMS,

$$\begin{Bmatrix} \hat{i} \\ \hat{j} \\ \hat{k} \end{Bmatrix} = \begin{bmatrix} \left(1 - \left[\frac{e_{12}^2 + e_{13}^2}{2}\right]\right) & (-e_{13} + e_{11}e_{12}) & (e_{12} + e_{11}e_{13}) \\ e_{13} & \left(1 - \left[\frac{e_{11}^2 + e_{13}^2}{2}\right]\right) & (-e_{11} + e_{12}e_{13}) \\ -e_{12} & e_{11} & \left(1 - \left[\frac{e_{11}^2 + e_{12}^2}{2}\right]\right) \end{bmatrix} \begin{Bmatrix} \hat{i}_1 \\ \hat{j}_1 \\ \hat{k}_1 \end{Bmatrix}$$

FIGURE B-3 TRANSFORMATION FROM BODY AXES $(\hat{i}_1, \hat{j}_1, \hat{k}_1)$
TO REFERENCE SYSTEM $(\hat{i}, \hat{j}, \hat{k})$

$$\hat{k} = \varphi \hat{i} + (1 - \varphi^2/2)\hat{k} \qquad (B-4)$$

$$\hat{j}_1' = \hat{j}_1 (1 - e_{11}^2/2) - e_{11}\hat{k}_1 \qquad (B-5)$$

$$\hat{k}_1'' = -e_{12}\hat{i}_1 + e_{11}\hat{j}_1 + \left(1 - \frac{e_{11}^2 + e_{12}^2}{2}\right)\hat{k}_1 \qquad (B-6)$$

Substituting ($\hat{i}_1$, $\hat{j}_1$, $\hat{k}_1$) for ($\hat{i}$, $\hat{j}$, $\hat{k}$) as indicated by the transformation of figure B-3, and retaining all second-order terms,

$$\vec{\omega}_1 = \left[\dot{e}_{11} - e_{13}\dot{\varphi} + \dot{\psi}(\varphi - e_{12}) - e_{12}\dot{e}_{13}\right]\hat{i}_1 +$$
$$+ \left[\dot{e}_{12} - \dot{\varphi} + \dot{\psi}(e_{11} - e_{13}\varphi) + e_{11}\dot{e}_{13}\right]\hat{j}_1 +$$
$$+ \left[\dot{e}_{13} + e_{11}\dot{\varphi} + \dot{\psi}\left\{1 + e_{12}\varphi - \left(\frac{e_{11}^2 + e_{12}^2 + \varphi^2}{2}\right)\right\} - e_{11}\dot{e}_{12}\right]\hat{k}_1 \qquad (B-7)$$

A similar result is obtained for $\vec{\omega}_2$.

C. KINETIC ENERGY CALCULATIONS

1. Translational Kinetic Energy

The kinetic energy will be computed using Konig's theorem, which states that the total kinetic energy of a moving body is the sum of that of an equal-mass particle located at the mass center, and the kinetic energy of rotation about the mass center.

The mass center of vehicle no. 1 moves with a velocity

$$\vec{V}_1 = -\left(\frac{M_2}{M_1 + M_2}\right)\left[\dot{x}\hat{i} + \dot{\psi}(r_0 + x)(1 - \varphi^2/2)\hat{j} + \dot{\varphi}(r_0 + x)\hat{k}\right] \qquad (B-8)$$

where once again cos ϕ has been approximated by $(1 - \phi^2/2)$. The translational kinetic energy of vehicle no. 1 is thus

$$T_{V_1} = \frac{1}{2}\left(\frac{M_1 M_2^2}{(M_1 + M_2)^2}\right)\left[\dot{x}^2 + (r_0 + x)^2\dot{\psi}^2(1 - \varphi^2/2) + \dot{\varphi}^2(r_0 + x)^2\right] \qquad (B-9)$$

Adding the translational kinetic energy of vehicle no. 2, and retaining only second-order terms,

$$T_V = \frac{1}{2}\left(\frac{M_1 M_2}{M_1+M_2}\right)\left[\dot{X}^2 + (r_0+X)^2(1-\varphi^2)\dot{\psi}^2 + r_0^2\dot{\varphi}^2\right] \qquad (B-10)$$

2. Rotational Kinetic Energy

If the angular velocity of vehicle no. 1, for example, is written

$$\vec{\omega}_1 = \omega_{11}\hat{i}_1 + \omega_{12}\hat{j}_1 + \omega_{13}\hat{k}_1 \qquad (B-11)$$

then the rotational kinetic energy is

$$T_{R_1} = \frac{1}{2}I_{11}\omega_{11}^2 + \frac{1}{2}I_{12}\omega_{12}^2 + \frac{1}{2}I_{13}\omega_{13}^2 - J_1\omega_{11}\omega_{12} - K_1\omega_{11}\omega_{13} - L_1\omega_{12}\omega_{13} \qquad (B-12)$$

The factors (J_1, K_1, L_1) represent cross-products of inertia. Equation (B-7) can be substituted into (B-12) to express T_{R_1} as a function of e_{ij}, $\dot{e}_{ij}$, φ, $\dot{\varphi}$, and $\dot{\psi}$. The total kinetic energy is then given by

$$T = T_{R1} + T_{R2} + T_V \qquad (B-13)$$

where T_{R_2} represents the rotational kinetic energy of vehicle no. 2, and is similar in form to T_{R_1}

D. POTENTIAL ENERGY CALCULATION

The potential energy of the system takes the form of strain energy stored in the structure connecting M_1 to M_2. Only the translation X or the rotations e_{ij} can affect the strain energy. Thus the potential energy, V, will have the form

$$\begin{aligned} V = {} & \frac{1}{2}K_{11}^* X^2 + K_{14}^* X e_{11} + K_{15}^* X e_{12} + K_{16}^* X e_{13} + \cdots + K_{19}^* X e_{23} + \\ & + \frac{1}{2}K_{44}^* e_{11}^2 + K_{45}^* e_{11}e_{12} + \cdots + K_{49}^* e_{23} + \\ & + \cdots \\ & + \frac{1}{2}K_{99}^* e_{23}^2 \end{aligned} \qquad (B-14)$$

The K_{ij}^* are, of course, the structural influence coefficients.

E. GENERALIZED FORCES

1. Form of Generalized Force Expressions

As mentioned earlier, the generalized forces must be computed by determining the work done by the external forces in an arbitrary displacement compatible with the constraints. To illustrate, consider an arbitrary translation of vehicle no. 1, denoted by $\delta\vec{x}_1$, and an arbitrary rotation, denoted by $\delta\vec{\gamma}_1$. The angular velocity analysis of paragraph B of this Appendix indicates that an arbitrary variation in the system coordinates will cause vehicle no. 1 to rotate by an angle

$$\begin{aligned}\delta\vec{\gamma}_1 = &\left[\delta e_{11} - e_{13}\delta\varphi + (\varphi - e_{12})\delta\psi - e_{12}\delta e_{13}\right]\hat{\imath}_1 + \\ &+\left[\delta e_{12} - \delta\varphi + e_{11}\delta\psi + e_{11}\delta e_{13}\right]\hat{\jmath}_1 + \\ &+\left[\delta e_{13} + e_{11}\delta\varphi + \delta\psi - e_{11}\delta e_{12}\right]\hat{k}_1\end{aligned} \qquad (B\text{-}15)$$

and the vehicle mass center to translate by an amount

$$\delta\vec{x}_1 = -\frac{M_2}{M_1+M_2}\left[\delta x\,\hat{\imath} + (r_0+x)\delta\psi\,\hat{\jmath} + (r_0+x)\delta\varphi\,\hat{k}\right] \qquad (B\text{-}16)$$

Second-order terms have been neglected in these expressions. Substituting for (i, j, k) from figure B-3, and retaining only first-order terms,

$$\begin{aligned}\delta\vec{x}_1 = -\frac{M_2}{M_1+M_2}\Big[&(\delta x + r_0 e_{13}\delta\psi - r_0 e_{12}\delta\varphi)\hat{\imath}_1 + (-e_{13}\delta x + [r_0+x]\delta\psi + e_{11}r_0\delta\varphi)\hat{\jmath}_1 + \\ &+(e_{12}\delta x - e_{11}r_0\delta\psi + [r_0+x]\delta\varphi)\hat{k}_1\Big]\end{aligned} \qquad (B\text{-}17)$$

The work done in this displacement is given by

$$\delta W_1 = \vec{T}_1\cdot\delta\vec{\gamma}_1 + \vec{F}_1\cdot\delta\vec{x}_1 \qquad (B\text{-}18)$$

where $\vec{T}_1$ is the torque about the mass center of vehicle no. 1, and $\vec{F}_1$ is the thrust through the mass center. Let

$$\vec{T}_1 = T_{11}\hat{\imath}_1 + T_{12}\hat{\jmath}_1 + T_{13}\hat{k}_1 \qquad (B\text{-}19)$$

$$\vec{F}_1 = F_{11}\hat{\imath}_1 + F_{12}\hat{\jmath}_1 + F_{13}\hat{k}_1 \qquad (B\text{-}20)$$

Then

$$\delta W_1 = -\frac{F_{11} M_2}{M_1+M_2}\delta x - \left(T_{12} + \frac{M_2 r_0 F_{13}}{M_1+M_2}\right)\delta\varphi + \left(T_{13} - \frac{M_2 r_0 F_{12}}{M_1+M_2}\right)\delta\psi +$$

$$+ T_{11}\delta e_{11} + T_{12}\delta e_{12} + T_{13}\delta e_{13} \qquad (B-21)$$

A similar expression is obtained from analysis of vehicle no. 2. Upon combination of these expressions, one finds that the generalized forces, denoted as Q, are as follows:

$$Q_x = \frac{M_1 F_{21} - M_2 F_{11}}{M_1+M_2} \qquad Q_{e_{21}} = T_{21}$$

$$Q_\psi = \frac{r_0(M_1 F_{22} - M_2 F_{12})}{M_1+M_2} + T_{13} + T_{23} \qquad Q_{e_{22}} = T_{22}$$

$$Q_{e_{23}} = T_{23}$$

$$Q_\varphi = \frac{r_0(M_1 F_{23} - M_2 F_{13})}{M_1+M_2} - T_{12} - T_{22} \qquad Q_{e_{12}} = T_{12}$$

$$Q_{e_{11}} = T_{11} \qquad Q_{e_{13}} = T_{13} \qquad (B-22)$$

2. Control Torque Inputs

The external torques, T_{ij}, include both disturbances and control torques. The latter torques will be assumed to have the form

$$T_{11}' = -\left[\alpha_{11}\omega_{11} + \alpha_{12}\omega_{12} + \alpha_{13}\omega_{13}' + \alpha_{14}\delta_{11} + \alpha_{15}\delta_{12} + \alpha_{16}\delta_{13}\right]$$

$$T_{12}' = -\left[\beta_{11}\omega_{11} + \beta_{12}\omega_{12} + \beta_{13}\omega_{13}' + \beta_{14}\delta_{11} + \beta_{15}\delta_{12} + \beta_{16}\delta_{13}\right]$$

$$T_{13}' = -\left[\gamma_{11}\omega_{11} + \text{---} + \gamma_{16}\delta_{13}\right]$$

$$T_{21}' = -\left[\alpha_{21}\omega_{21} + \text{---------} + \alpha_{26}\delta_{23}\right]$$

$$T_{22}' = -\left[\beta_{21}\omega_{21} + \text{---------} + \beta_{26}\delta_{23}\right]$$

$$T_{23}' = -\left[\gamma_{21}\omega_{21} + \text{---------} + \gamma_{26}\delta_{23}\right] \qquad (B-23)$$

where ω_{ij} is the inertial angular velocity of body i about its j^{th} axis and δ_{ij} is the pointing error rotation of body i about axis j. The variables ω'_{13} and ω'_{23} represent $(\omega_{13}-\Omega_o)$ and $(\omega_{23}-\Omega_o)$ respectively, where Ω_o is the nominal spin speed.

The pointing errors are related to the coordinate angles as follows:

$$\delta_{11} = e_{11}$$
$$\delta_{12} = e_{12} - \varphi$$
$$\delta_{13} = e_{13} \qquad (B-24)$$

Expressions for the inertial angular-velocity components were given in equations (B-7). Substitution of (B-7) and (B-24) into (B-23) yields expressions for the control torques in terms of the basic vehicle coordinates. This is the form desired for substitution into the equations of motion.

F. EQUATIONS OF MOTION

The equations of motion can now be obtained by substituting the partial derivatives of kinetic energy, the partial derivatives of potential energy, and the generalized force expressions into Lagrange's equations (B-1). The external torques, T_{ij}, and forces, F_{ij}, can then be separated into disturbance and control inputs, and the control-input portion handled as described above.

One further operation proves of value. Note that at this point, the disturbance torques, T_{13}, T_{23}, T_{12}, and T_{22}, will each appear in two of the equations of motion. (Note the form of $Q\psi$ and $Q\varphi$ in equation (A-22).) It is advantageous to eliminate T_{13} and T_{23} from the ψ equation by subtracting the other equations involving T_{13} and T_{23}. A similar remark applies to the φ equation. When this is done, the following equations of motion will be obtained:

$$[M]\{\ddot{y}\} + [C]\{\dot{y}\} + [K]\{y\} = \{f_o\} + \{f_a\} \qquad (B-25)$$

The data matrices [M], [C], and [K] are given in tables B-1, B-2, and B-3 respectively. Parameters C^*_{ij} have been introduced in the data matrix [C] to allow for the possibility of internal energy dissipation in the structure coupling M_1 to M_2.

The vector {y} is given by

$$\{y\} = \begin{Bmatrix} x \\ (\psi - \Omega_0 t) \\ \phi \\ e_{11} \\ e_{12} \\ e_{13} \\ e_{21} \\ e_{22} \\ e_{23} \end{Bmatrix} \tag{B-26}$$

The force vectors $\{f\}_o$ and $\{f\}_d$ are given by

$$\{f_o\} = \begin{Bmatrix} 0 \\ 0 \\ -L_1\Omega_0^2 \\ +K_1\Omega_0^2 \\ 0 \\ -L_2\Omega_0^2 \\ +K_2\Omega_0^2 \end{Bmatrix} \qquad \{f_d\} = \begin{Bmatrix} F_r \\ T_\Omega \\ T_\phi \\ T_{11} \\ T_{12} \\ T_{13} \\ T_{21} \\ T_{22} \\ T_{23} \end{Bmatrix} \tag{B-27}$$

where the following definitions apply:

$$F_r \equiv Q_x$$

$$T_\Omega \equiv Q_\psi - T_{13} - T_{23}$$

$$T_\Phi \equiv Q_\phi + T_{12} + T_{22} \tag{B-28}$$

The generalized forces Q_x, Q_ψ, and Q_ϕ are defined in equation (B-22). The vector $\{f_o\}$ can be considered as representing equivalent static imbalance torques due to the cross-products of inertia. The vector $\{f_d\}$ represents external disturbance torques.

TABLE B-1. DATA MATRIX [M]

	x	ψ	φ	e_{11}	e_{12}	e_{13}	e_{21}	e_{22}	e_{23}
x	$\frac{M_1M_2}{M_1+M_2}$	0	0	0	0	0	0	0	0
ψ	0	$\frac{M_1M_2}{M_1+M_2} r_0^2$	0	0	0	0	0	0	0
φ	0	0	$\frac{M_1M_2}{M_1+M_2} r_0^2$	0	0	0	0	0	0
e_{11}	0	$-K_1$	J_1	I_{11}	$-J_1$	$-K_1$	0	0	0
e_{12}	0	$-L_1$	$-I_{12}$	$-J_1$	I_{12}	$-L_1$	0	0	0
e_{13}	0	I_{13}	L_1	$-K_1$	$-L_1$	I_{13}	0	0	0
e_{21}	0	$-K_2$	J_2	0	0	0	I_{21}	$-J_2$	$-K_2$
e_{22}	0	$-L_2$	$-I_{22}$	0	0	0	$-J_2$	I_{22}	$-L_2$
e_{23}	0	I_{23}	L_2	0	0	0	$-K_2$	$-L_2$	I_{23}

TABLE B-2: DATA MATRIX [C]

	x	ψ	φ	e_{11}	e_{12}	e_{13}	e_{21}	e_{22}	e_{23}
x	C_{11}^*	$-\frac{2M_1M_2}{M_1+M_2} r_0 \Omega_0$	0	C_{14}^*	C_{15}^*	C_{16}^*	C_{17}^*	C_{18}^*	C_{19}^*
ψ	$\frac{2M_1M_2}{M_1+M_2} r_0 \Omega_0^2 - C_{16}^* - C_{19}^*$	0	0	$-C_{46}^* - C_{49}^*$	$-C_{56}^* - C_{59}^*$	$-C_{66}^* - C_{69}^*$	$-C_{76}^* - C_{79}^*$	$-C_{86}^* - C_{89}^*$	$-C_{96}^* - C_{99}^*$
φ	$C_{15}^* + C_{18}^*$	0	0	$C_{45}^* + C_{48}^*$	$C_{55}^* + C_{58}^*$	$C_{65}^* + C_{68}^*$	$C_{75}^* + C_{78}^*$	$C_{85}^* + C_{88}^*$	$C_{95}^* + C_{98}^*$
e_{11}	C_{14}^*	$2L_1\Omega_0 + d_{13}$	$(I_{12}+I_{11}-I_{13})\Omega_0^2 - d_{12}$	$C_{44}^* + d_{11}$	$(I_{13}-I_{11}-I_{12})\Omega_0^2 + C_{45}^* + d_{12}$	$2L_1\Omega_0 + C_{46}^* + d_{13}$	C_{47}^*	C_{48}^*	C_{49}^*
e_{12}	C_{15}^*	$\beta_{13} - 2K_1\Omega_0$	$-\beta_{12}$	$(I_{11}+I_{12}-I_{13})\Omega_0^2 + C_{45}^* + \beta_{11}$	$C_{55}^* + \beta_{12}$	$C_{56}^* + \beta_{13} - 2K_1\Omega_0$	C_{57}^*	C_{58}^*	C_{59}^*
e_{13}	C_{16}^*	γ_{13}	$-2K_1\Omega_0 - \gamma_{12}$	$-2L_1\Omega_0 + C_{46}^* + \gamma_{11}$	$2K_1\Omega_0 + C_{56}^* + \gamma_{12}$	$C_{66}^* + \gamma_{13}$	C_{67}^*	C_{68}^*	C_{69}^*
e_{21}	C_{17}^*	$2L_2\Omega_0 + d_{23}$	$(-I_{23}+I_{21}+I_{22})\Omega_0^2 - d_{22}$	C_{47}^*	C_{57}^*	C_{67}^*	$C_{77}^* + d_{21}$	$(I_{23}-I_{21}-I_{22})\Omega_0^2 + C_{78}^* + d_{22}$	$2L_2\Omega_0 + C_{79}^* + d_{23}$
e_{22}	C_{18}^*	$\beta_{23} - 2K_2\Omega_0$	$-\beta_{22}$	C_{48}^*	C_{58}^*	C_{68}^*	$(-I_{23}+I_{21}+I_{22})\Omega_0^2 + C_{78}^* + \beta_{21}$	$C_{88}^* + \beta_{22}$	$C_{89}^* + \beta_{23} - 2K_2\Omega_0$
e_{23}	C_{19}^*	γ_{23}	$-2K_2\Omega_0 - \gamma_{22}$	C_{49}^*	C_{59}^*	C_{69}^*	$-2L_2\Omega_0 + C_{79}^* + \gamma_{21}$	$2K_2\Omega_0 + C_{89}^* + \gamma_{22}$	$C_{99}^* + \gamma_{23}$

TABLE B-3 DATA MATRIX [K]

	x	ψ	φ	e_{11}	e_{12}	e_{13}	e_{21}	e_{22}	e_{23}
x	$K_{11}^* - \frac{M_1 M_2}{M_1+M_2}\Omega_0^2$	0	0	K_{14}^*	K_{15}^*	K_{16}^*	K_{17}^*	K_{18}^*	K_{19}^*
ψ	$-K_{16}^* - K_{19}^*$	0	$(L_1+L_2)\Omega_0^2$	$-K_{46}^* - K_{49}^*$	$-K_{56}^* - K_{59}^*$	$-K_{66}^* - K_{69}^*$	$-K_{76}^* - K_{79}^*$	$-K_{86}^* - K_{89}^*$	$-K_{96}^* - K_{99}^*$
φ	$K_{15}^* + K_{18}^*$	0	$\frac{M_1 M_2}{M_1+M_2} r_0^2 \Omega_0^2$	$K_{45}^* + K_{48}^*$	$K_{55}^* + K_{58}^*$	$K_{65}^* + K_{68}^* + -L_1\Omega_0^2$	$K_{75}^* + K_{78}^*$	$K_{85}^* + K_{88}^*$	$K_{95}^* + K_{98}^* + -L_2\Omega_0^2$
e_{11}	K_{14}^*	0	$J_1\Omega_0^2 + \alpha_{11}\Omega_0 + -\alpha_{15}$	$(I_{13}-I_{12})\Omega_0^2 + +K_{44}^* + \alpha_{12}\Omega_0 + +\alpha_{14}$	$-J_1\Omega_0^2 + K_{45}^* + -\alpha_{11}\Omega_0 + \alpha_{15}$	$K_{46}^* + \alpha_{16}$	K_{47}^*	K_{48}^*	K_{49}^*
e_{12}	K_{15}^*	0	$(I_{11}-I_{13})\Omega_0^2 + +\beta_{11}\Omega_0 - \beta_{15}$	$-J_1\Omega_0^2 + K_{45}^* + +\beta_{12}\Omega_0 + \beta_{14}$	$(I_{13}-I_{11})\Omega_0^2 + +K_{55}^* - \beta_{11}\Omega_0 + +\beta_{15}$	$K_{56}^* + \beta_{16}$	K_{57}^*	K_{58}^*	K_{59}^*
e_{13}	K_{16}^*	0	$\gamma_{11}\Omega_0 - \gamma_{15} + -L_1\Omega_0^2$	$K_{46}^* + +\gamma_{12}\Omega_0 + \gamma_{14}$	$K_{56}^* - \gamma_{11}\Omega_0 + +\gamma_{15}$	$K_{66}^* + \gamma_{16}$	K_{67}^*	K_{68}^*	K_{69}^*
e_{21}	K_{17}^*	0	$J_2\Omega_0^2 + \alpha_{21}\Omega_0 - \alpha_{25}$	K_{47}^*	K_{57}^*	K_{67}^*	$(I_{23}-I_{22})\Omega_0^2 + +K_{77}^* + \alpha_{22}\Omega_0 + +\alpha_{24}$	$-J_2\Omega_0^2 + +K_{78}^* - \alpha_{21}\Omega_0 + +\alpha_{25}$	$K_{79}^* + \alpha_{26}$
e_{22}	K_{18}^*	0	$(I_{21}-I_{23})\Omega_0^2 + +\beta_{21}\Omega_0 - \beta_{25}$	K_{48}^*	K_{58}^*	K_{68}^*	$-J_2\Omega_0^2 + K_{78}^* + +\beta_{22}\Omega_0 + \beta_{24}$	$(I_{23}-I_{21})\Omega_0^2 + +K_{88}^* + -\beta_{21}\Omega_0 + \beta_{25}$	$K_{89}^* + \beta_{26}$
e_{23}	K_{19}^*	0	$-L_2\Omega_0^2 + +\gamma_{21}\Omega_0 - \gamma_{25}$	K_{49}^*	K_{59}^*	K_{69}^*	$K_{79}^* + \gamma_{22}\Omega_0 + +\gamma_{24}$	$K_{89}^* + -\gamma_{21}\Omega_0 + \gamma_{25}$	$K_{99}^* + \gamma_{26}$

APPENDIX C

DERIVATION OF GENERALIZED CABLE INFLUENCE COEFFICIENTS

A. DISCUSSION

The cable spring gradients can be expressed in terms of partial derivatives of strain energy with respect to rotations of the end masses. Accordingly, an expression for the strain energy stored in an arbitrarily located cable will be developed, and appropriate partial-derivative computations performed.

The strain energy in a cable is a function of the amount of cable stretch. This stretch must be geometrically related to the angular rotations of the end capsules. The primary task, then, is to determine the amount of stretch induced in an arbitrarily located cable by specified motions of the end capsules.

B. GEOMETRIC CONSIDERATIONS

Denote the vector length of an arbitrarily located cable as $\vec{\ell}$. Let $\vec{d}_1$ and $\vec{d}_2$ denote vectors drawn from the mass centers of vehicles No. 1 and No. 2, respectively, to the points where the cable attaches to the capsules.

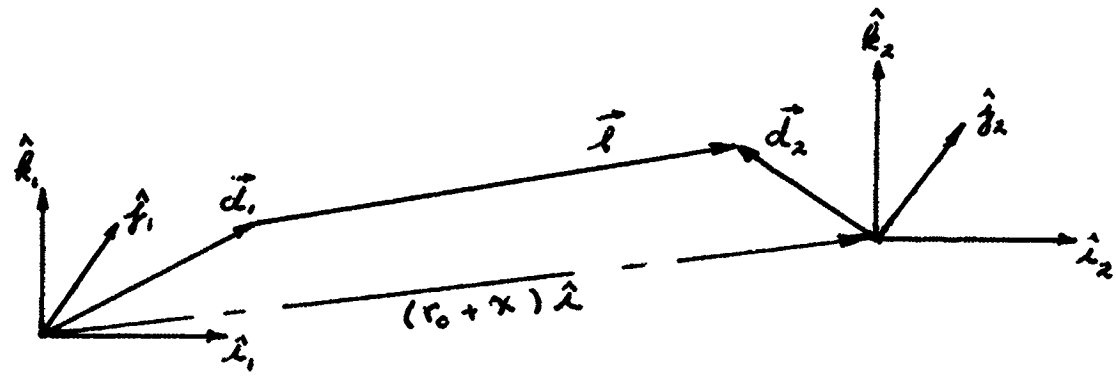

FIGURE C-1 DEFINITION OF CABLE LENGTH VECTOR

It can be seen from figure C-1 that

$$\vec{\ell} = -\vec{d}_1 + \vec{d}_2 + (r_o + x)\hat{\imath} \qquad (C-1)$$

Let the vectors $\vec{d}_1$ and $\vec{d}_2$ be expressed in terms of their body axis components (see Appendix B for definition of the various unit vectors):

$$\vec{d}_1 = d_{11}\hat{\imath}_1 + d_{12}\hat{\jmath}_1 + d_{13}\hat{k}_1 \qquad (C-2)$$

$$\vec{d}_2 = d_{21}\hat{\imath}_2 + d_{22}\hat{\jmath}_2 + d_{23}\hat{k}_2 \qquad (C-3)$$

Then substitution of $(\hat{\imath},\hat{\jmath},\hat{k})$ for $(\hat{\imath}_1,\hat{\jmath}_1,\hat{k}_1)$ and $(\hat{\imath}_2,\hat{\jmath}_2,\hat{k}_2)$, using the transformation of figure B-3 yields

$$\vec{d}_1 = \left\{d_{11}\left(1-\frac{e_{12}^2+e_{13}^2}{2}\right) + d_{12}(-e_{13}+e_{11}e_{12}) + d_{13}(e_{12}+e_{11}e_{13})\right\}\hat{\imath} +$$

$$+\left\{d_{11}e_{13} + d_{12}\left(1-\frac{e_{11}^2+e_{13}^2}{2}\right) + d_{13}(-e_{11}+e_{12}e_{13})\right\}\hat{\jmath} +$$

$$+\left\{-d_{11}e_{12} + d_{12}e_{11} + d_{13}\left(1-\frac{e_{11}^2+e_{12}^2}{2}\right)\right\}\hat{k} \qquad (C-4)$$

A similar expression is obtained for $\vec{d}_2$. Second-order terms have been retained because an energy analysis is being employed. Only a second-order energy change results from a first-order vehicle rotation. Thus, second-order terms must be retained in order to obtain first-order accuracy in the torque expressions.

It is expedient to introduce the reference lengths

$$\ell_1 = r_o + d_{21} - d_{11} \qquad (C-5)$$

$$\ell_2 = d_{22} - d_{12} \qquad (C-6)$$

$$\ell_3 = d_{23} - d_{13} \qquad (C-7)$$

The introduction of components of cable stretch, Δ_1, Δ_2, and Δ_3 is also of value:

$$\Delta_1 = (x-x_o) - d_{22}e_{23} + d_{23}e_{22} - \frac{d_{21}}{2}(e_{22}^2+e_{23}^2) + d_{22}e_{21}e_{22} +$$

$$+ d_{23}e_{21}e_{23} + d_{12}e_{13} - d_{13}e_{12} + \frac{d_{11}}{2}(e_{12}^2+e_{13}^2) - d_{12}e_{11}e_{12} - d_{13}e_{11}e_{13} \qquad (C-8)$$

$$\Delta_2 = d_{21}e_{23} - d_{23}e_{21} - \frac{d_{22}}{2}(e_{21}^2+e_{23}^2) + d_{23}e_{23}e_{22} - d_{11}e_{13} + d_{13}e_{11} +$$

$$+ \frac{d_{12}}{2}(e_{11}^2+e_{13}^2) - d_{13}e_{13}e_{12} \qquad (C-9)$$

$$\Delta_3 = -\alpha_{21} e_{22} + \alpha_{22} e_{21} - \frac{\alpha_{23}}{2}\left(e_{21}^2 + e_{22}^2\right) + \alpha_{11} e_{12} - \alpha_{12} e_{11} + \frac{\alpha_{13}}{2}\left(e_{11}^2 + e_{12}^2\right) \quad (C\text{-}10)$$

In the expression for Δ_1, the factor Xo represents the cable stretch due to centrifugal force alone, i.e., in the quiescent spinning condition, X = Xo. Substitution of (C-4) through (C-10) into (C-1) yields

$$\vec{\ell} = (\ell_1 + X_0 + \Delta_1)\hat{i} + (\ell_2 + \Delta_2)\hat{j} + (\ell_3 + \Delta_3)\hat{k} \quad (C\text{-}11)$$

Define

$$\ell_u = \sqrt{\ell_1^2 + \ell_2^2 + \ell_3^2} \quad (C\text{-}12)$$

$$\ell_1^* = \ell_1 + X_0 \quad (C\text{-}13)$$

$$\ell_1^{**} = \ell_1 + \frac{X_0}{2} \quad (C\text{-}14)$$

Then the magnitude of $\vec{\ell}$ is given by

$$\ell^2 = \ell_u^2\left[1 + \frac{2}{\ell_u^2}\left\{\ell_1^{**} X_0 + (\ell_1^* \Delta_1 + \ell_2 \Delta_2 + \ell_3 \Delta_3) + \frac{1}{2}(\Delta_1^2 + \Delta_2^2 + \Delta_3^2)\right\}\right] \quad (C\text{-}15)$$

The magnitude of $\vec{\ell}$g denoted ℓ, can be obtained by using the binomial expansion of (C-15) and neglecting third-order terms

$$\ell \approx \ell_u\left[1 + \frac{1}{\ell_u^2}\left\{\left(1 - \frac{\ell_1^{**} X_0}{2\ell_u^2}\right)\ell_1^{**} X_0 + \left(1 - \frac{\ell_1^{**} X_0}{\ell_u^2}\right)(\ell_1^* \Delta_1 + \ell_2 \Delta_2 + \ell_3 \Delta_3) + \right.\right.$$

$$+\left(1 - \frac{\ell_1^{**} X_0}{\ell_u^2} - \frac{\ell_1^{*2}}{\ell_u^2}\right)\frac{\Delta_1^2}{2} + \left(1 - \frac{\ell_1^{**} X_0}{\ell_u^2} - \frac{\ell_2^2}{\ell_u^2}\right)\frac{\Delta_2^2}{2} + \left(1 - \frac{\ell_1^{**} X_0}{\ell_u^2} - \frac{\ell_3^2}{\ell_u^2}\right)\frac{\Delta_3^2}{2} +$$

$$\left. \left. - \frac{\ell_1^* \ell_2}{\ell_u^2}\Delta_1\Delta_2 - \frac{\ell_1^* \ell_3}{\ell_u^2}\Delta_1\Delta_3 - \frac{\ell_2 \ell_3}{\ell_u^2}\Delta_2\Delta_3 \right\}\right] \quad (C\text{-}16)$$

C. STRAIN ENERGY EXPRESSION

The strain energy of a cable is given by

$$V = \frac{AE}{2\ell_u}(\ell - \ell_u)^2 \quad (C\text{-}17)$$

Substituting equation (C-16) leads to

$$V = \frac{1}{2}\left[a_0 X^2 + 2a_1\Delta_1 + 2a_2\Delta_2 + 2a_3\Delta_3 + b_1\Delta_1^2 + b_2\Delta_2^2 + \right.$$

$$\left. + 2g_1\Delta_1\Delta_2 + 2g_2\Delta_1\Delta_3 + 2g_3\Delta_2\Delta_3\right] \quad (C\text{-}18)$$

where

$$a_0 \equiv \left(1 - \frac{\ell_1^{**} X_0}{2\ell_u^2}\right)^2 \left(\frac{AE\,\ell_1^{**2}}{\ell_u^3}\right)$$

$$a_1 \equiv \left(1 - \frac{\ell_1^{**} X_0}{2\ell_u^2}\right)\left(1 - \frac{\ell_1^{**} X_0}{\ell_u^2}\right)\left(\frac{AE\,\ell_1^{**}\ell_1^{*} X_0}{\ell_u^3}\right)$$

$$a_2 \equiv \left(\frac{\ell_2}{\ell_1^{*}}\right) a_1$$

$$a_3 \equiv \left(\frac{\ell_3}{\ell_1^{*}}\right) a_1$$

$$b_1 \equiv \left[\left(1 - \frac{\ell_1^{**} X_0}{2\ell_u^2}\right)\left(1 - \frac{\ell_1^{**} X_0}{\ell_u^2} - \frac{\ell_1^{*2}}{\ell_u^2}\right)\left(\ell_1^{**} X_0\right) + \left(1 - \frac{\ell_1^{**} X_0}{\ell_u^2}\right)^2 \ell_1^{*2}\right]\left(\frac{AE}{\ell_u^3}\right)$$

$$b_2 \equiv \left[\left(1 - \frac{\ell_1^{**} X_0}{2\ell_u^2}\right)\left(1 - \frac{\ell_1^{**} X_0}{\ell_u^2} - \frac{\ell_2^2}{\ell_u^2}\right)\left(\ell_1^{**} X_0\right) + \left(1 - \frac{\ell_1^{**} X_0}{\ell_u^2}\right)^2 \ell_2^2\right]\left(\frac{AE}{\ell_u^3}\right)$$

$$b_3 \equiv \left[\left(1 - \frac{\ell_1^{**} X_0}{2\ell_u^2}\right)\left(1 - \frac{\ell_1^{**} X_0}{\ell_u^2} - \frac{\ell_3^2}{\ell_u^2}\right)\left(\ell_1^{**} X_0\right) + \left(1 - \frac{\ell_1^{**} X_0}{\ell_u^2}\right)^2 \ell_3^2\right]\left(\frac{AE}{\ell_u^3}\right)$$

$$g_1 \equiv \left[\left(1 - \frac{\ell_1^{**} X_0}{\ell_u^2}\right)^2 - \frac{\ell_1^{**} X_0}{\ell_u^2}\left(1 - \frac{\ell_1^{**} X_0}{2\ell_u^2}\right)\right]\left(\frac{AE\,\ell_1^{*}\ell_2}{\ell_u^3}\right)$$

$$g_2 \equiv \left[\left(1 - \frac{\ell_1^{**} X_0}{\ell_u^2}\right)^2 - \frac{\ell_1^{**} X_0}{\ell_u^2}\left(1 - \frac{\ell_1^{**} X_0}{2\ell_u^2}\right)\right]\left(\frac{AE\,\ell_1^{*}\ell_3}{\ell_u^3}\right)$$

$$g_3 \equiv \left[\left(1 - \frac{\ell_1^{**} X_0}{\ell_u^2}\right)^2 - \frac{\ell_1^{**} X_0}{\ell_u^2}\left(1 - \frac{\ell_1^{**} X_0}{2\ell_u^2}\right)\right]\left(\frac{AE\,\ell_2\ell_3}{\ell_u^3}\right) \qquad (C\text{-}19)$$

D. CALCULATION OF PARTIAL DERIVITIVES

The partial derivitives of the strain energy with respect to each parameter of interest are listed in table C-1. Only first-order terms have been retained in carrying out this final step.

$$K_{11}^{*} = b_1 \qquad K_{17}^{*} = -g_1 d_{23} + g_2 d_{22}$$

$$K_{14}^{*} = g_1 d_{13} - g_2 d_{12} \qquad K_{18}^{*} = b_1 d_{23} - g_2 d_{21}$$

$$K_{15}^{*} = -b_1 d_{13} + g_2 d_{11} \qquad K_{19}^{*} = -b_1 d_{22} + g_1 d_{21}$$

$$K_{16}^{*} = b_1 d_{12} - g_1 d_{11}$$

$$K_{44}^{*} = a_2 d_{12} + a_3 d_{13} + b_3 d_{12}^2 + b_2 d_{13}^2 - 2 g_3 d_{12} d_{13}$$

TABLE C-1, SHEET 1 OF 2: CABLE INFLUENCE COEFFICIENTS

$$K^*_{45} = -a_1 d_{12} - b_3 d_{11} d_{12} - g_1 d_{13}^2 + g_2 d_{12} d_{13} + g_3 d_{11} d_{13}$$

$$K^*_{46} = -a_1 d_{13} - b_2 d_{13} d_{11} + g_1 d_{12} d_{13} - g_2 d_{12}^2 + g_3 d_{11} d_{12}$$

$$K^*_{47} = -b_2 d_{13} d_{23} - b_3 d_{12} d_{22} + g_3 d_{13} d_{22} + g_3 d_{12} d_{23}$$

$$K^*_{48} = b_3 d_{12} d_{21} + g_1 d_{23} d_{13} - g_2 d_{12} d_{23} - g_3 d_{13} d_{21}$$

$$K^*_{49} = b_2 d_{13} d_{21} - g_1 d_{23} d_{13} + g_2 d_{12} d_{22} - g_3 d_{12} d_{21}$$

$$K^*_{55} = a_1 d_{11} + a_3 d_{13} + b_1 d_{13}^2 + b_3 d_{11}^2 - 2 g_2 d_{11} d_{13}$$

$$K^*_{56} = -a_2 d_{13} + g_1 d_{11} d_{13} + g_2 d_{11} d_{12} - g_3 d_{11}^2 - b_1 d_{13} d_{12}$$

$$K^*_{57} = b_3 d_{11} d_{22} + g_1 d_{13} d_{23} - g_2 d_{13} d_{22} - g_3 d_{11} d_{23}$$

$$K^*_{58} = -b_3 d_{11} d_{21} + g_2 d_{11} d_{23} + g_2 d_{13} d_{21} - b_1 d_{13} d_{23}$$

$$K^*_{59} = -g_1 d_{13} d_{21} - g_2 d_{11} d_{22} + g_3 d_{11} d_{21} + b_1 d_{13} d_{22}$$

$$K^*_{66} = a_1 d_{11} + a_2 d_{12} + b_1 d_{12}^2 + b_2 d_{11}^2 - 2 g_1 d_{11} d_{12}$$

$$K^*_{67} = b_2 d_{11} d_{23} - g_1 d_{12} d_{23} + g_2 d_{12} d_{22} - g_3 d_{11} d_{22}$$

$$K^*_{68} = b_1 d_{12} d_{23} - g_1 d_{11} d_{23} - g_2 d_{12} d_{21} + g_3 d_{11} d_{21}$$

$$K^*_{69} = -b_1 d_{12} d_{22} - b_2 d_{11} d_{21} + g_1 (d_{12} d_{21} + d_{11} d_{22})$$

$$K^*_{77} = -a_2 d_{22} - a_3 d_{23} + b_3 d_{22}^2 + b_2 d_{23}^2 - 2 g_3 d_{22} d_{23} - g_3 d_{23} d_{22}$$

$$K^*_{78} = a_1 d_{22} - b_3 d_{22} d_{21} - g_1 d_{23}^2 + g_2 d_{22} d_{23} + g_3 d_{23} d_{21}$$

$$K^*_{79} = a_1 d_{23} - b_2 d_{23} d_{21} + g_1 d_{23} d_{22} - g_2 d_{22}^2 + g_3 d_{22} d_{21}$$

$$K^*_{88} = -a_1 d_{21} - a_3 d_{23} + b_1 d_{23}^2 + b_3 d_{21}^2 - 2 g_2 d_{23} d_{21}$$

$$K^*_{89} = a_2 d_{23} - b_1 d_{23} d_{22} + g_1 d_{23} d_{21} + g_2 d_{21} d_{22} - g_3 d_{21}^2$$

$$K^*_{99} = -a_1 d_{21} - a_2 d_{22} + b_1 d_{22}^2 + b_2 d_{21}^2 - 2 g_1 d_{21} d_{22}$$

NOTE: $K^*_{ij} = 0$ FOR ALL NOT LISTED ABOVE

$K^*_{ij} = K^*_{ji}$ FOR ALL i AND j

TABLE C-1, SHEET 2 OF 2: CABLE INFLUENCE COEFFICIENTS

APPENDIX D

ACTUATOR COMPARISONS FOR ROLL/PITCH DAMPING

This appendix presents comparisons of several potential actuator systems which might be considered for meeting the damping requirements imposed on the roll and pitch axes of a spinning space station. The potential systems include

- Two-degree-of-freedom control-moment gyros
- Single-degree-of-freedom control-moment gyros
- Inertia wheels
- Reaction jets.

On the basis of the following analysis, a two-degree-of-freedom gyro has been selected for use in the system. The other candidates are compared to this actuator.

A. TWO SINGLE-DEGREE-OF-FREEDOM GYROS VS. TWO-DEGREE-OF-FREEDOM GYRO

There are two basic methods that can be used to compare alternate damping actuation systems. The first is to design and optimize competitive systems, using the alternate actuation schemes, and then compare overall system performance.

The second is to design an optimum damping system on the assumption that the required actuator torque-time histories can be obtained, by an unspecified method, and to then compare the competitive methods of obtaining the required torques. The second method has been chosen here, since the comparisons can be made completely independent of vehicle dynamics, and the relative advantages of the compared actuation systems can therefore be seen more clearly.

Figure D-1 illustrates the alternate damping actuators and defines the gyro parameters and coordinate systems.

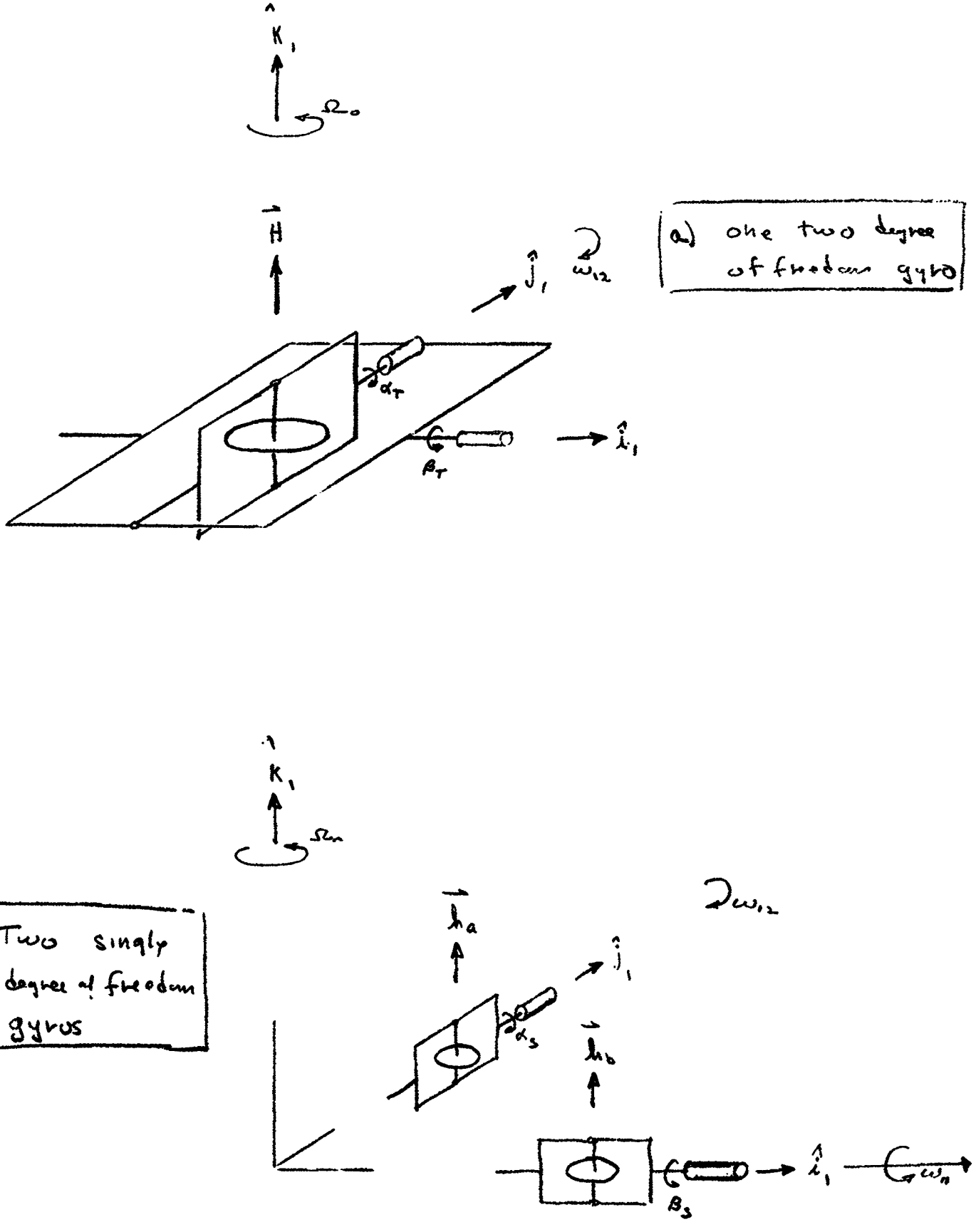

FIGURE D-1 CONTROL MOMENT GYRO ACTUATION FOR PITCH-ROLL DAMPING

1. Two-Degree-of-Freedom Gyro

The linearized equations of motion of the two-degree-of-freedom gyro may be written as

$$T_o = H\left[\dot{\alpha}_T + \Omega_o \beta_T + \omega_{12}\right]$$

$$T_I = H\left[-\dot{\beta}_T + \Omega_o \alpha_T - \omega_{11}\right] \qquad (D\text{-}1)$$

where

T_o = torque applied to outer gimbal

T_I = torque applied to inner gimbal

Ω_o = vehicle spin rate

ω_{11} = vehicle inertial roll rate

ω_{12} = vehicle inertial pitch rate.

Rearranging equations (D-1) gives

$$\dot{\alpha}_T = \frac{T_o}{H} - \Omega_o \beta_T - \omega_{12}$$

$$\dot{\beta}_T = -\frac{T_I}{H} + \Omega_o \alpha_T - \omega_{11} \qquad (D\text{-}2)$$

The factors T_o and T_I are the gyro torque histories required by the optimum control system, and are assumed known.

2. Single-Degree-of-Freedom Gyros

The linearized equations of motion for gyro (a) may be written

$$T_{ra} = h_a\left[\dot{\alpha}_s + \omega_{12}\right]$$

$$T_{pa} = h_a\left[\Omega_o \alpha_s - \omega_{11}\right] \qquad (D\text{-}3)$$

and those for gyro (b) may be written

$$T_{rb} = h_b \left[\Omega_o \beta_s + \omega_{12} \right]$$
$$T_{pb} = -h_b \left[\dot{\beta}_s + \omega_{11} \right] \qquad (D-4)$$

The total roll and pitch torques applied by the vehicle to the actuators is

$$T_r = h_a \dot{\alpha}_s + h_b \Omega_o \beta_s + (h_a + h_b)\, \omega_{12}$$
$$T_p = -h_b \dot{\beta}_s + h_a \Omega_o \alpha_s - (h_a + h_b)\, \omega_{11} \qquad (D-5)$$

Re-arranging equations (D-5) gives

$$\frac{h_a}{h_T} \dot{\alpha}_s = \frac{T_r}{h_T} - \frac{h_b}{h_T} \Omega_o \beta_s - \omega_{12}$$
$$\frac{h_b}{h_T} \dot{\beta}_s = -\frac{T_p}{h_T} + \frac{h_a}{h_T} \Omega_o \alpha_s - \omega_{11} \qquad (D-6)$$

where

$$h_T \equiv h_a + h_b$$

3. Comparison

For identical vehicle performance with the two actuation systems, it is evident from a comparison of equations (D-2) and (D-6) that the actuator torque outputs must be equal; i.e.,

$$\begin{Bmatrix} T_o \\ T_I \end{Bmatrix} = \begin{Bmatrix} T_r \\ T_p \end{Bmatrix} \qquad (D-7)$$

In general, vehicle motion will constitute a very small part of the total gimbal angles, so that equations (D-2) and (D-6) may be simplified to:

$$\dot{\alpha}_T \approx \frac{T_o}{H} - \Omega_o \beta_T$$

$$\dot{\beta}_T = -\frac{T_I}{H} + \Omega_o \alpha_T$$

$$\dot{\alpha}_s = \frac{T_o}{h_a} - \frac{h_b}{h_a}\Omega_o \beta_s \qquad (D\text{-}8)$$

$$\dot{\beta}_s = -\frac{T_I}{h_a} + \frac{h_a}{h_b}\Omega_o \alpha_s$$

It is evident from (D-8) that for $\alpha_s = \alpha_T$ and $\beta_s = \beta_T$, we must have

$$h_a = h_b = H \qquad (D\text{-}9)$$

so that

$$h_T = 2H \qquad (D\text{-}10)$$

The single-degree-of-freedom gyro system therefore requires twice the total angular momentum as the two-degree-of-freedom gyro system. This implies, essentially, a factor of two advantage in both weight and power for the two-degree-of-freedom gyro system.

B. TWO INERTIA WHEELS VS TWO-DEGREE-OF-FREEDOM GYRO

The rate damper actuators are required to deliver sinusoidal torques oscillating at the wobble frequency, ω_o. The inertia wheel configuration shown in figure D-2 can provide such torques on both vehicle axes by controlling the wheel speeds such that

$$\omega_a = \frac{T_{MAX}}{(\Omega_o + \omega_o) I_W} \sin \omega_o t$$

$$\omega_b = -\frac{T_{MAX}}{(\Omega_o + \omega_o) I_W} \cos \omega_o t \qquad (D\text{-}11)$$

in which case the vehicle torques are:

$$T_r = -T_{MAX} \cos \omega_o t$$

$$T_p = -T_{MAX} \sin \omega_o t \qquad (D\text{-}12)$$

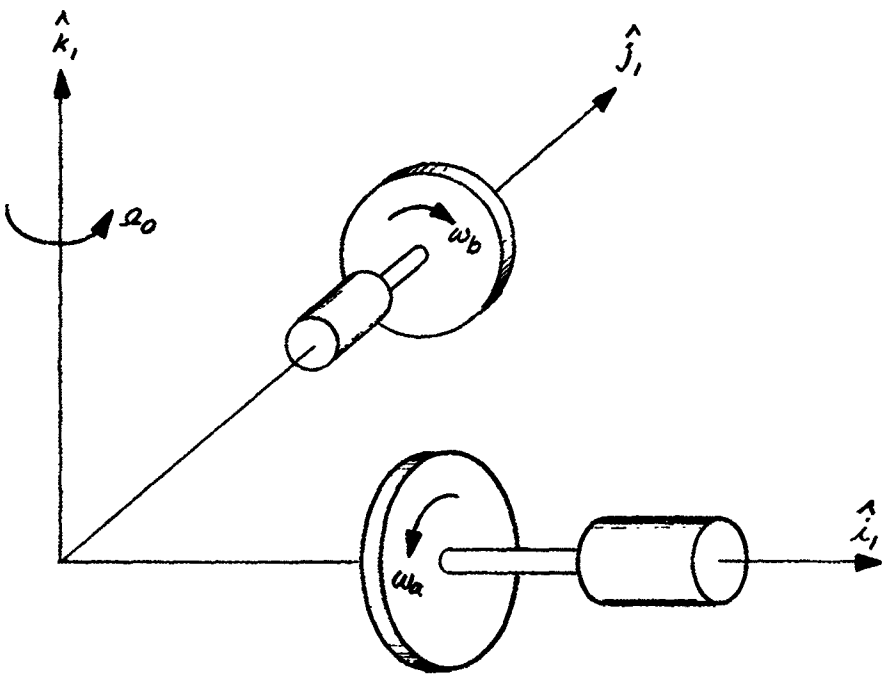

$$T_R = I\omega(\dot{\omega}_a - \omega_b \Omega_0)$$

$$T_P = I_W(\dot{\omega}_b + \omega_a \Omega_0)$$

FIGURE D-2 INERTIA WHEEL ACTUATION FOR PITCH-ROLL DAMPING

The cross-coupling effect of vehicle spin is included in equation (D-12).

The instantaneous power of torquer A is

$$P_a = I_w \dot{\omega}_a \omega_a = \frac{T_{MAX}^2 \omega_o}{2(\Omega_o + \omega_o)^2 I_w} \sin 2\omega_o t \qquad (D\text{-}13)$$

so that the torquers must provide peak powers up to

$$P_{a_{MAX}} = \frac{T_{MAX}^2 \omega_c}{2(\Omega_o + \omega_o)^2 I_w} \qquad (D\text{-}14)$$

In comparison, the control moment gyro torque output is (equation D-1 neglecting small effects of ω_{11} and ω_{12})

$$T_o = H\left[\dot{\alpha}_T + \Omega_o \beta_T\right]$$
$$T_I = H\left[-\dot{\beta}_T + \Omega_o \alpha_T\right] \qquad (D\text{-}15)$$

These torques can be obtained by controlling α_T and β_T such that

$$\alpha_T = \alpha_{MAX} \sin \omega_c t$$
$$\beta_T = \beta_{MAX} \cos \omega_c t \qquad (D\text{-}16)$$

From equations (D-15) and (D-16) it can be seen that

$$T_{MAX} = H(\Omega_o + \omega_o)\alpha_{MAX} \qquad (D\text{-}17)$$

and

$$T_o = T_{MAX} \cos \omega_o t$$
$$T_I = T_{MAX} \sin \omega_o t \qquad (D\text{-}18)$$

Solving (D-17) for α_{max} and substituting in (D-16) gives

$$\alpha_T = \frac{T_{MAX}}{H(\Omega_o+\omega_o)} \sin \omega_o t$$

$$\beta_T = \frac{T_{MAX}}{H(\Omega_o+\omega_o)} \cos \omega_o t \qquad (D\text{-}19)$$

Thus, for the control moment gyro, the torquer power is

$$P_g = T_o \dot{\beta}_T = \frac{T_{MAX}^2 \omega_o}{2H(\Omega_o+\omega_o)} \sin 2\omega_o t \qquad (D\text{-}20)$$

so that the peak gyro torquer power is

$$P_{g\,MAX} = \frac{T_{MAX}^2 \omega_o}{2H(\Omega_o+\omega_o)} \qquad (D\text{-}21)$$

For equal weight in the inertia-wheel system and the two-degree-of-freedom gyro system, the gyro wheel will be approximately twice as heavy as one of the two inertia wheels, so that

$$I_g = 2 I_w \qquad (D\text{-}22)$$

and

$$H = 2 I_w \omega_g \qquad (D\text{-}23)$$

In this case, the ratio of inertia-wheel torquer power to gyro torquer power is

$$\frac{P_{a\,MAX}}{P_{g\,MAX}} = \frac{2\omega_g}{\Omega_o+\omega_o} \qquad (D\text{-}24)$$

In general, the gyro rotor speed, ω_g, is about 500 radians per second. In addition, for the range of vehicle parameters considered in this report, the maximum value of spin speed plus wobble frequency, $(\Omega_o + \omega_o)$, is approximately unity, so that the gyro system enjoys a minimum power advantage of 1000:1 over the inertia-wheel system. In Section VIII it is

shown that the peak gyro-torquer power to be expected is approximately 11 watts. This implies that a 14 horsepower servo would be required with each inertia wheel for adequate rate damping. Further consideration of inertia-wheel actuators for the pitch and roll axes does not appear warranted.

C. REACTION JET SYSTEM VS TWO-DEGREE-OF-FREEDOM CONTROL MOMENT GYRO

A direct torque or power comparison between the use of a two-degree-of-freedom control-moment gyro and reaction-jet thrusting for roll/pitch damping cannot, of course, be made. It is useful, however, to estimate the order of magnitude of propellant requirements for a jet-damping system for consideration in comparing the two systems. Figure D-3 shows typical computer runs obtained for a reaction-jet-damping system. These records use the vehicle model discussed in Section V. In this case, a 0.1-degree-per-second damping threshold has been assumed, and various small reaction jets mounted on seven-foot moment arms have been used. It is evident that the propellant consumption will be approximately 1.5 pounds per disturbance. It can be shown that adequate vehicle damping can be obtained for the same disturbance inputs as noted on figure D-3 with a two-degree-of-freedom control-moment gyro system having an angular momentum of 56 ft lb sec. Such a gyro would weigh approximately 45 pounds, so that the weight crossover point is reached at 30 disturbances. This crossover occurs at a low enough point to obviate the use of reaction jets for damping the vehicle, at least for missions of relatively long duration.

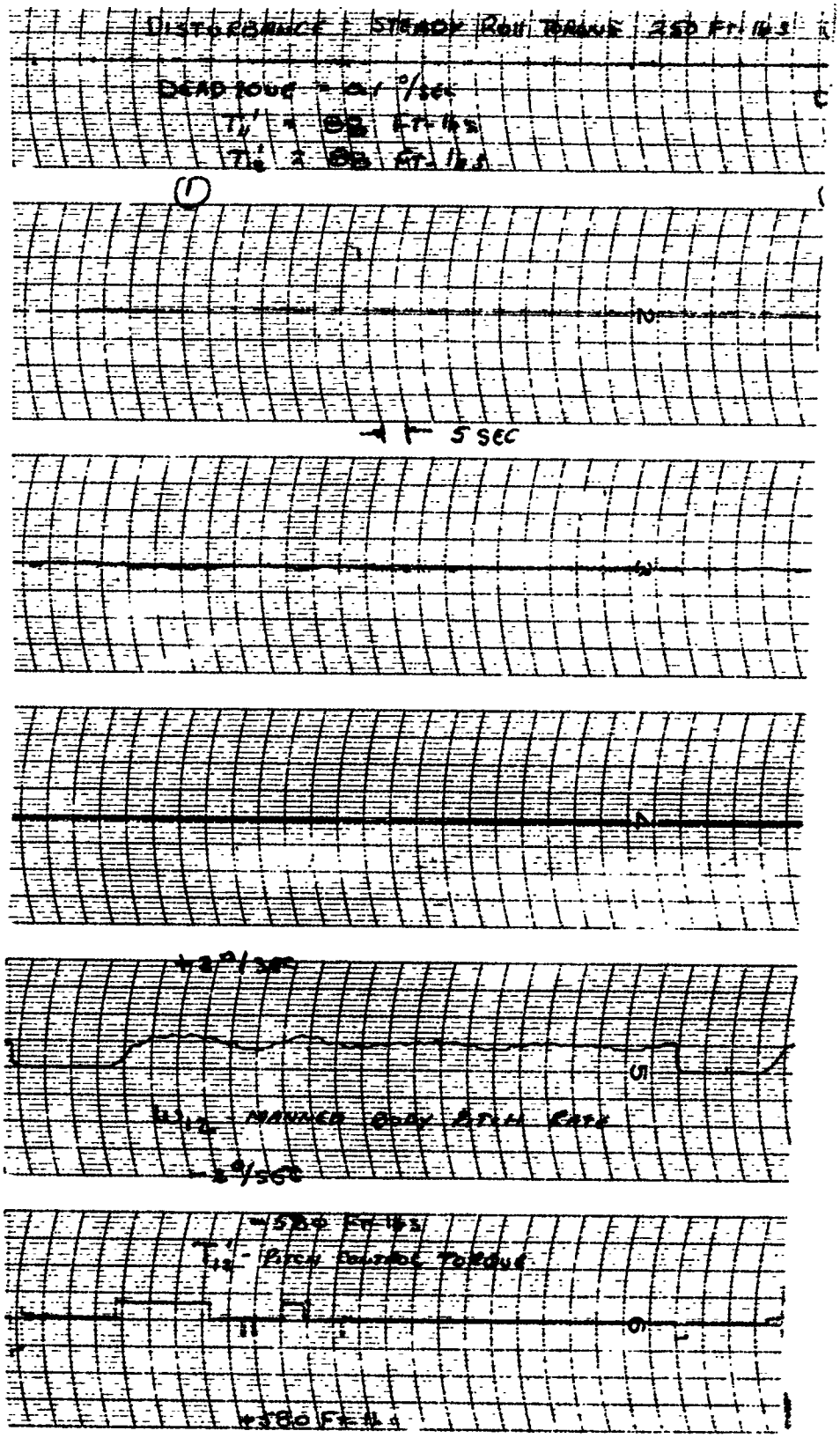
DISTURBANCE STEADY ROLL TORQUE 250 FT-LBS
DEAD BAND = 0.1°/SEC
5 SEC
+2°/SEC
-2°/SEC
+250 FT-LBS
+380 FT-LBS

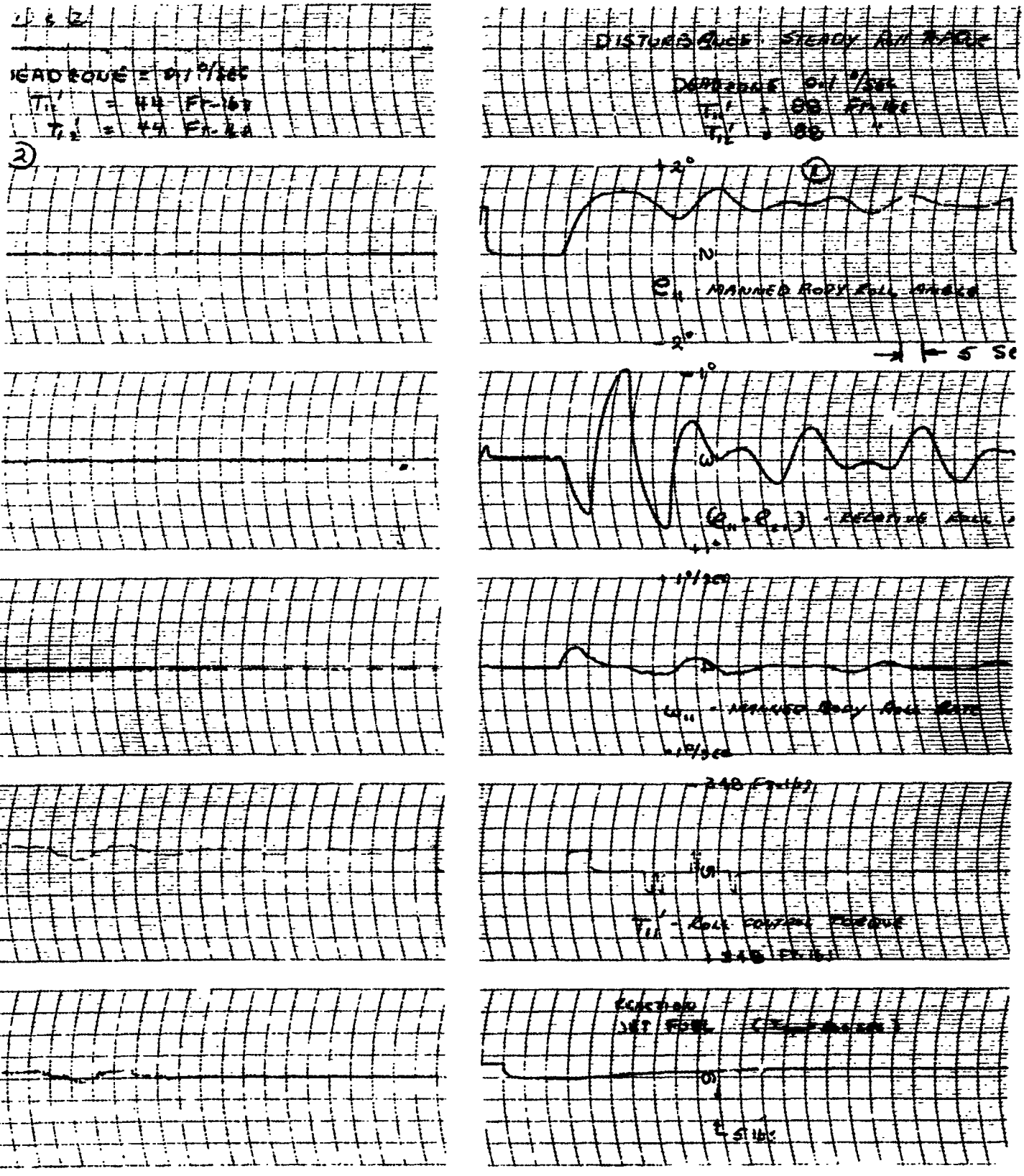

D-3-2

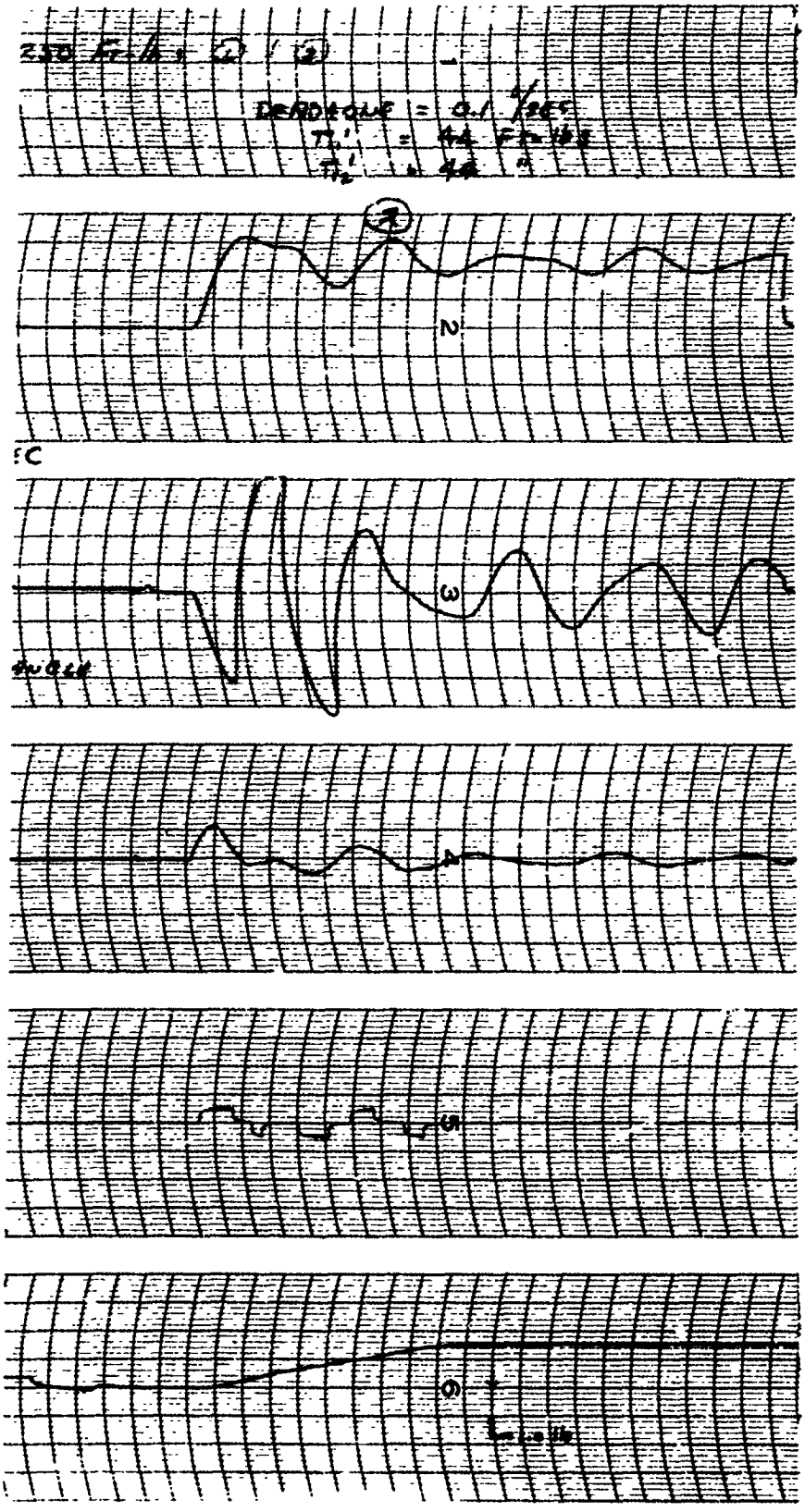

FIGURE D-3 RATE STABILIZATION SYSTEM PERFORMANCE USING REACTION JETS.

APPENDIX E

DERIVATION OF EQUATIONS FOR EXTENSION-RETRACTION MODEL

A. VEHICLE DYNAMICS

The extension-retraction model presented here is restricted to the four degrees of vehicle freedom that are contained in the spin plane. These consist of the following:

- The separation of the centers of mass of the two rigid bodies, r.
- The spin speed of the two rigid bodies about their common mass center, Ω.
- The yaw angle between the principal axis of the manned body and the line of centers of the two bodies, e_{13}.
- The similar yaw angle for the booster, e_{23}.

The equations of motion for this four-degree-of-freedom model are as follows, using symbols defined in Appendix A and equation (B-26):

$$F_r = M_T (\ddot{r} - r\Omega^2)$$

$$T_\Omega = 2M_T \Omega r \dot{r} + M_T r^2 \dot{\Omega} + I_{13}(\ddot{e}_{13} + \dot{\Omega}) + I_{23}(\ddot{e}_{23} + \dot{\Omega})$$

$$T_{13} = I_{13}(\ddot{e}_{13} + \dot{\Omega})$$

$$T_{23} = I_{23}(\ddot{e}_{23} + \dot{\Omega}) \qquad (E-1)$$

The cable configuration employed in this model consists of four parallel cables, symmetrically arranged so that two of them are superimposed upon two others when they are projected into the spin plane. Figure 28 illustrates this arrangement, with the forces F_A and F_B each representing the combined tension forces in a pair of equally loaded cables. Other loads for the model shown in figure 28 are the spin jet force, F_j, and a yaw damper torque, T_{13}', both acting on the manned body. With the assumption that the yaw angles, e_{13} and e_{23}, are small, the following expressions can be derived to represent the forces and moments used in equations (E-1):

$$F_r = -\frac{M_T}{M_1} F_J e_{13} - F_A - F_B \qquad (E-2)$$

$$T_\Omega = F_J \left(X_J + \frac{M_T}{M_1} r \right) + T_{13}' \qquad (E-3)$$

$$T_{13} = d_{22}(F_A - F_B) - \frac{d_{11} d_{21}' (F_A + F_B)}{l_u} (e_{23} - e_{13}) + - \frac{d_{11}(F_A + F_B)}{l_u} (l_u + d_{11} + d_{21}') e_{13} + F_J X_J + T_{13}' \qquad (E-4)$$

$$T_{23} = -d_{22}(F_A - F_B) + \frac{d_{11} d_{21}' (F_A + F_B)}{l_u} (e_{23} - e_{13}) + - \frac{d_{21}' (F_A + F_B)}{l_u} (l_u + d_{11} + d_{21}') e_{23} \qquad (E-5)$$

A symmetric configuration, where $d_{12} = d_{22}$, has been assumed.

B. CABLE FORCES

If each of the four cables has an unloaded length, l_u, the stretch of each pair of cables is represented by

$$\Delta l_A = l_A - l_u = r - d_{11} - d_{21}' - d_{22} e_{13} + d_{22} e_{23} - l_u$$

$$\Delta l_B = l_B - l_u = r - d_{11} - d_{21}' + d_{22} e_{13} - d_{22} e_{23} - l_u \qquad (E-6)$$

Cable slacking effects are introduced by defining the combined forces for each pair of cables in the following manner:

$$\begin{aligned} F_A &= 0 \quad \text{WHEN} \quad \Delta l_A \leq 0 \\ F_B &= 0 \quad \text{WHEN} \quad \Delta l_B \leq 0 \\ F_B &= \frac{k \Delta l_B}{l_u} \quad \text{WHEN} \quad \Delta l_B > 0 \\ F_A &= \frac{k \Delta l_A}{l_u} \quad \text{WHEN} \quad \Delta l_A > 0 \end{aligned} \qquad (E\text{-}7)$$

where k is a constant that represents the stiffness per unit length for a pair of cables in parallel.

C. SIMPLIFYING ASSUMPTIONS FOR ANALOG COMPUTATION

The two yawing moment equations, (E-4) and (E-5), each contain terms that are multiples of cable forces and yaw angles. It can be shown that the second term of these equations will be small compared to the first term, that is,

$$d_{22}(F_A - F_B) \gg \frac{d_{11} d_{21}' (F_A + F_B)}{l_u} (e_{23} - e_{13}) \qquad (E\text{-}8)$$

if the following conditions are met:

- If both pairs of cables are in tension:

$$\frac{d_{22}^2}{d_{11} d_{21}'} \gg \frac{\Delta l_A + \Delta l_B}{2 l_u} \qquad (E\text{-}9)$$

- If one pair of cables is slack:

$$\frac{d_{22}}{d_{11} d_{21}'} \gg \frac{|e_{23} - e_{13}|}{l_u} \qquad (E\text{-}10)$$

- If both pairs of cables are slack, both sides of (E-8) disappear.

Since it appeared reasonable to assume that these conditions would hold true, the terms in question were neglected in the analog computer program. The program results justified the assumption.

Further simplification of equations (E-4) and (E-5) is obtained by assuming that the yaw angles, e_{13} and e_{23}, vary slowly, compared to the

oscillating total cable force associated with relative translation. This permits the use of the following approximation in computing the third term of these equations:

$$(F_A + F_B) \approx M_T (\ell_u + d_{11} + d_{21}') \Omega^2 \qquad (E-11)$$

Equations (E-4) and (E-5) can now be rewritten, with the above assumptions, as

$$T_{13} = d_{22}(F_A - F_B) - M_T \Omega^2 d_{11} \left[\ell_u + 2(d_{11} + d_{21}') + \frac{(d_{11} + d_{21}')^2}{\ell_u}\right] e_{13}$$

$$+ F_J X_J + T_{13}' \qquad (E-12)$$

$$T_{23} = -d_{22}(F_A - F_B) - M_T \Omega^2 d_{21}' \left[\ell_u + 2(d_{11} + d_{21}') + \frac{(d_{11} + d_{21}')^2}{\ell_u}\right] e_{23}$$

$$(E-13)$$

By combining equations (E-1), (E-2), (E-3), (E-12) and (E-13), the following equations of motion are obtained, subject to the assumptions (E-9), (E-10) and (E-11):

$$F_r = -\frac{M_T}{M_1} e_{13} F_J - (F_A + F_B) = M_T (\ddot{r} - r\Omega^2)$$

$$T_\Omega = \left(\frac{M_T}{M_1} r + X_J\right) F_J + T_{13}' = M_T (2r\dot{r}\Omega + r^2\dot{\Omega}) + T_{13} + T_{23}$$

$$T_{13} = d_{22}(F_A - F_B) - M_T \Omega^2 d_{11} \left[\ell_u + 2(d_{11} + d_{21}') + \frac{(d_{11} + d_{21}')^2}{\ell_u}\right] e_{13} +$$

$$+ X_J F_J + T_{13}' = I_{13} (\ddot{e}_{13} + \dot{\Omega})$$

$$T_{23} = -d_{22}(F_A - F_B) - M_T \Omega^2 d_{21}' \left[\ell_u + 2(d_{11} + d_{21}') + \frac{(d_{11} + d_{21}')^2}{\ell_u}\right] e_{23} =$$

$$= I_{23} (\ddot{e}_{23} + \dot{\Omega})$$

$$(E-14)$$

D. NOMINAL VEHICLE PARAMETERS

Values of the various vehicle parameters chosen for the analog computer study were:

Manned-body mass, M_1 = 1220 slugs

Booster mass, M_2 = 557 slugs

Equivalent combined mass, $M_T = M_1 M_2/M_1 + M_2$ = 384 slugs

Manned-body yaw inertia, I_{13} = 173,000 slug ft^2

Booster yaw inertia, I_{23} = 73,000 slug ft^2

Minimum mass-center separation, r_{min} = 37.6 ft

Cable length, unloaded, l_u = 2 to 102 ft

Distance, mass center to cable-attachment point, $d_{11} = d_{21}'$ = 17.8 ft

Distance, center line to cable-attachment point, d_{22} = 5 ft

Distance, manned-body mass center to spin-jet line of action, x_j = 4 ft

Stiffness per unit length of two cables in parallel, in slack range, k = 250,000 lbs/ft/ft

APPENDIX F

EFFECT OF SPIN SPEED-SEPARATION PROFILE ON EXTENSION-RETRACTION IMPULSE REQUIREMENTS

In order to obtain a general expression for spin jet impulse requirements, consider the four-degree-of-freedom model of Appendix E, with the further restrictions that yaw is restrained and that there is no yaw damper. The spinning moment equation can then be written as:

$$\left(\frac{M_T}{M_1} r + X_J\right) F_J = 2 M_T r \Omega \frac{dr}{dt} + \left(M_T r^2 + I_{13} + I_{23}\right) \frac{d\Omega}{dt} \qquad (F-1)$$

By transposing, we get:

$$F_J\, dt = \left[\frac{2 M_T r \Omega}{\frac{M_T}{M_1} r + X_J}\right] dr + \left[\frac{M_T r^2 + I_{13} + I_{23}}{\frac{M_T}{M_1} r + X_J}\right] d\Omega \qquad (F-2)$$

The jet impulse required during a transition between states (r_a, Ω_a) and (r_b, Ω_b) can now be obtained by integrating both sides of the above expression:

$$\left(F_J\, t\right)_{ab} = \int_{r_a}^{r_b} \left[\frac{2 M_T r \Omega}{\frac{M_T}{M_1} r + X_J}\right] dr + \int_{\Omega_a}^{\Omega_b} \left[\frac{M_T r^2 + I_{13} + I_{23}}{\frac{M_T}{M_1} r + X_J}\right] d\Omega \qquad (F-3)$$

Now assume that the overall transition maneuver consists of three linear segments, as shown in figure F-1. In the segment that provides the transition between states (r_o, Ω_o) and (r_M, Ω_E), it is implicitly assumed that the extension rate is being continuously varied so as to achieve the desired linear relation between separation and spin speed while thrusting with constant force. In this segment, therefore, the following relationships hold:

$$\Omega = \frac{\Omega_E(r - r_o) - \Omega_o(r - r_M)}{(r_M - r_o)} \qquad (F\text{-}4)$$

$$d\Omega = \left[\frac{\Omega_E - \Omega_o}{r_M - r_o}\right] dr \qquad (F\text{-}5)$$

By substitution, the total impulse for the three-segment transition can be expressed as:

$$(F_J t) = \left[\frac{M_T r_o^2 + I_{13} + I_{23}}{\frac{M_T}{M_1} r_o + X_J}\right]\Omega_o + \int_{r_o}^{r_M} \left[\frac{3M_T r^2 - 2M_T r_o r + I_{13} + I_{23}}{(r_M - r_o)\left(\frac{M_T}{M_1} r + X_J\right)}\right.$$

$$\left.(\Omega_E - \Omega_o) + 2M_T(r_M - r_o) r \Omega_o\right] dr + \left[\frac{M_T r_M^2 + I_{13} + I_{23}}{\frac{M_T}{M_1} r_M + X_J}\right](\Omega_M - \Omega_E) \qquad (F\text{-}6)$$

Integrating and collecting terms, we get the following general expression for the total impulse for the three segments:

$$(F_J t) = \left[\frac{M_T r_o^2 + I_{13} + I_{23}}{\frac{M_T}{M_1} r_o + X_J} + 2\frac{M_T(r_M - r_o)}{\frac{M_T}{M_1}} - \frac{2M_T X_J}{\left(\frac{M_T}{M_1}\right)^2} \ln \frac{\left(\frac{M_T}{M_1}\right) r_M + X_J}{\left(\frac{M_T}{M_1}\right) r_o + X_J} + \right.$$

$$\left. - \frac{M_T r_M^2 + I_{13} + I_{23}}{\frac{M_T}{M_1} r_M + X_J}\right]\Omega_o + \left[\frac{3M_T X_J^2 + 2M_T X_J r_o\left(\frac{M_T}{M_1}\right) + (I_{13} + I_{23})\left(\frac{M_T}{M_1}\right)^2}{\left(\frac{M_T}{M_1}\right)^3 (r_M - r_o)}\right.$$

$$\ln \frac{\left(\frac{M_T}{M_1}\right) r_M + X_J}{\frac{M_T}{M_1} r_o + X_J} + \frac{M_T(3r_M - r_o)}{2\left(\frac{M_T}{M_1}\right)} - \frac{3M_T X_J}{\left(\frac{M_T}{M_1}\right)^2} - \frac{9M_T X_J^2}{2\left(\frac{M_T}{M_1}\right)^3 (r_M - r_o)} +$$

$$\left. - \frac{M_T r_M^2 + I_{13} + I_{23}}{\left(\frac{M_T}{M_1}\right) r_M + X_J}\right](\Omega_E - \Omega_o) + \left[\frac{M_T r_M^2 + I_{13} + I_{23}}{\left(\frac{M_T}{M_1}\right) r_M + X_J}\right]\Omega_M \qquad (F\text{-}7)$$

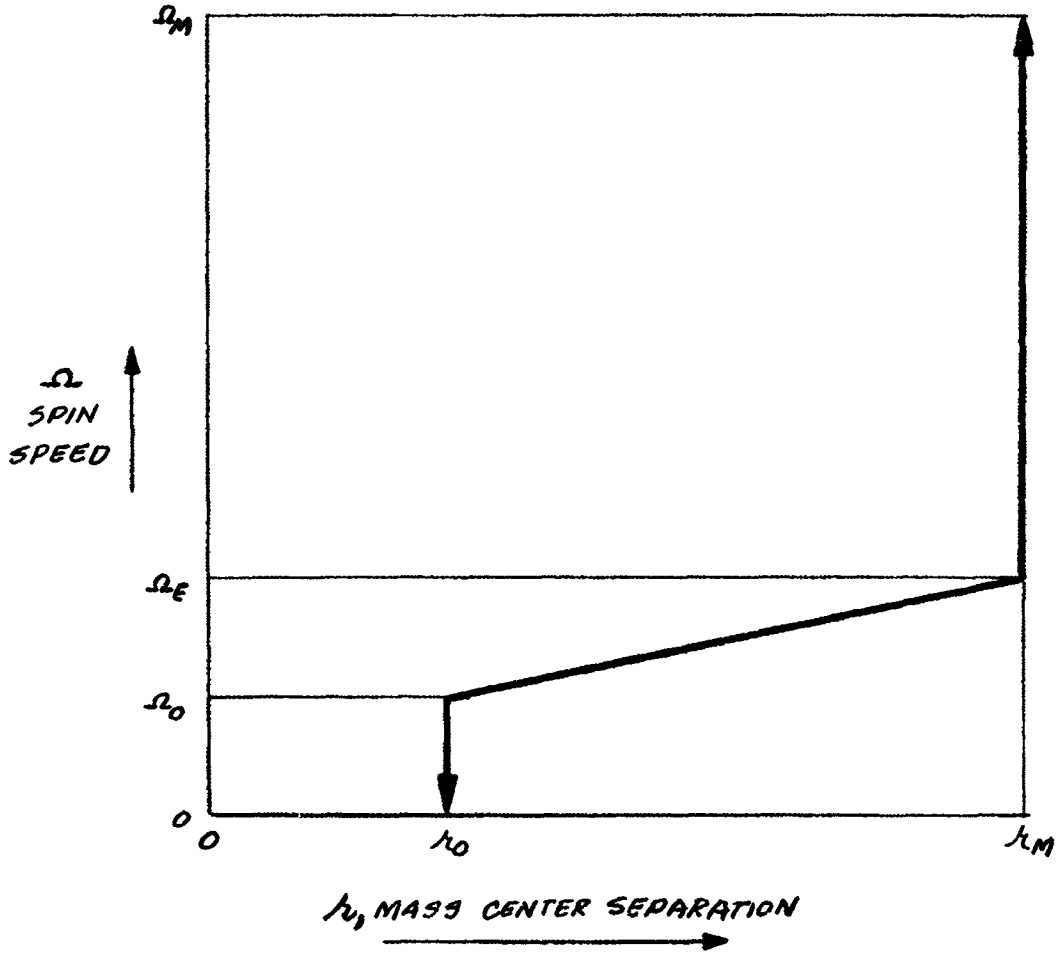

FIGURE F-1 TRANSITION PROFILE ASSUMED FOR IMPULSE REQUIREMENT STUDY

Using nominal values of the various parameters as given in Appendix E, the total impulse can be written as:

$$(F_j t) = 101{,}700\,\Omega_o + 42{,}300(\Omega_E - \Omega_o) + 159{,}000\,\Omega_M \quad \text{lb-sec} \qquad (F\text{-}8)$$

If the spin jets are considered to be located at the center of the manned body, instead of four feet outboard, the required impulse increases to:

$$(F_j t)_{x_j=0} = 136{,}000\,\Omega_o + 65{,}000(\Omega_E - \Omega_o) + 174{,}000\,\Omega_M \quad \text{lb-sec} \qquad (F\text{-}9)$$

Figure 29 illustrates those relationships graphically.

APPENDIX G

PROPELLANT REQUIREMENTS FOR SOLAR TRACKING

A. GRAVITY GRADIENT TORQUES

Consider the vehicle shown in figure G-1. The gravity force in the unit mass element dm is

$$\vec{df} = -g_o\left(\frac{R_o}{\rho_T}\right)^2\left(\frac{\vec{R}+\vec{\rho}}{\rho_T}\right)dm \qquad (G\text{-}1)$$

where

g_o = acceleration of gravity at earth's surface

R_o = radius of earth

$\vec{R}$ = position of c.m. with respect to earth center

$\vec{\rho}$ = position of (dm) with respect to c.m. of vehicle

$\vec{\rho}_T = \vec{R} + \vec{\rho}$

The torque on (dm) about the mass center is

$$\vec{dT_g} = \vec{\rho} \times \vec{df} = -\frac{g_o R_o^2}{\rho_T^3}\left(\vec{\rho}\times\vec{R}\right) \qquad (G\text{-}2)$$

Since R is much larger than ρ, we can write

$$\rho_T = \sqrt{\vec{\rho}_T \cdot \vec{\rho}_T} \approx R\left[1 + \frac{\vec{\rho}\cdot\vec{R}}{R^2}\right] \qquad (G\text{-}3)$$

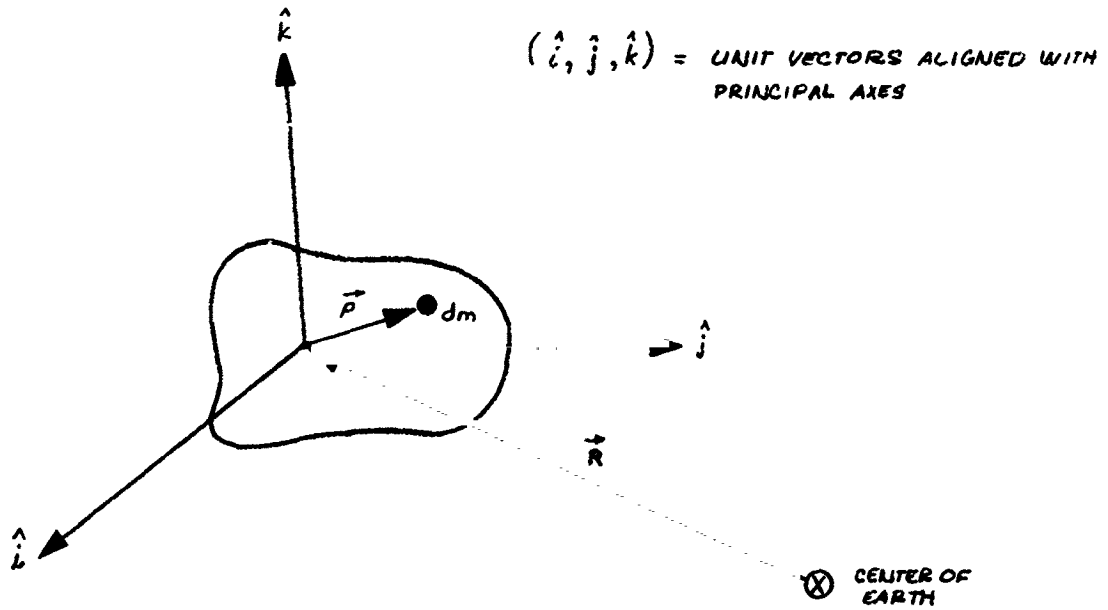

FIGURE G-1. BODY COORDINATE SYSTEM

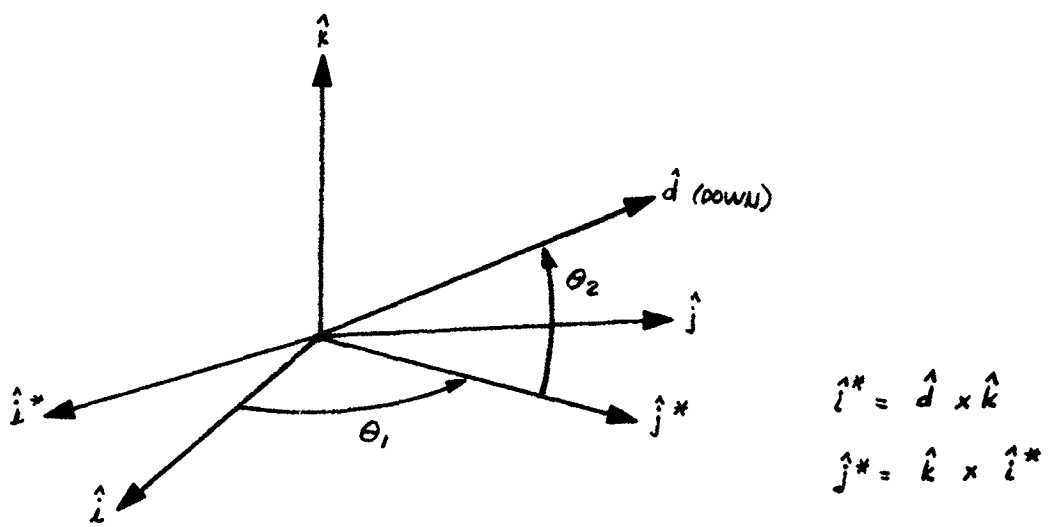

FIGURE G-2. POSITION OF LOCAL VERTICAL IN BODY AXES

The total gravity torque on the vehicle then becomes

$$\vec{T}_g = \frac{g_o R_o^2}{\rho^3} \iiint_M \left[1 - \frac{3\vec{\rho}\cdot\vec{R}}{R^2}\right](\vec{\rho}\times\vec{R})\,dm \qquad (G\text{-}4)$$

Let

$$\vec{R} = \xi\hat{i} + \eta\hat{j} + \nu\hat{k} \qquad (G\text{-}5)$$

and let (θ_1, θ_2) define the position of the local vertical in body axes as shown in figure G-2. Performing the operations indicated in (G-4), one obtains

$$\left.\begin{aligned}
T_\xi &= -\frac{g_o R_o^2}{R^2}\iiint_M \left[\nu\sin\theta_1\cos\theta_2 - \eta\sin\theta_2\right]\left[1 + \frac{3}{R}\left(\xi\cos\theta_1\cos\theta_2 + \eta\sin\theta_1\cos\theta_2 + \nu\sin\theta_2\right)\right] dm \\
T_\eta &= -\frac{g_o R_o^2}{R^2}\iiint_M \left[\xi\sin\theta_2 - \nu\cos\theta_1\cos\theta_2\right]\left[1 + \frac{3}{R}\left(\xi\cos\theta_1\cos\theta_2 + \eta\sin\theta_1\cos\theta_2 + \nu\sin\theta_2\right)\right] dm \\
T_\nu &= -\frac{g_o R_o^2}{R^2}\iiint_M \left[-\xi\sin\theta_1\cos\theta_2 + \eta\cos\theta_1\cos\theta_2\right]\left[1 + \frac{3}{R}\left(\xi\cos\theta_1\cos\theta_2 + \eta\sin\theta_1\cos\theta_2 + \nu\sin\theta_2\right)\right] dm
\end{aligned}\right\} \qquad (G\text{-}6)$$

where

$$\vec{T}_g = T_\xi\hat{i} + T_\eta\hat{j} + T_\nu\hat{k} \qquad (G\text{-}7)$$

Since the point $(\xi = 0,\ \eta = 0,\ \nu = 0)$ is the vehicle center of mass by definition, and since $(\hat{i},\ \hat{j},\ \hat{k})$ are principal axes, equations (G-6) reduce to

$$\left.\begin{aligned}
T_\xi &= -\frac{3g_o R_o^2}{R^3}(I_2 - I_3)\sin\theta_1\sin\theta_2\cos\theta_2 \\
T_\eta &= -\frac{3g_o R_o^2}{R^3}(I_3 - I_1)\cos\theta_1\sin\theta_2\cos\theta_2 \\
T_\nu &= -\frac{3g_o R_o^2}{R^3}(I_1 - I_2)\sin\theta_1\cos\theta_1\cos^2\theta_2
\end{aligned}\right\} \qquad (G\text{-}8)$$

For the vehicle under study, the individual body inertias represent a very small portion of the total pitch and yaw inertias, so that we can approximate the total station inertias as

$$\left.\begin{aligned} I_1 &= 0 \\ I_2 &= M_T r^2 \\ I_3 &= M_T r^2 \end{aligned}\right\} \quad (G\text{-}9)$$

where

$$r = r_1 + r_2$$

$$M_T = \frac{M_1 M_2}{M_1 + M_2}$$

Equations (G-8) may now be written as

$$\left.\begin{aligned} T_\xi &= 0 \\ T_\eta &= -\frac{3 g_0 R_0^2}{R^3}\left(M_T r^2\right)\cos\theta_1 \sin\theta_2 \cos\theta_2 \\ T_\nu &= \frac{3 g_0 R_0^2}{R^3}\left(M_T r^2\right)\sin\theta_1 \cos\theta_1 \cos^2\theta_2 \end{aligned}\right\} \quad (G\text{-}10)$$

The gravity gradient torques may be transformed to the $(\hat{i}^*, \hat{j}^*, \hat{k})$ coordinate system of figure G-2:

$$\begin{aligned} \vec{T}_g = &\left[\frac{3 g_0 R_0^2}{R^3}\left(M_T r^2\right)\cos^2\theta_1 \sin\theta_2 \cos\theta_2\right]\hat{i}^* + \\ &-\left[\frac{3 g_0 R_0^2}{R^3}\left(M_T r^2\right)\sin\theta_1 \cos\theta_1 \sin\theta_2 \cos\theta_2\right]\hat{j}^* + \\ &-\left[\frac{3 g_0 R_0^2}{R^3}\left(M_T r^2\right)\sin\theta_1 \cos\theta_1 \cos^2\theta_2\right]\hat{k} \end{aligned} \quad (G\text{-}11)$$

Since the $(\hat{i}^*, \hat{j}^*, \hat{k})$ coordinate system rotates very slowly with respect to the vehicle spin rate $(\vec{\Omega} = \Omega\hat{k})$, it is meaningful to average the torques in this coordinate system over a spin cycle. In this case we get

$$\vec{T}_g = \frac{3g_0}{2R_0}(M_T r^2)\sin\theta_2\cos\theta_2\,\hat{i}^* \qquad (G\text{-}12)$$

In (G-12) a low orbit has been assumed, i.e., $R \approx R_0$. Note from figure (G-2) that

$$\hat{d}\cdot\hat{k} = \sin\theta_2$$
$$\hat{d}\times\hat{k} = \cos\theta_2\,\hat{i}^*$$

so that (G-12) can be written as

$$\vec{T}_g = \frac{3g_0}{2R_0}(M_T r^2)(\hat{d}\cdot\hat{k}) \qquad (G\text{-}13)$$

In this equation, $\hat{d}$ is parallel to the local vertical and points down, while $\hat{k}$ is parallel to the vehicle spin axis. Normally $\hat{k}$ points at the sun.

Figure G-3 shows the coordinates necessary to define the position of the vehicle in orbit. It follows from figure G-3, and the associated coordinated conversion, that

$$\hat{d} = -\sin\lambda\sin i\,\hat{I} + (\sin\lambda\cos i\sin\Omega - \cos\lambda\cos\Omega)\hat{J} - (\cos\lambda\sin\Omega + \sin\lambda\cos i\cos\Omega)\hat{K} \qquad (G\text{-}14)$$

$$\hat{k} = \cos\mu\,\hat{J} + \sin\mu\,\hat{K} \qquad (G\text{-}15)$$

where

$(\hat{I}, \hat{J}, \hat{K})$ = unit vectors centered at the earth and having a fixed inertial alignment with the normal to the plane of the ecliptic and aligned with the vernal equinox

i = inclination of vehicle orbit with respect to the ecliptic

Ω = position of the ascending mode in the ecliptic

λ = position of the vehicle in its orbit

μ = position of the sun in the ecliptic.

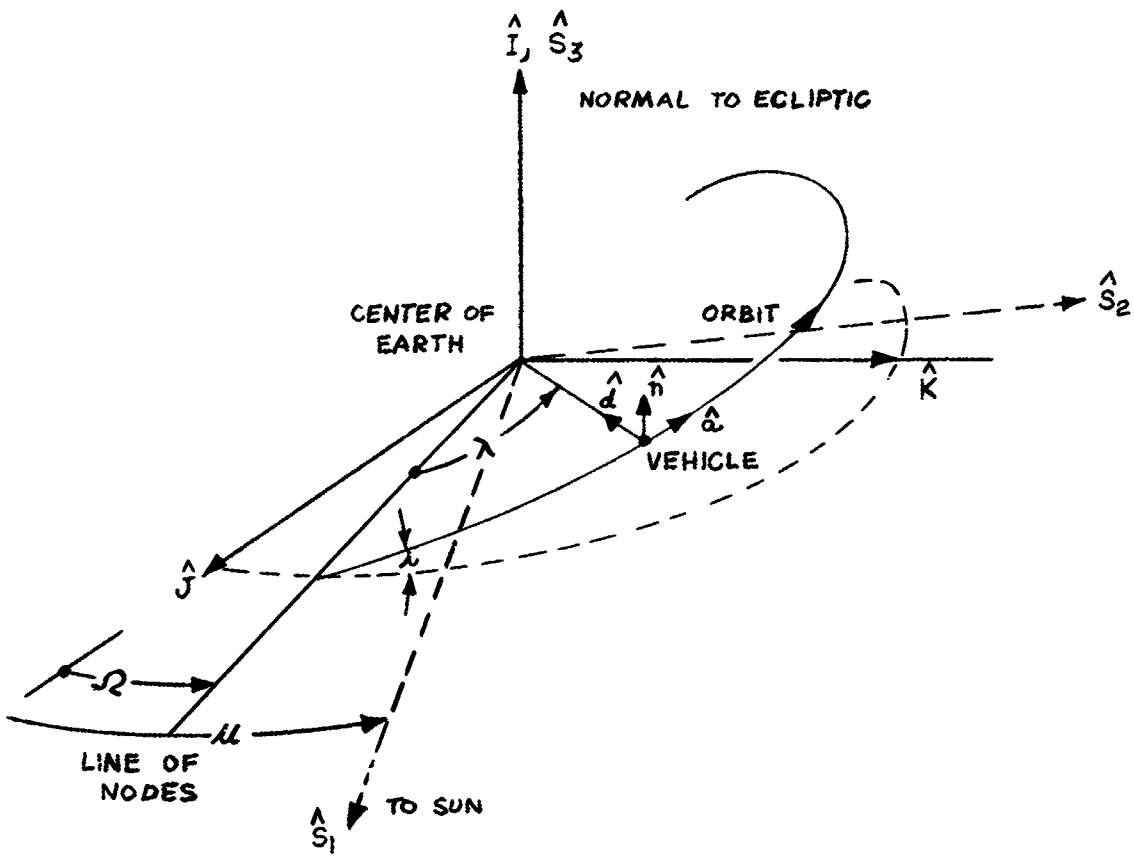

$$\begin{Bmatrix} \hat{d} \\ \hat{n} \\ \hat{a} \end{Bmatrix} = \begin{bmatrix} 0 & -\cos\lambda & -\sin\lambda \\ 1 & 0 & 0 \\ 0 & -\sin\lambda & \cos\lambda \end{bmatrix} \begin{bmatrix} \cos i & 0 & -\sin i \\ 0 & 1 & 0 \\ \sin i & 0 & \cos i \end{bmatrix} \begin{bmatrix} 1 & 0 & 0 \\ 0 & \cos\Omega & \sin\Omega \\ 0 & -\sin\Omega & \cos\Omega \end{bmatrix} \begin{Bmatrix} \hat{I} \\ \hat{J} \\ \hat{K} \end{Bmatrix}$$

FIGURE G-3 ORBITAL PARAMETERS

Using these definitions, we get

$$(\hat{d}\cdot\hat{k})(\hat{d}\times\hat{k}) = \Big[\sin^2\lambda\cos^2 i\,\sin(\Omega-\mu)\cos(\Omega-\mu) - \cos^2\lambda\sin(\Omega-\mu)\cos(\Omega-\mu) + \\ -\cos\lambda\sin\lambda\cos i\cos^2(\Omega-\mu) + \sin\lambda\cos\lambda\cos i\sin^2(\Omega-\mu)\Big]\hat{I} + \\ + \Big[\sin^2\lambda\sin i\cos i\sin\mu\sin(\Omega-\mu) - \cos\lambda\sin\lambda\sin i\cos(\Omega-\mu)\Big]\hat{J} + \\ + \Big[\cos\lambda\sin\lambda\cos\mu\sin i\cos(\Omega-\mu) - \sin^2\lambda\sin i\cos i\cos\mu\sin(\Omega-\mu)\Big]\hat{K} \qquad (G\text{-}16)$$

The average value of this factor over one orbit is

$$(\hat{d}\cdot\hat{k})(\hat{d}\times\hat{k}) = \frac{1}{4}\Big[-\sin^2 i\sin 2(\Omega-\mu)\,\hat{I} + \sin 2i\sin(\Omega-\mu)\sin\mu\,\hat{J} - \sin 2i\sin(\Omega-\mu)\cos\mu\,\hat{K}\Big] \qquad (G\text{-}17)$$

If a sun-oriented coordinate system is introduced, as shown in figure G-3, (G-17) becomes

$$(\hat{d}\cdot\hat{k})(\hat{d}\times\hat{k}) = -\frac{1}{4}\Big[\sin 2i\sin(\Omega-\mu)\,\hat{S}_2 + \sin^2 i\sin 2(\Omega-\mu)\,\hat{S}_3\Big] \qquad (G\text{-}18)$$

Thus, the average torque for one orbit is

$$\overrightarrow{T_{av}} = -\frac{3g_0}{8R_0}(M_T r^2)\Big[\sin 2i\sin(\Omega-\mu)\,\hat{S}_2 + \sin^2 i\sin 2(\Omega-\mu)\,\hat{S}_3\Big] \qquad (G\text{-}19)$$

using

$$g_o = 32.2 \text{ ft/sec}^2$$

$$R_o = 2.09 \times 10^7 \text{ ft}$$

$$M_r r^2 = 7.25 \times 10^6 \text{ slug-ft}^2$$

$$\overrightarrow{T_{av}} = -4.2\left[\sin 2i \sin(\delta_b - \mu)\hat{S}_2 + \sin^2 i \sin 2(\delta_b - \mu)\hat{S}_3\right] \qquad (G\text{-}20)$$

For a general orbit, earth oblateness causes a regression of the nodes, so that i and Ω vary with time. For this reason, further averaging of the gravity gradient torques is extremely difficult. Reasonable fuel estimates can be made, however, by considering the special case of an equatorial orbit. In this case, the orbit inclination with respect to the ecliptic is 23°, and there is no orbit regression. Arbitrarily starting with $\Omega = 0$ gives

$$\overrightarrow{T_{av}} = 3 \sin\mu \hat{S}_2 + .64 \sin 2\mu \hat{S}_3 \qquad (G\text{-}21)$$

B. REQUIRED CONTROL TORQUES

In order to precess the vehicle spin vector to follow the sun line as the earth moves in its orbit, it is necessary to obtain a precession torque of

$$\overrightarrow{T_s} = H_v \dot{\mu} \hat{S}_2 \qquad (G\text{-}22)$$

where

H_v = vehicle angular momentum

$\dot{\mu}$ = earth orbital velocity

For the nominal vehicle, the required torque is

$$\vec{T}_c = 0.6\,\hat{S}_2 \qquad (G\text{-}23)$$

It is evident that a control torque, $\vec{T}_c$, must be applied to the vehicle such that gravity gradient torques are nullified, and the vehicle tracks the sun. Let

$$\vec{T}_c = T_{c_2}\,\hat{S}_2 + T_{c_3}\,\hat{S}_3 \qquad (G\text{-}24)$$

Then it follows from equations (G-21) and (G-23) that the required torque is

$$\vec{T}_c = (0.6 - 3\sin\mu)\,\hat{S}_2 - (0.64\sin 2\mu)\,\hat{S}_3 \qquad (G\text{-}25)$$

C. PROPELLANT REQUIREMENTS

The propellant required to maintain solar orientation of the vehicle can be estimated from equation (G-25). The required propellant weight, W, is given by

$$W = \frac{1}{r_1^* I_{sp}} \int_0^t |T_c|\, d\tau \qquad (G\text{-}26)$$

where

r_1^* = reaction jet moment arm

I_{sp} = propellant specific impulse

Equation (G-26) is based on an orientation control system where fuel is expended only when the vehicle cable line is essentially normal to the required torque vector. This equation is also based on the assumption that no solar pointing error can be tolerated. Since T_c varies as a complex function of time as the earth moves in its orbit around the sun, it is

convenient to integrate equation (G-26) graphically. Figure G-4 shows the yearly variation in required control torque, T_c. The yearly average of this torque is found to be 2.0 ft-lbs.

This value, together with a reaction-jet moment arm of 47 feet and a specific impulse of 300 seconds, yields a yearly propellant requirement for solar orientation of

$$W = 4500 \text{ pounds.} \qquad \text{(G-27)}$$

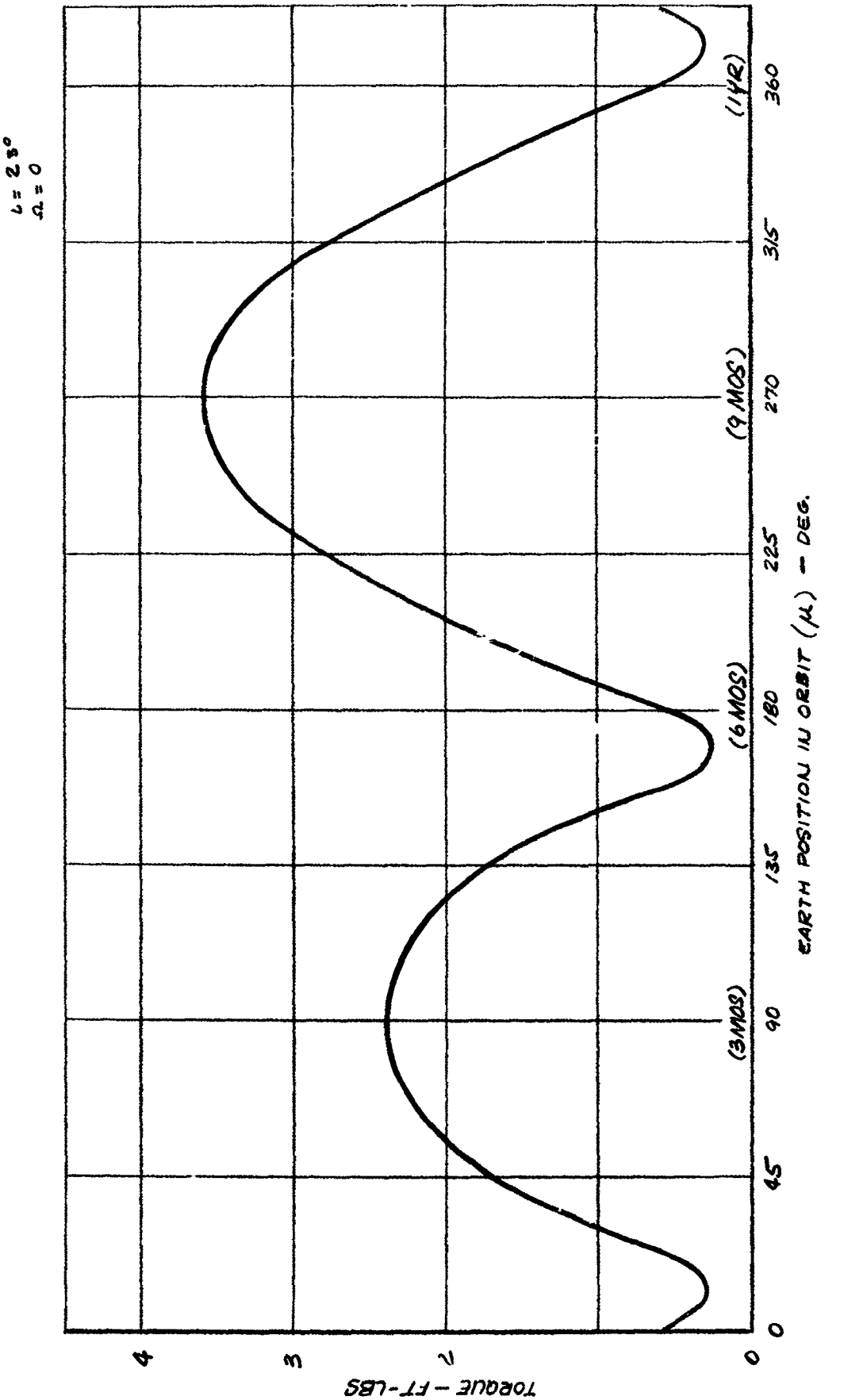

FIGURE G-4 REQUIRED CONTROL TORQUE, T_c, TO MAINTAIN SOLAR ORIENTATION

APPENDIX H

ACTUATOR SIZING CALCULATIONS FOR NONSPINNING MODE

A. NONSPINNING VEHICLE CONFIGURATION

It is assumed the cables will be fully retracted whenever the vehicle is not spinning and that the vehicle will be as shown in figure H-1.

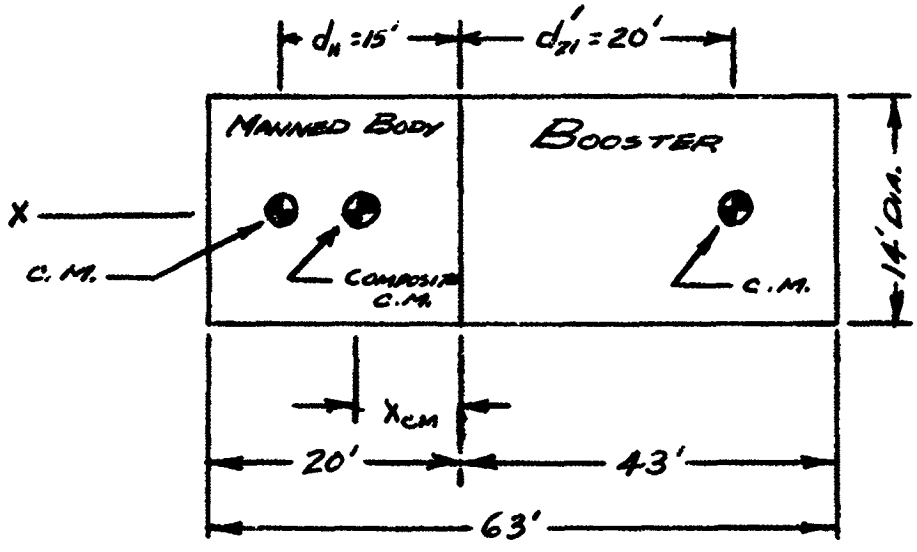

FIGURE H-1 NONSPINNING VEHICLE CONFIGURATION

The mass and inertias of the booster and manned capsule are as follows:

	Manned Body	Booster
Mass	M_1 = 1220 slugs	M_2 = 557 slugs
Roll Inertia	I_{11} = 1 x 10^5 slug ft^2	I_{21} = 3 x 10^4 slug ft^2
Pitch Inertia	I_{12} = 9.05 x 10^4	I_{22} = 7.3 x 10^4
Yaw Inertia	I_{13} = 1.73 x 10^5	I_{23} = 7.3 x 10^4

Then, the composite vehicle has the following parameters:

Mass $$\bar{M} = M_1 + M_2 = 1777 \text{ slugs} \qquad (H\text{-}1)$$

Composite center of Mass

$$x_{cm} = \frac{m_1 d_{11} - m_2 d_{21}'}{\bar{M}} = \frac{(1220)(15) - (20)(557)}{1777} = 4.04'$$

Inertias

Roll $$I_1 = I_{11} + I_{21} = 1 \times 10^5 + 0.3 \times 10^5 = 1.3 \times 10^5 \text{ slug-ft}^2 \qquad (H\text{-}2)$$

Pitch

$$I_2 = I_{12} + M_1 d_1^2 + I_{22} M_2 d_2^2 \qquad (H\text{-}3)$$

$$I_2 = 6.32 \times 10^5 \text{ slug-ft}^2$$

Yaw

$$I_3 = I_{13} + 1.7_1 d_1^2 + I_{23} + m_2 d_2^2 \qquad (H\text{-}4)$$

$$I_3 = 7.14 \times 10^5 \text{ slug-ft}^2$$

B. ORBITAL ORIENTATIONS

The two vehicle orientations considered for illustrating disturbance-level variations are depicted in figure H-2. The solar-oriented vehicle is pointed so that the longitudinal (x) body axis is aligned with the sun's rays. Roll orientation is optional, but for the present analysis, the vehicle is assumed to remain inertially fixed in roll.

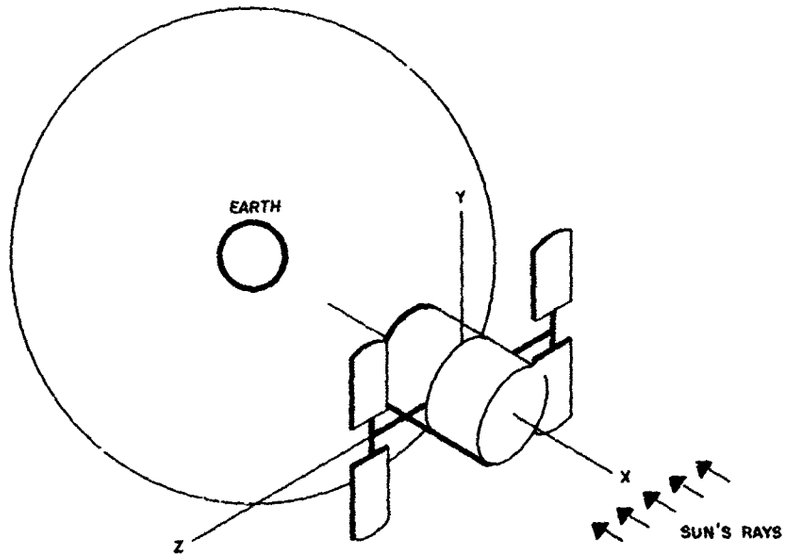

a. SOLAR ORIENTATION

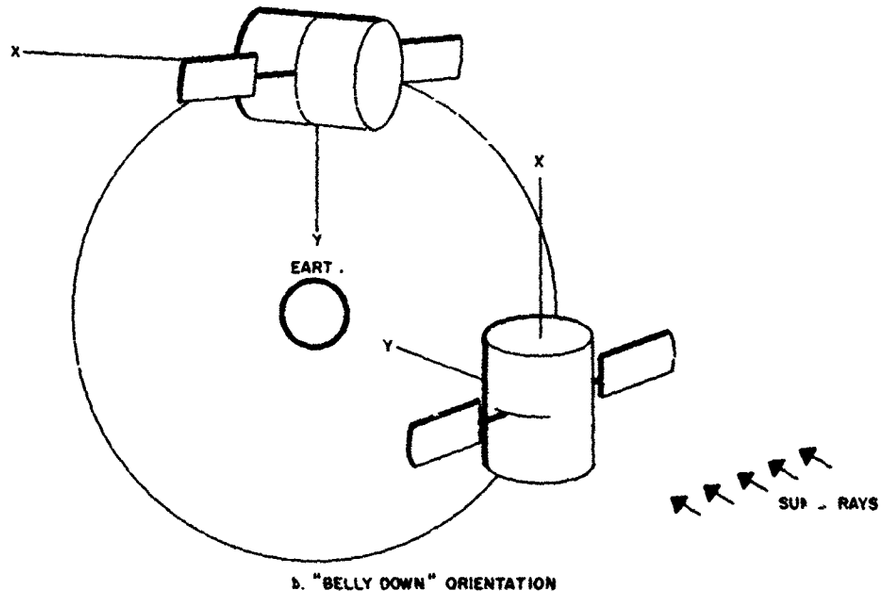

b. "BELLY DOWN" ORIENTATION

FIGURE H-2 ORBITAL ORIENTATIONS

In the "belly down" orientation, the y-axis is aligned with the local vertical and the x-axis is held in the orbital plane. It should be noted that the pitch and yaw definitions used here are consistent with the definitions used in the spinning vehicle studies.

C. GRAVITY GRADIENT TORQUES

The body axis torques acting on an orbiting vehicle due to gravity gradient are as follows:

$$\text{Roll } T_\xi = \frac{3g_o R_o^2}{R^3}(I_3 - I_2)\left(\frac{\eta}{R}\right)\left(\frac{\nu}{R}\right) = K_{T1}\left(\frac{\eta}{R}\right)\left(\frac{\nu}{R}\right) \text{ FT-LB} \qquad (H\text{-}5)$$

$$\text{Pitch } T_\eta = \frac{3g_o R_o^2}{R^3}(I_1 - I_3)\left(\frac{\xi}{R}\right)\left(\frac{\nu}{R}\right) = K_{T2}\left(\frac{\xi}{R}\right)\left(\frac{\nu}{R}\right) \text{ FT-LB} \qquad (H\text{-}6)$$

$$\text{Yaw } T_\nu = \frac{3g_o R_o^2}{R^3}(I_2 - I_1)\left(\frac{\xi}{R}\right)\left(\frac{\eta}{R}\right) = K_{T3}\left(\frac{\xi}{R}\right)\left(\frac{\eta}{R}\right) \text{ FT-LB} \qquad (H\text{-}7)$$

where

R_o = radius of earth = 20.9×10^6 ft

g_o = surface value acceleration of gravity = 32.2 ft/sec^2

R = orbital radius = 21.9×10^6 ft (175-nm orbit)

(I_1, I_2, I_3) = principal moments of inertia (ft lb sec^2)

(ξ, η, ν) = body axis components of radius vector to vehicle (ft) (ξ, η, ν are a function of vehicle position on orbit and orientation)

therefore,

$\frac{\xi}{R}, \frac{\eta}{R}, \frac{\nu}{R}$ are direction cosines.

Evaluating these torques for the vehicle shown in figure H-1, the constant factors are

K_{T1} = 0.33 ft lb
K_{T2} = 2.35 ft lb
K_{T3} = 2.02 ft lb

When the vehicle is in the "belly down" orientation, the y-body axis intersects the center of the earth; therefore, $R_x = R_y = 0$ Thus,

$$T_\zeta = K_{T1}\left(\frac{\eta}{R}\right)\left(\frac{v}{R}\right) = 0 \qquad (H\text{-}8)$$

$$T_\eta = K_{T2}\left(\frac{\zeta}{R}\right)\left(\frac{v}{R}\right) = 0 \qquad (H\text{-}9)$$

$$T_v = K_{T3}\left(\frac{\zeta}{R}\right)\left(\frac{\eta}{R}\right) = 0 \qquad (H\text{-}10)$$

provided this orientation is held.

For the solar oriented vehicle, ζ, η and v depend on the location of the orbital plane, the sun, and on the vehicle position in orbit. For the purpose of estimating actuator sizing requirements, the worst case will be assumed, giving the following maximum torques:

$$T_{\zeta MAX} = 0.5\, K_{T1}$$

$$T_{\eta MAX} = 0.5\, K_{T2}$$

$$T_{v MAX} = 0.5 K_{T3}$$

These torques will oscillate at twice the orbital frequency, giving maximum oscillatory components of

$$T_\zeta = (0.5)(0.33)(\sin 2\omega_e t) = (0.165\ ft\text{-}lb)\sin 2\omega_e t \qquad (H\text{-}11)$$

$$T_\eta = (0.5)(2.35)(\sin 2\omega_e t) = (1.175\ ft\text{-}lb)\sin 2\omega_e t \qquad (H\text{-}12)$$

$$T_v = (0.5)(2.02)(\sin 2\omega_e t) = (1.01\ ft\text{-}lb)\sin 2\omega_e t \qquad (H\text{-}13)$$

where ω_e is orbit frequency (1.14×10^{-3} rad/sec for a 175 nmi orbit).

The impulse required to counteract these torques is given by

$$\mathcal{I} = Impulse = T_{MAX}\int_0^{\frac{T}{4}} \sin 2\omega_e t\, dt = \frac{T_{MAX}}{\omega_e} \qquad (H\text{-}14)$$

where

$$T = \frac{2\pi}{\omega_e}$$

This gives the following values when evaluated for the above torques:

$$\text{Roll } \mathcal{J}_1 = 144.7 \text{ ft lb sec}$$
$$\text{Pitch } \mathcal{J}_2 = 1030 \text{ ft lb sec}$$
$$\text{Yaw } \mathcal{J}_3 = 885 \text{ ft lb sec}$$

Assuming that the yaw reaction wheel can be operated from full speed one direction to full speed the other direction to absorb the yaw torque impulse, a minimum wheel capacity would be 443 ft lb sec (slug ft^2/sec). Extra wheel capacity may be needed to counteract cross-coupling from the control moment gyro, depending on its specific implementation.

A two-degree-of-freedom control moment gyro for pitch and roll would be sized by the pitch torque impulse. Assuming here, too, that hardover-to-hardover operation is acceptable, the gyro angular momentum (based on 60-degree gimbal deflection) would be

$$\int_{-\frac{\pi}{3}}^{\frac{\pi}{3}} H \cos \alpha_T \, d\alpha_T = 1030 \text{ ft-lb-sec} \qquad (H\text{-}15)$$

where α_T is the gyro gimbal angle.

$$H = \frac{1030}{1.732} \approx 600 \text{ ft-lb-sec}$$

In addition to the oscillatory components assumed to be counteracted by momentum storage devices, there will also be secular gravity gradient torques that will require reaction jet fuel consumption. The maximum values of these secular torques would be

$$T_\xi = 0.0825 \text{ ft-lb}$$
$$T_\tau = 0.505 \text{ ft-lb}$$

The fuel required to oppose these secular torques depends on the actual vehicle ephemeris.

D. AERODYNAMIC TORQUES

Aerodynamic torques on a space station depend on its geometric shape as well as its orbital altitude and orientation. Attachments, such as solar panels, may also contribute major aerodynamic torques. Therefore,

a detailed analysis of the aerodynamic torques would necessitate establishing nonspinning vehicle configuration parameters to a depth not consistent with this study. However, some measure of the potential importance of these torques can be obtained by considering the simplified vehicle model shown in figure H-3, and neglecting the effects of solar panels.

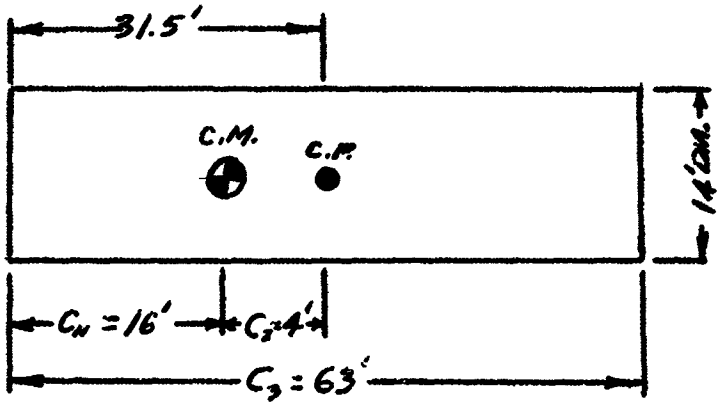

FIGURE H-3 AERODYNAMIC VEHICLE MODEL

For the solar orientation, the vehicle angle-of-attack α will go through 360 degrees in the course of each orbit. To a first approximation, the maximum moment will occur when the angle-of-attack is 90 degrees. This moment can be calculated readily using the equations developed by Davison* based on free-molecule aerodynamics.

The drag coefficient based on frontal area for a cylinder normal to the relative wind is given by (Davison, p. 16, eq. 37)

$$C^*_{D_{\alpha=\pi/2}} = \frac{\pi^{3/2}}{4 S_-}\sqrt{\frac{T_w}{T_\infty}} + \frac{\sqrt{\pi}}{2(C_3/C_4) S_-} + 2 \qquad (H\text{-}16)$$

- - - - - - -

*Paul H. Davison, Passive Aerodynamic Stabilization of Near Earth Satellites, Volume II - Aerodynamic Analysis, WADD TR61-133, Wright Air Development Division, WPAFB, Ohio, March 1961.

where

S_∞ = molecular speed ratio

T_w = vehicle skin temperature

T_∞ = free stream temperature

These parameters are all evaluated by Davison and are presented in the reference cited as a function of orbital altitude. For a 175-nm orbit,

$$S_\infty = 7.25$$

$$\frac{1}{S_\infty}\sqrt{\frac{T_w}{T_\infty}} = 6.4 \times 10^{-2}$$

And for

$$C_3/C_4 = \frac{63}{14} = 4.5$$

the resultant drag coefficient becomes

$$C_{D_{\alpha/2}}^{*} = \frac{5.58}{4}(6.4 \times 10^{-2}) + \frac{1.775}{(2)(4.5)(7.25)} + 2 = 2.117 \qquad \text{(H-17)}$$

and the drag is

$$D = C_D^* C_3 C_4 q$$

$$D = (2.117)(63)(14)(1.42 \times 10^{-5}) = 0.0264 \text{ lb}$$

where

$q = \frac{1}{2}\rho^* V^2$

ρ^* = atmospheric density

V = orbital velocity

(evaluated for 175-nm orbit)

giving a resultant moment of

Torque = Drag x C_2 (mass center to center of pressure distance)

= (2.64×10^{-2} lb) (15.5 ft)

= 0.41 ft lb

If the aerodynamic torque is approximated by a sinusoid at orbital frequency having this peak value, the maximum impulse is

$$\mathcal{I} = \int_{c}^{T/2} 0.41 \sin \omega_e t \, dt \qquad (H\text{-}18)$$

$$= \frac{(0.41)(2)}{(1.14 \times 10^{-3})} = 720 \text{ FT-LB-SEC}$$

where

ω_e = orbit frequency (1.14×10^{-3} rad/sec for 175-nm orbit)

This would certainly be significant in sizing momentum storage devices.

E. MOMENTUM STORAGE FOR MANEUVERING

It may be desirable to employ momentum storage actuators for maneuvering control during some phases of the mission. One advantage of such a procedure is the conservation of reaction jet fuel; another is the capability of more precise pointing control. However, with the large vehicle inertias involved, even low maneuvering rates require significant momentum storage capacity. For example, maneuvering at a rate as low as 0.05 degree per second will require the following:

Yaw: ΔH yaw = (0.05 deg/sec)(1/57.3)(7.14×10^5 ft lb sec^2) = 623 ft lb sec

Pitch: ΔH pitch = (0.05)(1/57.3)(6.32×10^5) = 552 ft lb sec

Roll: ΔH roll = (0.05)(1/57.2)(1.3×10^5) = 114 ft lb sec

Thus, if an orbital orientation which minimizes external disturbances is selected, the capacity of the momentum exchange actuators may well be determined by the maneuvering control requirements.